Study on Hydro-morphological Characteristics of Meandering Channels with Groynes

KARKI Saroj

2019

Study on Hydro-morphological Characteristics of Meandering Channels with Groynes

A dissertation submitted in partial fulfillment for the requirement of

Doctoral Degree in Civil and Earth Resources Engineering

by

KARKI Saroj

Supervised by Prof. NAKAGAWA Hajime

Laboratory of Hydroscience and Hydraulic Engineering

Department of Civil and Earth Resources Engineering

Graduate School of Engineering

Kyoto University

Japan

2019

Abstract

This thesis, through experimental and numerical simulation, focused on investigating the effects of meandering channel geometric parameters such as sinuosity, deflection angle, ratio of radius of curvature to the channel width (R_c/B ratio) on the flow characteristics and morphological evolution. Meandering channels vary from one another in different aspects and their role on channel flow and morphology have already been realized. Thus it wouldn't be rational to generalize all meandering channels into a single category of analysis. Acknowledging this fact, experiments were conducted in two sine-generated meandering channels of different sinuosity (1.2 and 1.35) with corresponding maximum deflection angle of 45^0 and 60^0 respectively under the erodible bed and erodible banks. It was observed that the initial bed development process is more rapid in low sinuous channels. Accordingly, the rate of bank erosion was higher for such channels. The common characteristics of meandering channels like point bar and deep pools were also more distinct in low sinuous channels. With increasing sinuosity, the bed morphology tend to be more complicated. Another important observation was the location of the maximum bank erosion which was different for each channels. In low sinuosity (and low deflection angle) channel, maximum bank erosion zone extended between crossover to further downstream near inner (convex) bend apex while that located around crossover to further upstream near the outer (concave) bend apex in higher sinuosity channel. The main reason was the angle of approach of the flow in the bends which varied with changing deflection angle.

The next emphasis of the experiments was to examine the channel flow and morphological response in the presence of groynes and at the same time, analyze the role of groynes in reducing bank erosion. From several preliminary experiments, the location of groynes were decided and placed slightly downstream of the outer bank apex. Results showed that the erosion of the outer banks can be significantly reduced by implementing groynes. The high-velocity zone was shifted away from the banks around the groynes field which suppressed the growth and expansion of the point bar on the opposite inner bank. However, the strong recirculation in the embayment can cause the erosion to continue in that area. At the same time, it was observed that the first groynes where the impact of approach flow is higher, greater scour occurs near the tip increasing the risk of failure of the groynes. Although groynes reduced the erosion at some locations, they also tend to transfer the erosion from one point to another. Experiments revealed higher erosion in the near-bank area upstream of the first groynes in higher sinuosity channels suggesting increased protection of the area. This tendency was relatively lower in low sinuous channel which is due to the convergence of approach flow downstream of the apex with less attack on the first groynes.

The third focus was to investigate numerically the channel response under different arrangement of groynes such as varying angle of groynes and changing the position of groynes from outer bank apex to further downstream. The objective was to determine the appropriateness of groynes position and angle on reducing erosion of the near-bank area under different sinuosity. Validation results revealed that the 2D models can reasonably predict the bed morphological evolutions in different meandering channels. The application of 2D models to this study showed that in low sinuosity channel, the groynes positioned downstream of the apex are more effective in reducing the scour depth at the groynes tip, shifting high-velocity core and high near-bank shear stress towards the channel. However, with increasing sinuosity, the position of groynes needs to be shifted upstream around the apex for improving the performance. As it was recognized for high sinuosity and deflection angle channel that the groynes positioned exactly at the apex have a better effect of shifting the high velocity core and high bed shear stress away from the banks.

The application of model to the real field cases reproduced the observed trend quite well. In case of Gowain River, it was observed that the groynes oriented at 90^0 are more effective in shifting the high velocity from the banks but could promote erosion behind the initial groynes at the entry of the bend. On the other hand, groynes placed at 120^0 induce greater deposition in the initial groynes. Therefore it was concluded that rather than adopting a single orientation, a combination of two or more arrangements would enhance the effectiveness of the groynes depending upon the field condition. Simulation in Uji River suggested that the overall channel evolution is insignificant but the bank erosion is dominant at several locations. It was also concluded that the bank erosion is mainly caused by the undercutting of the bank toe due to the low flow condition which induce high bed shear stress and high near bank velocity. With higher flow discharge, the zone of maximum velocity tend to shift more towards the channel center. Results of the prediction of bank erosion indicated that fluvial erosion due to the scour near the bank toe is dominant at most of the locations in Uji River.

The final focus was to investigate the three dimensional flow field through 3D numerical simulation which couldn't be investigated by using the depth-averaged 2D model. Results indicated that the cross-sectional flow variability is higher in high curvature bend i.e. 45^0 channel (R_c/B=1.25) showed greater variability than 60^0 channel (R_c/B =2.25). The cross-sectional variation of velocity field is dominant at the entry and the exit of the bend whereas the secondary flow is mostly stronger at the apex sections in both channels. The divergence of flow relative to the channel apex begin more upstream in high sinuosity and high deflection angle channel. At the bend apex, the secondary flow effect was higher in ch-60 compared to ch-45.

Keywords: Meandering channels, Sinuosity, Bed morphology, Bank erosion, Groynes

Acknowledgements

Each page of this thesis is the outcome of three years of persistent efforts accompanied by challenges, successes and failures. It wouldn't have come to the timely conclusion without the support of a number of people around me- my family, my supervisors, friends, laboratory staffs, Kyoto University staffs and many others.

I am exceedingly grateful to my supervisor Prof. Dr. Hajime Nakagawa for giving me an honorable opportunity to work under him and believing in my abilities. His very positive attitude, well-directed guidance, generosity, time, patience, and regular advice helped me overcome several challenges during my study as well as provided an inspiration to work harder. I am also thankful to my co-supervisor Assoc. Prof. Dr. Kenji Kawaike for his support, precise comments and for always being available to any inquiry regarding my research. Similarly, I would also like to thank Asst. Prof. Dr. Kazuki Yamanoi for his suggestions and comments to improve the thesis.

I would like to extend my sincere gratitude to the reviewer of my thesis, Prof. Dr. Masaharu Fujita, DPRI, Kyoto University whose constructive comments and valuable suggestions aided to improve this thesis.

I want to thank my parents for their wholehearted dedication and patience in bringing me where I am today. No words would be enough to mention their contributions. They have always been there for me during the ups and downs of my life, given me inspiration and incredible strength to march forward in life. I would also like to thank my brother, sisters, hajur-aama, thulo mummy, mama-maiju, dada-bhauju, buwa-aama and everyone for their support and belief on me.

More than anyone else, it's my wife Suchana and daughter Sarseej whose presence fueled me with positive energy during the most turbulent times. The way my wife single-handedly controlled the pressure of managing home, taking care of Sarseej and continuing her studies deserves a big applause. I love you Soltu and Betu.

It wouldn't be fair if I don't mention Prof. Dr. Narendra Man Shakya and Prof. Dr. Durga Prasad Sangroula (Tribhuvan University, Nepal) who encouraged me right from my Master's degree for research works and eventually recommended me for a PhD course at Kyoto University.

Thank you all

~To all the mothers in the World~

Table of contents

x

Chapter 1

Introduction

1.1 General

River channel forms one of the dynamic systems of planet earth. With the ability to shape its path through the transport of sediment, rivers continuously evolve over time if they are unconstrained by external factors. While rivers have been utilized to serve various human-related purposes but lack of their proper management, have resulted in adverse impacts such as flooding, bank erosion and channel migration. Therefore studies on the river morphology have been a subject of great interest for river morphologists, scientists, engineers and a challenge at the same. They recognize that any engineering effort in rivers must be based on a proper understanding of the morphological characteristics (Chang, 2008). In general, Rivers are classified as straight, meandering and braiding depending upon its planform (Leopold and Wolman, 1957). Various factors such as flow discharge, sediment properties, channel geometry, etc. govern the evolution of a river into any of the above-mentioned types. However, most of the natural streams, regardless of its size, are characterized by the absence of long straight reaches and the presence of frequent sinuous reversals of curvature (Leopold and Langbein, 1960). Such behavior of river channels led to the evolution of a unique subject in fluvial geomorphology-the meandering channels and increased the attention of people from all related disciplines to study this dynamic river form.

This dissertation is focused on the study of meandering channels with varying geometric characteristics like sinuosity, deflection angle and curvature. Effects of these geometric parameters on the channel bed morphology and bank erosion were investigated through laboratory experiments. Experiments involving the simultaneous evolution of bed and banks in the presence of groynes are also performed. Further, the effectiveness of different arrangement of groynes on mitigating bank erosion is investigated through numerical simulation including field application.

1.2 Previous studies on meandering channels

Meandering rivers are defined as single thread channels with a sinuous planform, consisting a series of alternate loops, frequently depicted as regular and simple in form and size, but in reality often having some irregularity, asymmetry, and complexity (Hooke, 2013). They are distinct from braided channel patterns, which consists of multiple channels or multiple free bars within the course, and straight channels, which have very low sinuosity **(Figure 1.1)**. Hooke (2003) mentions "River meanders have been subject to much analysis, of various kinds, in fluvial geomorphology because of their remarkable forms, their ubiquity, their dynamism and the practical consequences of their movement". According to Güneralp et al. (2012), interest in the dynamics of meandering river channels is scientific and includes concerns related to river engineering and management, such as flood control, navigation, bank erosion, and the protection of land and infrastructure.

Research on river meanders has been undertaken in a range of disciplines, including geomorphology (in geography and earth sciences), engineering, mathematics, fluid dynamics, etc. The shift from the subjective to more quantitative approach in the study of river meander morphology and processes began in the 1950s, continuing through the 1960s, with the pivotal contribution of Leopold and Wolman (1957,1960), Leopold and Langbein (1966), Leopold et al., 1964, and Schumm (1960,1963). These work laid the foundations for modern fluvial geomorphology and the basic understanding of river meanders (Hooke, 2013). Meandering channels were approximated to fit a sine-generated curve following the theory of energy
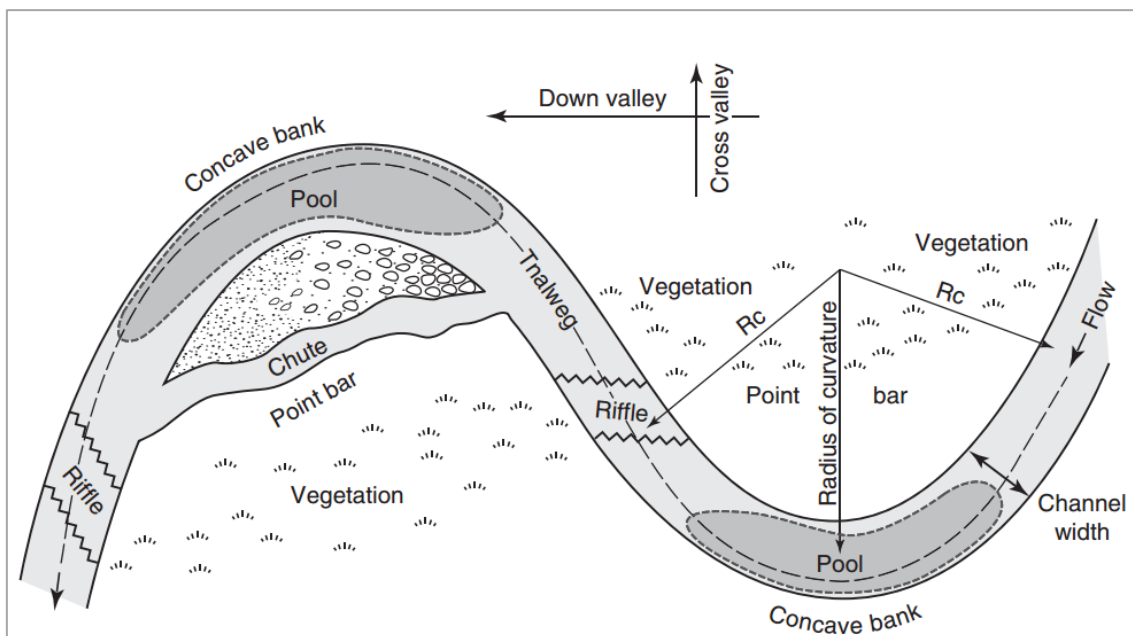

Figure 1.1 Characteristic features of meandering channels (Adapted from Hooke, 2013)

2

distribution and minimum variance. Morphometric and process form relations, for example, between meander wavelength and discharge, were quantified. It is evident that erosion and deposition processes occur naturally in alluvial rivers and help to shape their channel form. But why do the river meanders? Rhoads and Welford (1991) reviewed different theories and arguments on the reason behind the river meandering. These arguments include Coriolis force, energy arguments (excess, minimization), bank erosion and sediment effect, helical and secondary flows, an inherent property of turbulent flow, the interaction between flow and mobile channel, bar theory and bend theory.

Based on the review of different theoretical analysis, Seminara (2006), elucidated that meandering is mainly related to fundamental instability mechanisms due to the interaction of the flow and erodible boundary. He summarized that ''any small random perturbation of channel alignment eventually grows, leading to a meandering pattern, as shown by bend instability theory.'' From the 'bend theory,' it can be summarized that a straight channel is intrinsically unstable, provided the banks are erodible.

Table 1.1 Different areas of focus on meandering channel study

S.N	Focus area	Bed Condition	Bank Condition	References
1	Local flow structure and hydrodynamics	Fixed (F) or Erodible (E)	Fixed (F)	Blanckaert, K 2011 Tape, W.,2001
2	Meander Development	E	E	Dulal and Shimizu, 2010 Braudrick et al.,2009
3	Bank erosion	E, F	E	Ebrahimi, M., 2015 Langendoen et al., 2016
4	Bed Morphology	E	F	Engelund, 1974 Xu and Bai, 2012 Struiksma et al., 1985
5	Sinuosity and Curvature	E	E,F	da Silva et al., 2006, Song et al., 2016 Hickin and Nanson, 1984
6	Flow/bed evolution with river training structures	E,F	F	Bhuiyan et al.,2010 Giri and Shimizu, 2004 Kashyap, 2012
7	Real field cases	E	F,E	Elhakeem et al., 2017 Xiao et al., 2016

From the river engineering point of view, studies on meandering channels range from the understanding of the fundamentals through laboratory works to the engineering applications for real field problem. Most rivers take some type of meandering form which consists of a series of alternating curved reaches with pools at the outer banks, and deposition along the inner banks (Knighton, 1988). Therefore the concern is to reduce the adverse impact of these erosion-deposition processes in meandering channels. **Table 1.1** outlines the different area of focus on meandering channel research in recent years. In the next subsection, we review different works in meandering channels focusing on the experiments and numerical simulations particularly from the aspects of flow, bed, bank interaction, sediment transport, etc. and application of bank erosion countermeasures.

1.2.1 Experimental studies

The experimental studies on meandering channels are challenging due to the fact that the continuous and rapid erosion of bank causes the river to take a braided channel form. Thus it is difficult to maintain the single thread planform (Hooke, 2013). In this regard, most of the engineering application related experimental studies concentrated on flow patterns and bed topography are performed under fixed banks. Some experiments use complex, high sinuosity channels or sharp-angle bends. Termini carried out experiments in a large amplitude meander bend to study the channel morphological features and the flow pattern. Similarly, da Silva and El-Tahawy (2008) studied on the location of the erosion-deposition pattern in an SG generated meandering channel having a deflection angle of 60^0. Most experiments are run with constant discharge and uniform sediment size. Experimental results are mainly used for validating theoretical or numerical simulation model results.

However, few studies have tried to consider erodible bed and erodible bank (Dulal and Shimizu, 2010; Song et al., 2016) for examining the meander channel evolution. Braudrick et al., 2009 studied the conditions necessary to sustain meandering channels. They concluded that the experimental meander migration was fast compared to most natural channels which caused nearly all of the bedload sediment to exchange laterally, such that bar growth was primarily dependent on bank sediment supplied from upstream lateral migration. Apart from the meandering channels, various studies considering single bend of different angle (like 90^0 bend, 135^0 bend, 180^0 bend) have been undertaken. Studies considering the river training structures were mostly performed under such bends. Lyn and Cunningham (2010) carried out experiments in a 90^0 channel bend to evaluate the performance of bendway weir against bank erosion. Similarly, Jamieson et al. (2013) investigated 3D flow and sediment dynamics with and without stream barbs in a 135^0 sharp channel bend. Most of these studies considered a meandering channel of single sinuosity or a single channel bend. The studies concerning the effect of channel sinuosity and other meander parameters on channel morphological changes are very few. Understanding the effect of channel geometry on the morphological response can be vital in the planning of river management works. Xu and Bai (2013) investigated experimentally the bed topography evolution in alluvial meandering channels with various sinuousness. They showed that bed topography evolution becomes more uncertain with increasing sinuosity. Similarly, the increase in sinuousness in channel bends leads to the increase in both the spatial and the temporal fluctuation of bedforms. Whiting & Dietrich (1993b) indicated that the location in flow plan of the erosion-deposition zones varies depending on the stream plan shape i.e. deflection angle and ratio of meander wavelength to the channel width. In their experimental study on meandering channels with different sinuosity, da Silva et al. (2006) concluded that each sinuosity has its own convective flow pattern i.e. its own distribution of convergence-divergence zones of flow which will

ultimately dictate the location of erosion and deposition. Their studies, however, were performed under the condition of fixed banks. Not only the inside channel morphology depends on the channel geometry but also the location and extent of bank erosion are likely to be influenced by the channel sinuosity and curvature. Song et al. (2016) investigated the influence of initial channel parameters on the short-term development of sine-generated meandering channels considering different sinuosity, inflow discharges and channel widths. Their analysis showed that the overall channel migration is mainly controlled by channel sinuosity and discharge. Similarly, studies suggest that the channel migration is influenced by the centerline curvature (ratio of the radius of curvature, R_c to the channel width, B) with higher migration for low R_c/B and vice versa (Hickin and Nanson, 1984). However, previous studies were mainly focused on channel migration and meander development phenomena. The spatial and temporal change in the location of critical bank erosion zones in different sinuosity channels were not analyzed. Also, none of the previous studies to date has analyzed the performance of different groynes arrangement under varying channel sinuosity. Identifying potential bank erosion locations would be helpful to appropriately plan and implement riverbank protection works.

1.2.2 Numerical studies

Numerical modeling is another important approach to study the dynamic interaction of flow, bed and banks in meandering channels. Some models are aimed at solving practical problems and providing a means of prediction and design while others aimed at elucidating the bases of river meandering by testing fundamental theory (Hooke, 2013). Models ranging from 1D to more complicated 2D and 3D have been developed incorporating different processes. The application of numerical models to study the river morphodynamics has increased in the recent years with the development of a number of computational models (Abad et al., 2008; Guan et al., 2015; Wu, 2004). But unlike the straight channels, the formation of complex flow features due to the presence of helical (secondary) flows, makes it challenging to accurately model morphodynamics in meandering channels (Blanckaert, 2015; De Vriend, 1977; Johannesson and Parker, 1989; Song et al., 2012). Some models consider only the bed evolution while others consider simultaneous bed and bank evolution. A depth-averaged 2D model could be used with some confidence for modeling channel hydraulics and morphology at a natural bend provided that secondary flow features are corrected and grain-size parameterization is undertaken (Guan et al., 2016). The objective of this study is not to analyze the meandering development but the channel morphological variations, we, therefore, considered 2D and 3D models of flow and sediment transport without the lateral bank migration. However, in our experiments, erosion of banks are considered to identify the critical locations of bank erosion. For computing the bank erosion, we used an uncoupled model. The purpose of the 2D simulation was to investigate at first the channel

bed evolution and identify critical locations of erosion-deposition. And next, to examine the channel response under a various arrangement of groynes for identifying the suitable position and orientation. Since the presence of groynes induces a complex 3D flow structure, we finally, formulated a 3D model to identify the role of 3D flow characteristics on the erosion-deposition pattern.

1.3 Problems associated with meandering channels

Erosion and migration of riverbank are one of the major problems in many rivers around the world. For example, river erosion is a serious problem in Bangladesh which poses a major challenge in river management (Nakagawa et al., 2013). The problem of bank erosion and planform evolution become more complicated in meandering rivers due to their unique morpho-dynamics resulting from the interactions of flow, sediment transport and channel curvature (Hooke, 2003;Seminara 2006).

Natural alluvial rivers self-organize into distinct morphologies that can be considered as a continuum of patterns from incoherent (braided) to highly organized (meandering) (Tal et al., 2010). Alluvial channels are formed on the sediments that they have transported and deposited, (Church, 2006). Accordingly, the channel is self-formed. Banks may be composed of either cohesive or non-cohesive materials which are usually fragile and can be easily erodible by fluvial force. This fragility of the banks attributes to the self-forming characteristics of alluvial channels. Alluvial channels may take various planform shape depending on the flood discharge, bank characteristics, amount of sediment, its size and type, etc. Of the common morphological channel pattern observed in the natural alluvial channels is the meandering, about which this study is focused on. Meandering channels are one of the most studied topics in fluvial geomorphology due to its unique morpho-dynamics. However, various channel processes governing meander planform are yet to be understood fully. One of the most challenging aspects of the meandering channel research is the unpredictability of bank erosion and channel migration. Based on the previous studies as well as natural observation in meandering channels, it is evident that the erosion occurs at the outer bank forming deep pools and the deposition occurs at the inner bank forming a point bar which can be visualized in **Figure 1.2**. These phenomena are responsible for channel migration. Erosion-deposition induced channel migration causes loss of hundreds of hectares of mainland floodplain, agriculture affecting the livelihood of the people. In this regard, various countermeasures are usually implemented to prevent riverbank from erosion and migration processes and hence preserve channel planform. In the analysis of river-related problems, along with the flow characteristics, channel morphological characteristics need to be equally considered. Whenever river training structures are introduced for preventing bank erosion, channel morphology is altered. Conversely, morphological change may affect the effectiveness
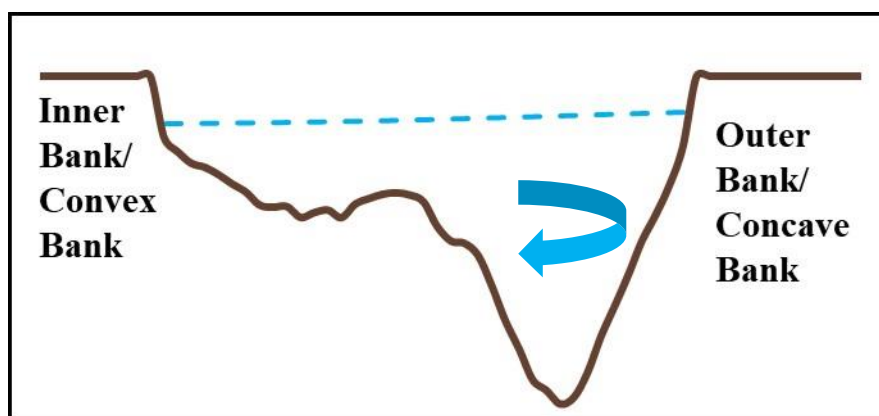
Figure 1.2 Typical cross-sectional profile in meandering channels

and functioning of the river training structures itself.

Riverbank erosion can eventually lead to channel migration, which can be difficult to predict accurately. For this reason, river erosion and migration can pose substantial risks to existing infrastructures such as houses, agricultural land, roads and bridges years after their construction (Lagasse et al., 2004)

Counter-measures like groynes are usually implemented to control the riverbank erosion process and hence prevent the shifting of river planform (Elhakeem et al., 2017). In this context, studies are therefore necessary to understand the dynamics of channel bed and planform evolution in the presence of river training structures like groynes. Most of the previous studies on groynes considered straight channels where the focus was on the flow and sediment dynamics only around groynes (Yossef and Vriend, 2010; Zhang and Nakagawa, 2009). Laboratory experiments in meandering channel with groynes have been conducted either in fixed bed and fixed bank (FBFB) or in erodible bed and fixed bank (EBFB) condition (Bhuiyan et al., 2010; Giri and Shimizu, 2004) Some experiments in FBFB considered single or series of spur dikes where local flow field around the structures was studied (Sharma and Mohapatra, 2012; Giri et al., 2003). While experimental study with a series of countermeasures in EBFB condition focused on the local scour, 3-D flow pattern and bed topography near the structures. However, in such cases, the simultaneous interaction of changing channel planform and bed morphology on the groynes field or vice versa couldn't be studied. Of the few experimental studies that considered both erodible bed and erodible bank (EBEB) channel, were conducted in a single channel bend where the effect of countermeasures like stream barbs or bendway weirs (submerged groynes) on flow field dynamics and sediment transport were analyzed (Jamieson et al., 2013; Lyn and Cunningham, 2016). However, the temporal variation in erosion/deposition mechanism including the overall channel evolution was not analyzed. In addition, the analysis was performed at the equilibrium stage and the phenomena leading to the equilibrium were not discussed. Also, the effect of the different

arrangement of groynes was not studied. Therefore in this study, we first tried to investigate the channel morphology and bank erosion phenomena through laboratory experiments with and without groynes and later numerical simulations were performed under several arrangements of groynes in order to determine the effectiveness of groynes.

1.4 Bank erosion and its mitigation measures

It is important to protect river banks from erosion, particularly in meandering channels, in order to maintain the stable dimensions, patterns and profile of a river (Bhuiyan et al., 2010). In general, two modes are attributed to the erosion of a riverbank (Langendoen, 2000); 1) Hydraulic or fluvial force that detaches and entrains surface particles from bank and bed, 2) geotechnical instabilities of soil mass leading to the mass failure. However, in most of the cases, the combination of both of these modes are prevalent. Hydraulic or fluvial force leads to the erosion of riverbank whenever the local boundary shear stress exerted by the flow near the bank exceeds the critical value (Langendoen, 2000). Similarly, the geotechnical stability of the soil mass with respect to mass failure depends on the balance between the driving forces of gravity that tends to drive the soil mass downward and the resisting force of friction and cohesion that tend to resist the downward movement. In meandering channels, due to secondary flow effect and other complicated flow structure, scouring near the outer (concave bank) is naturally high. This erosion of the toe or near-bank bed triggers the failure of the banks. Therefore special attention is needed for mitigating bank erosion and channel migration processes in meandering channels.

Based on previous studies as well as observation in natural channels, erosion occurs at the outer bank forming deep pools and deposition occurs at the inner bank forming a point bar (Hickin and Nanson, 1984; Struiksma et al., 1985). This morphological phenomena in meandering channels create adverse impact by eroding banks and damaging people's houses, lands, agriculture and other public structures. Such problem has inspired the search for different bank protection countermeasures to improve outer bank stability and minimize erosion (Cunningham and Lyn, 2016). Although bank protection countermeasures such as submerged vanes, bendway weirs, stream barbs, bank-attached vanes, bandal like structures, etc. have been tested (Jamieson et al., 2013; Bhuiyan et al., 2010; Teraguchi et al., 2011; Cunningham and Lyn, 2016), groynes are still one of the most widely implemented countermeasures for bank protection especially in natural bends or meandering channels (Teraguchi, 2011). Groynes are linear structures projecting perpendicular or at a certain inclination from the bank towards the river as depicted in **Figure 1.3**. Groynes help to protect the riverbank from erosion by deflecting high-velocity flow away from the banks to the channel center (Uijttewaal, 2005; Dehghani et al., 2013). Groynes perform three main functions, they deflect flow and secondary currents away from the river bank, they disrupt

high velocity gradients in the near bank region, and they shift the thalweg closer to the channel centerline (Kashyap, 2012; Matsuura and Townsend, 2004). In this way they tend to provide a longer-term solution to mitigate bank erosion (Mosselman et al., 2000). However, studies suggest that the performance of groynes in real field cases have been variable (Jia et al., 2009). Also, there lacks a comprehensive research and guidelines on the appropriate arrangement of groynes in meandering channels (Lagasse et al., 2009). Different cases have been observed where the
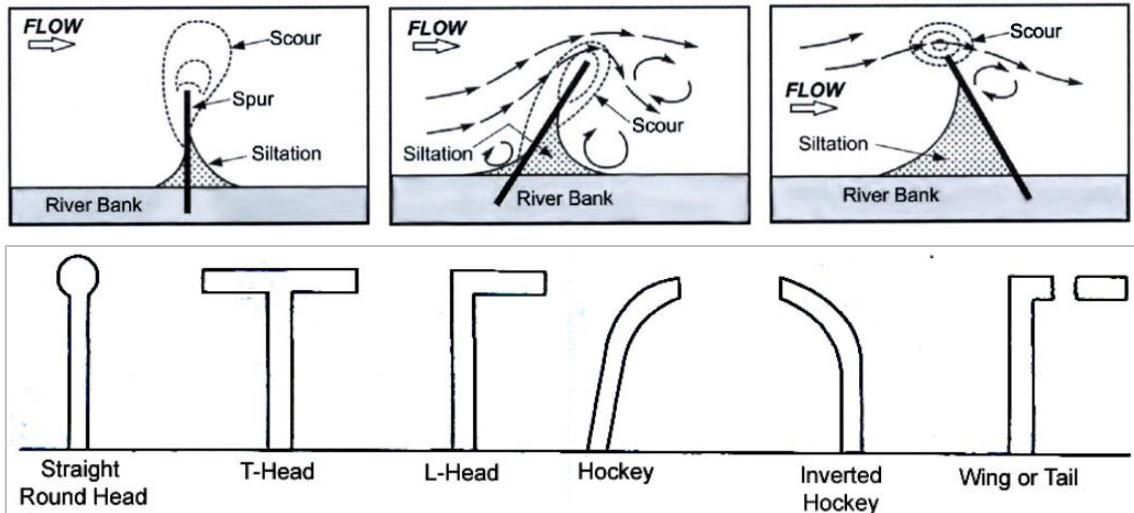

Figure 1.3 Groynes with different orientation to the flow (top) and shape head (bottom) (Adapted from (Barkdoll et al., 2007; Kashyap, 2012; Przedwojski, 1995))
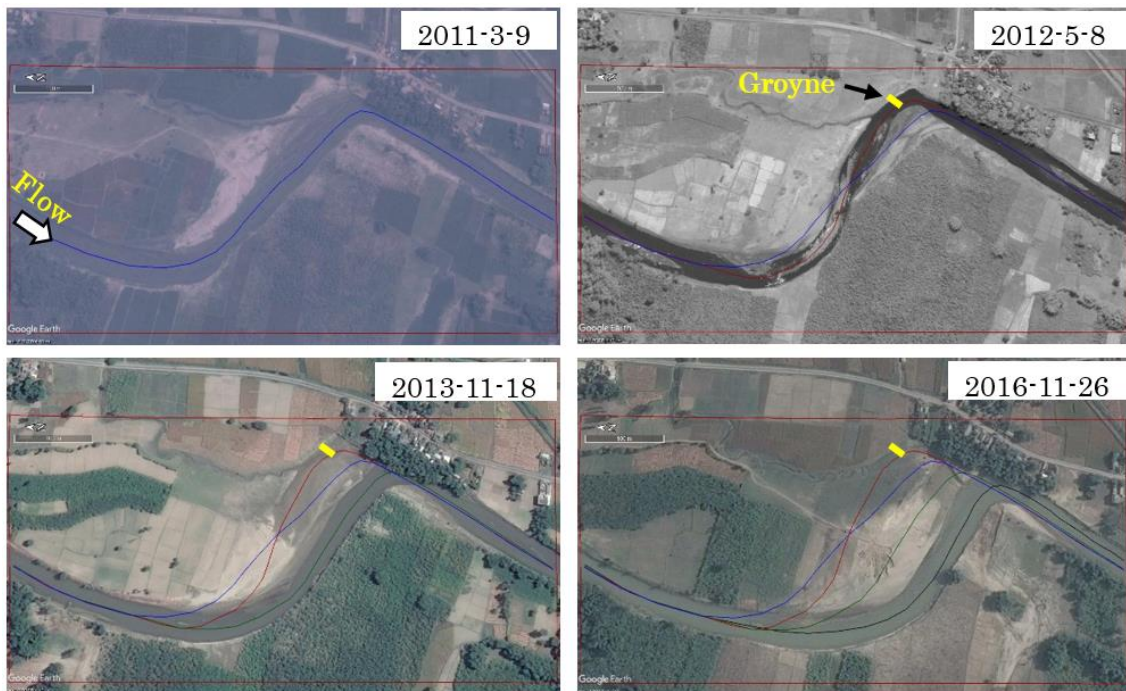

Photo 1.1 Time series (google earth) images showing the impact of groyne on channel evolution.

9

implemented groynes have led to the adverse impact on the channel processes (Karki et al., 2018).

Photo 1.1 shows time series images of the impact of rectangular impermeable groyne on the erosion-deposition process in the bend of an alluvial river. Due to the deposition induced by the groyne field, a significant portion of land has been reclaimed on the adjacent bank. However, nearly the same amount of land has been lost to erosion on the opposite bank.
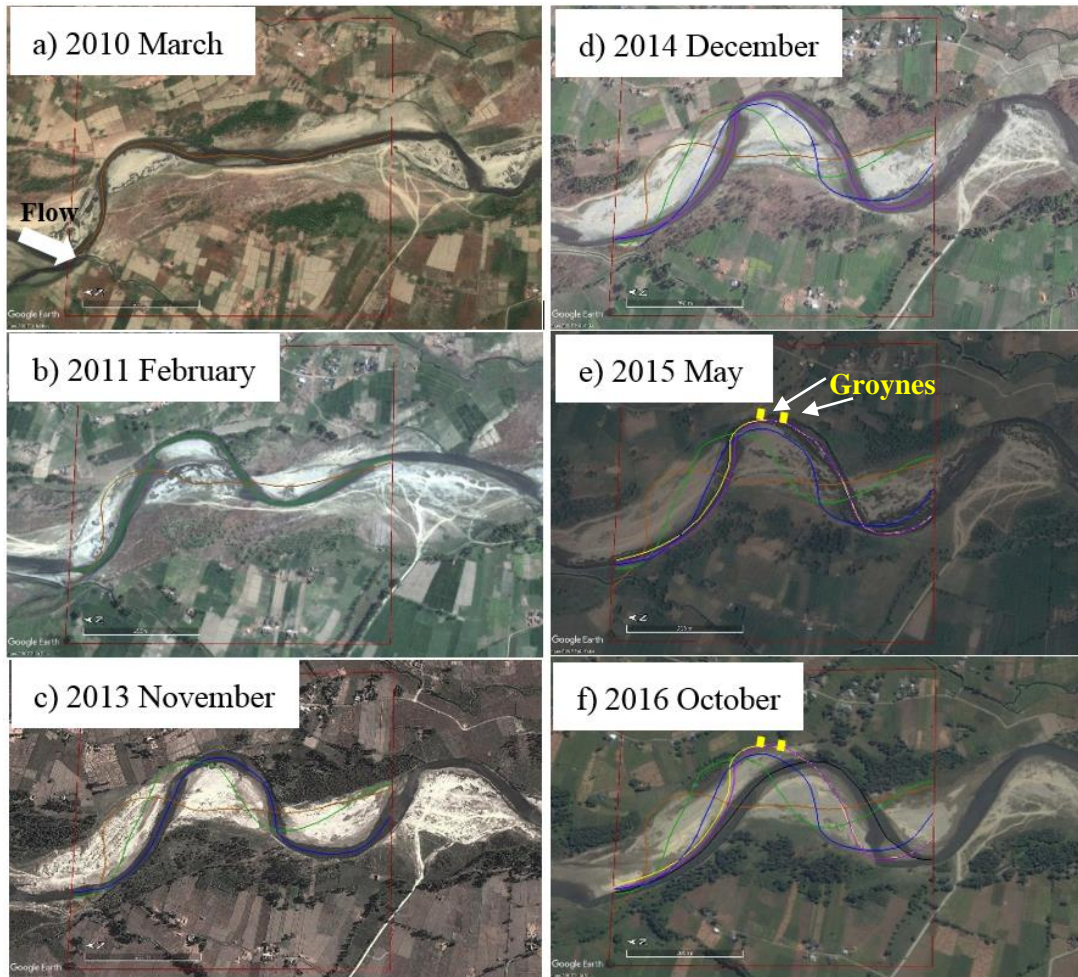

Photo 1.2 Time series (google earth) images showing the impact of groynes on the evolution of alluvial meandering channels.

Photo 1.2 illustrates the evolution of an alluvial meandering channel before and after the implementation of two rectangular impermeable groynes on the outer bank. Before the implementation of groynes in **Photo 1.2 (a-e)**, due to the erosion of the outer bank near the apex and further downstream, the channel centerline continuously shifted downstream. The implementation of groynes protected bank erosion by inducing deposition and shifting the flow away from the bank. However, the erosion now shifted to the downstream portion as well as the opposite bank **(Photo 1.2 f and 1.3)**. It can be clearly seen from the shift in the channel centerline that the channel has the overall tendency to migrate downstream. Another important aspect to be

analyzed is the formation and movement of point bars in the meandering channel as they have a significant effect on the overall channel development. Bar formation and growth signifies that the channel migration is active in the channel. In this regard, there is a need to identify the appropriate arrangement of groynes for the mitigation of bank erosion and which induce a minimum effect on the opposite banks.

Photo 1.3 Bank erosion and implementation of groynes in the channel shown in photo 1.2

1.5 Research gaps and objectives of present study

Meandering channels of different geometric characteristics, grain size distributions, flow regimes, etc., exist in nature and in any given channel the conditions may vary from one meander loop to another (da Silva et al., 2006). Despite the awareness of the effect of channel sinuosity and curvature on the flow pattern and morphology, most of the researches have focused on meandering channels of single sinuosity (Giri and Shimizu, 2004; Bhuiyan et al., 2010). In contrast, few previous studies on meandering channels have considered the role of sinuosity and curvature on the flow pattern and channel morphology (da Silva et al., 2006; Xu and Bai, 2013). Studies on the variation of sinuosity in sine-generated (SG) meandering channels showed that the flow in meandering channels consists of convergence-divergence zones occurring due to the deflection of streamlines and the converging flow near one bank causes divergence near the

opposite bank. Accordingly, each SG channel has its own distinct flow and morphological pattern. Consequently, the variation of the sinuosity and channel curvature significantly influence the sediment transport and bed topography. Similarly, studies suggest that the channel migration is influenced by its centerline curvature (ratio of the radius of curvature, R_c to the channel width, B) with higher migration for low R_c/B ratio channels and vice-versa (Hickin and Nanson, 1977). Thus, it may not be realistic to generalize the meandering channel morphological evolution under single channel sinuosity as it can be influenced by dominant channel characteristics. While the role of meandering channel geometry on the flow pattern and channel morphology have been addressed, the effect of groynes on channel evolution pattern under different sinuosity have not been examined yet. In this context, the counter-measures implemented for the mitigation of bank erosion in meandering channels may also perform differently under varying channel characteristics. For example, a study has shown that the increase in bend radius leads to a decrease in maximum scour depth in curved channels with cross-vane structures (Kurdistani and Pagliara, 2017). Several research works in the past have studied the application of different bank protection measures in meandering channels. However, studies considering the effect of channel sinuosity and curvature on the performance of bank protection counter-measures like groynes have not been tested. Moreover, most of the laboratory studies in the meandering channel with counter-measures were performed either under the fixed bed and fixed bank (FBFB) or erodible bed and fixed bank (EBFB) channel condition. In such channels, the interaction of flow with the bank erosion and subsequent planform changes couldn't be studied.

Realizing the above-mentioned gaps in the previous works, the current study first attempts to investigate how the channel sinuosity and curvature influence the channel and bank morphology as well groynes performance through experimental analysis under the erodible bed and erodible bank (EBEB) channel condition. Secondly, the effectiveness of several arrangements of groynes (orientation and position) in shifting the erosion zone and high-velocity zone away from the banks are investigated through 2D numerical simulation considering movable bed and fixed bank. 2D numerical models are computationally efficient in investigating different scenarios of groynes application. Applications of the 2D numerical models have shown that they can reproduce the meandering channel morphological phenomena with reasonable accuracy(Nagata et al., 2000). We then apply the validated model to a real field alluvial meandering channels. The real field application of the numerical model is a challenging task due to the heterogeneity of various variables as well as data availability. Finally, to better understand the complex flow structure in meandering channels with and without groynes, 3D simulations are carried out. Therefore, this is the first study of its kind where the effect of sinuosity on groynes performance are examined. Similarly, studies considering the simultaneous bed and bank evolution in the presence of countermeasures are very few which this study has incorporated. Finally, no previous studies have

analyzed the response of meandering channels (with different sinuosity) to the different arrangement of groynes.

Protecting the river bank against erosion is an important aspect of river management and restoration process in meandering channels. In this context, groynes (both impermeable and permeable) have been widely implemented around the world to deter the erosion along the outer bank of meandering channels or sharp bends. However, the performance of groynes in the field has been variable which have necessitated a further understanding of the flow and morphological process to better optimize their performance. For the effective functioning of the implemented bank protection measures, it is first necessary to understand the channel response to these structures. Under this scenario, this study was undertaken with the following objectives:

- To review the previous works in meandering channels with a focus on the channel morphology including the application of bank protection works.
- To analyze experimentally the channel bed morphology including bank erosion phenomena in meandering channels.
- To investigate the effect of channel geometric characteristics like sinuosity, deflection angle and R_c/B ratio on the overall evolution of meandering channels through experimental study.
- To formulate a numerical model for analyzing the effectiveness of different scenarios of groynes arrangement in meandering channels under different sinuosity.
- To study challenges involved in the real field application of numerical models for identifying suitable design parameters of bank protection works.
- To understand the flow and morphological dynamics in meandering channels with groynes through 3-dimensional simulation.

1.6 Outlines of the dissertation

This dissertation is grouped into 6 chapters whose contents are outlined as follows:

Chapter 1 includes the general background of the study, review of the previous studies in meandering channels and objectives of the study,

Chapter 2 describes the laboratory experimental works, objectives, procedures, measurements and analysis of the results,

Chapter 3 presents the formulation of a 2D numerical model, its validation and simulation results of the different case scenarios.

Chapter 4 incorporates the application of the 2D model formulated in chapter 3 to the real field cases of meandering Gowain River, Bangladesh and Uji River, Japan.

Chapter 5 consists of the 3-dimensional simulation of flow and morphology in meandering channels with and without groynes.

Chapter 6 concludes this dissertation with major findings and their implications and also possible recommendations for future studies.

Chapter 2

Experiments on the evolution of meandering channels

2.1 Introduction

Alluvial meandering channels continuously evolve due to erosion-deposition phenomena leading to the lateral expansion and downstream migration by eroding banks. This tendency of channel evolution might not be the same for all meandering channels. In order to understand the channel evolution mechanism including the erosion of banks, experimental works were performed. The objective was to investigate the effect of meandering geometry on the channel evolution pattern and also evaluate the channel response to the bank protection structures. In this chapter, the results of the laboratory experiments carried out on two different sine-generated meandering channels having different sinuosity, curvature and the deflection angle are discussed. Analysis of the channel bed morphology, bank erosion rate, sediment transport and velocity are presented.

2.2 Experimental Setup

The experimental works presented herein were carried out in the Ujigawa Open Laboratory under Disaster Prevention Research Institute (DPRI), Kyoto University. The schematic diagram of the experimental set-up is shown in **Figure 2.1.** The experiments were conducted in two SG meandering channels of different sinuosity whose centerline is defined by **Eq. [2.1]**. The upstream and downstream ends of the channel were connected to a 50 cm and 100 cm long straight channels, respectively, having rigid bed and banks. As shown in **Photo 2.1 (a & b)**, the meandering channels were excavated within a 400 cm long and 200 cm wide domain filled with non-uniform [d_{mean}=0.72mm and $\sigma=(d_{84}/d_{16})^{0.5}$ =1.38], non-cohesive sediments of density 1410 kg/m^3. The

initial channel cross-section was rectangular with vertical banks of height 6cm from the bed. Experiments were performed under a clear water condition and a steady uniform discharge for a duration of one hour. The use of light sediment material with low specific gravity enabled the deposition/erosion phenomena to be observed even with low flow velocities. In this study, we considered two sine-generated meandering channels of different sinuosity. **Photo 2.1** shows the two experiment-ready channels excavated using a pre-fabricated template of the channels within the erodible domain.

To prepare an erodible meandering channel, first, the channel bed was compacted and levelled, then bank materials were filled and compacted around a prefabricated wooden channel. Two separate prefabricated wooden channels following SGC were constructed to prepare experimental meandering channels of two different sinuosities. The same type of sediment was used in the bed as well as in the bank. After the bank materials were compacted and levelled, the prefabricated channel was carefully removed to obtain the designed rectangular experimental channel having an initial width of 20 cm and a depth of 6 cm. For both the channels, same procedure was adopted.
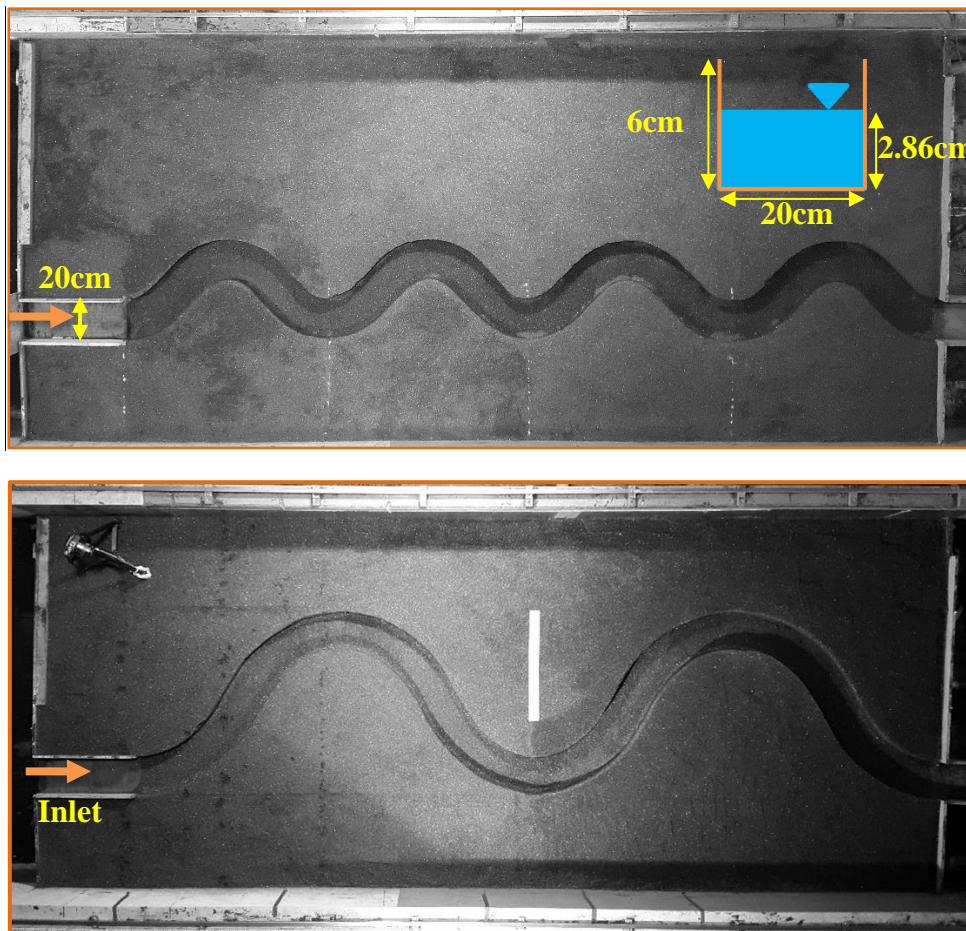

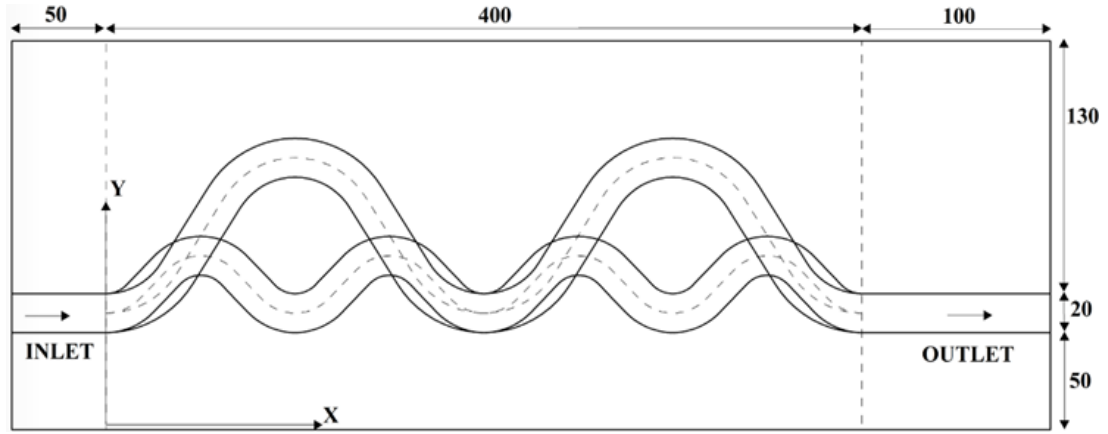**Photo 2.1** Channel set-up for the experiments; Ch-45 (top) and Ch-60 (bottom)

Figure 2.1 Layout plan of the experimental channels [Dimensions in cm]

2.2.1 Channel parameters

The sine-generated curve (SGC) defined by **Eq. [2.1]** was used to delineate the meandering channels within the erodible boundary. **Figure 2.2** illustrates the definition sketch with different parameters of a meandering channel. The main parameters determining SGC are channel-wise wavelength (*L*) and maximum deflection angle (ω) (Langbein and Leopold, 1966).

$$\emptyset = \omega . \cos(2\pi \frac{l_c}{L})$$

[2.1]

Where

$\emptyset$ = local deflection angle

ω = maximum deflection angle

l_c = length along the channel centerline

L = wavelength of one meander

As mentioned earlier, in this experiment, two SG channels were prepared whose different parameter values are listed in **Table 2.1**. Each meandering channels have their own value of those parameters. The two channels are denoted as Ch-45 and Ch-60 and will be used throughout this thesis. Ch-45 refer to the lower sinuosity channel with a maximum deflection angle of 45^0 whereas Ch-60 indicate the higher sinuosity channel having a maximum deflection angle of 60^0. The ratio of the radius of curvature (R_c) to the channel width (*B*) for Ch-45 and Ch-60 was 1.25 and 2.25 respectively. This ratio indicates the sharpness of the bend curvature with higher ratio signifying low sharpness and vice versa. The choice of these parameters was mainly decided by the size of the available experimental facility as well as the working condition. Also, maneuvering the channel template during the preparation process would have been extremely difficult for the bigger size channels.
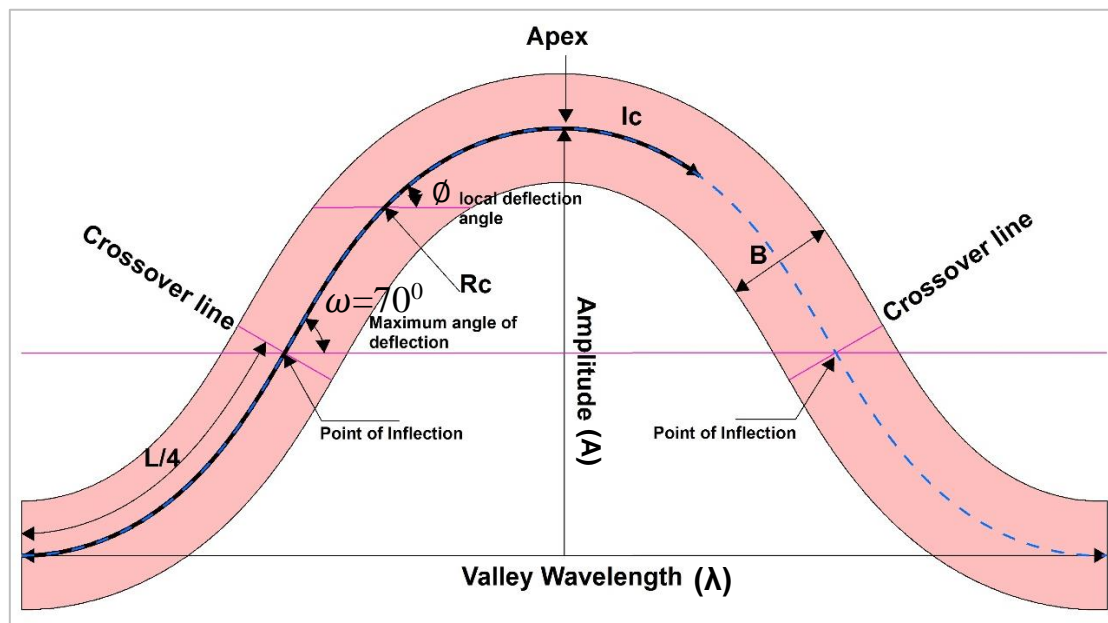
17

Figure 2.2 Definition Sketch of a sine-generated meandering channel

Table 2.1 Parameters of the channels designed for the experiments

Parameter (cm)	Ch-45	Ch-60
Channel width (B)	20	20
Radius of curvature (R_c)	25	45
R/B ratio	1.25	2.25
Amplitude (A)	30	80
Channel-wise wavelength (L)	120	270
Valley wavelength (λ)	100	200
Sinuosity ($K=L/\lambda$)	1.2	1.35
Maximum deflection angle(ω)	45^0	60^0

2.2.2 Hydraulic conditions for the experiment

Determining the appropriate hydraulic condition is an important step in any fluvial experimental studies. However, the hydraulic condition is governed by several factors. In this study, the flow rate for experiments was partially governed by the size of the channel as well as non-cohesive sediments used for making the erodible channel. Preparing a larger channel would have been extremely difficult requiring a large volume of sediments and very long channel preparation time. Also, due to the non-cohesive sediments, the selection of a higher discharge would have resulted in high and rapid erosion of channel forcing us to shorten the experimental time. A discharge was chosen that transports sediment but does not overtop the banks of the designed channel.

The critical shear velocity was calculated using Iwagaki Formula (Iwagaki, 1956). The details of the hydraulic conditions are shown in **Table 2.2**.

The calculation of Iwagaki's $R*$ is given by Eq. 2.2,

$$R^* = \frac{\sqrt{\left(\frac{\rho_s}{\rho_w} - 1\right) * g * (d_m)^3}}{\vartheta}$$

[2.2]

where,

ρ_s and ρ_w= Density of sediment and water respectively (kg/m^3)

g=acceleration due to gravity (m/s^2)

ϑ=Kinematic viscosity of water (m^2/s)

Table 2.2 Details of the hydraulic conditions

Discharge (l/s)	Mean flow depth (cm)	Mean velocity, V_{av} (cm/s)	Channel slope, S_o	Shear Velocity (cm/s)	Mean bed shear stress , τ_0(N/m^2)	Froude number	Reynolds number
0.95	2.86	16.6	1:550	1.99	0.397	0.31	5322

2.2.3 Sediment properties

Sediment is mainly characterized by its size and density. The use of the sediment is dependent on the purpose and the phenomena intended to study. Since our objective was to study the channel evolution processes only considering the bed-load transport, we used non-uniform, non-cohesive sediment with relatively lower density (1410kg/m^3). Teraguchi (2011) used the same sediment to carry out the experimental works on the bed evolution with different types of groynes. The use of lighter particles allowed the erosion-deposition phenomena to be observed more clearly. Banks and the bed were composed of the same sediment. Seive analysis were carried out on the sample sediment. The mean diameter (d_{mean}) of the sediment is 0.72mm. The particle size distribution curve is shown in **Figure 2.3**. The ratio $\sigma = (d_{84}/d_{16})^{0.5}$ which indicate the non-uniformity of the sediment was found to be 1.38.
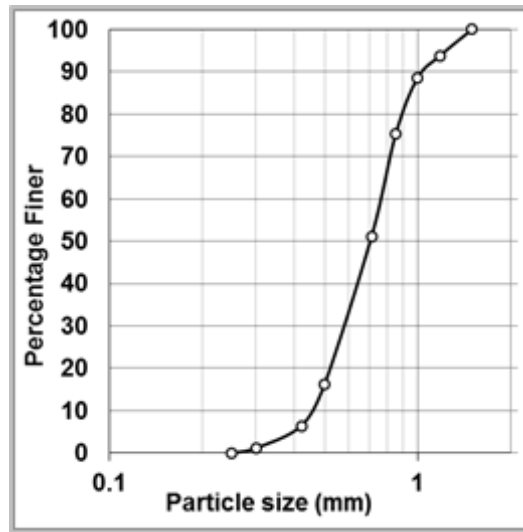
Figure 2.3 Sediment size distribution

2.3 Measurement techniques

Different parameters were measured during the experiment, namely: 2D surface velocities, channel bed topography at a different time interval, water level variation, and water discharge (see **Table 2.3**).

Table 2.3 Equipment used to measure different variables in experiment

Measurement Variables	Measurement Device
Bed Topography	Laser Displacement Sensor
2D Surface Velocity	Particle Image Velocimetry (PIV) technique
Water Level	Ultrasonic Sensor
Water Discharge	V-notch weir and Bucket and time method

2.3.1 HD video camera and Particle Image Velocimetry (PIV) technique

PIV technique is a widely adopted efficient and powerful technique for measuring instantaneous surface velocity indirectly by measuring the velocity of the tracer particles within the flow. For field measurement with large-scale flows, an extension of PIV, the LSPIV (Large-scale particle image velocimetry) is usually used. In hydraulic engineering, this technique has so far mainly been applied for surface velocity measurements of water (Fujita et al., 1998). An HD video camera mounted on the top of the experimental channel was used to record the video. The flow was seeded by white PVC (polyvinyl chloride) particles of mean diameter equal to 50 µm. The recorded video (30 fps) was converted to individual frames and were systematically processed using MATLAB PIVLab software. The details on PIV analysis based on this method can be found in (Thielicke and Stamhuis, 2014).

2.3.2 Laser displacement sensor

The laser displacement sensor (Keyence – LK 2500: Body and Keyence – LK 500: sensor) was used to measure the final bed deformation after each experiment for all different cases. This equipment consists of a controller and a sensor head (**Photo 2.2**), that measures the distance of one point of a bed surface to the laser displacement through a sensor installed to capture the time interval for this laser beam go and return to the source place.
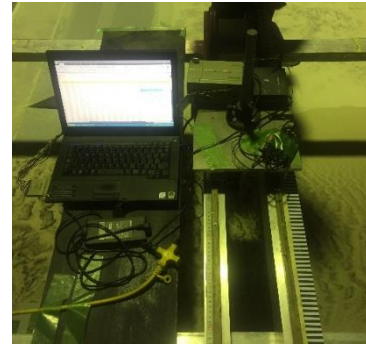
Laser displacement sensor   Sample measurement
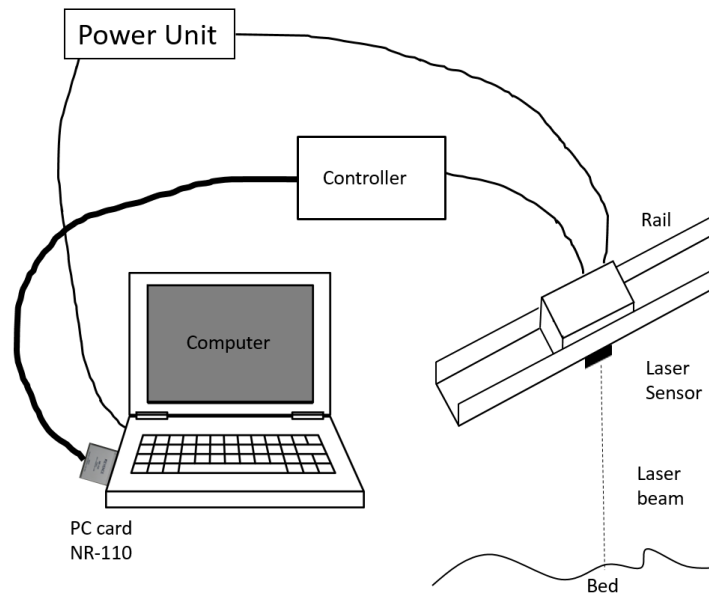
Photo 2.2 Measurement of bed level

The output data of bed level measurements are analogical voltage values which were saved in laptop using a data collection system. Before the bed level measurement, a calibration of equipment, using 4 cylindrical steel plates with pre-defined thickness as reference levels, were used to determine the relation between the voltage registered by the equipment and the measured bed level. One example of this calibration curve can be seen in **Figure 2.4**. For each experimental cases, these calibration results are different. The bed level measurements were done after the bed was completely dried out due to the presence of water could cause measurements errors.
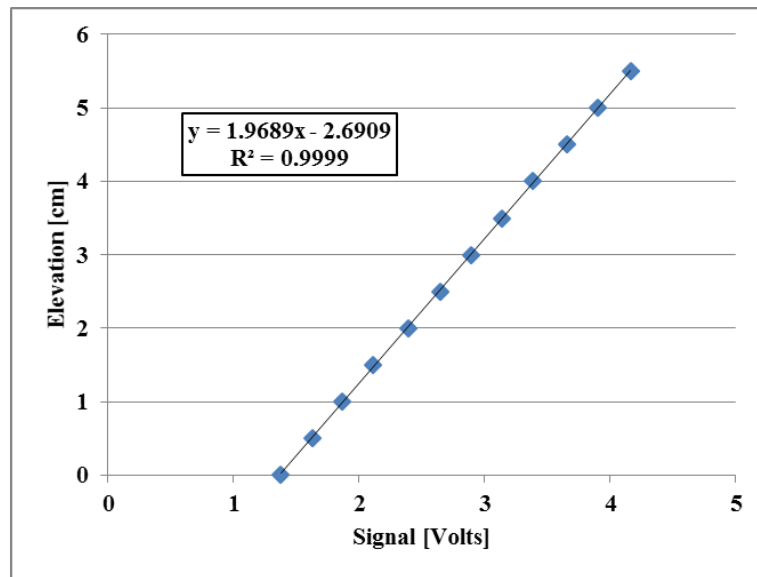
Figure 2.4 Typical calibration curve of the laser displacement sensor

The laser displacement sensor was mounted on an instrument carriage that moves the device on the rails over the channel.

2.3.3 Ultra sonic water level sensor

The ultrasonic water level sensor (Keyence FW-H07) was used to measure the water level with a contactless method. This equipment consists of a transducer in stainless steel (**Photo 2.3**), that measures the distance of one point of a water level using ultrasonic wave. This method is similar to the laser. The measurement is unaffected by optical factors like colour and transparency.
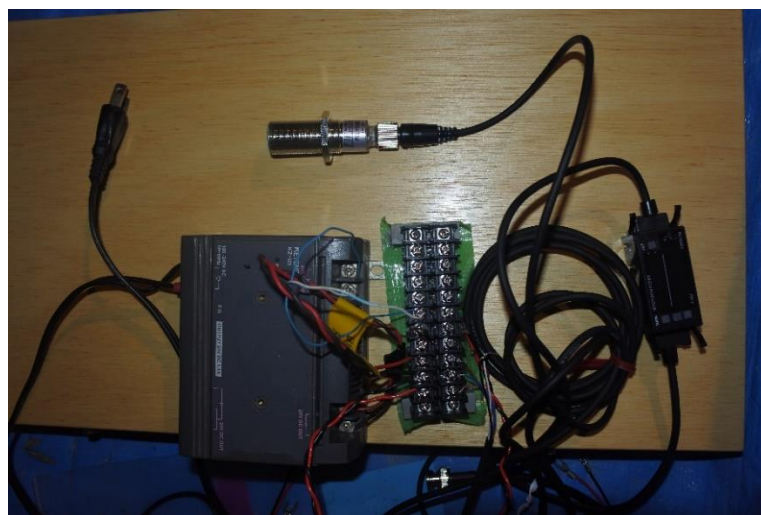
Photo 2.3 Ultrasonic water level sensor

The output data of water level measurements are analogical voltage values which were saved in laptop using a data collection system similar to above mentioned for the measurement of bed level. Before the water level measurement, a calibration of equipment, using 4 cylindrical steel

plates with pre-defined thickness as reference levels, were used to determine the relation between the voltage registered by the equipment and the measured height. One example of this calibration curve can be seen in **Figure 2.5**. For each experimental cases, these calibration results are different. The water level measurements were taken at specific cross-sections along the target area of the study. For each cross-section, water-levels were taken at the right bank, center and the left bank.
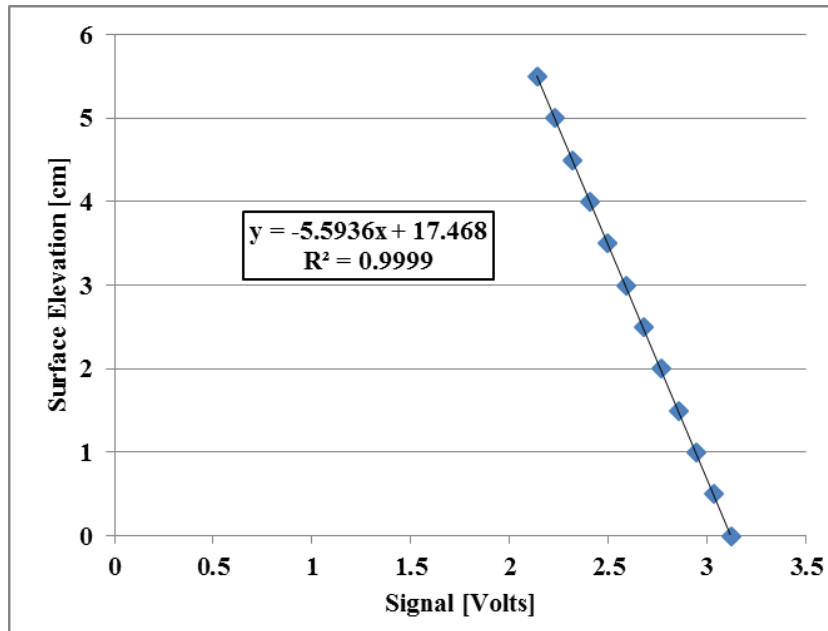

$$y = -5.5936x + 17.468$$
$$R^2 = 0.9999$$

Figure 2.5 Typical calibration curve of ultrasonic water level sensor

2.3.4 Water discharge measurement

The inflow discharge through the water pump was monitored by a V-notch weir during the experiments. The water was collected in an upstream pond which flowed into the channel inlet. The outflow discharge was measured by bucket and time method. The flow rate is obtained simply by dividing the volume of the container by the time to fill up.

Photo 2.4 V-notch weir for water discharge control

2.4 Experimental methods and procedures

As mentioned at the beginning of this chapter, all the experiments in this study were conducted in two different meandering channels under the condition of erodible bed and erodible banks. Series of preliminary experiments were conducted before the main experiments in order to identify the problem and issues related. Consequently, the main experiments could be run without any problems and results were not affected by any situation during the experiments.

Experiments were conducted without any implementation of groynes as well as the implementation of groynes. First, the experiments were conducted without implementing any countermeasures. After taking information from this case, groynes were placed at appropriate locations for the next cases. Two types of groynes were examined, one the rectangular and the other triangular. A total of six cases are discussed in this thesis, two each without groynes, with rectangular groynes and two with triangular groynes as listed in **Table 2.4**. Experiments were conducted under clear water (no sediment supply upstream) condition for a duration of 1 hour in the case without groynes and with rectangular groynes while in case of triangular groynes, it was conducted for 40 minutes. In both cases, a constant discharge of 0.95 l/s was supplied by a pump to the upstream storage pond through which water gradually entered the channel inlet. The target area for detailed analysis is illustrated in **Figure 2.1.** The definition of outer-bank and inner-bank are split at the initial point of inflection with a maximum deflection angle. The concave bank is outer-bank while the convex bank is an inner bank as shown in **Figure 2.2**.

Table 2.4 List of experiments discussed in this thesis

Cases	Symbol		Duration
	Ch-45	**Ch-60**	
No groynes	Ch-45-NG	Ch-60-NG	60 minutes
Rectangular Groynes	Ch-45-R	Ch-60-R	60 minutes
Triangular Groynes	Ch-45-T	Ch-60-T	40 minutes

2.5 Results and discussions

To understand the channel morphological changes as well as the location of potential erosion and deposition, experiments were conducted under the erodible bed and erodible banks. During the experiments, channel bed topography was measured at every 20min interval using the laser displacement sensor when the bed became dry after stoppage of inflow discharge. In order to characterize the spatiotemporal mechanism of channel evolution phenomena under different sinuosity and deflection angle, analysis of the channel morphological changes were performed based on the measured bed topography. Similarly, analysis of the rate of bank erosion

phenomenon was done. For understanding the effect of sinuosity and deflection angle on the flow and channel morphology, both types of channels are grouped under one heading. The details analysis of results and the discussions for each case of experiments are presented next.

2.5.1 Without groynes

1) Channel Evolution

The continuous interaction of flow and channel bed is made further complex due to the lateral expansion of the channel by the erosion of banks. **Figure 2.6** and **2.7** depict the channel evolution, dz in cm for the first 20 minutes (min) and at the end of one hour of experiment,
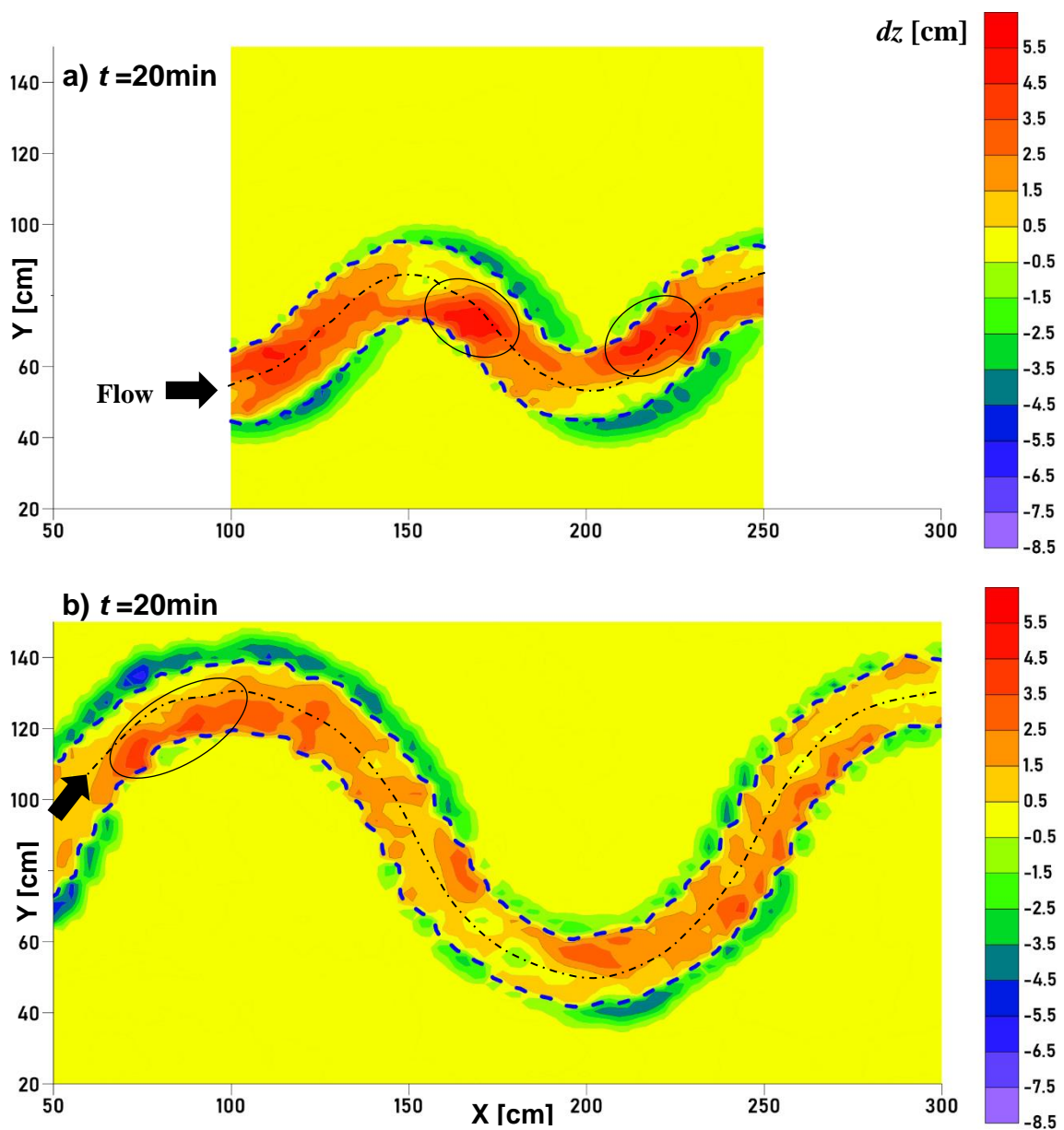
Figure 2.6 Channel evolution, dz [cm] for the first 20min a) Ch-45-NG and b) Ch-60-NG

respectively for ch-45-NG and ch-60-NG. Positive and negative values respectively signify channel erosion and deposition. The thick blue dashed line represents the initial channel bankline whereas the thin dashed black line indicates the initial channel centerline. The flow direction is from the left to the right.

It can be seen from **Figure 2.6 (a & b)** that the initial bed development process is more rapid and symmetric in Ch-45-NG where the formation of point bar along the inner or convex bank and deep pools along the concave or outer bank occurred. In Ch-60-NG, these features of bed morphology were less distinct in the early stage as seen in **Figure 2.6 (b).** The size and location of the point bar growth were also different in two channels. In Ch-45-NG, point bar formed just below the apex of the convex bend while it formed beginning from slightly upstream of the apex in Ch-60-NG, see **Figure 2.7 (a & b)**. This phenomenon is basically governed by the channel deflection angle which has an effect on the flow pattern causing the location of the erosion-deposition zone to vary. With increasing channel sinuosity and deflection angle, the channel morphology tend to become more complex as shown by the comparison between Ch-45-NG and Ch-60-NG. The non-uniformity of the channel bed after the development of bar and pool tend to further accelerate the bank erosion as can be seen from **Figure 2.7 (a & b)**. In fact, there is a two-way interaction among the bar development and bank erosion phenomena. Since no sediments were supplied externally to the channel, all the sediment must be derived from the bed and bank erosion. Sediment from erosion deposits to form point bar which in turn further pushes the flow towards the bank and increase erosion. The channel erosion-deposition and bank erosion pattern suggest that the low sinuosity and low deflection angle channel tend to migrate downstream whereas higher sinuosity and higher deflection angle tend to expand laterally.
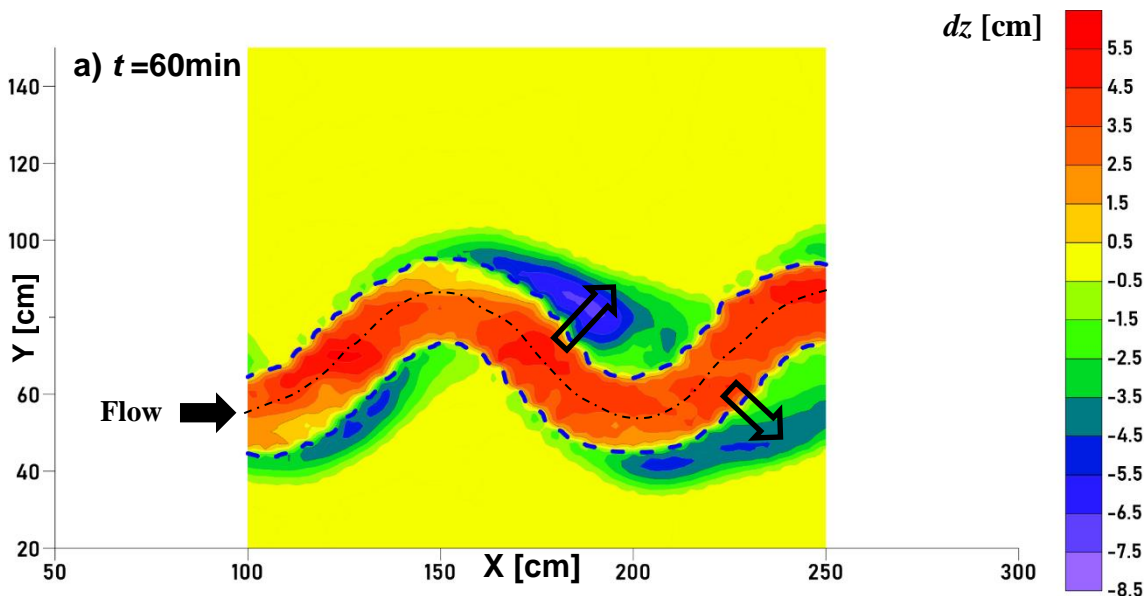

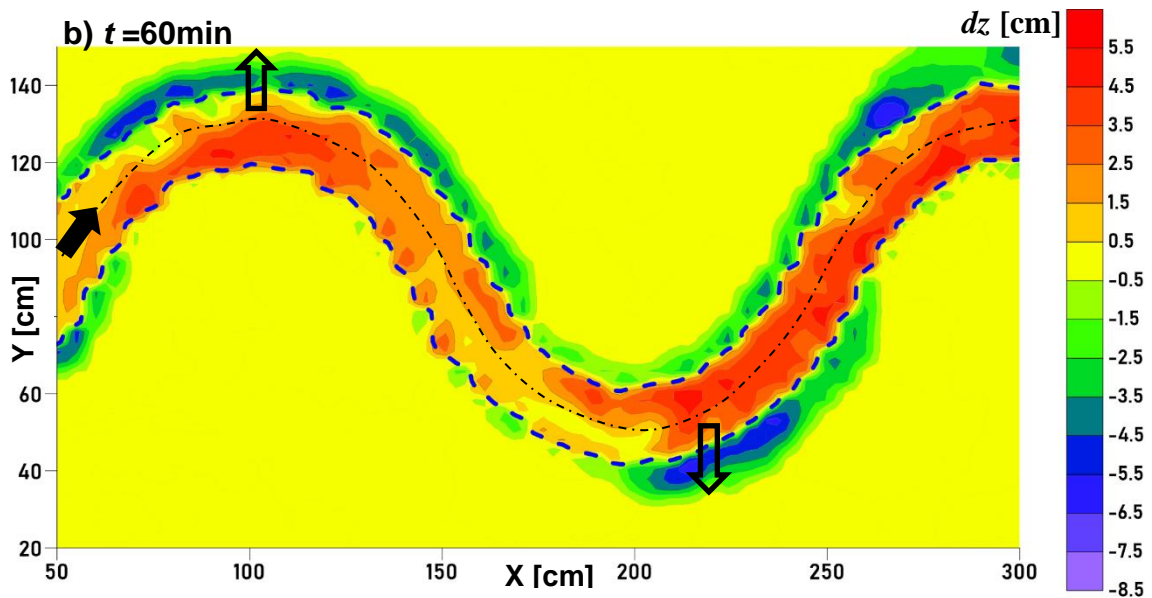**Figure 2.7 a** Channel evolution, dz at the end (*t*=60min) of the experiment for Ch-45-NG

Figure 2.7 b Channel evolution, dz at the end (t=60min) of the experiment for Ch-60-NG
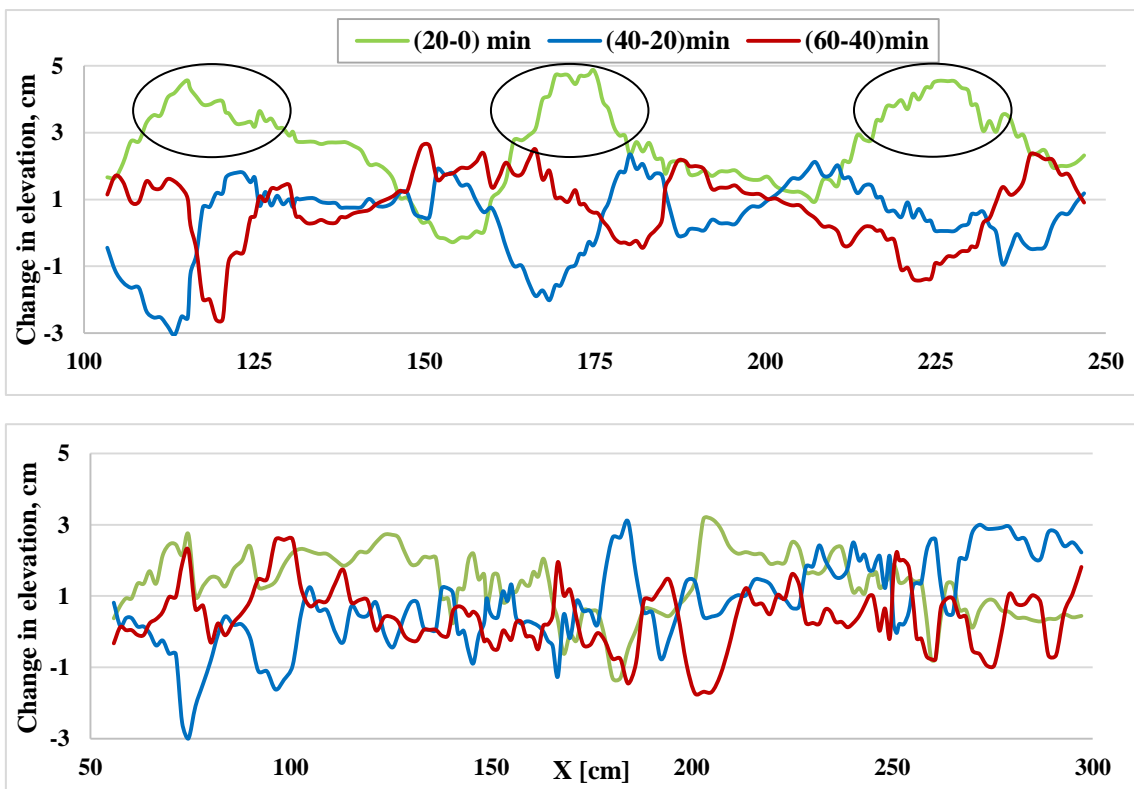

Figure 2.8 Temporal change in elevation along the original centerline (top) Ch-45-NG and (bottom) Ch-60-NG

Figure 2.8 represents the temporal change in the elevation along the original centerline for both Ch-45- NG (top) and Ch-60-NG (bottom) where the values above zero represent the aggradation and below zero represents the degradation. **Figure 2.9** illustrates the sediment volume eroded or
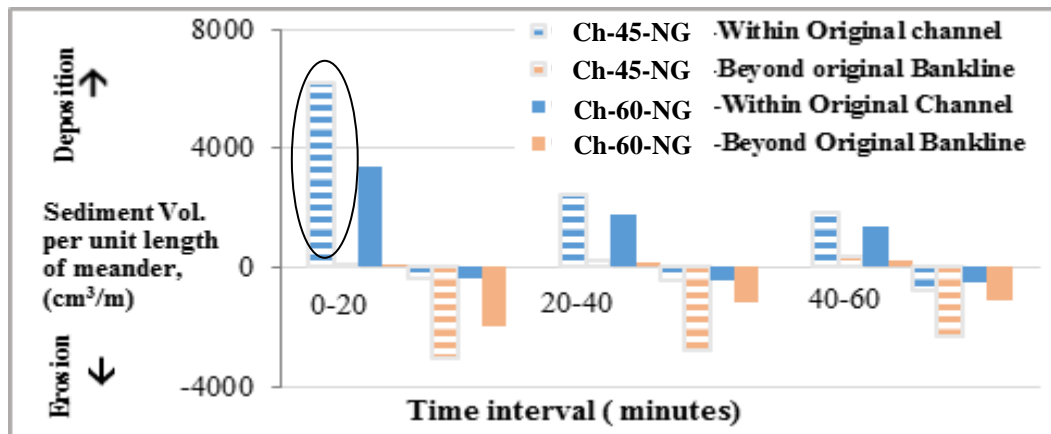
Figure 2.9 Comparison of temporal change in erosion/deposition volume for no groynes

deposited within the target area. The changes in elevation at all the three intervals in Ch-45-NG in **Figure 2.8** (top) suggest that the channel has consistently aggraded throughout the period. It can be seen that the erosion and deposition locations are distinctly visible in the case of ch-45-NG. In the initial phase of bed development, the overall channel transport capacity is higher, as a result, higher deposition occurred between 0-20min. In the remaining stages, the rate of aggradation decreased gradually. This can be verified from **Figure 2.9** where the deposition volume is higher in the initial period of 20min and decreased gradually. The location of the point bar can also be clearly seen from the deposition hills along the channel centerline which is just below the apex section i.e. between *X*=100-125, 150-175 and 200-275 cm. On the other hand, the pattern of change in elevation is quite random in ch-60-NG. The overall channel aggradation is lower in ch-60-NG which is also shown by the total deposition-erosion volume in **Figure 2.9**. As suggested by Song *et*. al (2016), the bed morphology becomes more complex with increasing sinuosity.

2) Bank Erosion

Bank erosion occurs through two processes, namely fluvial erosion and mass failure (Langendoen, 2000). Fluvial erosion is the continuous erosion of bank material due to the direct effect of near-bank flow whereas mass failure is an intermittent failure causing a collapse of the bank material due to the geotechnical instability. According to (Motta et al., 2012), fluvial erosion is the dominant mode in channels consisting of non-cohesive and homogenous bank material.

In both channels, at the beginning of the experiment, the erosion at the bank toe caused the bank materials to fail as a mass, which was transported by the flow. In the later stages, the bank slope adjusted to the flow conditions and thus mass failure did not occur. However, due to higher near-bank velocity, fluvial erosion continued at specific locations along the channel banks resulting in the lateral widening of the channel. **Figure 2.10 (a & c)** shows the bank erosion rate (cm per min)

plotted against the ratio of channel length (l_c) to the meander wavelength (L) during the first 20min for Ch-45-NG and Ch-60-NG respectively. The dashed black line indicates the general alignment of the channel centerline between the two consecutive apexes within the target area of the study. Similarly, **Figure 2.10 (b & d)** illustrate the bank erosion rate during the remaining 40min (i.e. between 20-60min) of the experiment. Erosion rate was higher in general for both the channels during the first 20min. Comparatively, the rate was higher for Ch-45-NG. In the later stages, the erosion continued in ch-45-NG whereas except for slight scour near the bank, no any significant erosion occurred in ch-60-NG. From **Figure 2.7** and **2.10**, a considerable difference in the location and the extent of bank erosion could also be found between the two channels. The bank erosion extended throughout the outer bank in Ch-45-NG while in Ch-60-NG, erosion shifted to the opposite bank after passing the crossover region.   In Ch-45-NG, maximum erosion occurred around downstream of the crossover region toward the convex bend apex. In contrast, higher erosion was observed around the crossover and further upstream toward the concave bend apex in case of Ch-60-NG. This can be clearly seen from **Figure 2.10 (a & c)** that higher erosion rates are located upstream and downstream of apex in Ch-45-NG while those concentrate around the apex region in Ch-60-NG. This finding is in agreement with the results of da Silva and El-Tahawy (2008) who concluded that the maximum erosion occurs near the crossover region for channels of small deflection angle while it occurs around the apex area for greater deflection angle. The rate of erosion in the real field might be slower but the important issue for river management works is to identify where the bank will erode higher and quicker.
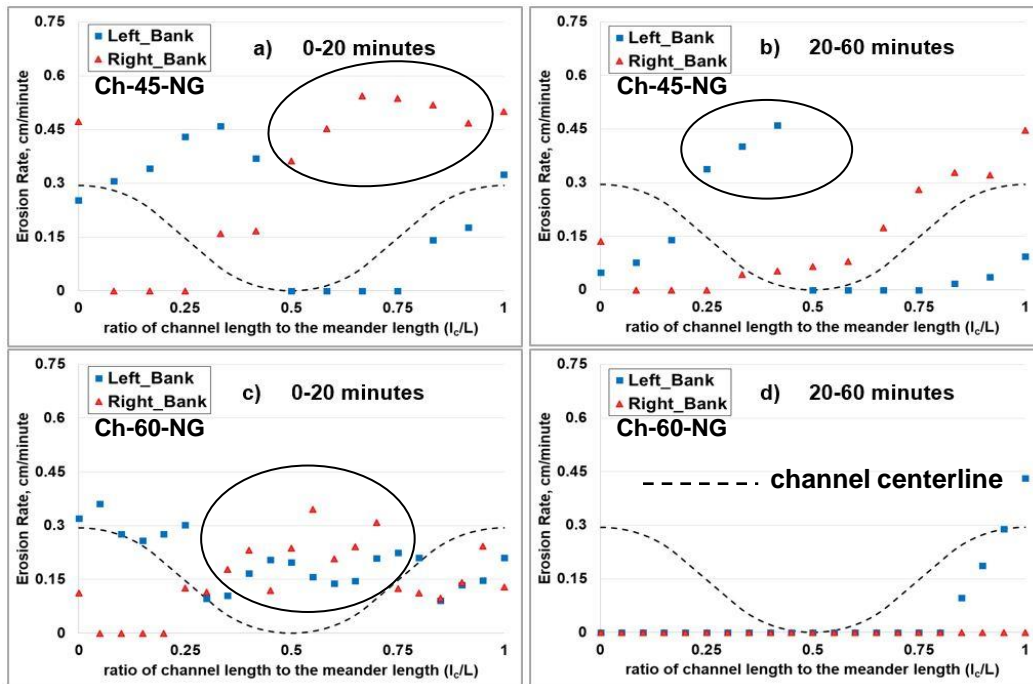

Figure 2.10 Rate of bank erosion for 0-20 and 20-60 minutes (a, b) Ch-45-NG (c, d) Ch-60-NG

3) Surface velocity distribution

To analyze the relationship between the velocity distribution and the channel evolution including bank erosion, 2D surface velocity field was plotted based on the PIV measurement during the experiments. **Figure 2.11** shows such the spatial distribution of surface velocity computed using PIV techniques at a different time of the experiment in both the channels. The continuous evolution of channel bed and planform largely affects the velocity distribution both longitudinally as well as in transverse direction.

In ch-45-NG at t=20min from the start of the experiment, it is observed that the flow is more or less well distributed within the channel. However, higher velocity zone is concentrated around the inner bend apex downstream of the crossover region. As a result, a higher rate of fluvial erosion occurred around these locations which can be correlated with **Figure 2.10** & **2.7** of bank erosion rate and channel morphological changes. The velocity leaving one bank converged downstream of the outer bank apex of the next bend. A recirculating region was formed between the downstream of the inner bank and upstream of the outer bank. This recirculating region increased in size as the channel expanded by the lateral erosion of the banks. At t=60 mins as shown in **Figure 2.11(b)**, the velocity distribution became more non-uniform with the overall increase in magnitude due to the asymmetry of the channel caused by bank erosion. In comparison to ch-45-NG, the overall distribution of velocity distribution is more uniformly distributed within the channel. The cross-sectional variation is also relatively less. The size of the low-velocity recirculating region is also small relative to the ch-45-NG. The other difference is the convergence of velocity around the outer bank apex due to which higher erosion zone was located around apex area. The higher bank erosion rate around the apex area in **Figure 2.10** supports this conclusion.
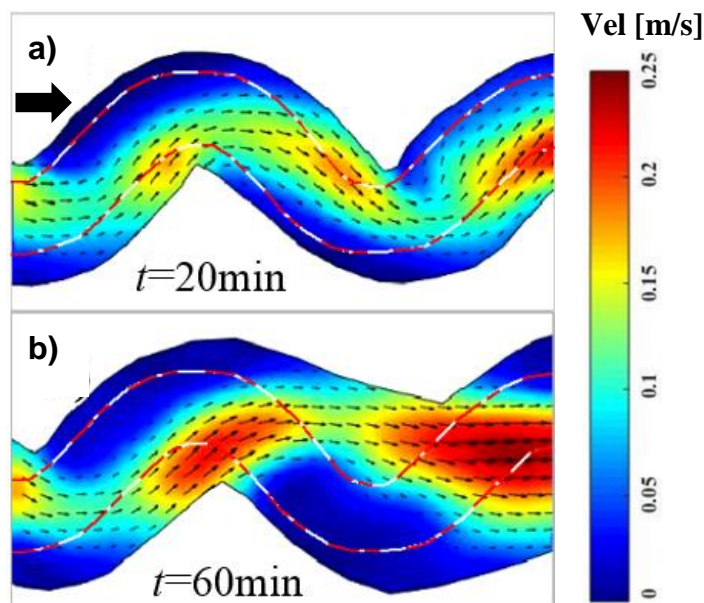

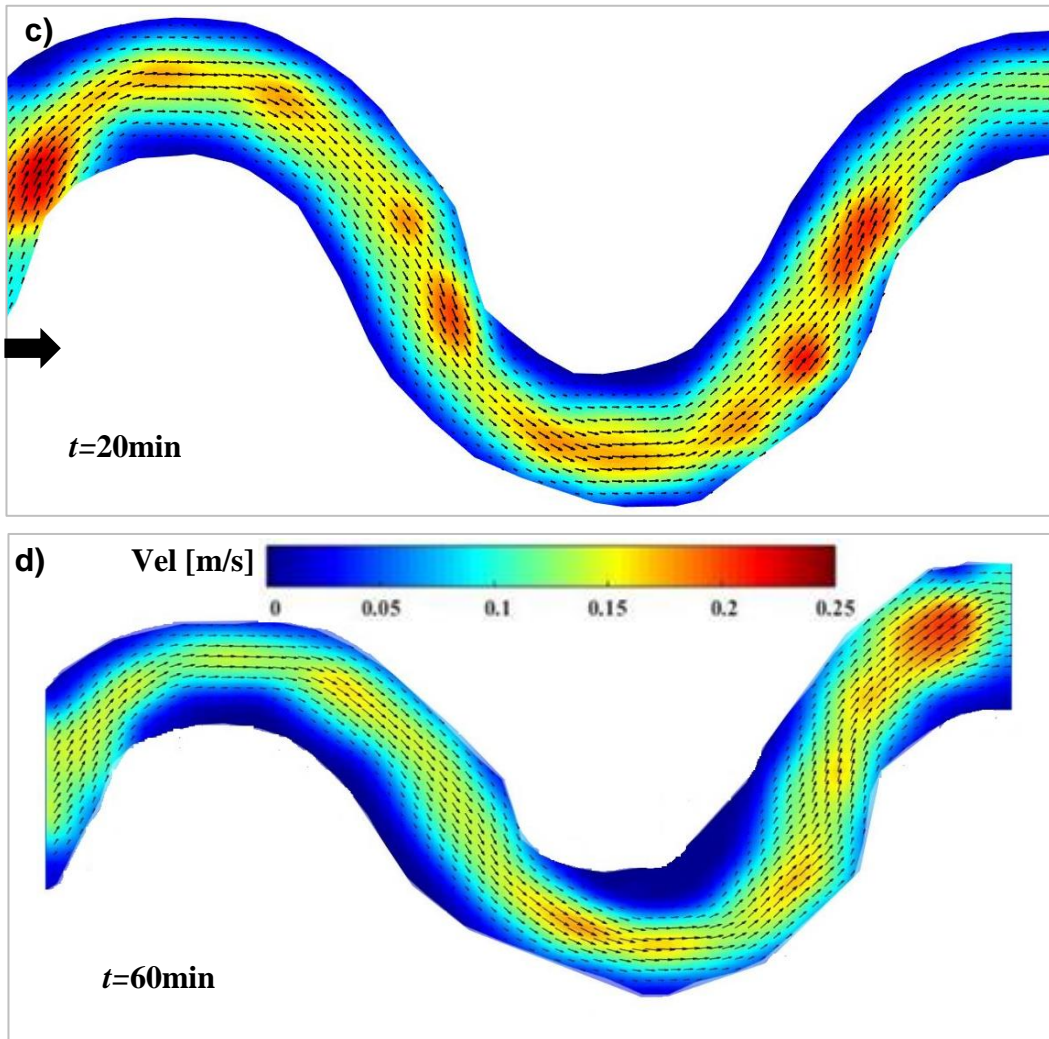**Figure 2.11 (a & b)** Surface velocity distribution for Ch-45-NG

Figure 2.11(**c & d**) Surface velocity distribution Ch-60-NG

2.5.2 With rectangular groynes

The dimensions of the groynes were set based on the previous experience while the location of groynes was decided based on a series of preliminary experiments.
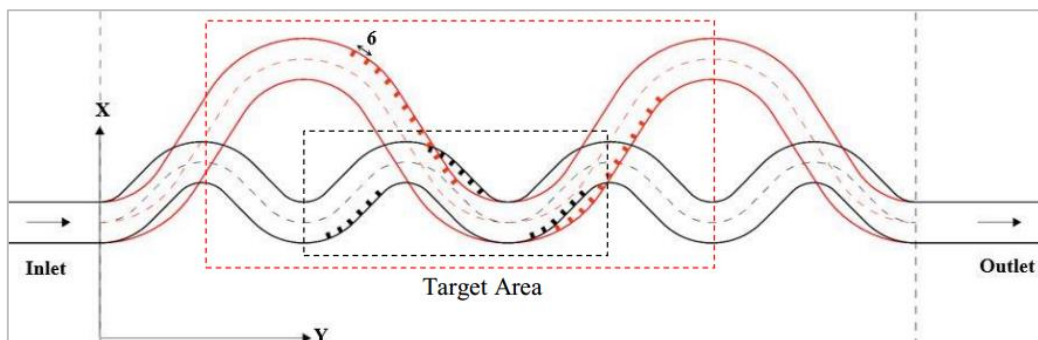

Figure 2.12 Sample layout of the groynes arrangement in the experimental channels

1) Channel evolution

In the next step, experiments were conducted with groynes. **Figure 2.13** (**a & b**) respectively represent the morphological changes in ch-45-R and ch-60-R for the first 20min of the experiment. The initial channel adjustment process in the presence of groynes as shown in **Figure 2.13 (a & b)** was more or less similar to the without groynes cases described in the previous section. The erosion/deposition volume in **Figure 2.15** is also almost similar compared to the same in the case of no groynes in **Figure 2.9**. However, the presence of groynes significantly reduced the erosion volume in the successive time periods which shows improved bank protection. Although the overall bank erosion minimized in both the cases with groynes, the erosion of the bank in the
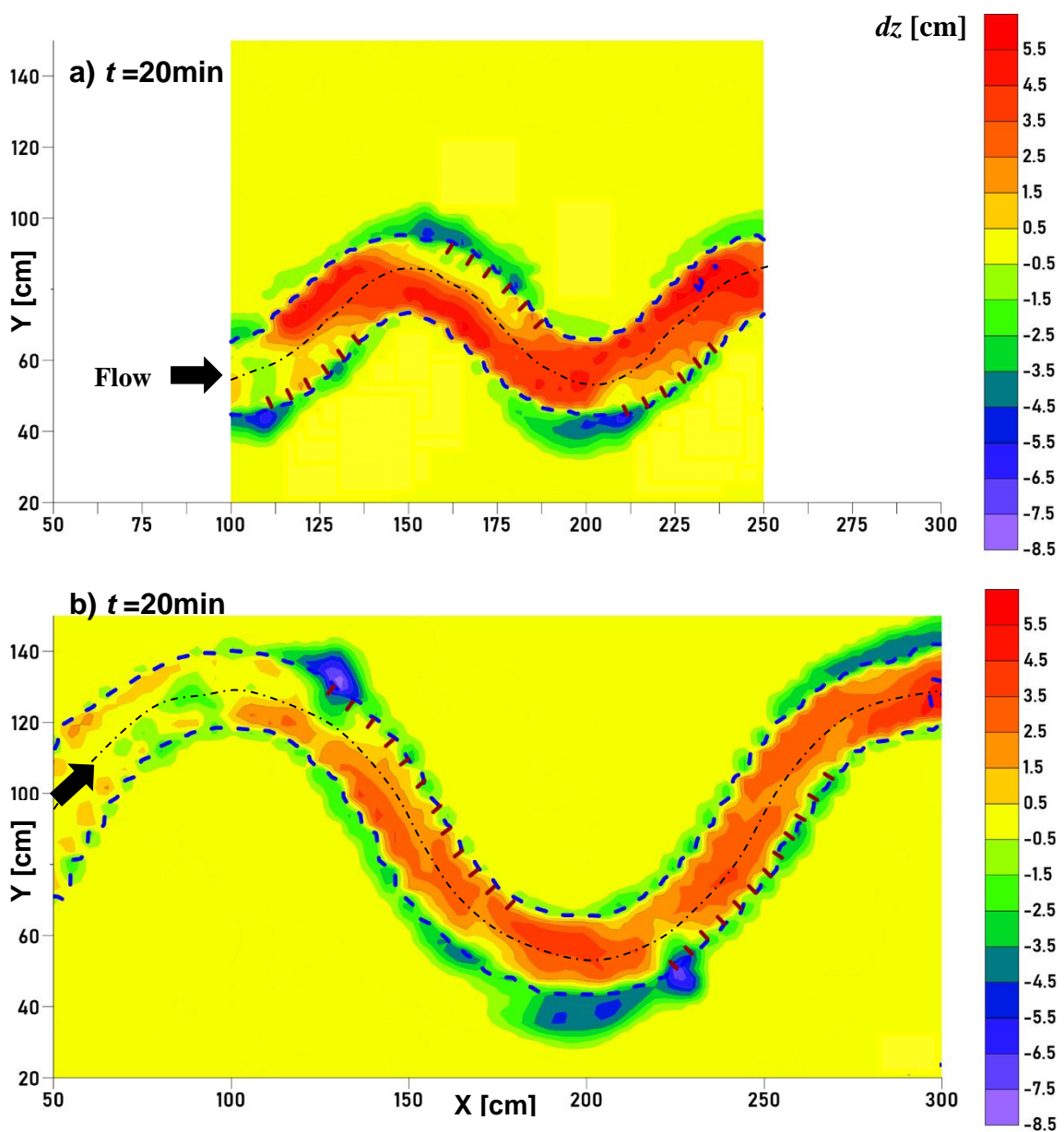
Figure 2.13 Channel evolution, *dz* [cm] for the first 20min a) Ch-45-R & b) Ch-60-R
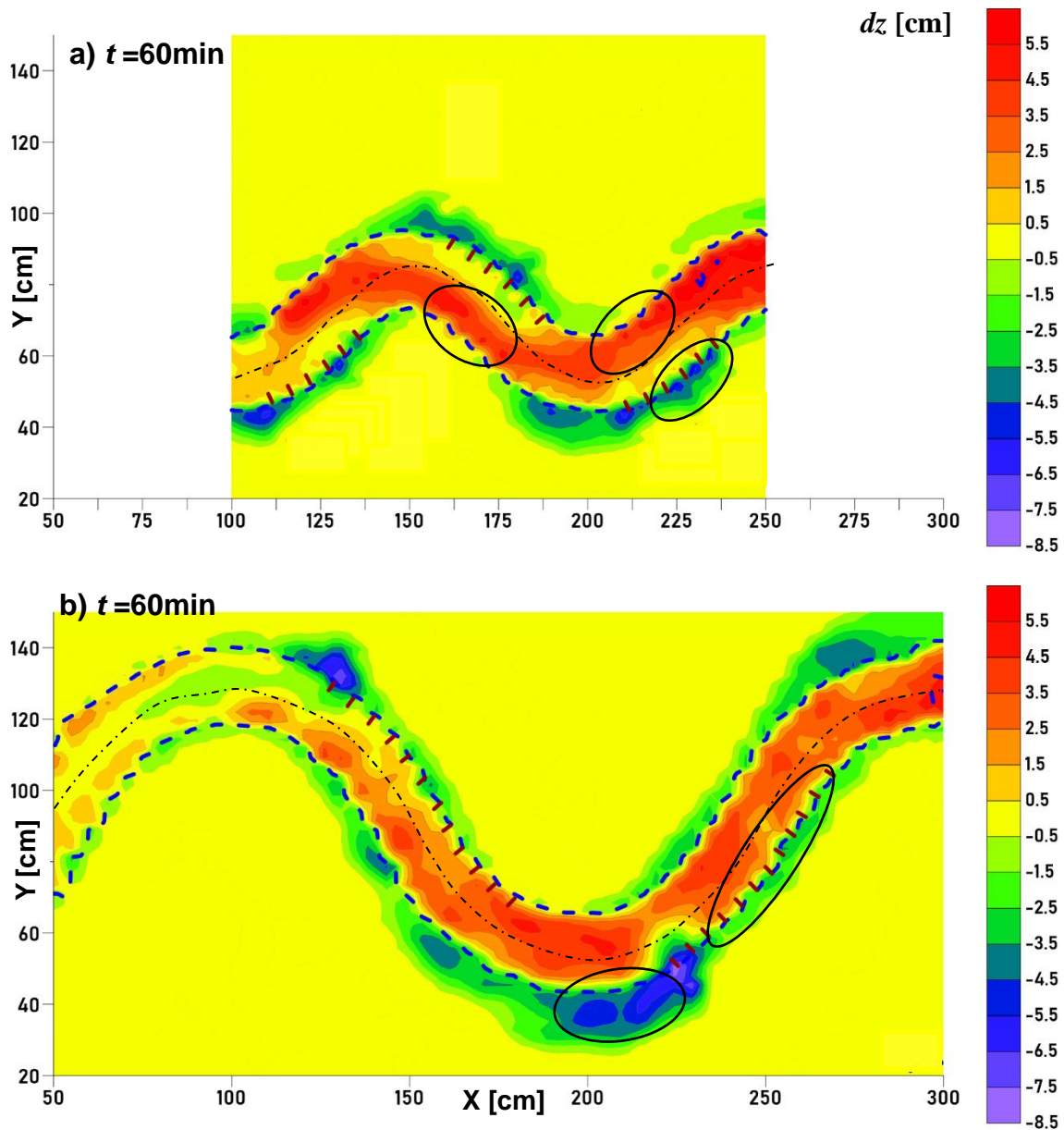
Figure 2.14 Channel evolution, *dz* [cm] at the end of the experiment a) Ch-45-R & b) Ch-60-R

space between the groynes still continued and was slightly higher in ch-45-R channel. The presence of groynes controlled the erosion of the outer banks downstream of the apex but the erosion increased near and upstream of the outer bank apex in both cases ch-45-R and ch-60-R compared to the cases of no groynes. Erosion of the outer bank apex was higher for case ch-60-R in comparison to the case ch-45-R seen from x-sectional change in **Figure 2.16 (a & b)** and **2.14 (a & b).** The reason for increased erosion near the outer bank apex in both cases was due to the increased flow velocity leaving past the groynes from the opposite bank as well as the formation of recirculation zones behind the initial groynes around the outer bank apex. This suggested that
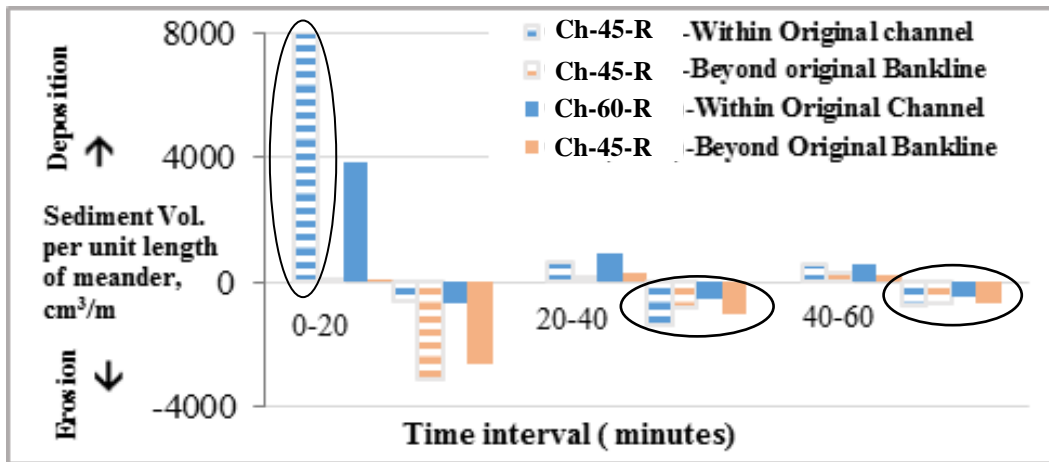
Figure 2.15 Comparison of temporal change in erosion/deposition volume for groynes cases
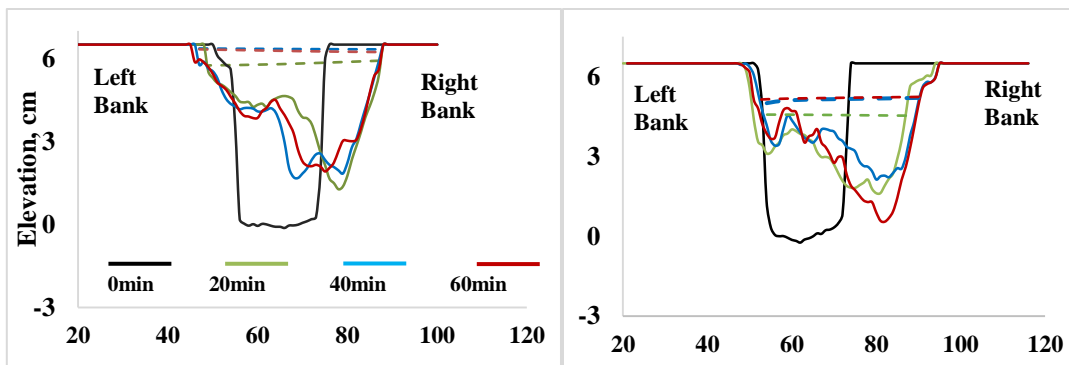

Figure 2.16 Cross-sectional change and water level variation at the apex (*X*=200cm) for case
(a) Ch-45-R and b) Ch-60-R

the installation of groynes control the bank erosion but it also tends to shift the point of erosion from one location to another. The presence of groynes also significantly reduced the size of the point bar in case of ch-45-R channel.

Similarly, **Figure 2.17** represents the temporal change in the elevation along the original channel centerline. During the initial channel adjustment process, the overall aggradation of the channel occurred in both cases ch-45-R and ch-60-R. The shift of the channel thalweg towards the bank due to erosion and the consequent transverse bed load transport caused aggradation of the channel. The aggradation tends to increase slightly in the downstream direction. After the initial channel adjustment process in the first 20mins, the overall change in the channel centerline elevation was not so significant for the remaining time period. This can be correlated with the reduced erosion volume in **Figure 2.15** as the supply of the sediment is minimized due to the control of bank erosion.

To see the effect of groynes on the temporal evolution of the channel thalweg line**,** the plot in **Figure 2.18** depicts the temporal change in the channel thalweg line at every 20mins during the
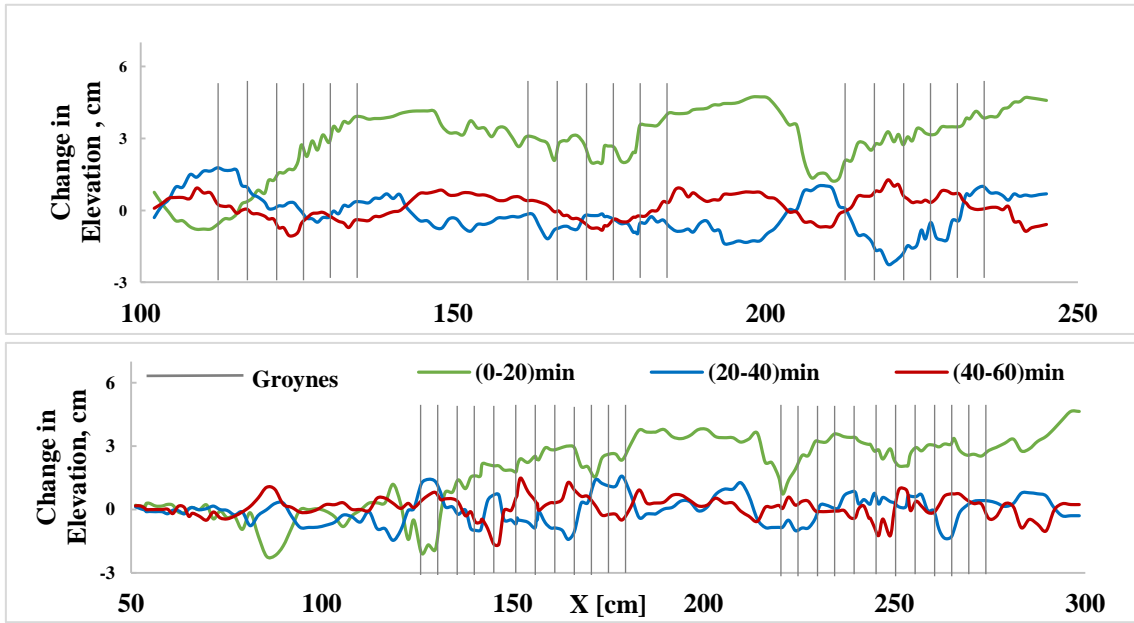
Figure 2.17 Temporal difference in elevation along the original centerline (top) ch-45-R and (bottom) ch-60-R
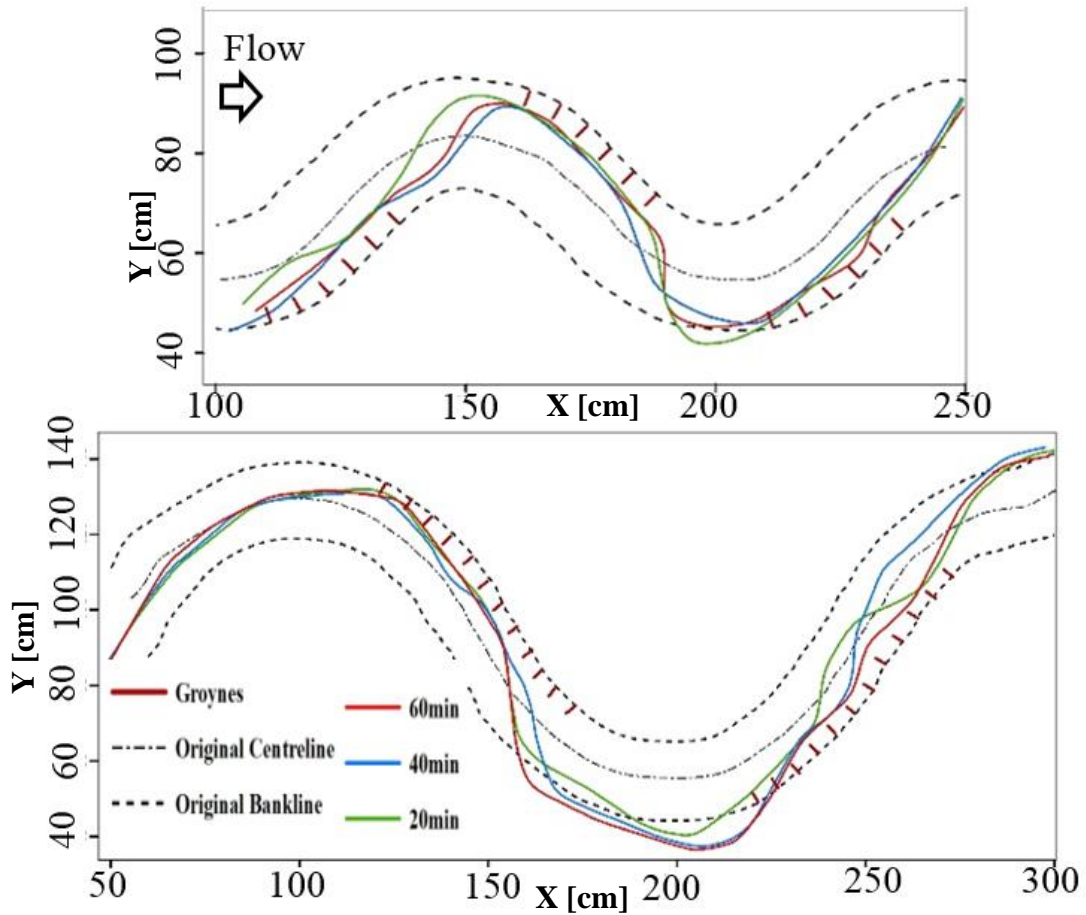

Figure 2.18 Temporal change in the channel thalweg line in (a) case ch-45-R and (b) ch-60-R

experiments with groynes. In both cases ch-45-R and ch-60-R, once the channel adjusted to new morphology, the thalweg also adjusted accordingly. However, initially adjusted thalweg line didn't change much for the remaining time period mainly due to the control of bank erosion by groynes. The thalweg line was located around the groynes in the outer bank in both channels. However, due to the higher erosion of the bank near the outer bend apex, the thalweg shifted slightly more beyond the original bankline in case of ch-60-R as seen in **Figure 2.18** (**bottom**).

3) Velocity distribution

In case ch-45-R with groynes, **Figure 2.19** shows that zone of high velocity is contained inside the channel rather than near the banks as compared to no groynes case ch-45-NG. One of the main function of groynes is to deflect the high-velocity currents towards the channel center which holds true in this study too. This resulted in a decrease in the size of the point bar and the effective flow area was maintained. A zone of circulation or rotational flow developed immediately upstream of the groynes near the apex of the outer bank as seen in **Figure 2.20**. This region was nearly stagnant in case ch-45-NG. The strength of this circulation flow was enhanced by the increased flow
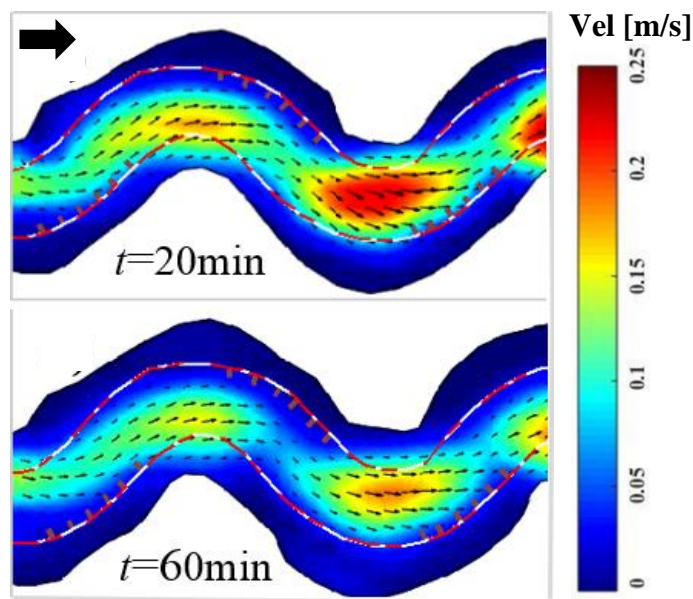

Figure 2.19 Temporal change in Surface velocity distribution for case ch-45-R

Figure 2.20 Typical streamlines of surface flow in case ch-45-R with groynes
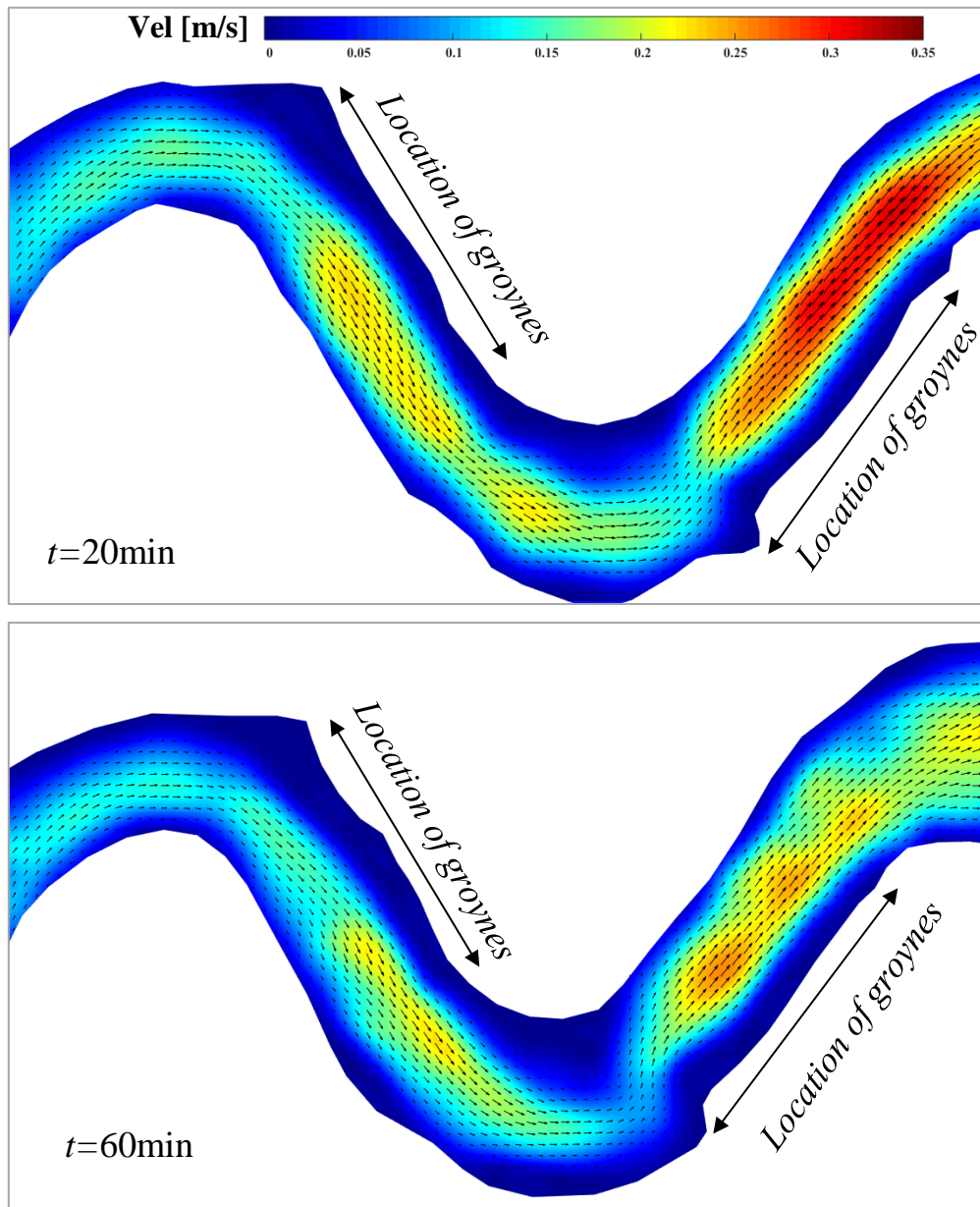
Figure 2.21 Temporal change in surface velocity distribution for case ch-60-R

velocity leaving past the groynes from the opposite banks.

In the case of ch-60-R, velocity is generally higher around the groynes field. The velocity distribution pattern is more or less uniform along the channels which can be seen from **Figure 2.21**. This is mainly due to the fact that the overall erosion of the banks was less. As a result, channel symmetry didn't change. However, the velocity was slightly higher around the crossover region. And this higher velocity can correspond to the higher erosion around those regions as shown in **Figure 2.7**. At t=60min, the channel section changed due to erosion at some locations

37

as well as the bed topography already adjusted to the flow condition which resulted in the overall decrease in the velocity.

2.5.3 With sloped-crested groynes

To check the effect of groynes head on the overall turbulence and scour pattern, the tip of the groynes was modified in the next experimental case. Groynes modified for the present studies consisted of a triangular portion inclined from the bank top towards the channel and a rectangular portion inserted inside the banks to prevent the flow outflanking around the structures. Compared to the rectangular groynes, the sloping crest from the bank towards the channel caused minimum flow constriction, less turbulence and safe passage of flow. The dimensions and a schematic layout of the groynes are shown in **Figure 2.22**.

The position of the groynes along the outer bank is shown in **Figure 2.22** for both channels. Groynes are placed starting from upstream of the apex to the crossover or the point of inflection along the outer bank. Accordingly, due to the difference in channel length, the number of groynes in each type of channel varied from one to another. The groynes from upstream up to the apex
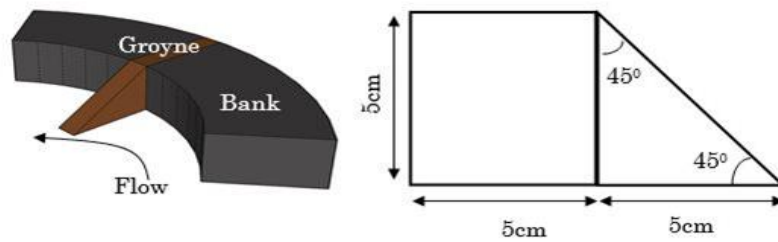

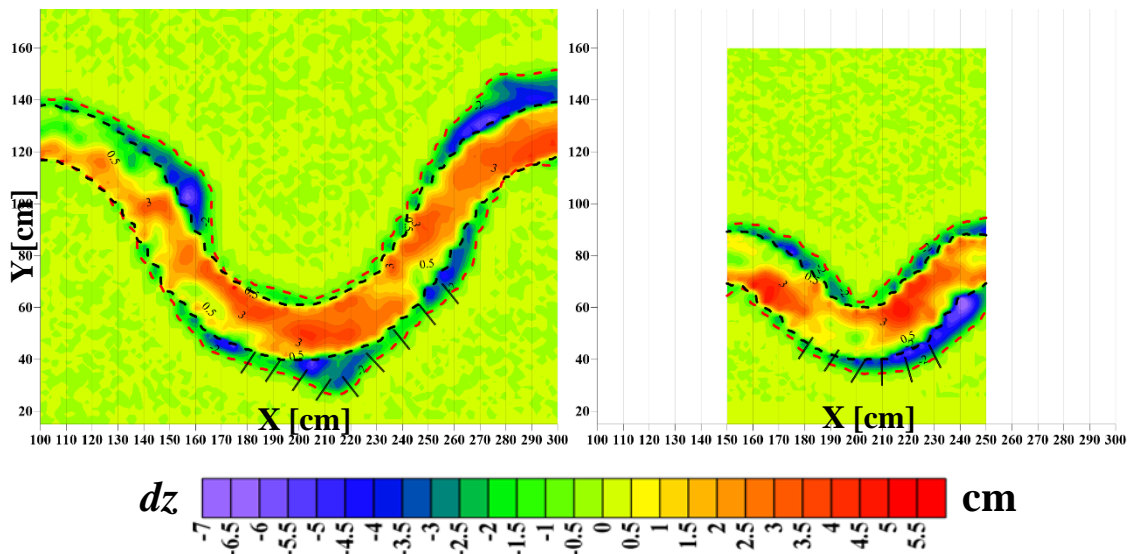**Figure 2.22** Schematic layout and geometry of the groynes

Figure 2.23 Position of the groynes and the change in the channel bed elevation between time, t=20 mins and t=0 mins for cases Ch-45-S and Ch-60-S.

were inclined at 120^0 to the upstream bank in order to ensure a smooth flow approach towards the downstream groynes whereas the groynes downstream of the apex were placed at right angles to the bankline. During the initial channel adjustment period, the pattern, location and the extent of the bank erosion varied from one channel to another as shown by the change in channel elevation ($dZ=Z_{20\ min}-Z_{0\ min}$) between t=20 mins and t=0 min in **Figure 2.23**. Due to this non-uniformity in the bank erosion process, the positioning of the groynes was also affected. The bank erosion process after the implementation of groynes is discussed in the next section.

1) Channel evolution

The morphology of a meandering channel continuously evolves due to the interaction of flow, sediment transport and channel planform. **Figure 2.24 (a & b)** shows the difference ($dZ=Z_{40}$ min-Z_0 min) in channel elevation between the end (t=40 min) and the start (t=0 mins) of the experiment for case Ch-45-S and **Figure 2.25 (a & b)** for Ch-60-S (the flow is from the left to the right). The black dashed line in the figure represents the original bankline (t=0 min) while the red dashed line indicates the bankline at the end of the 20-minute experiment, just at the time of implementation of the groynes. Positive values in the figure signify deposition while negative values indicate erosion.

The ratio of the radius of curvature (R) of the channel centerline to the channel width (B), which signifies the sharpness or the tightness of the channel curve is an important parameter controlling the channel erosion and migration (Hickin and Nanson, 1975) in meandering channels. The ch-60 channel, due to the longer flow path and high value of the R_c/B ratio, had smooth flow transition and thus less erosion occurred in the Ch-60-NG case. However, the ch-45 channel had a shorter channel flow path and low R_c/B ratio, which caused rapid flow transition and resulted in higher erosion in the ch-45-NG case. As discussed earlier, in Ch-60-NG case shown in **Figure 2.7**, maximum erosion occurred near the point of inflection or crossover region whereas, in the case of Ch-45-NG, channel erosion occurred near the apex of the inner bend and gradually shifted in the upstream direction. The extent of erosion or channel expansion had an effect on the direction of the flow approach, which in turn dictated the performance of the groynes.

With the installation of groynes, the erosion near the outer bank apex was controlled in both the Ch-45 and Ch-60 channels. The erosion at the downstream of the apex was also greatly reduced in the case of Ch-45-S but slightly higher erosion occurred in Ch-60-S as shown in **Figure 2.24** and **2.25**. Within the field of the groynes, erosion was minimized, however, it continued on the downstream end after exiting the groynes field. The size of the deep pools, as well as the scours at the outer bank in the case of Ch-45-S, were also reduced to some extent as compared to those in the Ch-45-NG case in **Figure 2.7**. Although scour at the tip of the groynes was observed
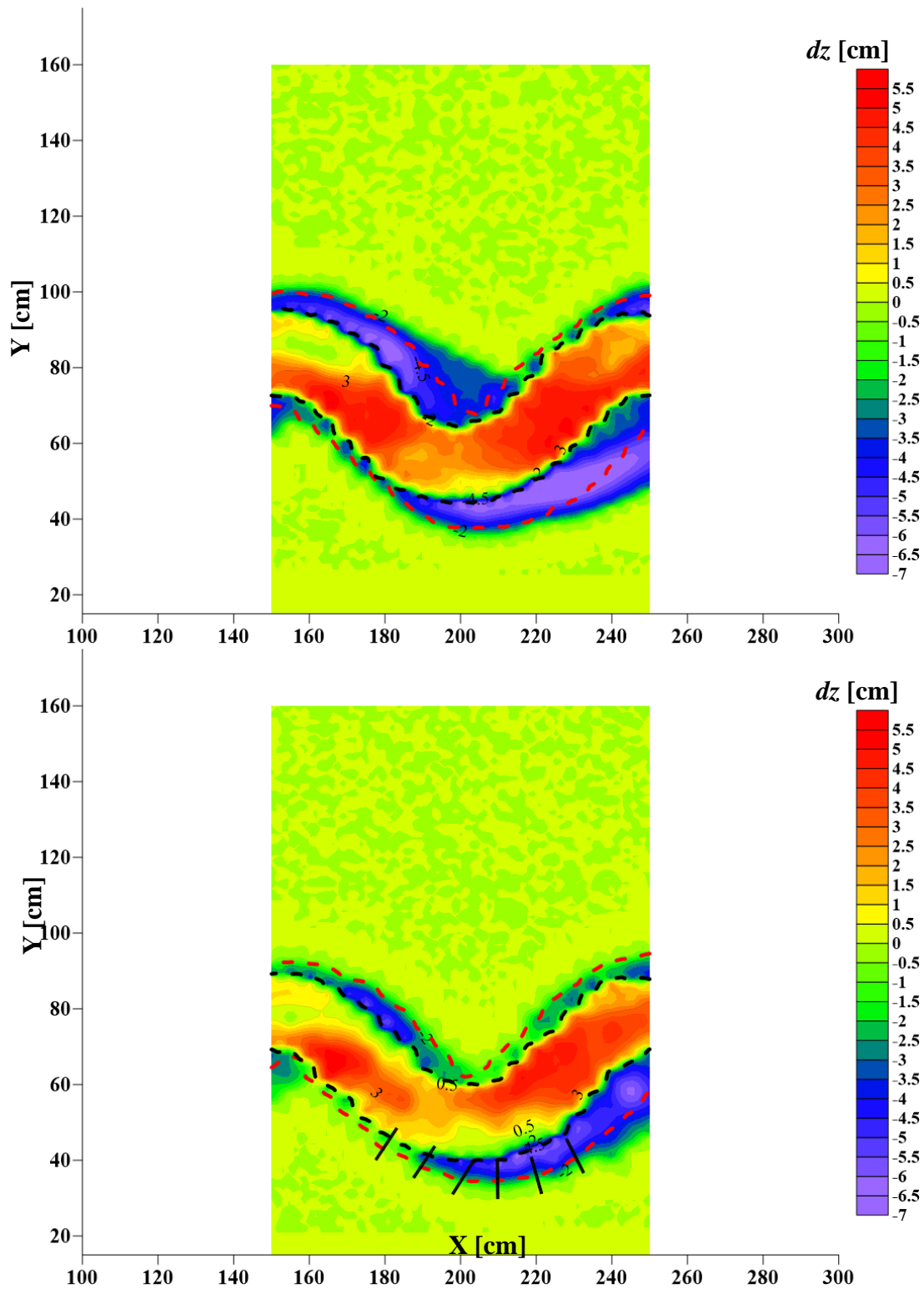
Figure 2.24 Change in the channel bed elevation between the final (*t*=40 min) and the initial
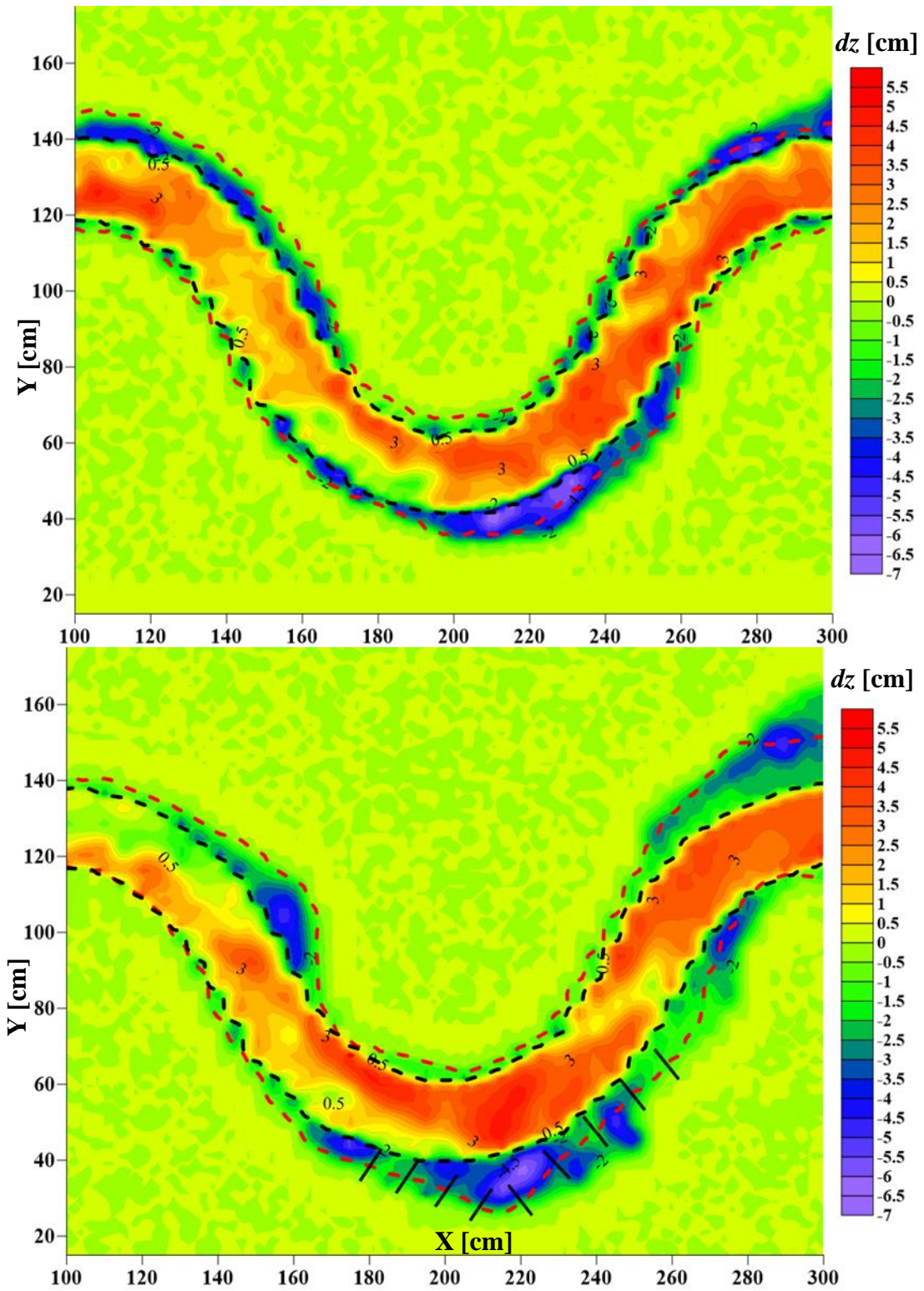
(*t*=0 min) for case Ch-45-S

Figure 2.25 Change in the channel bed elevation between the final (*t*=40 min) and the initial (*t*=0 min) for case Ch-60-S

in one or two groynes, the overall scour at the tip of the groynes was not so significant. Considerable erosion occurred in the space between the groynes in the case of Ch-60-S compared to that of the Ch-45-S. The deep pools in the case of Ch-45-S caused the incoming flow velocity to be more moderate and thus reduced the turbulence whereas, in the case of Ch-60-S, the approach on the groynes occurred with higher velocity thereby causing more recirculation behind the groynes. This angle of approach might also be influenced by the deflection angle of the meandering channel since the Ch-60 channel had a deflection angle of 60^0 compared to the 45^0 of the Ch-45 channel.

2) Erosion-Deposition Pattern

The erosion-deposition pattern of the channel was analyzed in order to determine the sediment transport behaviour of the channel. **Figure 2.26** depicts the temporal change in the erosion-deposition volume for cases ch-45-S and ch-60-S.

The erosion-deposition volume between the successive time periods was calculated based on the change in measured bed elevation at different time periods. The erosion, as well as deposition volume, was higher in the first 20min for all cases as the channel underwent rapid adjustment under the given flow conditions. Although the volume was slightly different even for the same type of channel, the overall initial channel adjustment behaviour was similar. After the implementation of groynes, the erosion and deposition volume was significantly reduced in the case of ch-45-S as compared to that of ch-45-NG as shown in **Figure 2.8**. This suggests that the groynes effectively reduced the erosion and enhanced channel transport capacity. However, in the case of ch-60-S, the erosion-deposition volume changed little compared to that of the ch-60-NG case. This might suggest that the channel adjustment process was still active in the ch-60 channel.
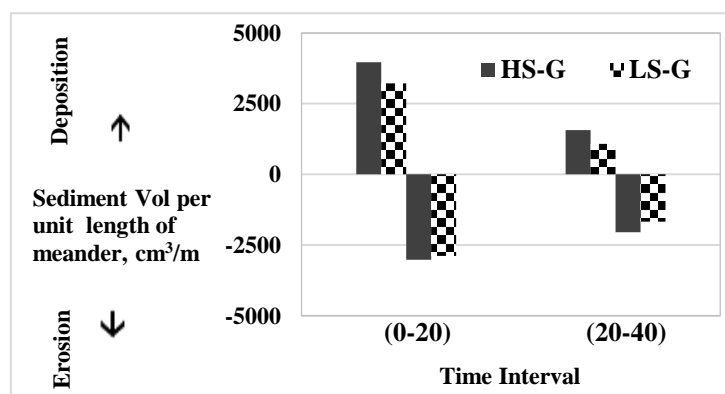

Figure 2.26 Temporal change in the erosion-deposition volume for different experiment cases.

Figure 2.27 (a-d) shows the change in the channel elevation ($dZ=Z_{40min}-Z_{20min}$) along the initial channel centerline as well as along the initial right bankline between time $t=40min$ to $t=20min$, i.e. after the implementation of groynes. Channel erosion is represented by negative values while

42

deposition is given by positive values. The comparison between the Ch-45-NG and Ch-45-S
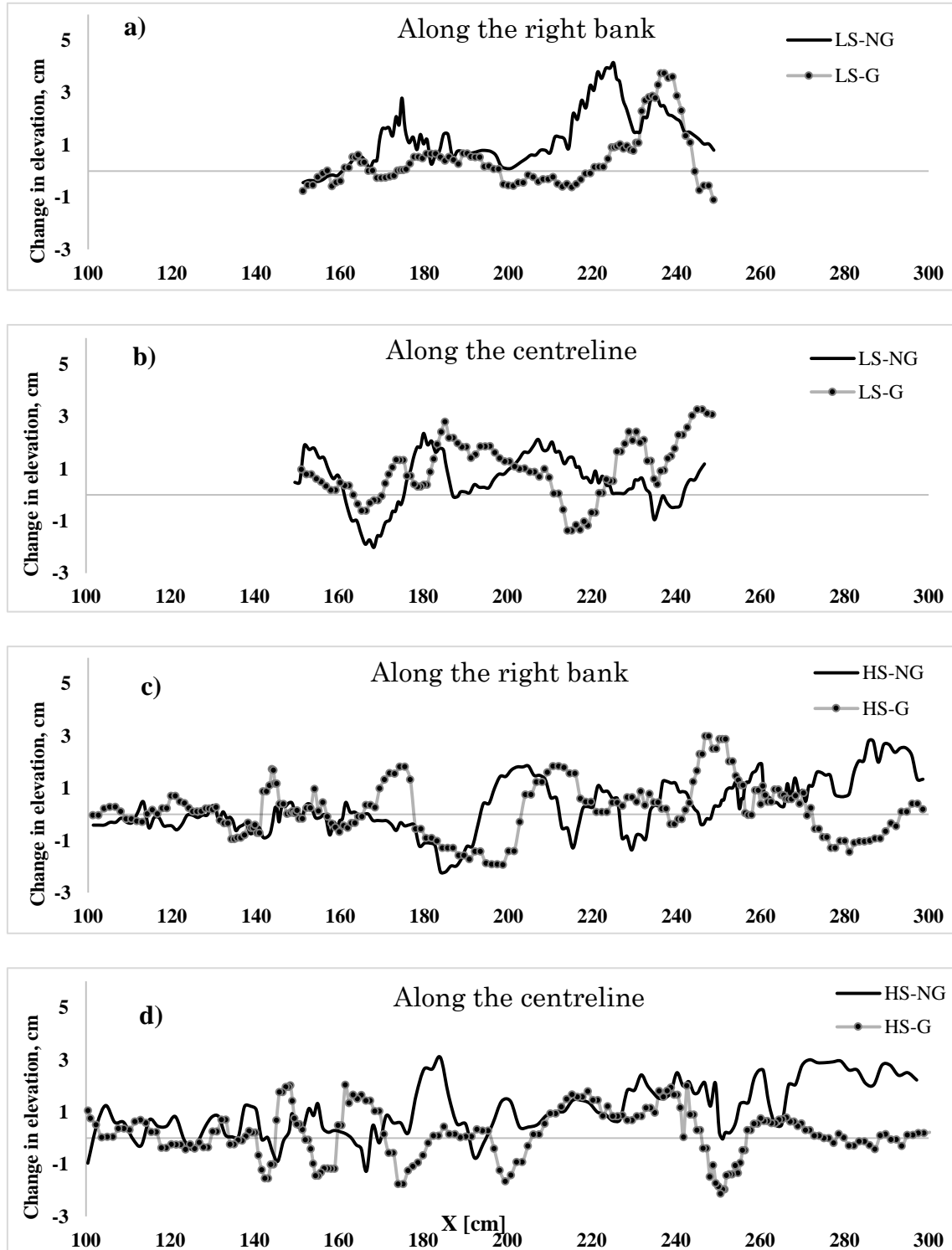(**Figure. 2.27(a)**) shows that the presence of groynes caused degradation along the right

Figure 2.27 (a-d) Difference in the elevation between t=40min and t=20min along the original
channel centerline and along the original right bankline

bank due to local scouring particularly downstream of the apex. However, along the channel centerline, as shown in **Figure 2.27(b),** the channel was continuously aggraded due to the transport of eroded sediment from the bank towards the center. In the case of the Ch-60 channel, the channel aggradation-degradation pattern changed little even in the presence of groynes. Along the right bank, slight deposition occurred upstream of the apex and slight degradation was seen just near the apex region (**Figure. 2.27(c)**). A similar pattern of elevation change was also observed along the channel centerline as shown in **Fig. 2.27(d).**

3) Velocity distribution

The continuous change in the channel planform as well as the channel bed due to erosion-deposition phenomena largely affects the distribution of velocity in both the longitudinal as well as transverse direction. Conversely, velocity distribution dictates the channel morphological evolution. In fact, these phenomena proceed simultaneously. Surface velocity distribution obtained by the PIV technique was analyzed to determine how the morphological evolution process is related to the velocity distribution in the channel. **Figure 2.28** shows the distribution of the surface velocity before implementing the groynes (first 20min) and after implementing the groynes (next 20 mins) in the cases of Ch-45-S.
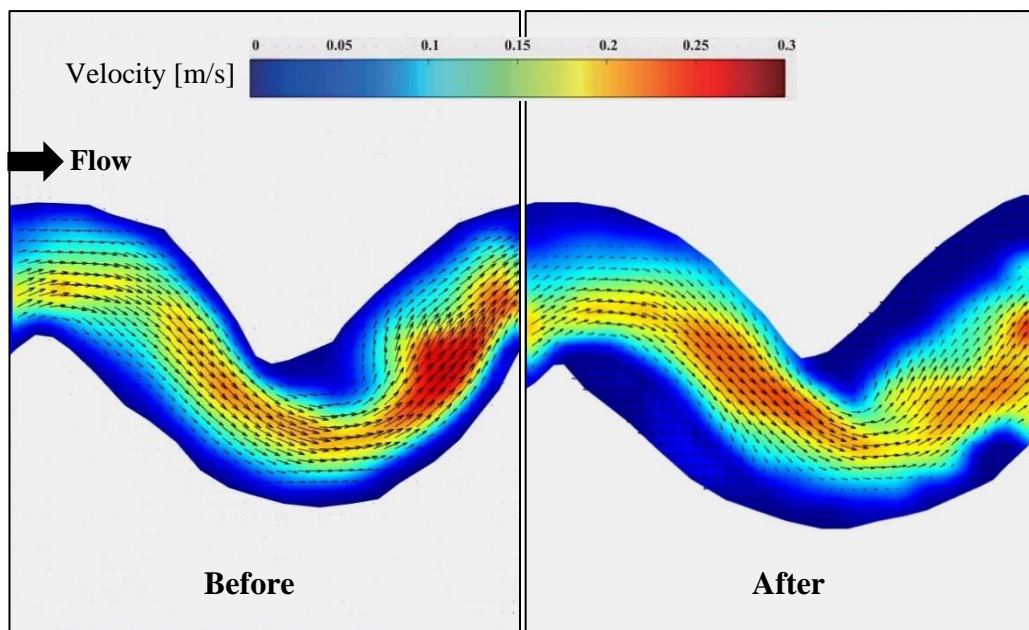

Figure 2.28 Velocity distribution along the channel before (first 20mins) and after (last 20mins) implementation of the groynes in ch-45-S.

During the initial 20min where the channel adjustment process was dominant, the velocity distribution within the channel was nearly uniform. After the channel adjusted to the given flow conditions by undergoing morphological changes, the distribution of velocity also tends to be

non-uniform. Due to the longer flow path as well as the R_c/B ratio, smooth flow transition occurred in the Ch-60-S case. Consequently, the velocity was more or less uniformly distributed across
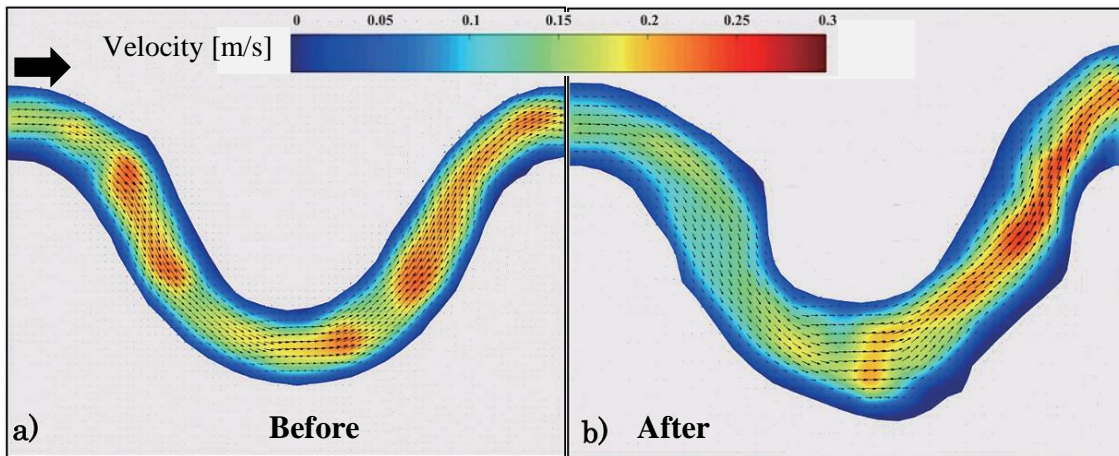

Figure 2.29 Velocity distribution along the channel before (first 20min) and after (last 20min) implementation of the groynes in Ch-60-S.

channel section as well as along the channel as shown in **Figure 2.29(a)**. However, the velocity was slightly high at the point of inflection between the two apices because of which higher erosion was observed around those areas. Similarly, in the case of Ch-45-S, before the implementation of groynes, the high velocity was concentrated near the apex of the inner bend as shown in **Figure 2.28(a),** which caused higher erosion around that region. The transverse velocity component in the case of the Ch-45 channel was higher because of which more bed load transport occurred forming deep pools near the outer bank and point bar near the inner bend. After the implementation of the groynes, the near bank velocity was significantly reduced in both Ch-45 and Ch-60 (**Figure 2.28** (**b) and 2.29 (b)**). However, apart from the slight deflection around the groynes region, no noticeable change in velocity distribution within the channel was observed. Velocity around the groynes was reduced but it tends to increase after exiting the groynes field as shown in the same figures. Some previous studies on straight rectangular groynes showed a higher flow deflection, which resulted in higher bank erosion on the opposite bank. In the case of Ch-45-S, a stagnant or dead zone extending from upstream of the outer bank apex to the inner bend apex was observed (**Figure 2.28**(**b**)).
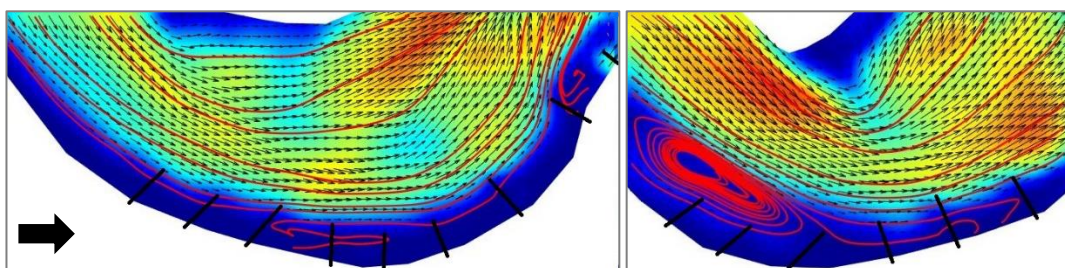

Figure 2.30(a-b) Streamlines and velocity around the groynes: (a) ch-60-S (b) ch-45-S

Similarly, **Figure 2.30 (a** and **b),** shows the streamlines and velocity near the groynes area in the case of Ch-45-S and Ch-60-S, respectively. For Ch-60-S, a stagnant zone did not develop upstream of the apex. However, in the space between the groynes downstream of the apex, strong recirculation flow was observed, which resulted in higher erosion in that region. Similarly, the flow deflection around the groynes was slightly higher in the case of the ch-60. This was mainly because of the direction of the approach flow towards the groynes. In the case of ch-60-S, the erosion in the previous bend (X=150-200 cm) in **Figure 2.30** was minimum due to which the flow smoothly approached towards the initial groynes. However, in the case of ch-45-S, due to higher erosion in the preceding bend (X=175-200 cm) in **Figure 2.2,** the flow of approach was towards the end groynes and further downstream. Consequently, less flow deflection, as well as higher erosion downstream of the groynes, was observed.

2.6 Summary

This chapter presented the results and analysis of the experimental works performed in two different SG meandering channels. The objective of the experimental study was to understand the phenomena of bed evolution and bank erosion. And eventually to identify the effect of bank protection countermeasures on reducing the bank erosion.

Results showed that the bed development phenomena was more rapid and dominant in low sinuosity channels. Eventually, the channel bank erosion was also higher in low sinuosity and low deflection angle channels requiring a greater degree of bank protection. The characteristic features of meandering channels such as point bar and deep pools were more distinct in low sinuosity channels whereas bed morphology was more irregular and complex in higher sinuosity channels. Also, it was found out that the extent and the location of bank erosion varied with channel geometric parameters. This was mainly due to the flow direction which attacked downstream of apex in 45-degree channel whereas as in 60-degree channel, the approach was more towards upstream of the apex. Such findings could be useful while planning the real field bank protection measures.

The implementation of groynes indicated that the overall channel erosion-deposition pattern could be greatly modified in the presence of bank protection structures. There was a net reduction in channel bank erosion. However, the erosion in between the groynes could still be higher due to the strong recirculation which depends on the groynes orientation, spacing, etc. The orientation and the position of the first groynes were vital because the erosion behind the first groynes was higher in both channels. Another, important point to be mentioned is the effect of groynes on the erosion of the opposite banks which could significantly increase. It was observed that the size of the point bar on the opposite bank reduced while the erosion on the opposite banks also increased.

Chapter 3

2-Dimensional numerical modeling of bed evolution

3.1 Introduction

Due to various constraints, it was difficult to perform a different scenario in the experiments. Nevertheless, the results and information obtained from the experiments were useful in determining the next step of work and analysis. To overcome that difficulty, we carried out 2D numerical simulations that are discussed in this chapter. The objective of the 2D simulations was to analyze the channel response to the different arrangement of groynes and also analyze the performance of the different groynes arrangement in minimizing the vulnerability of bank erosion.

3.2 Two-dimensional coupled model of flow and sediment transport

An open source depth-averaged hydrodynamic model Telemac2D coupled internally with the sediment transport model SISYPHE from the TELEMAC-MASCARET suite of solvers (www.opentelemac.org) was applied to study the channel hydrodynamics and morphological changes. Telemac-2D solves the shallow water equations (momentum and continuity) using the finite-element in an unstructured (triangular elements) computational mesh. The sediment transport model sisyphe and the hydrodynamic model Telemac2D are internally coupled where at each time step, sisyphe receives the spatial distribution of the main hydrodynamic variables: water depth h, horizontal depth-averaged flow velocity components V_x and V_y, and bed shear

47

stress τ calculated by the hydrodynamic model. Telemac2D has been validated for various analytical, experimental and real-field cases (Hervouet and Bates, 2000).

3.2.1 Hydrodynamic model

Telemac2D solves the depth-averaged RANS equations as shown in **Eq. [3.1-3.3]**. In this study, the $k\text{-}\epsilon$ turbulence model was used for modeling turbulence closure.

$$\frac{\partial h}{\partial t} + \frac{\partial (hV_x)}{\partial x} + \frac{\partial (hV_y)}{\partial y} = 0 \tag{3.1}$$

$$\frac{\partial V_x}{\partial t} + V_x \frac{\partial (V_x)}{\partial x} + V_y \frac{\partial (V_x)}{\partial y} = -g \frac{\partial Z_s}{\partial x} + F_x + \frac{1}{h} \nabla[hv_T \vec{\nabla}(V_x)] \tag{3.2}$$

$$\frac{\partial V_y}{\partial t} + V_x \frac{\partial (V_y)}{\partial x} + V_y \frac{\partial (V_y)}{\partial y} = -g \frac{\partial Z_s}{\partial x} + F_x + \frac{1}{h} \nabla[hv_T \vec{\nabla}(V_y)] \tag{3.3}$$

Where,

t = time

x, y = horizontal Cartesian coordinates

Z_s = water surface

v_T = turbulent viscosity

F_x, F_y = source terms which includes friction forces

3.2.2 Sediment transport and bed evolution model

Sediment transport is modelled only considering the bed-load transport while the suspended sediment transport is neglected. In the current study, we considered a non-uniform sediment transport using the active layer concept (Hirano, 1971). The uppermost bed layer is subdivided into two layers: an active layer which is in contact with the flow, and a substrate layer directly below. The active layer supplies sediment to be transported as bed load as well as receives the sediment for deposition. The role of the lower substratum layer is to exchange sediment with the active layer so as to maintain its thickness. The sediment material is divided into N size-fractions (five size-class in this study), each characterized by a diameter, d_k, and a volume percentage of occurrence, p_k. The sediment transport is assumed to adapt instantaneously to the driving hydrodynamics and is computed according to the availability of each grain size fraction (El Kadi Abderrezzak et al. 2016). The bed load rate per unit width for the kth fraction size, q_{bk}, was calculated using the Meyer-Peter and Müller (1948) empirical formula and weighted depending on the proportion of the kth fraction in the sediment mix. Modifications of the critical Shield's parameter due to hiding/exposure effect was calculated using Ashida-Michiue's (1973) formula. The magnitude and direction of the bed load are influenced by the transverse bed slope.

We used Koch & Flokstra (1980) formulation to account for this effect. The bed evolution was calculated using sediment mass conservation equation or the Exner equation.

$$(1-p)(\frac{\partial z_b}{\partial t})_k + \frac{\partial(q_{bk}\cos\alpha_k)}{\partial x} + \frac{\partial(q_{bk}\sin\alpha_k)}{\partial y} = 0 \qquad [3.4]$$

The total bed level change is given as

$$\frac{\partial z_b}{\partial t} = \sum_{k=1}^{n}(\frac{\partial z_b}{\partial t})_k \qquad [3.5]$$

Where,

p = porosity of bed material

α_k = angle between the bedload direction and the x-axis

$(\frac{\partial z_b}{\partial t})_k$ = rate of change in bed elevation corresponding to the kth fraction size.

To account for the effect of secondary currents in curved channels, Engelund's (1974) formulation has been incorporated. The transverse bed evolution in curved channels can be well reproduced in 2D models using this formulation. The direction of bed shear stress relative to the flow direction is modified depending on the water-depth h, and the local radius of curvature, r_s. The radius, unknown in the model, can be substituted using the formulation for the slope of the free surface, $\partial Z_s/\partial y$ such that $g\,(\partial Z_s/\partial y) = \alpha'U^2/r_s$ in bends. The correction factor α' is the only calibration parameter and should be chosen between 0.75, in the presence of bedforms, and 1, for flat-bed conditions which was considered in this study (Villaret et al., 2013).

> **Coupling of hydrodynamic and bed evolution**

Morphological models may be used fully coupled (Cao et al., 2002) and decoupled (de Vriend, 1987). The approach used by Sisyphe follows the decoupled treatment, i.e., to alternate between the simulation of flow and bed evolution. This procedure, also known as an asynchronous solution, considers that the bottom is fixed when the flow variables are computed (Tassi, 2018).
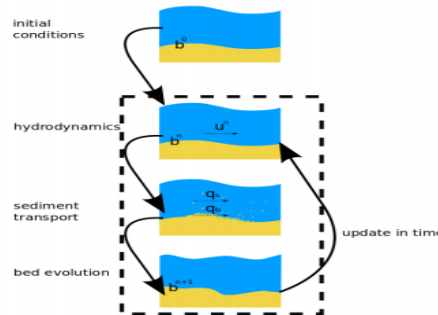

Figure 3.1 Coupling of Telemac2D hydrodynamic & Sisyphe sediment transport model
[Adapted from (Tassi, 2018)]

The hydrodynamic solution is therefore to solve the hydrodynamic continuity and momentum equations on a short time scale. During this hydrodynamic step, the bottom is frozen and the discretized sediment equation is subsequently solved separately. The coupling mechanism is illustrated in **Figure 3.1** (Tassi, 2018).

> **Bed-load transport calculations**

Critical shields parameter

The critical bottom shear stress τ_c is calculated as a function of non-dimensional grain size D_*

$$D_* = d_{50} \left[\frac{\left(\frac{\rho_s}{\rho_w} - 1 \right) g}{\nu^2} \right]^{1/3} \qquad [3.6]$$

$$\frac{\tau_c}{g(\rho_s - \rho_w)d_{50}} = \begin{cases} 0.24D^{-1}, & D_* \leq 4 \\ 0.14D_*^{-0.64}, & 4 < D_* \leq 10 \\ 0.04D_*^{-0.1}, & 10 < D_* \leq 20 \\ 0.013D_*^{0.29}, & 20 < D_* \leq 150 \\ 0.045, & D_* > 150 \end{cases} \qquad [3.7]$$

Meyer-Peter and Muller bed load formulation

MPM approach is one of the widely used empirical method for the calculation of bed load transport in river studies (El Kadi Abderrezzak et al., 2016). Wide range of sediment size can be considered in this method [d_{50}=0.4-29mm]. In general, bed-load transport rate is calculated as a function of shield's number (θ) as

$$\theta = \frac{\tau_b}{(\rho_s - \rho_w)gd_{50}} \qquad [3.8]$$

With τ_b the bottom shear stress [Pa].

The dimensionless current induced sediment transport rate is given as;

$$\boldsymbol{\Phi}_b = \begin{cases} 0, & \theta < \theta_{cr} \\ \alpha_{mpm}(\theta - \theta_{cr})^{\frac{3}{2}}, & otherwise \end{cases} \qquad [3.9]$$

Where,

α_{mpm} is MPM coefficient whose value is taken as 8 in this study and θ_{cr} is the critical shield's parameter.

The dimensionless current-induced sediment transport rate $\boldsymbol{\Phi}_b$ is expressed by,

$$\boldsymbol{\Phi}_b = \frac{Q_b}{\sqrt{g\left(\frac{\rho_s}{\rho_w} - 1\right)d_{50}^3}} \qquad [3.10]$$

Q_b is the bedload transport rate per unit width.

➢ **Correction of magnitude and direction of bed-load transport**

The empirical approach of bed-load transport is valid under certain assumptions. Whenever these assumptions are not satisfied, corrections have to be applied to modify the direction and the magnitude of the bed-load transport. The three major corrections adopted in this study as depicted in **Figure 3.2** are,

i) The effect of the local bed slope,

ii) Secondary flow effect due to the channel meandering,

iii) Skin friction correction on bed shear stress and drag force due to the presence of bedforms.
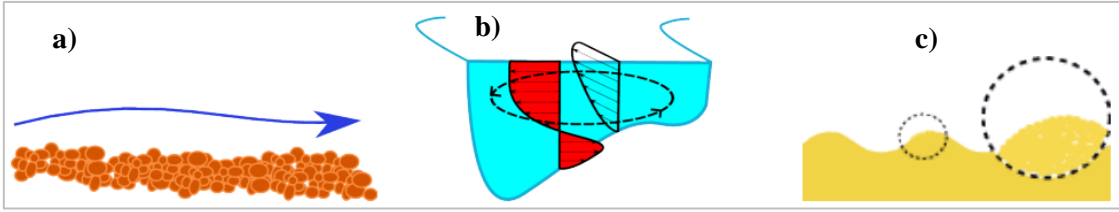
Figure 3.2 Schematic showing the effect of (a) bed slope, (b) secondary flow and (c) the bedforms [Adapted from (Tassi, 2018)]

i) Due to the combined action of transverse slope and secondary currents, the angle α between the direction of sediment transport and the x-axis will deviate from that of the bed shear stress.

$$\tan \alpha = \frac{\sin \delta - \dfrac{1}{f(\theta)} \dfrac{\partial z_b}{\partial y}}{\cos \delta - \dfrac{1}{f(\theta)} \dfrac{\partial z_b}{\partial x}}$$ [3.11]

Where,

$\dfrac{\partial z_b}{\partial x}$, $\dfrac{\partial z_b}{\partial y}$ = longitudinal and transverse bed slopes respectively

z_b = position of the bed

δ = the angle between the sediment transport vector and the flow direction modified by the spiral flow.

The sediment shape function $f(\theta)$ weighs the influence of the transverse bed slope and is expressed as a function of the non-dimensional shear stress or Shields parameter, θ. It can be computed according to Koch and Flokstra (1980):

$$f(\theta) = \frac{4}{6\theta}$$ [3.12]

ii) Correction of the effect of secondary flow on the direction of bed shear stress

In curved channels, due to the effect of secondary flow, the direction of the sediment transport will no longer coincide with the direction of the bed shear stress:

$$\delta = \tan^{-1}\left(\frac{v}{u}\right) - \tan^{-1}\left(\frac{A}{r_s}h\right) = \delta^* - \Delta\delta \qquad [3.13]$$

The terms highlighted in red accounts for the effect of the spiral motion on the sediment flux.

A = spiral flow coefficient

$\delta^*, \Delta\delta$ = the direction of the bed shear stress (which coincides with the direction of the
depth-averaged velocity) and the direction due to the effect of secondary currents

iii) The total bed shear stress is due to skin friction and bed form drag but only the component due to skin friction acts on bedload. The shear stress due to skin friction is expressed as:

$$\tau' = \mu\tau_b \qquad [3.14]$$

Where, $\tau_b = 0.5\rho_s C_f (V_x^2 + V_y^2)$ is the total bed shear stress and μ is the friction factor:

$$\mu = \frac{C_f'}{C_f} \qquad [3.15]$$

Where, C_f is the friction coefficient due to form drag plus skin friction (specified in the hydrodynamics module), and C_f' the friction coefficient due only to skin friction, which is computed as:

$$C_f' = 2\left(\frac{\kappa}{\log\left(\frac{12h}{k_s'}\right)}\right)^2 \qquad [3.16]$$

where k is the von Kármán coefficient (= 0:40), the roughness height $k_s' = \alpha_{ks}d_{50}$, α_{ks} the calibration parameter (Mendoza et al., 2016)

3.2.3 Solution steps

The different terms of the **Eq. [3.1-3.3]** are solved in one or more steps (in the case of advection by the method of characteristics which is considered in this study) following the finite element approach (Hervouet, 2007).

1. In the first step, advection terms corresponding to the transport of physical quantities V_x, V_y and h, k, ϵ. (The details on k-ϵ will be presented later in chapter 5)

2. In the second step, the remaining equations of propagation, diffusion and source terms are solved. This stage is resolved by finite element technique; the elimination of non-linear terms are made possible through time discretization. The variational formulation including time and space discretization then allows the transformation of continuous equations into a discrete linear system whose unknowns are the value of the physical quantities V_x, V_y and h at the nodes of the mesh. This system is then resolved by an iterative method of conjugate gradient type.

3.3 Model Validation

Before applying the model to the cases of this study, it was first validated on the experimental data from the published work. The experimental data used to validate the model was derived from the works of Da Silva and El-Tahawy (2008). As depicted in **Figure 3.3**, their experiment was performed in a sine-generated meandering channel consisting of two full meander length with a deflection angle 70^0. The inlet was connected to a straight channel measuring 2m in length. Constant steady discharge of 9.8l/s with average flow depth 5cm was supplied to the inlet rectangular channel of width 80cm having fixed banks. Non-uniform sand having median diameter d_{50}=0.65mm was used as bed material in the channel of bed slope of 1:250 along the centerline. The experiment was conducted for a duration of 170 minutes. The details hydraulic condition is presented in **Table 3.1**

Table 3.1: Hydraulic condition in the experiments of Da Silva and El-Tahaway (2008)

Run no.	Q (l/s)	h_{av}(cm)	S_0	V_{av}(m/s)	B/h_{av}	$(C_f)_{av}$	R_e	F_r	Re_*
4	9.8	5	1/250	0.25	16	15.4	12250	0.35	58
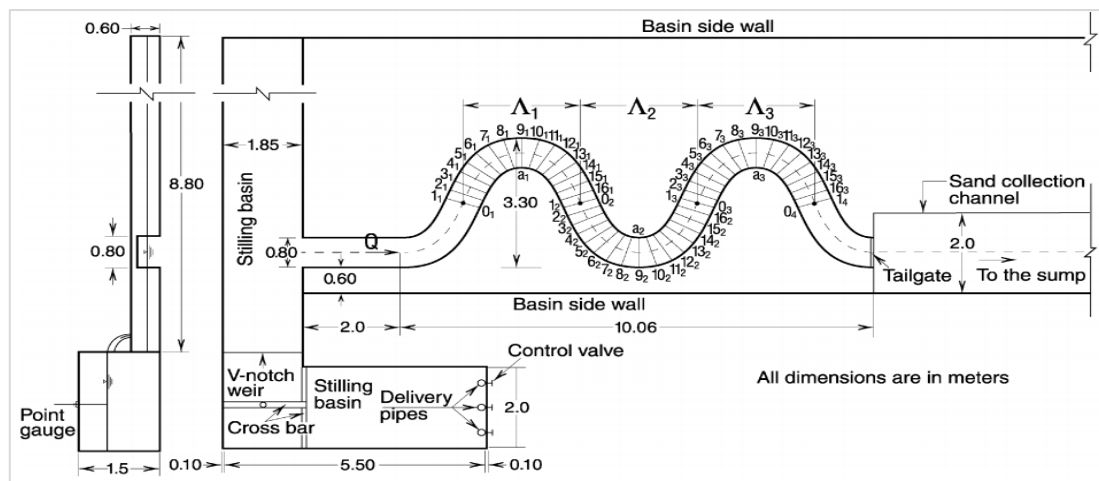
Figure 3.3 Experimental arrangement of Da Silva and El-Tahawy (2008)

Figure 3.4 (top and bottom) respectively represent the bed elevation changes at the end of the experiment and the simulation period of 170min. Negative values represent erosion while the positive ones represent the deposition. As can be seen, simulated results are in a close agreement with the observed ones in terms of the pattern of channel evolution. Simulation has satisfactorily reproduced the various bed morphological features obtained in the experiments like deep scour along the outer banks as well as the point bar along the inner bank. The location and the extent of erosion and deposition are nearly the same in both the experiments and the simulation. Apart from

a marginal underestimation of the erosion depth at some locations, the overall channel evolution in terms of both position and degree of erosion-deposition is almost the same. Based on these results, we can be sure of the reliability of the model used for analyzing the channel bed development in meandering channels.
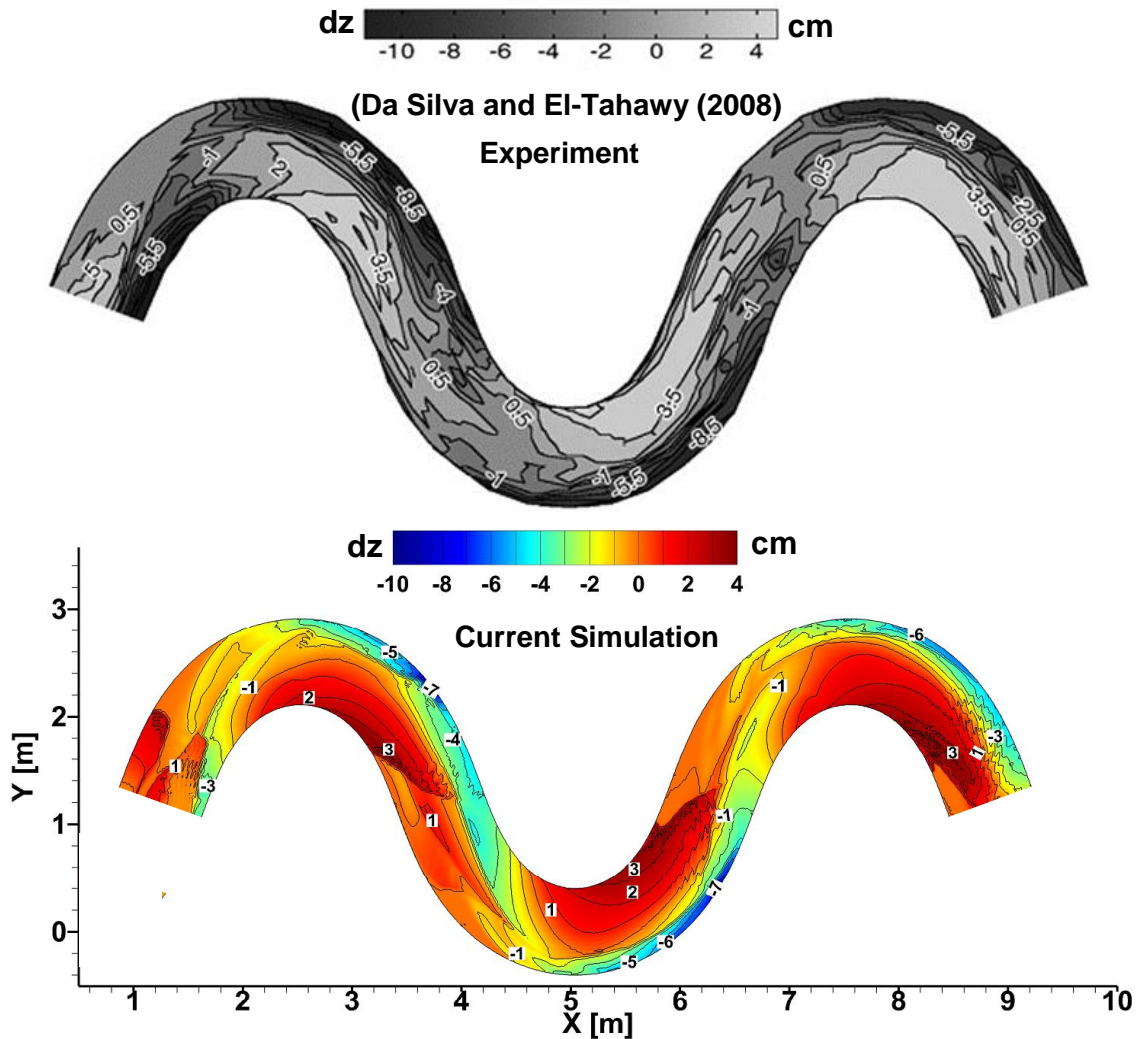
Figure 3.4 Comparison of the experimental (top) and simulated (bottom) bed evolution.

3.4 Description of the simulation cases

After validating the model, different cases were performed in the current experimental channels, both with and without groynes. In each of the channels, first, the simulation was carried out without groynes. The objective was to see whether the erosion-deposition zones match the experimental results. In the cases with groynes, scenarios were created changing the position and orientation. Two positions, one starting at the apex and the other starting downstream of the apex were considered. In terms of the orientation, 90^0 and 120^0 to the bankline in upstream direction

were tested. **Table 3.2** represents the different simulation cases as explained here. Altogether 12 simulation cases were performed. The flow, channel hydraulic condition and sediment properties in the simulation were kept the same as that of the experiment.

Table 3.2 Representation of the 2D simulation cases presented in the study

	NO GROYNES	IMPERMEABLE GROYNES				PERMEABLE GROYNES
ORIENTATION		90^0		120^0		90^0
POSITION		Apex	D/S of apex	Apex	D/S of apex	Apex
Channels						
Ch-45	Ch45NG	Ch45AP90	Ch45DS90	Ch45AP120	Ch45DS120	Ch45AP/PM90
Ch-60	Ch60NG	Ch60AP90	Ch60DS90	Ch60AP120	Ch60DS120	Ch60AP/PM90

3.4.1 Design and arrangement of Groynes

The design of the groynes namely its length, the spacing and the orientation were based on the findings from the previous researches as well as the available guidelines (Lagasse et al., 2009). The length of the groynes was fixed to 3cm i.e. 15% of the channel width whereas the spacing between the groynes was set 6cm i.e. 2 times the length of the groynes. Lagasse et al. (2009) suggested that the length of the impermeable groynes should be less than 20% of the channel width. Yossef (2002) suggested that the spacing of the groynes should be between 2-6 times the channel widths for better bank protection. For the position of groynes, in case 2 groynes started from the apex and ended at 75% of the valley length between the next outer bank apex. In case 3 where groynes started from downstream of the apex, they were positioned in the middle half of the distance between the successive outer bank apices. Accordingly, the number of groynes in each of the channels were different. **Figure 3.5** shows the arrangement of groynes in two types of channels used in this study. Groynes were placed in two successive outer banks. In **Figure 3.6** (**a-d**), the exact and detailed positioning of the groynes is shown for Ch-45.

Figure 3.5 Sample arrangement of groynes for case Ch45DS90 (black) and Ch60DS90 (red)

Figure 3.6 Positioning of groynes for different cases in Ch-45

The positioning of the groynes is exactly the same in Ch-60. However, due to the longer length of the channel, the number of groynes were higher in Ch-60 case.

3.4.2 Boundary Condition

For the upstream or the inlet boundary, we set constant discharge whereas, for the downstream or the outlet boundary, the average water depth of the initial flat-bed condition i.e. 2.86cm was fixed. There was no supply of sediment from outside i.e. clear water simulation. In all cases, simulation was carried out for a duration of one hour. The straight channels at the upstream and the downstream ends were set as a non-erodible bed. All the simulations started with uniform depth (2.86cm) of water everywhere in the domain.

3.5 Results and Discussions

The validated model was applied to the current experimental cases of this study. Taking information from the experimental results discussed in chapter 2, we performed numerical simulations to analyze the channel flow and morphological response to the different scenario of groynes arrangement. The simulation was performed considering the movable bed and fixed bank. Results are discussed separately for each case and comparison is made between both channels.

3.5.1 Without Groynes

First, the simulation was done without considering the groynes. The objective was to see whether the location of erosion-deposition zones will resemble the experimental observations. Consequently, the locations of the placement of the groynes could be decided.

1) Channel morphological variations

Figure 3.7 shows the channel evolution and the bed shear stress distribution at the end of the simulation (t=60 min). Flow direction is from left to the right. **Figure 3.7** (a and b) represent Ch45NG whereas **Figure 3.7** (c and d) represent Ch60NG.
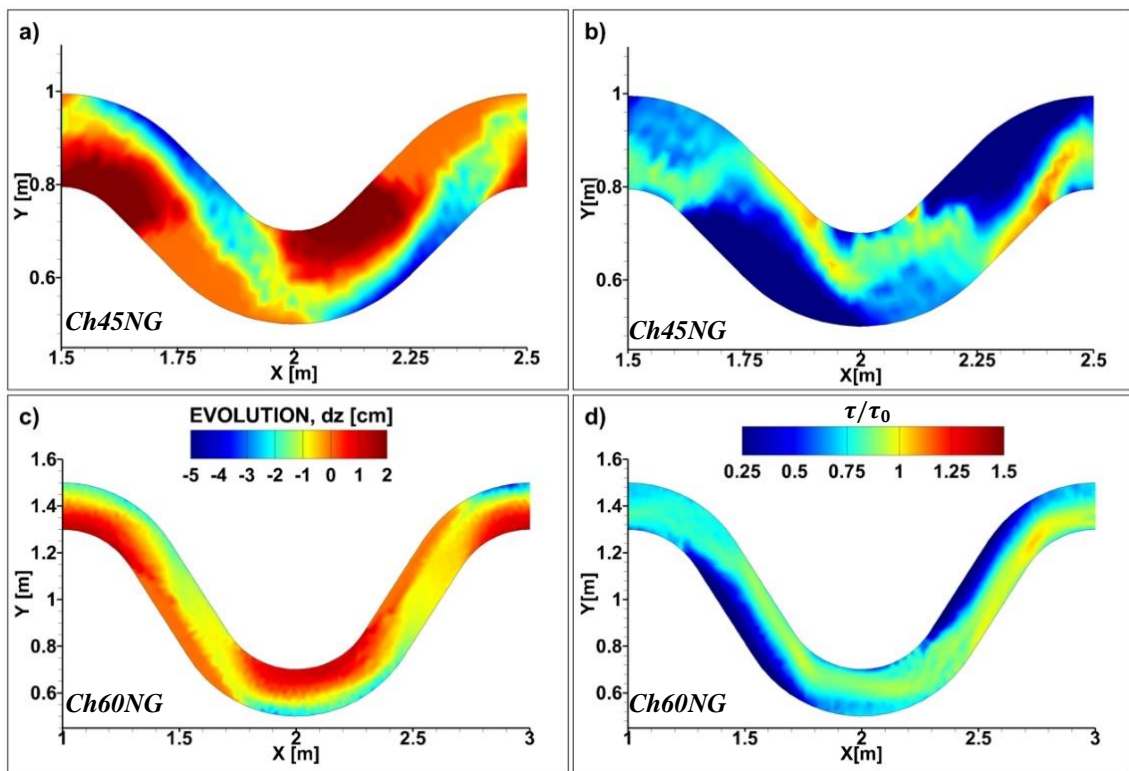
Figure 3.7 (a, c) Bed evolution and (b, d) distribution of τ/τ_0 at the end (t=60 min)

Results showed that in low sinuosity channel, erosion of the bed near the outer bank started slightly downstream of the apex and erosion extended nearly throughout the outer bank length. But as the sinuosity increase as that in Ch60NG, the erosion zone shifted upstream of the apex and the maximum erosion zone was located around the outer bank apex as shown in **Figure 3.7** (a & c). The location, as well as the size of the point bar, also varied according to the channels. The point bar formed downstream of the apex of the inner bend with a bigger size relative to the channel length in low sinuosity Ch45NG. But in case of Ch60NG, point bar formed from the upstream of inner bend apex with relatively shorter length downstream. Bed shear stress (τ) was

made dimensionless dividing by the channel average value ($\tau_0 = \gamma R S_0 = 0.397 \text{N/m}^2$) corresponding to the initial flat bed, where γ=specific gravity of water and R= hydraulic radius. Distribution of bed shear stress as shown in **Figure 3.7** (b & d) suggests that higher bed shear stress were concentrated around the exit of the bend. The pattern of channel evolution phenomena in terms of erosion-deposition zones closely resemble the experimental results described in the **section 3** as the locations of bed having higher erosion near the bank is the same in both the simulation and experiment. And the banks are likely to be eroded at the same locations where the bed adjacent to them is eroded (da Silva and El-Tahawy, 2008).
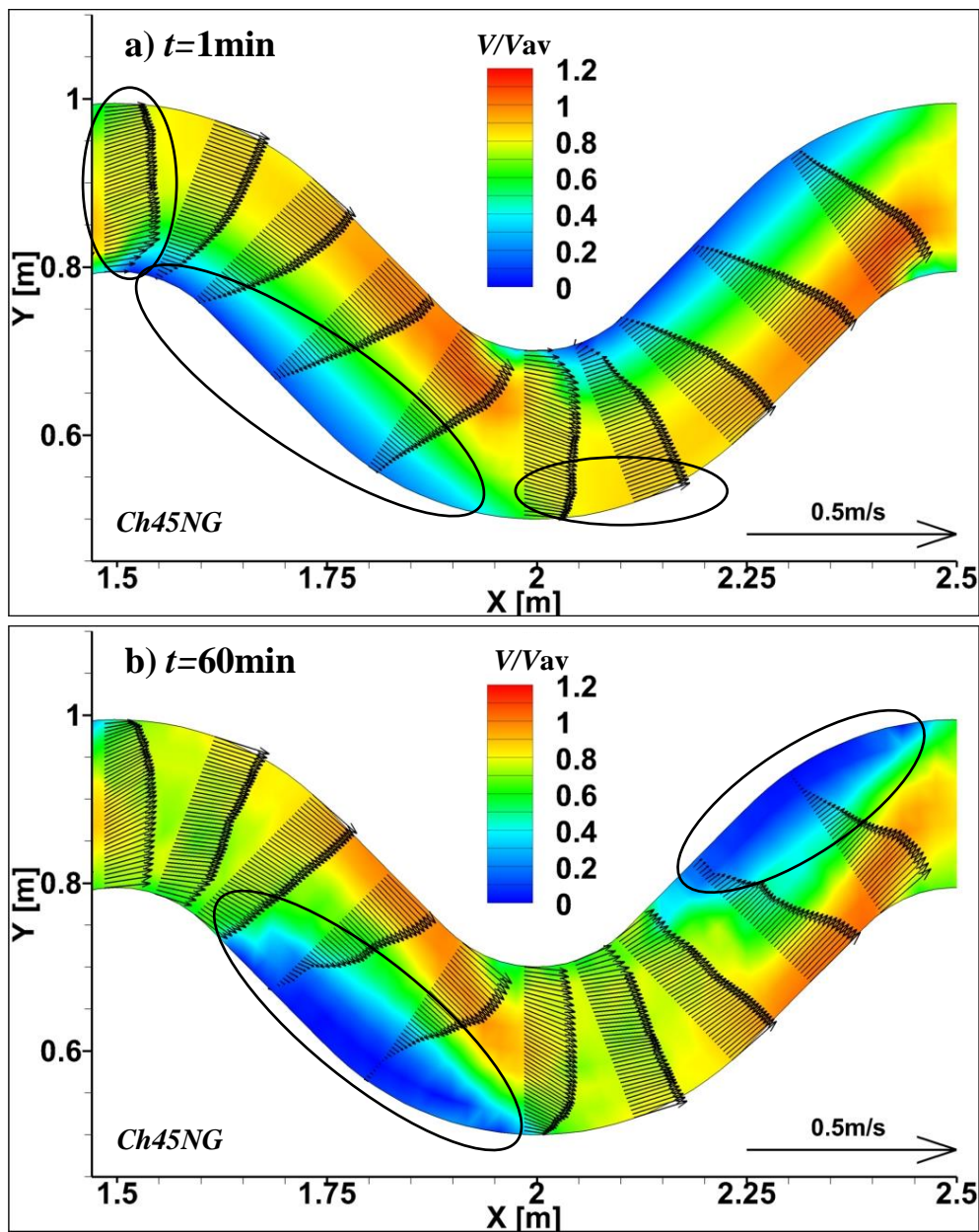
Figure 3.8 (a & b) Distribution of *V/V*av and the cross-sectional velocity vectors for Ch45NG
a) *t*=1min b) *t*=60min.

58
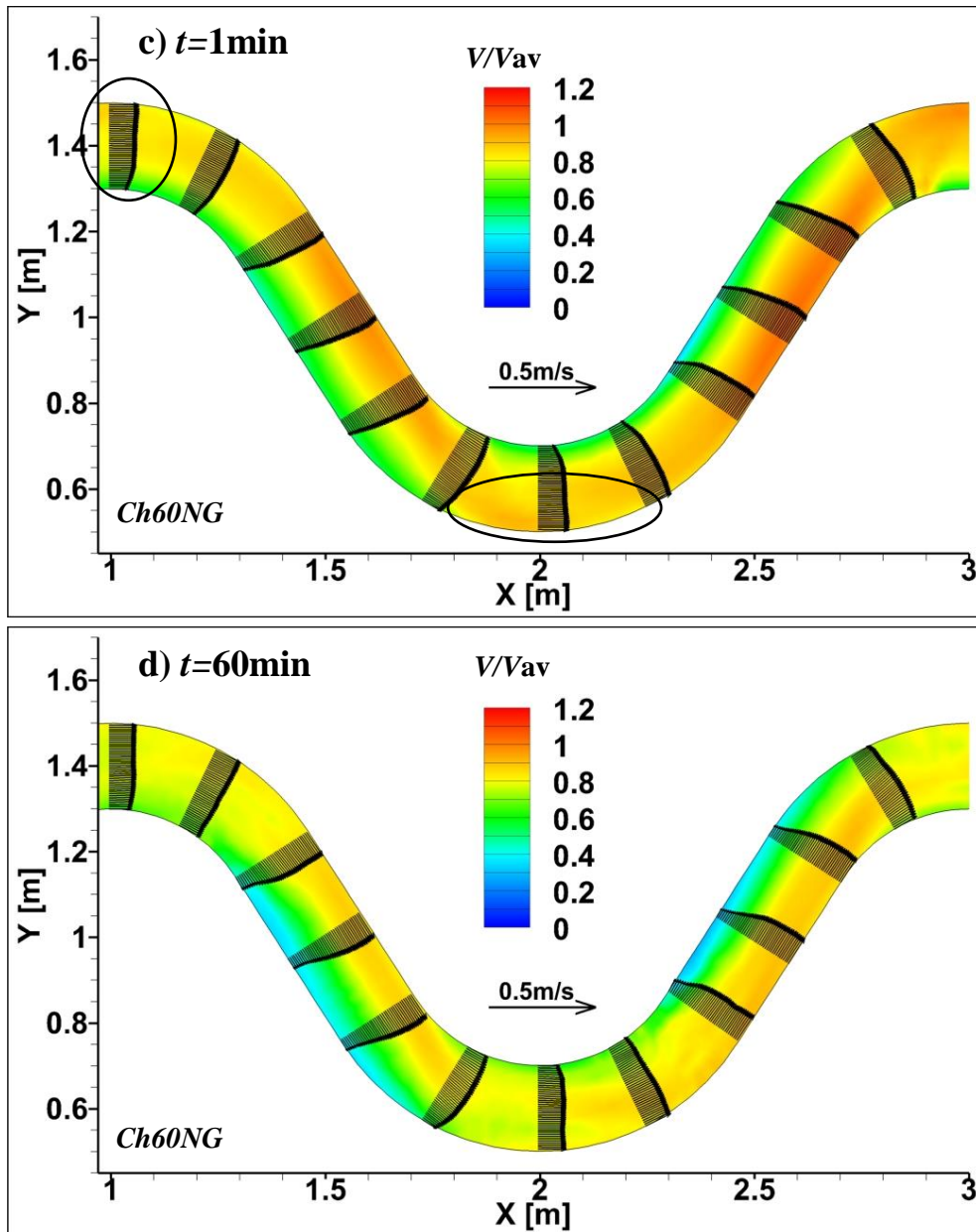
Figure 3.8 (c & d) Distribution of *V/V*av and the cross-sectional velocity vectors for Ch60NG
c) *t*=1min d) *t*=60min.

To correlate the channel erosion-deposition process with the velocity pattern, we plotted the velocity distribution including the cross-sectional velocity vectors. The depth-averaged velocity (*V*) is normalized by the channel averaged velocity (*V*av=16.6cm/s) corresponding the initial flat-bed condition. **Figure 3.8** (**a-b** and **c-d**) illustrates the distribution of *V/V*av for case Ch45NG and Ch60NG respectively. Comparing **Figure 3.8 (a & b)** for Ch45, the cross-sectional velocity gradient further increased with time. The recirculation region of low velocity increased across the channel width but reduced in length. For both channels, velocity field was higher in the initial time *t*=1min and decreased in the final stage *t*=60min as a result of the bed development and

channel adjustment. The recirculation region in Ch60 was relatively smaller. The flow separation begin slightly upstream of the apex in Ch60 (**Figure 3.8c**) while it was slightly downstream of inner bend apex in Ch45 (**Figure 3.8a**).Comparing all the plots of channel Ch-45 and Ch-60, it can be seen that cross-sectional velocity variation is more pronounced in Ch45NG. For Ch45, higher velocities in general are concentrated close to the inner bend apex whereas in Ch60, higher velocities located around the crossover region and slightly downstream. The erosion of the bank were higher in the same location as presented in the experimental results in chapter 2. A recirculating region of low velocity was formed starting from the crossover region to the apex. The zone of higher velocities converged downstream of the apex in the next bend in Ch45. On the other hand, the overall distribution of V/V_{av} was more uniform in Ch60NG. The recirculating zone of low velocity was smaller. Similarly, the cross-stream velocity variation was also lesser. The higher velocities after leaving the apex converged upstream of the apex. This is due to the fact that the formation of point bar was around the apex area whereas in case of Ch45NG, point bar formed downstream of the apex. As a result, the approach flow was deflected before it reached the apex in Ch60NG.

3.5.2 Groynes at the Apex
1) Perpendicular to the bankline
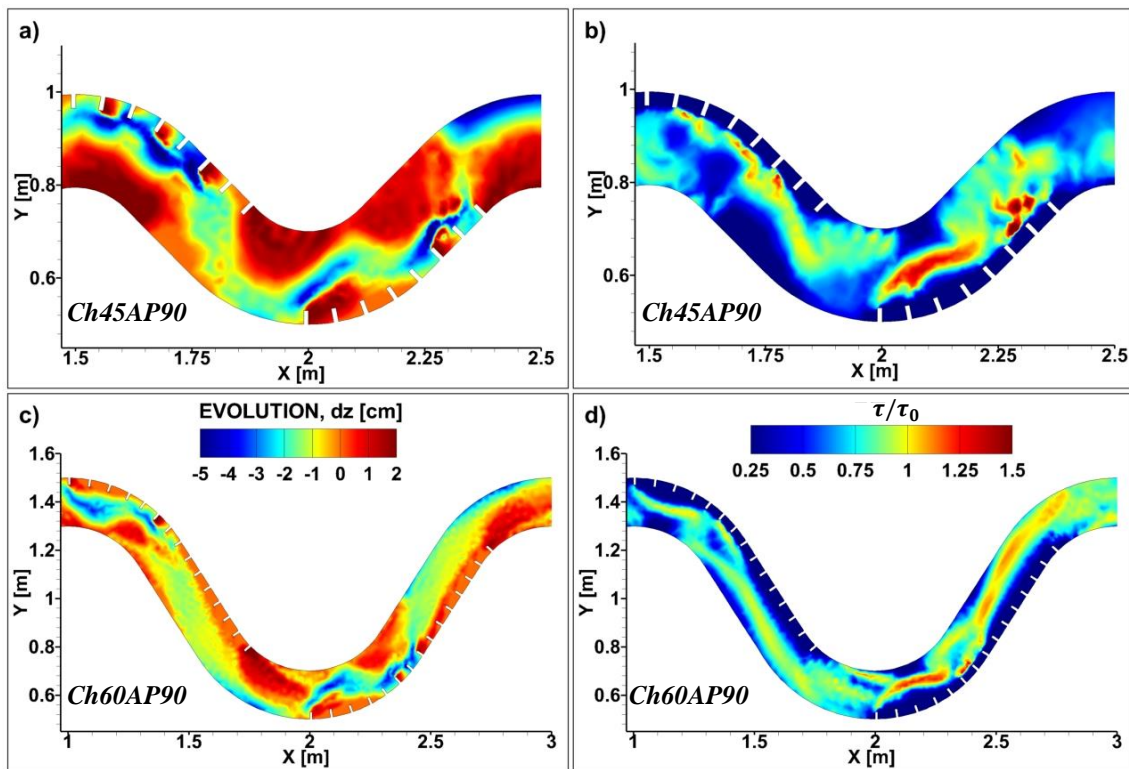
Figure 3.9 (a, c) Bed evolution and (b, d) distribution of τ/τ_0 at the end (t=60 min)

Figure 3.9 represents the bed evolution and the bed shear stress distribution at the end of 60min of simulation. In the first bend of Ch45AP90 where the undisturbed flow approached the first series of groynes, deep scour greater than 5cm was formed at the groynes tip and erosion was also higher in the embayment area as shown in **Figure 3.9(a)**. This phenomenon continued up to the crossover region. However, in Ch60AP90 of higher sinuosity, scour was less and closer to the channel center rather than the groynes tip. After passing the crossover region, due to the divergence of flow, a significant deposition occurred immediately downstream of the last groynes in both the channels and consequently, erosion was shifted to the opposite bank. This tendency was similar in both the channels which can be seen in **Figure 3.9 (a & c)**. The size of the point bar in the first inner (convex) bend also reduced due to the effect of groynes. In the second series of groynes in the next bend, the channel morphology was quite similar to the first bend for Ch60AP90. However, in Ch45AP90, considerable deposition occurred in between most of the groynes. One of the important issue to be considered in implementing the river bank protection measures like groynes is the safety of the opposite bank. We can see from **Figure 3.9 (a)** that after exiting from the groynes in the next bend significant erosion occurred compared to the case of no groynes in Figure **3.7 (a).** Comparing the distribution of bed shear stress in **Figure 3.9 (b & d)** suggest that the shifting of the higher bed shear stress zone towards the channel center is more prominent in Ch60AP90 as the higher bed shear stress is mostly concentrated around the groynes tip in Ch45AP90.

The distribution of V/V_{av} in **Figure 3.10 (top)** shows that the higher velocities are concentrated around the groynes tip for Ch45AP90. In the first bend, where the undisturbed flow approached the groynes, the deflection of velocity was insignificant until the groynes of the crossover. This is because, in channels of lower deflection angle, velocity is concentrated downstream of the apex. However, the groynes near the exit deflected the high velocities towards the opposite bank upstream of the apex. As a result, in the second bend, higher deflection could be seen in the first groynes of the second bend. But the effect of the remaining groynes was minimum in deflecting the high-velocity zone towards the channels. This clearly suggests the need for different groynes positioning for low sinuosity channels.

The overall functionality of the groynes was better achieved in case Ch60AP90 which can be clearly observed from the distribution of V/V_{av} in **Figure 3.10 (bottom)** where the zone of maximum velocity is more pushed towards the channel center. In case of Ch60AP90, the deflection started from the first groynes. This deflected velocity again reattached around the groynes approximately near the crossover region. After leaving the crossover region, the deflected velocity converged on the opposite banks which suggest that the groynes further downstream of the crossover might not be required. Nearly all the groynes indicate some deflective action against high velocity in Ch60AP90.
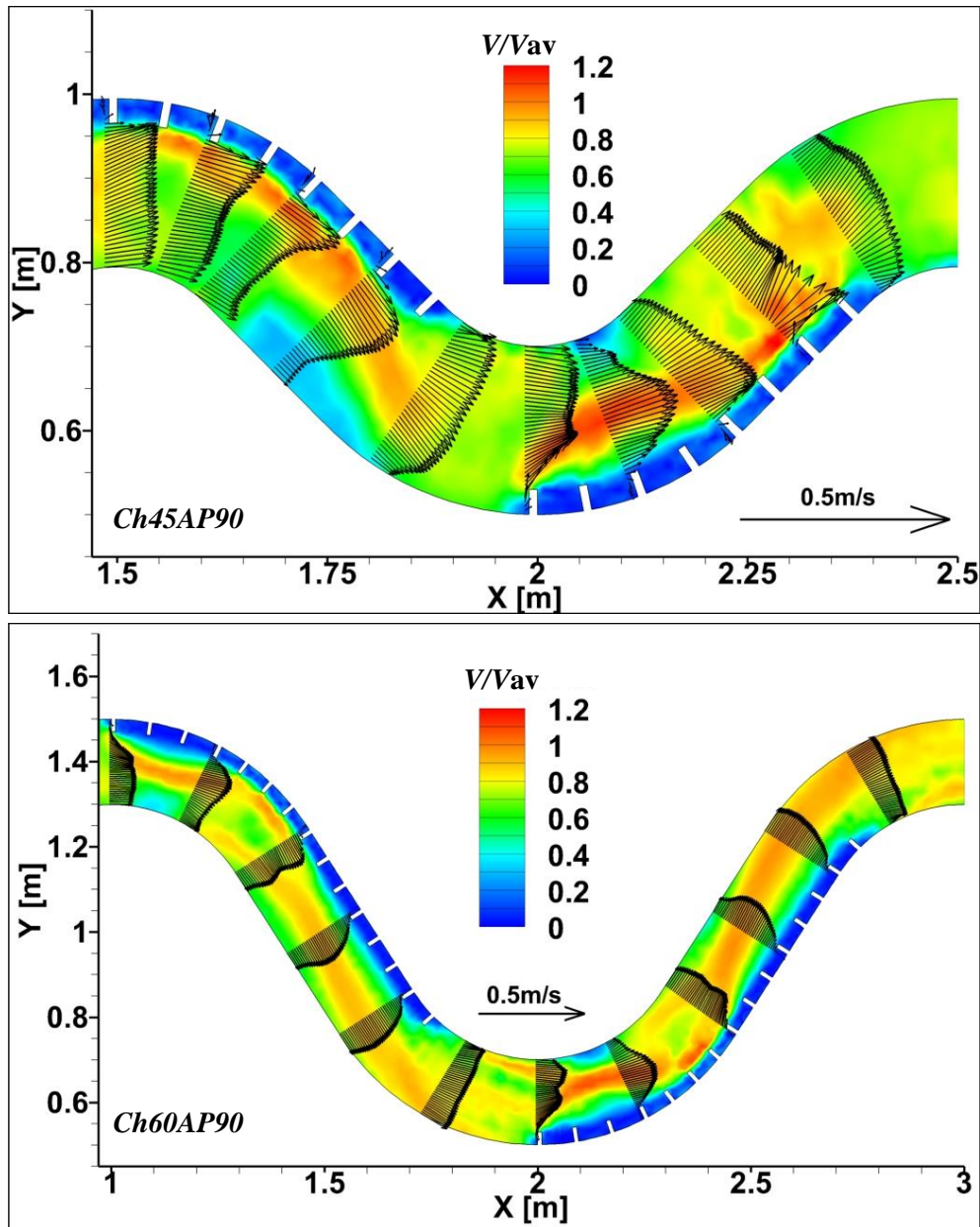
Figure 3.10 Distribution of V/V_{av} and the cross-sectional velocity vectors

2) 120-degree to the bankline

Next, the orientation of the groynes was changed from 90 to 120 degree but the position were kept the same. **Figure 3.11** represents the channel evolution and the distribution of τ/τ_0 for case Ch45AP120 and Ch60AP120.

Similar to the previous case Ch45AP90, the scour around the initial groynes are also higher for this case. The erosion of the opposite bank after leaving the first series of groynes is significantly increased. This is mainly due to the deflection of velocity by the groynes around the crossover region. It is also evident from **Figure 3.11 (a)** that the deposition in the region of groynes
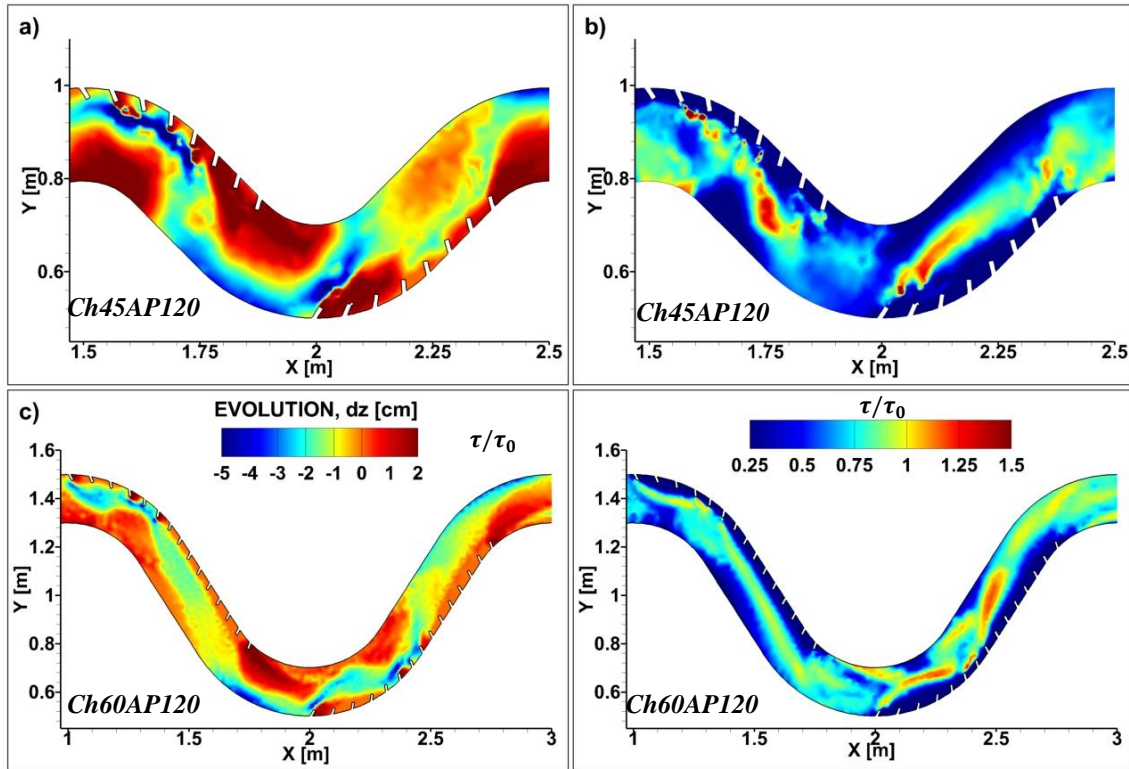
Figure 3.11 (a, c) Bed evolution and (b, d) distribution of τ/τ_0 at the end (t=60min)

downstream of crossover is also high. Also from **Figure 3.12 (top),** it can be seen that the deflection of velocity is comparatively higher in Ch45AP120 than that in case Ch45AP90. Consequently, the point bar in the second bend is nearly entirely eroded due to the deflection by the groynes.

In Ch60AP120, the overall tendency was similar to that of Ch60AP90 with minimum differences. The deposition in the point bar in the first bend was higher in this case. This is because the 120-degree groynes caused less deflection than 90-degree groynes. In the case Ch60AP90, the erosion in the first opposite bend started around the crossover region whereas in the case Ch60AP120, the erosion was shifted downstream. Consequently, the degree of erosion near the upstream of the next outer bank apex was higher. The bed shear stress distribution pattern is more or less similar to the previous case. Exactly at the apex, the point bar was eroded. However, in the downstream and the upstream, the deposition was nearly the same. The velocity in the zone of maximum velocity was slightly lower than the previous case Ch60AP120. The deflection of the velocity by the groynes causes the convergence of higher velocities near the crossover of the opposite bank in the second bend. Consequently, near the bank higher erosion could be seen in **Figure 3.11**. Based on the above observations, it could be said that the overall impact or the sensitiveness of the angle of inclination of the groynes in such channels are minimum.
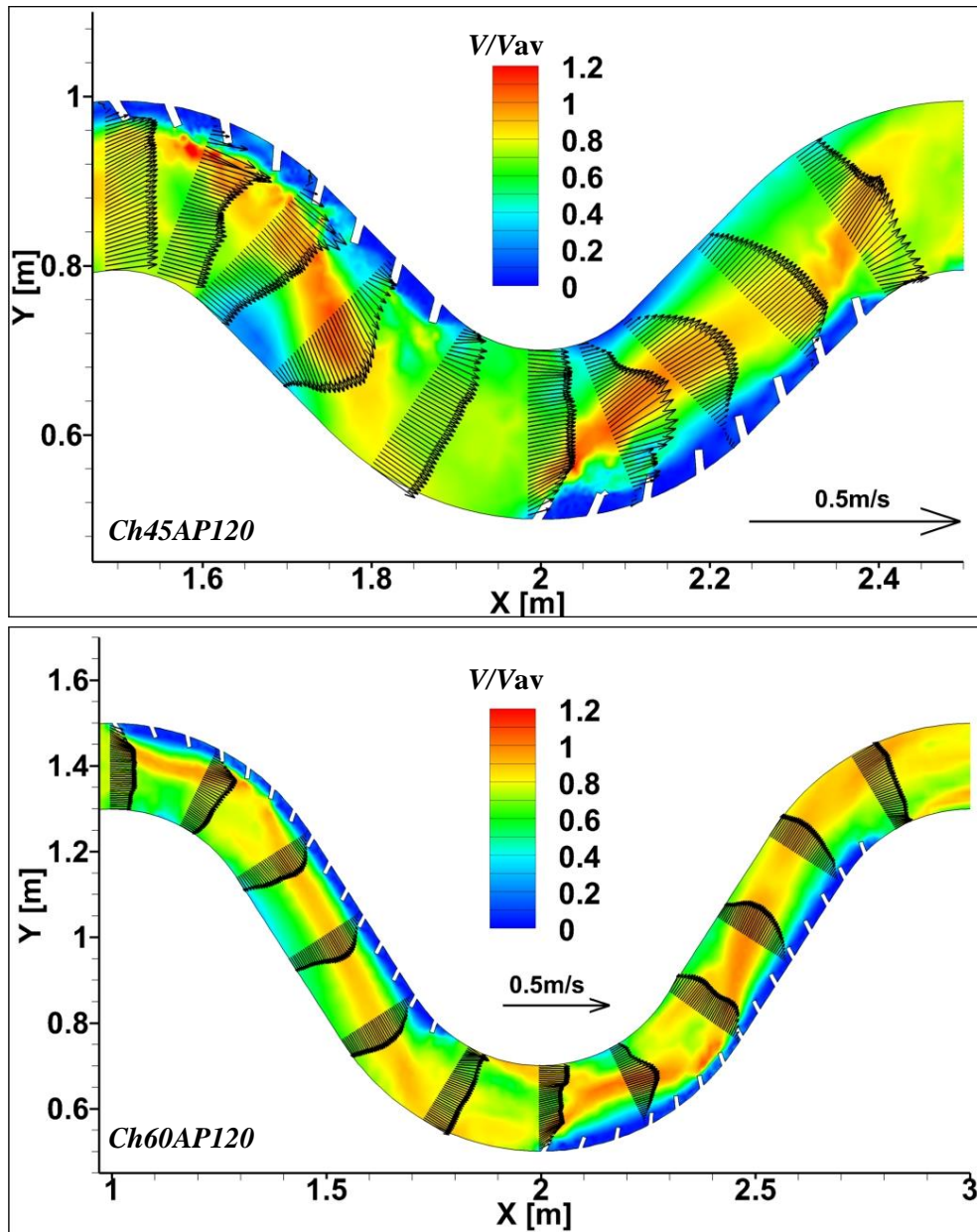
Figure 3.12 Distribution of V/V_{av} and the cross-sectional velocity vectors

3.5.3 Groynes at downstream of Apex

1) Perpendicular to the bankline

In this case, the position of the groynes was changed with the first groynes beginning from the downstream of the apex. The series of groynes were placed such that the first and the last groynes of each series lie in the middle half of the distance between two successive apices. Accordingly, the first groynes are positioned downstream of the apex. **Figure 3.13** illustrates the channel evolution and the bed shear stress distribution at the end of the simulation of 60min.
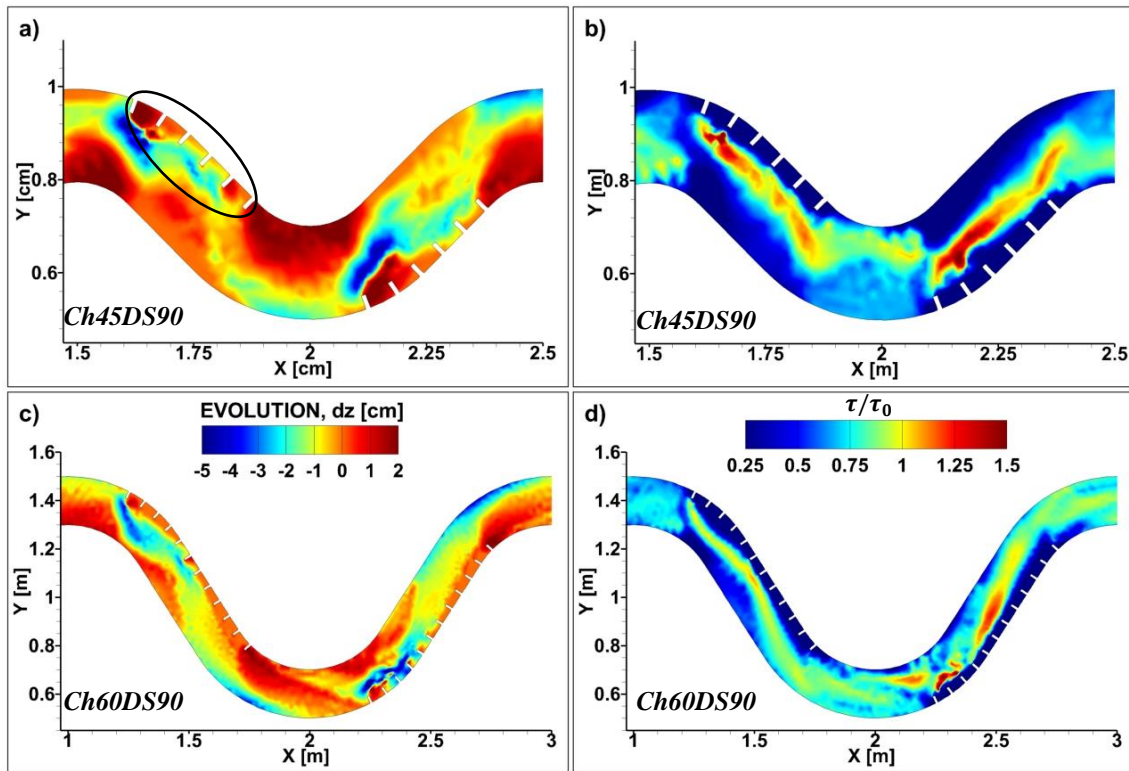
Figure 3.13 (a, c) Bed evolution and (b, d) distribution of τ/τ_0 at the end (t=60min)

As compared to the previous groynes arrangement beginning from the apex, the performance was quite different and improved. The major difference was in the formation of deep scour and the erosion in space between the groynes. From **Figure 3.13 (a)** and **3.9 (a)** of ch-45, it can be clearly differentiated that the scour holes near the tip of most of the groynes considerably decreased. Similarly, the erosion between the groynes was less severe in Ch45DS90. At the same time, the size of the point bar in the convex bend in front of both first and second series of groynes was also reduced. This is mainly due to the fact that in the channel of lower sinuosity and low angle of deflection, the approach flow is more concentrated downstream of the apex. Consequently, the flow could be more deflected by the initial groynes. The erosion of the opposite bank after exiting the second series of groynes was also lower in this case which further suggests its effectiveness. The bed shear stress distribution pattern as shown in Figure **3.13 (b)** is also more uniform and higher stress zone is more shifted to the channel center as compared to **Figure 3.9 (b)** of Ch45AP90. In Ch-60 as compared to Ch-45, differences between Ch60AP90 and Ch60DS90 were less distinct. The area of erosion in the first bend is slightly less. Although the bed shear stress distribution pattern is similar to Ch60AP90, the shift of higher bed shear stress towards the channel center is slightly less as shown in **Figure 3.13(d)** which shows the effect of the change in groynes orientation is dependent on the meandering channel characteristics.

65
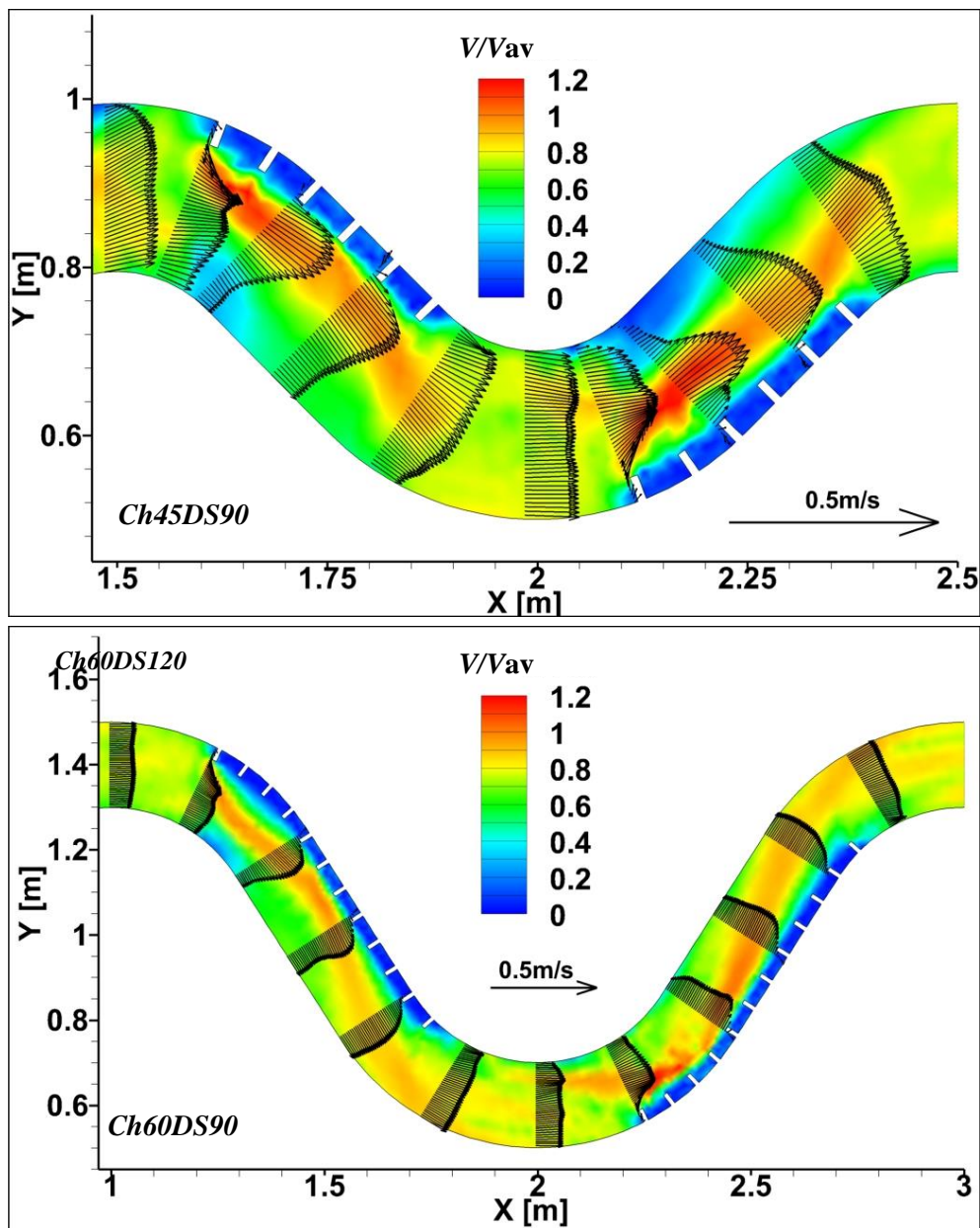
Figure 3.14 Distribution of V/V_{av} and the cross-sectional velocity vectors

The distribution of velocity also clearly suggests that the higher velocity zone was more deflected towards the channel in Ch45DS90 as compared to the case of Ch45AP90. Notice the deflection at the first groynes in **Figure 3.14 (top)** and comparing it with **Figure 3. 10 (top),** it can be said that in channels of lower deflection angle, the effectiveness of the groynes can be increased if it is placed downstream of the apex. However, in Ch60DS90, the overall difference is quite insignificant as seen from **Figure 3.14 (bottom)**. This suggests that the lower sinuosity channels are more sensitive to the change in the groynes position. Therefore while planning the bank protection works, these factors need to be taken care of.

2) 120^0 to the bankline
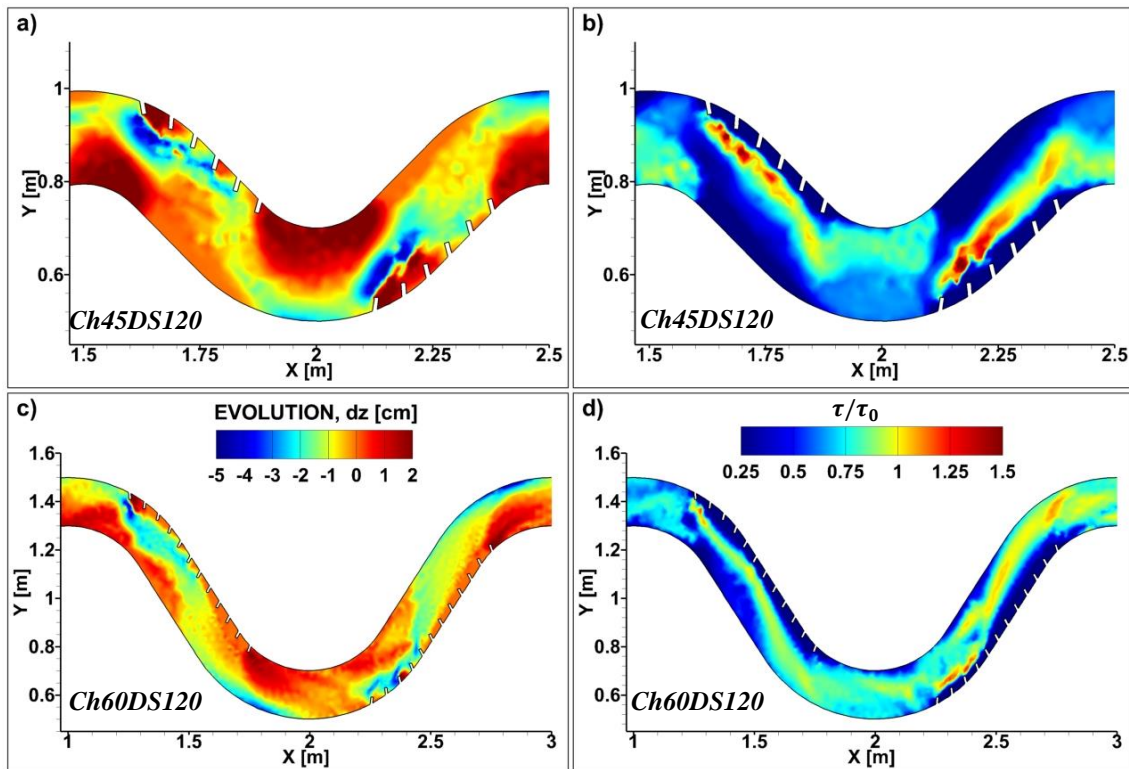
Figure 3.15 (a, c) Bed evolution and (b, d) distribution of τ/τ_0 at the end (t=60min)

As discussed in **section 3.5.2 (2)**, the variations in the overall pattern of the bed evolution in case of 120^0 groynes were not very different compared to that of 90^0 cases which can be seen in **Figure 3.15 (a & c)**. In the first series of groynes in Ch-45, the scour around the groynes tip was higher as well as the groynes with higher scour were greater in number. Consequently, the effect of the groynes on the shifting of erosion towards the channel and the opposite bank was slightly lower as compared to the case Ch45DS90. The deposition in the embayment was higher in the initial 1 or two groynes as in the case of Ch45DS90. Similarly, the shift of the higher bed shear stress zone towards the channel was lower in Ch45DS120 compared to Ch45DS90 which can be seen from **Figure 3.15 (b).**

Similarly, in Ch60DS120, the scour depth at the first groynes tip was higher. Also, the erosion in the embayment area was higher in the first series of groynes where the flow first approached towards them. The comparison between the 90^0 and 120^0 groynes suggest that the role of the initial groynes are vital in determining the overall effectiveness of the remaining groynes. As we observed that the effect of the change in orientation was minimum in the overall change in channel evolution and other bed patterns. Therefore the position of the groynes is more vital in determining the effect of groynes on the channel development and bank erosion.
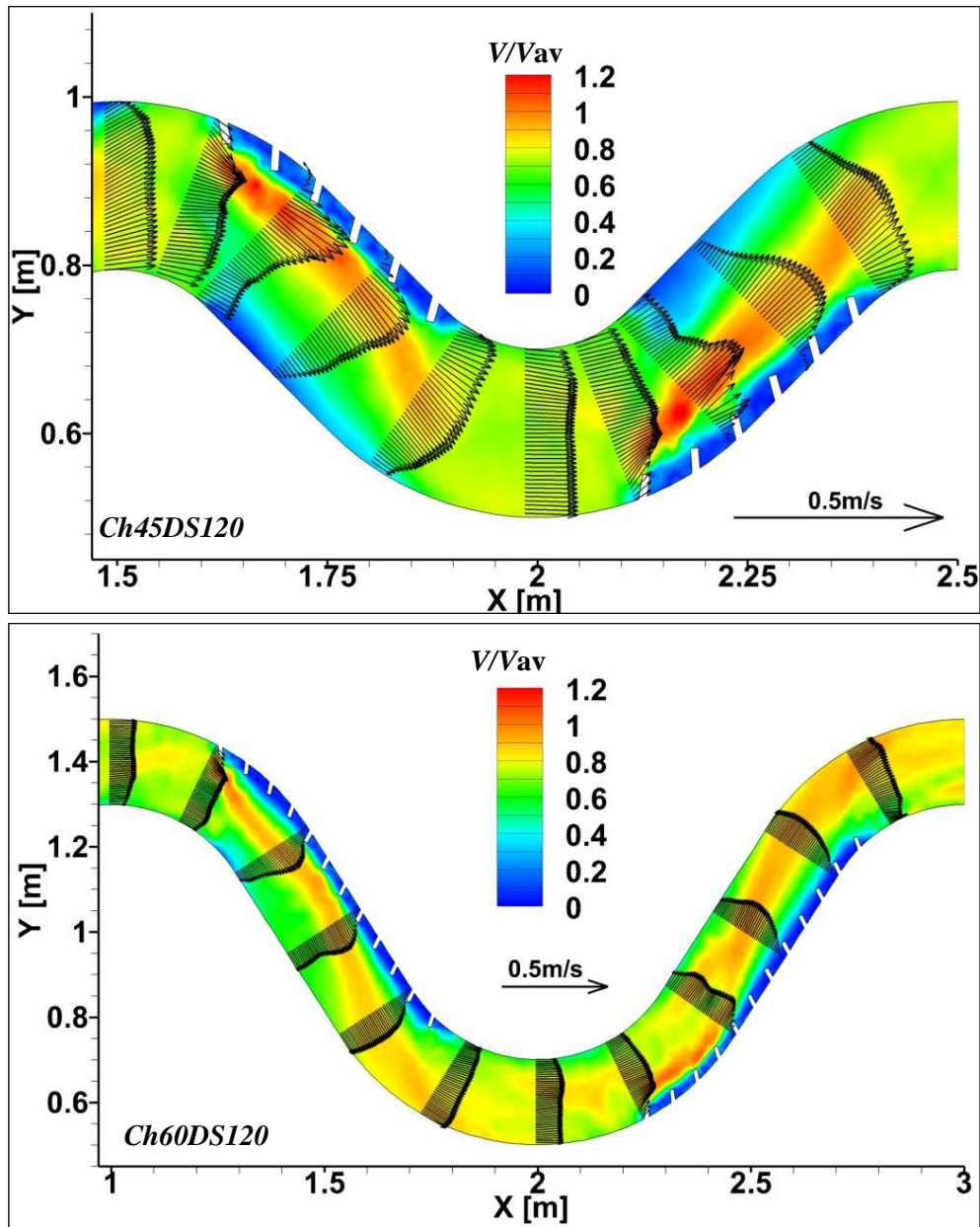
Figure 3.16 Distribution of V/V_{av} and the cross-sectional velocity vectors

The distribution of V/V_{av} shows that the high velocity is close to the groynes in case Ch45DS120 along with both the series of groynes. This clearly indicates that the deflection of high velocity is achieved better in the case of 90^0 groynes. As a result of the lower deflection, the extent of the stagnant zone of low velocity in the opposite inner bend was greater than Ch45DS90, especially in the first bend. In Ch-60, the difference is relatively smaller in comparison to Ch-45. The flow separation due to the first groynes tends to reattach again around the cross-over region. The deflection tendency is more or less similar. However, the overall channel-averaged velocity was slightly lower in this case.

3.5.4 Permeable type

a) Ch45AP/PM90

Legend

Gridlines

- - - - Centreline

Channel45

Piles

b) Ch60AP/PM90
Gridlines

Leg

—— Gridlines

- - - - Centreline

Channel60

Piles
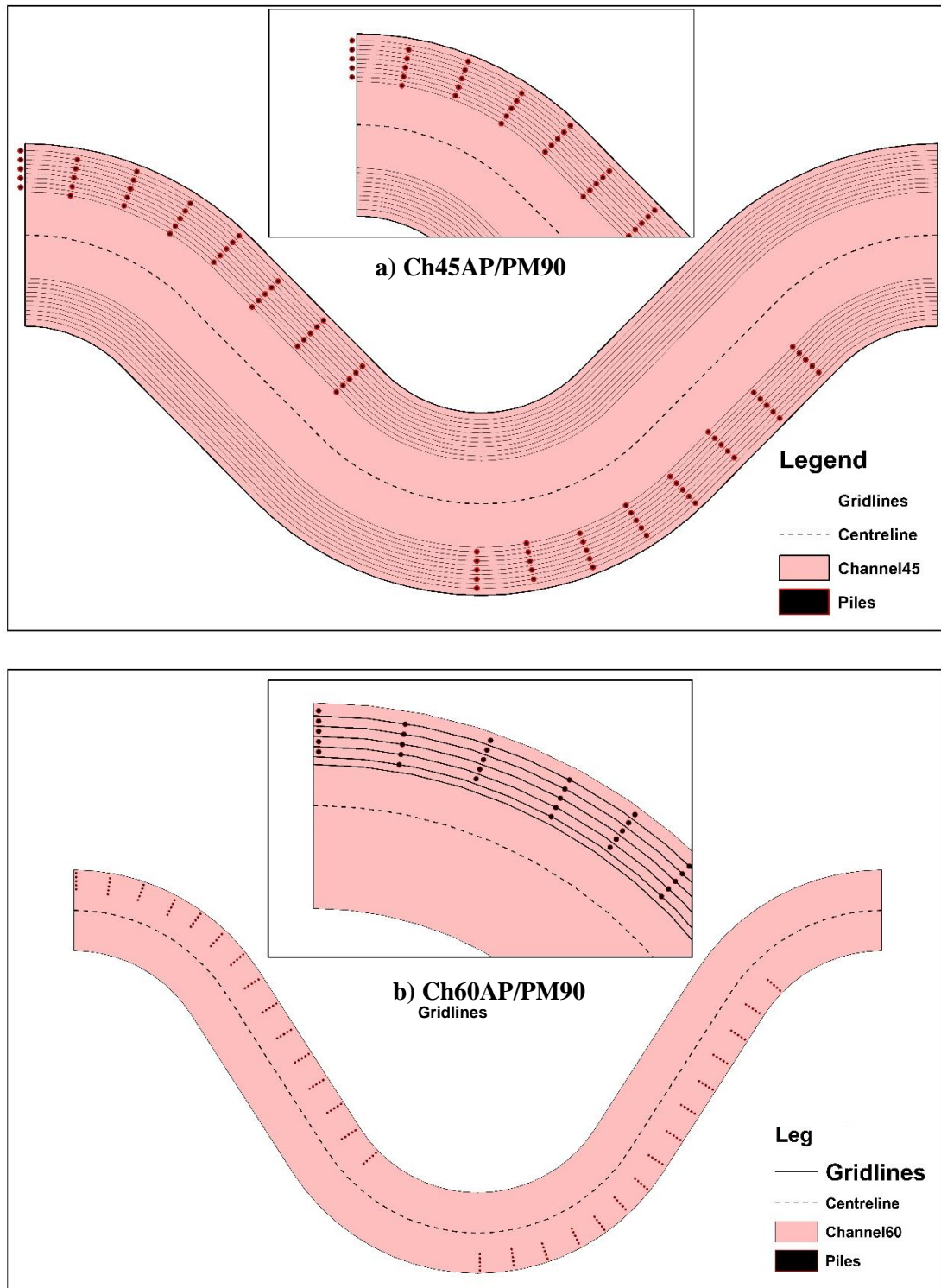
Figure 3.17 Schematic layout of the arrangement of permeable type structures in
a) Ch45AP/PM90 and b) Ch60AP/PM90
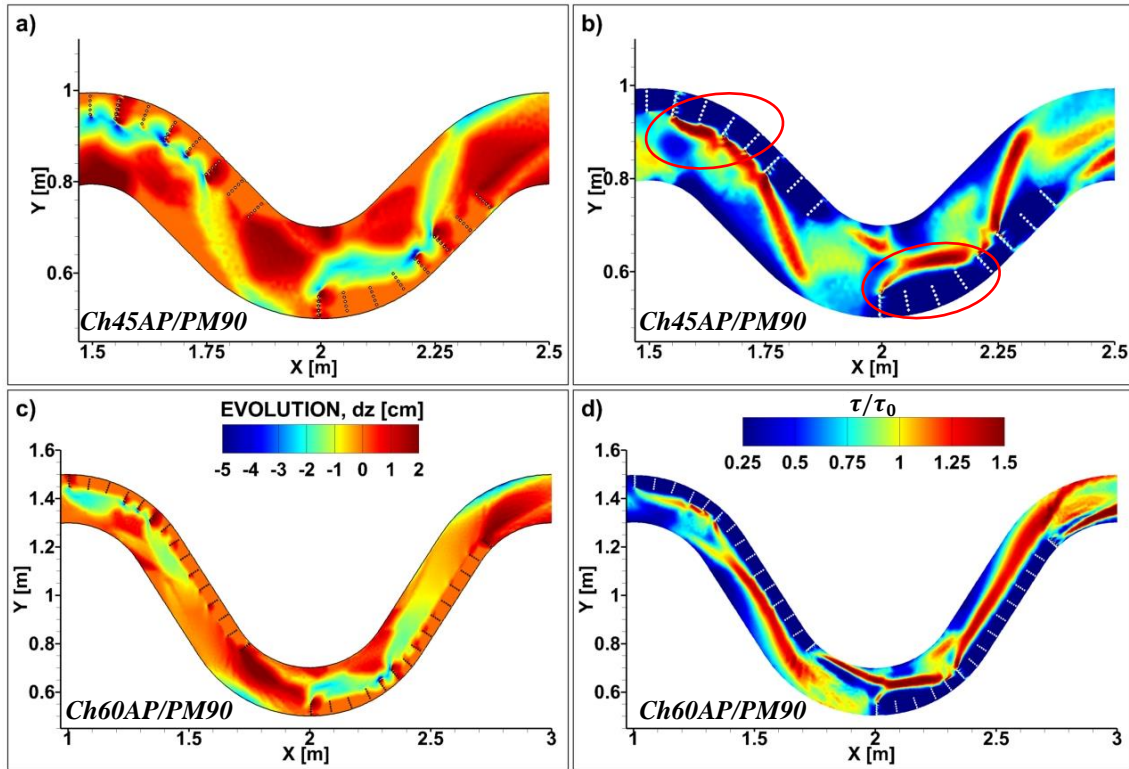
Figure 3.18 (a, c) Bed evolution and (b, d) distribution of τ/τ_0 at the end (t=60min).

In the next case, we considered permeable type structures consisting of 5 piles each of diameter 5mm and spaced 1cm center to center. The schematic layout of the arrangement of permeable type groynes consisting of the circular piles are illustrated in **Figure 3.17 a** and **b.** The spacing between the two successive pile series along the channel bank was 6cm. The two successive piles are arranged in a staggered grid such that the flow leaving from the space between the two piles will strike the pile in the next series. Permeable groynes are used as an alternative to the impermeable groynes.

With permeable groynes, the overall area of the erosion was smaller in both the channels. The scour was again higher around the groynes tip and the embayment area in Ch-45 [**Figure 3.18 (a)**]. However, the erosion didn't reach the bank area. Similar to the case of impermeable groynes, after the crossover region [X=1.75m], the erosion tends to shift away from one bank to the opposite bank. But the degree of erosion of the opposite bank was smaller. Higher bed shear stress as depicted in **Figure 3.18 (b)** is concentrated around the groynes tip until the crossover region [X=1.6-1.75m] and [X=2-2.25m] and after leaving this region, there is a sharp shift towards the channel. In Ch-60, the pattern of channel evolution and bed shear stress distribution is similar to the impermeable case as illustrated in **Figure 3.18 (c)**. However, deposition in the embayment

area was higher in this case. Also, the shift of the higher bed shear stress zone towards the channel was not as sharp as compared to that of Ch-45.
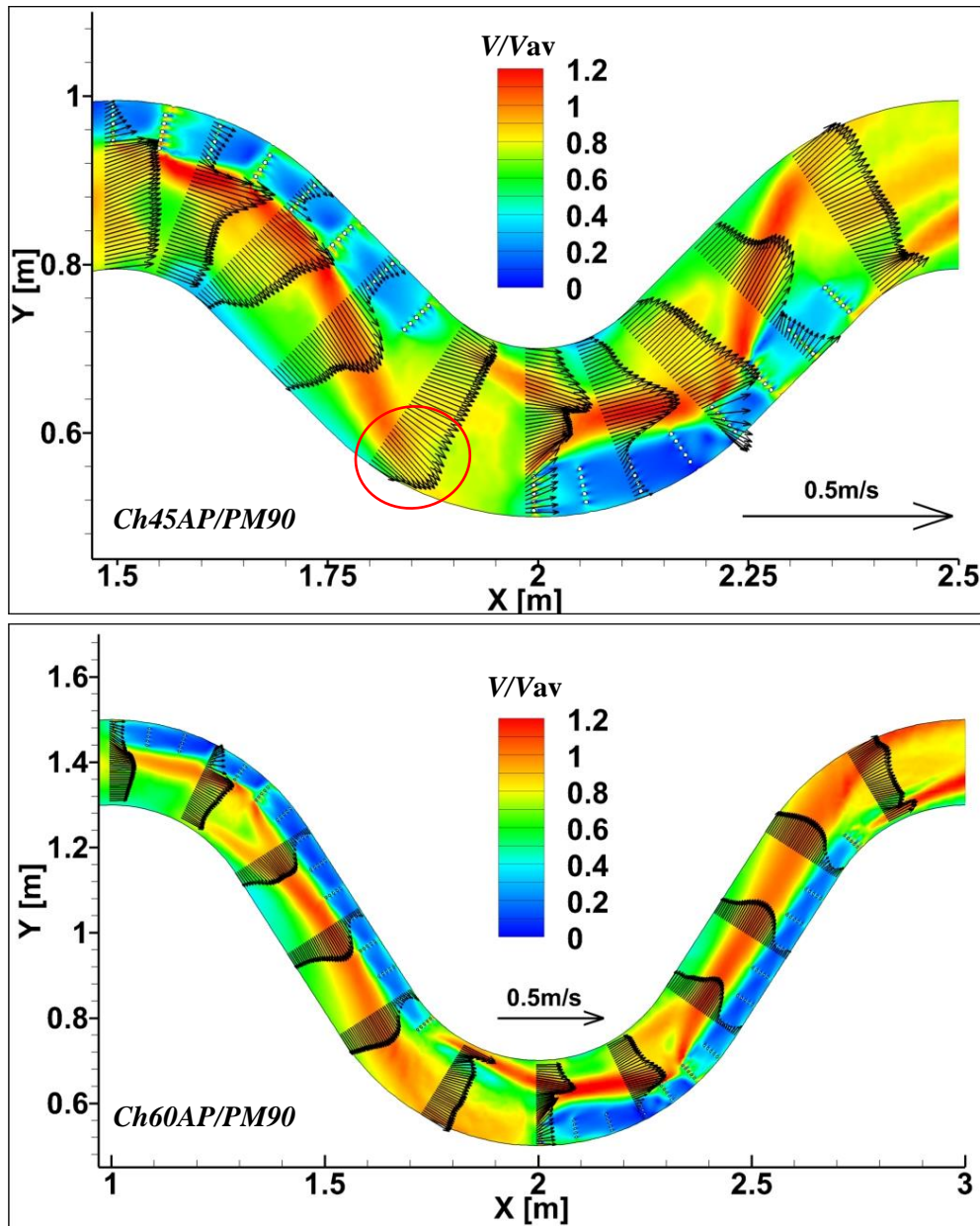
Figure 3.19 Distribution of V/V_{av} and the cross-sectional velocity vectors

The distribution of V/V_{av} shown in **Figure 3.19** suggests that velocity in both channels is slightly higher compared to the impermeable groynes case (**Figure 3.10**). Since the channel bed changed little due to lesser erosion, the impact on the velocity was lower. It was also observed that the flow passed through the piles with higher velocity in Ch-45. Velocity was particularly higher around the piles at their immediate upstream and downstream where the flow strikes and leaves those piles. Also, the near bank velocity was higher compared to the impermeable groynes

case which might induce erosion of banks. Therefore, the selection of the permeable and impermeable groynes is a choice between the channel condition and the desired objective.

3.6 Summary

The results and analysis discussed in this chapter suggest that channel morphological development is strongly influenced by channel geometric properties. Consequently, the channel flow and morphological response to the bank protection countermeasures are not the same. We examined the suitability of different arrangement of groynes under two different channel sinuosity. The zone of maximum bank erosion is located around the apex for the channel of higher sinuosity and higher deflection angle whereas the maximum erosion zone shifts downstream with decreasing sinuosity and deflection angle as in Ch-45 where it was located downstream of the crossover. The positioning of the groynes showed that in low sinuosity channels, the performance in terms of reduced scour depth, a greater shift in high bed shear stress away from the banks, reduced erosion of the opposite bank, etc. is more improved if the groynes are placed starting from downstream of the apex. With increasing sinuosity and deflection angle, the position of the groynes needs to be shifted upstream around the apex for achieving better functionality as in Ch-60 where groynes positioned at the apex showed slightly better performance. The change in the angle of groynes caused a minimal difference in the channel response indicating that the channel evolution is more sensitive to the position of groynes in meandering channels. In permeable type groynes, the overall bed evolution were relatively small. However, the near-bank velocity tend to be higher for permeable groynes compared to impermeable ones, which indicates that the bank erosion risk may increase.

Chapter 4

Real field application of 2D simulation model in meandering channels

4.1 Introduction

In chapter 3, the formulation of a 2D numerical model and its validation including the application to analyze different scenarios were discussed. The 2D model reasonably reproduced the experimental observations. Even though the flow field in real rivers is highly 3-dimensional, the application of the 3D model to the real field cases is computationally expensive owing to the scale of the study domain. As already discussed in Chapter 1, studies have shown that 2D models are quite capable of simulating real field scenarios. In this regard, we employed the 2D model developed in chapter 3 to study the hydro-morphological behavior of natural meandering channels. This chapter discusses the results of the field application of the model. The chapter is divided into two parts, the first part discusses the application case of Bangladesh whereas the second part, will talk about the case of Uji River in Japan. These two river reaches were chosen mainly due to two reasons; one due to their meandering nature and second due to the river bank erosion problems. In the case of Gowain River, Bangladesh the river bank erosion along with the flash flood events greatly impacts the agriculture-based livelihood of the people in the study area. Similarly, the river bank erosion has accelerated at some particular locations of Uji River in recent years. Although the river is protected by embankment along both the banks, the erosion problem persists.

In each field case, we first performed the satellite imagery analysis to identify the historical channel bankline changes followed by the description of input data to set-up the model. Finally, the results of different field cases are analyzed. We also examined the role of low and high flow discharges in the variation of channel bed and other hydro-morphological features.

4.2 Gowain River, Bangladesh

Bangladesh is a south Asian country which drains some of the largest rivers of the world namely Padma and Jamuna. The other medium and small rivers are often overshadowed due to the dynamic behaviour of these big rivers. However, the problems of river erosion, inundation, etc. are severe not only in big rivers but the medium to small rivers too are equally affected by these issues. One river facing the problem of river bank erosion is chosen for the field application. Gowain River is located in Jaflong, Gowainghat Upazila, Sylhet Division the north-eastern part of Bangladesh. The majority of its catchment lies in Meghalaya, India. Due to the steep slope, the occurrence of flash floods is a common phenomenon during the monsoon. The target area chosen for this study includes a meandering reach where more than 200m of the bank has eroded since 2011. The area adjacent to this bank consists of tea garden which is greatly affected by the river bank erosion process **Figure 4.1** depicts the location of the study reach. The total length of the study reach is about 8km. The channel slope is approximately 1 in 1000. The channel consists of point bars some of which have taken permanent form. At the apex, the channel thalweg is closer to the outer bank which can be seen from **Figure 4.1**. Haphazard mining of the river bed materials has further exacerbated the problem of river bank erosion. It is first necessary to understand the channel behavior and flow characteristics. In this regard, analysis of channel morphological changes could be vital in identifying the critical zones of erosion and appropriate planning of river management works.
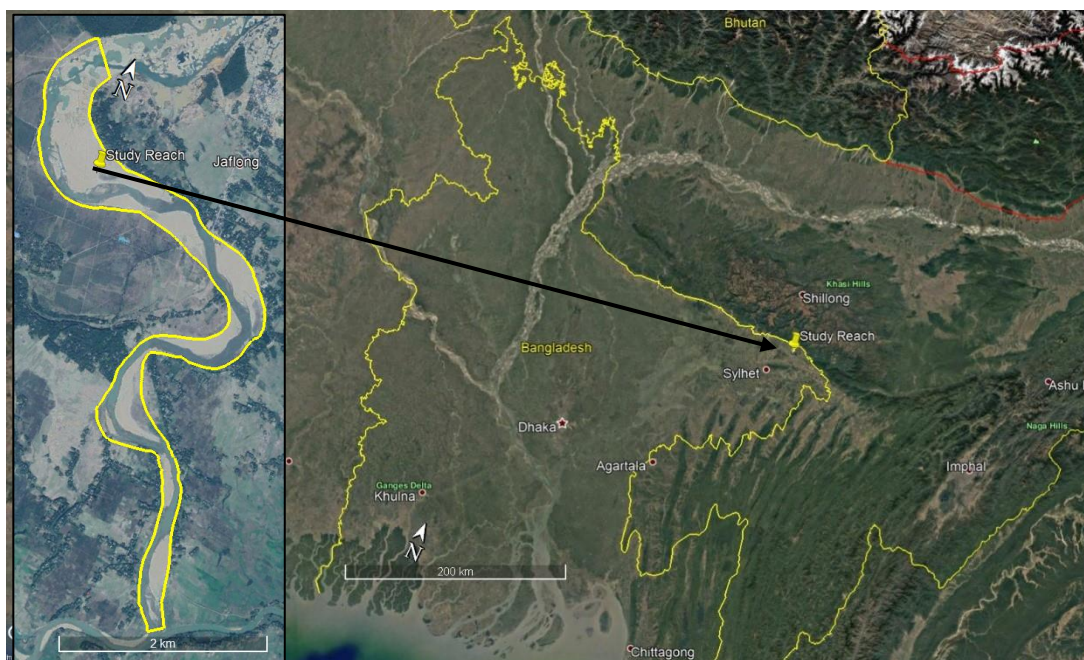
Figure 4.1 Location map of the study river reach in Bangladesh (google earth, 2019)

4.2.1 Satellite Imagery Analysis of Channel changes
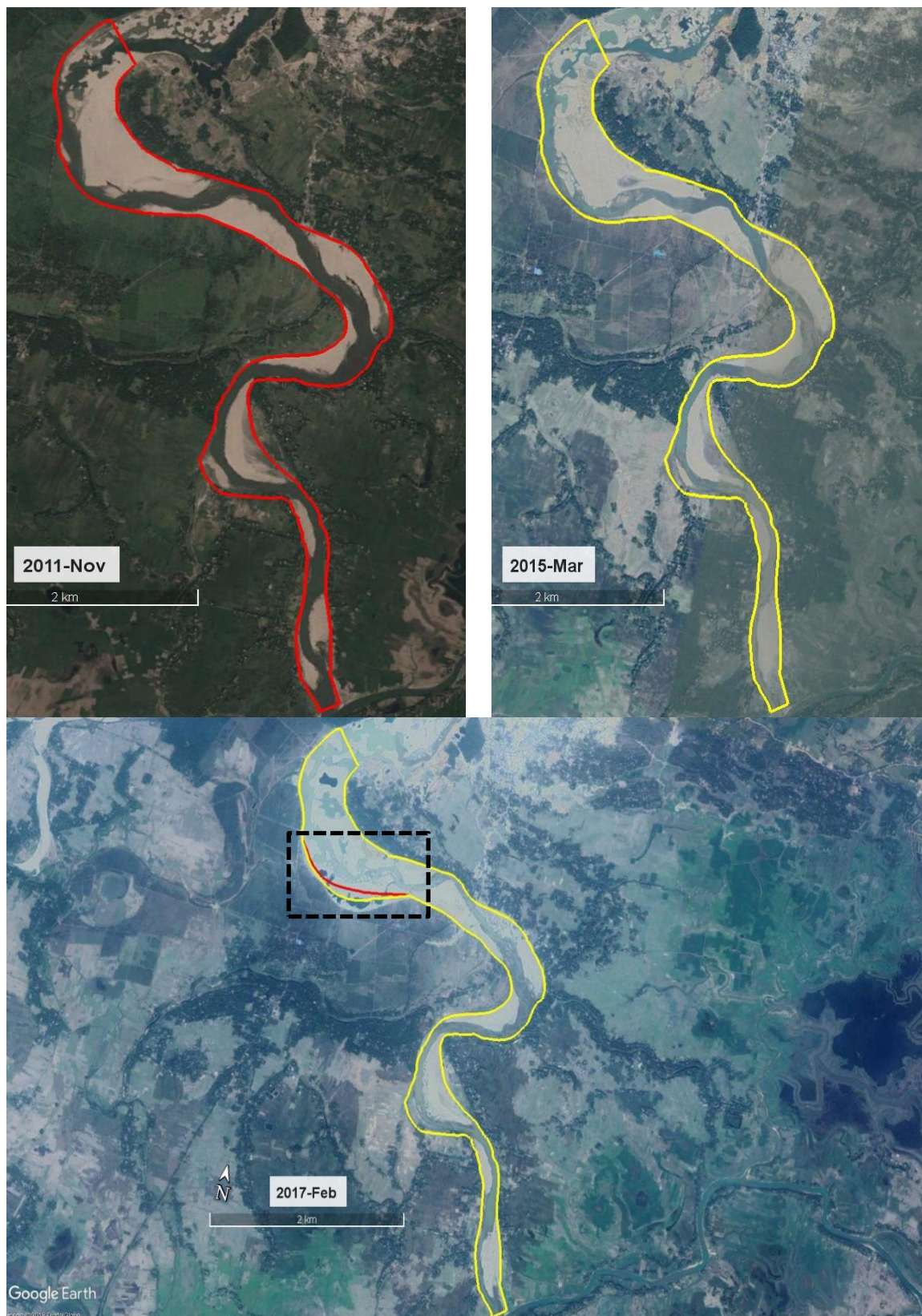
Figure 4.2 Channel bankline changes traced from the google earth images (google earth, 2019)

Satellite images greatly assist in the early stage of any real river-related research work. In this context, we extracted the google earth mages of three different years from 2011 and traced the bankline. The analysis showed that the outer/concave bend of the right bank has been continuously shifting due to bank erosion. Erosion more than 200m has occurred over a period of about 5 years from 2011 to 2017. The width of the point bar attached along the opposite inner bend has also increased which has caused the thalweg to push towards the outer bank. The image of Feb 2017 shows scour holes distributed in the channel bed close to the bank erosion area. These are created by the sand miners. The other portion of the river shows nearly no change in the channel bankline even though slight changes in the river bed was seen.

4.2.2 Model Input data

Availability of the data is a challenging issue in any real field cases. The different data necessary for running the simulation are bathymetry data, observed discharge and water level and sediment distribution and its properties. This section deals with a brief description of these datasets.

1) River Bathymetry
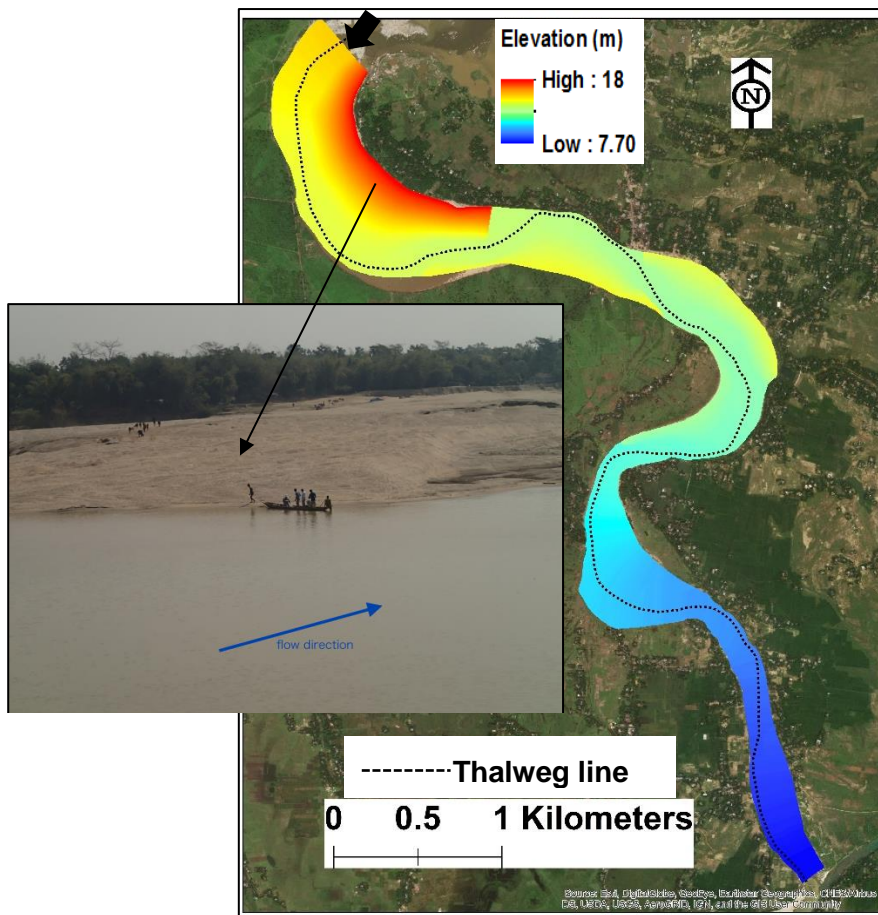
Figure 4.3 Bed topography of the study reach of Gowain River
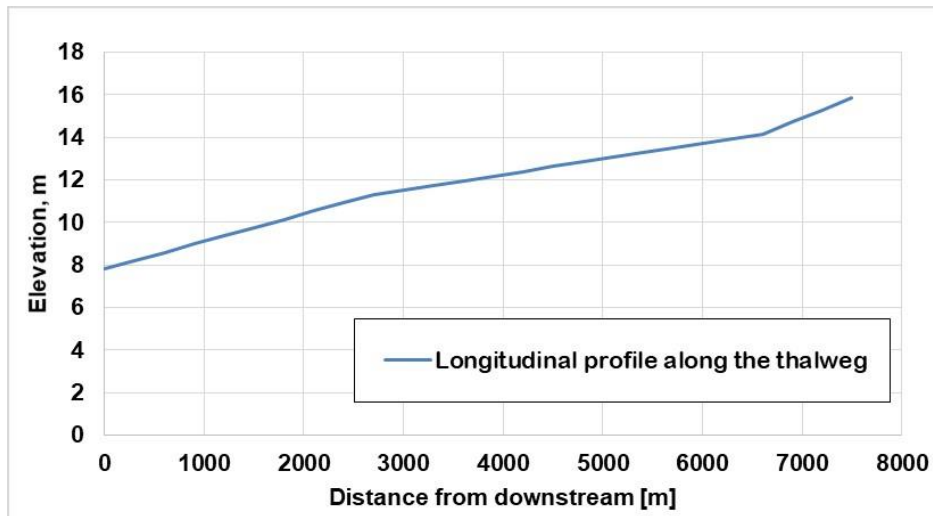
Figure 4.4 Longitudinal profile along the channel thalweg

The river survey data that were obtained from different sources in Bangladesh were found to have discrepancies and hence couldn't be considered as reliable. Therefore those data couldn't be used directly. In this regard, we used the river bathymetry data from the previous works of (Hashimoto et al., 2017) who compared the adjacent floodplain elevation and the river bed data from the SRTM3 DEM data. The total length along the channel thalweg was about 9 Kilometer. The channel was divided into three stretches having a different slope of the bed. The longitudinal elevation was varied according to the bed slope while the cross-stream was considered uniform elevation i.e. horizontal. The bank width was extracted from the satellite image of Nov 2011. Within the study domain, we interpolated the channel elevation data to get the river bathymetry. In addition, we also extracted the shape of the channel point bars from the satellite images and were superimposed on the river bed map. The elevation along the channel bar was determined from the relative elevation difference obtained from the surveyed data. **Figure 4.3** presents the channel bathymetry data used in the current analysis. The longitudinal profile of the river is shown in **Figure 4.4.**

2) Flow and Water Level

Observed river discharge and water-level are the other data required for performing the numerical simulation. The observed data of the Jaflong spill observation station were available only until the year 2006. For the current simulation, we used the data from May 2000 to the end of September 2000 i.e. the monsoon period. These time period included varieties of flow including the low as well as peak events. The discharge and the downstream water-level were used as the upstream and the downstream boundary conditions respectively. The observed discharge and the corresponding water-level data used for the simulation is illustrated in **Figure 4.5**.
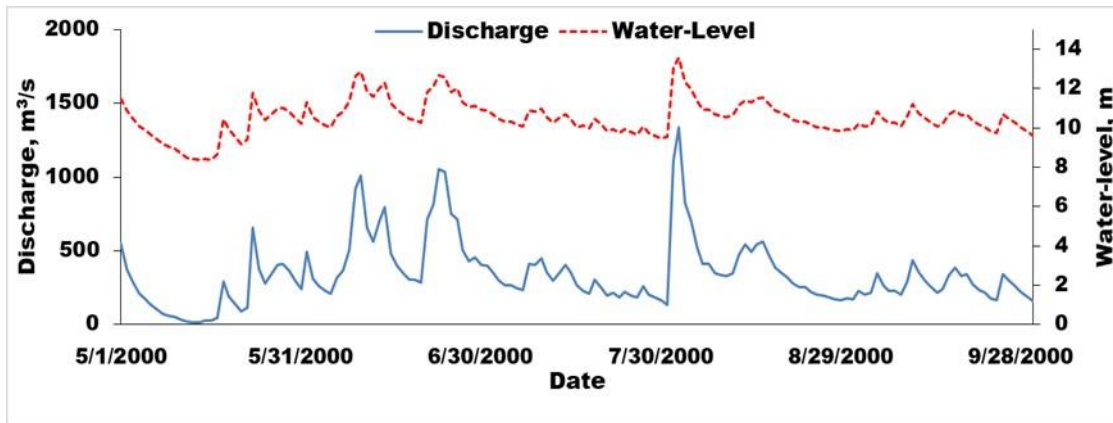
Figure 4.5 Observed River discharge and water-level at the Jaflong gauging station

3) Sediment properties

The sediment data required for simulating the channel bed evolution process were obtained from the field data collected and analyzed jointly by the team from Bangladesh University of Engineering and Technology and the Kyoto University. The sediment distribution curve is shown in **Figure 4.6.** The mean diameter was 0.93mm while $(d_{84}/d_{16})^{0.5}$ was 2.7 indicating the non-uniformity of the sediment. The density of the sediment was 2650 kg/m^3.
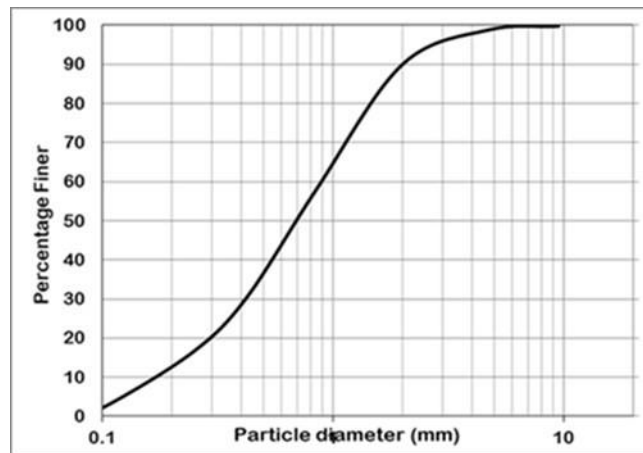
Figure 4.6 Sediment distribution curve of the bed materials

4.2.3 Different Simulation Cases

After preparing the input data, the mesh was generated for the study reach of the river where four different cases of simulations were performed. The average size of the mesh for no groynes case was 20m as illustrated in **Figure 4.7**. First, the hydrodynamic simulation was carried out considering a fixed bed for calibrating the model. After the model was calibrated, we performed a simulation with sediment transport. The coupled flow and bed evolution simulation was conducted for three cases; without groynes, with groynes at 90^0 and with groynes at 120^0. For the

78

cases with groynes, rectangular impermeable groynes were implemented as done in the case of experimental channels. The results and discussions for each case are presented next.
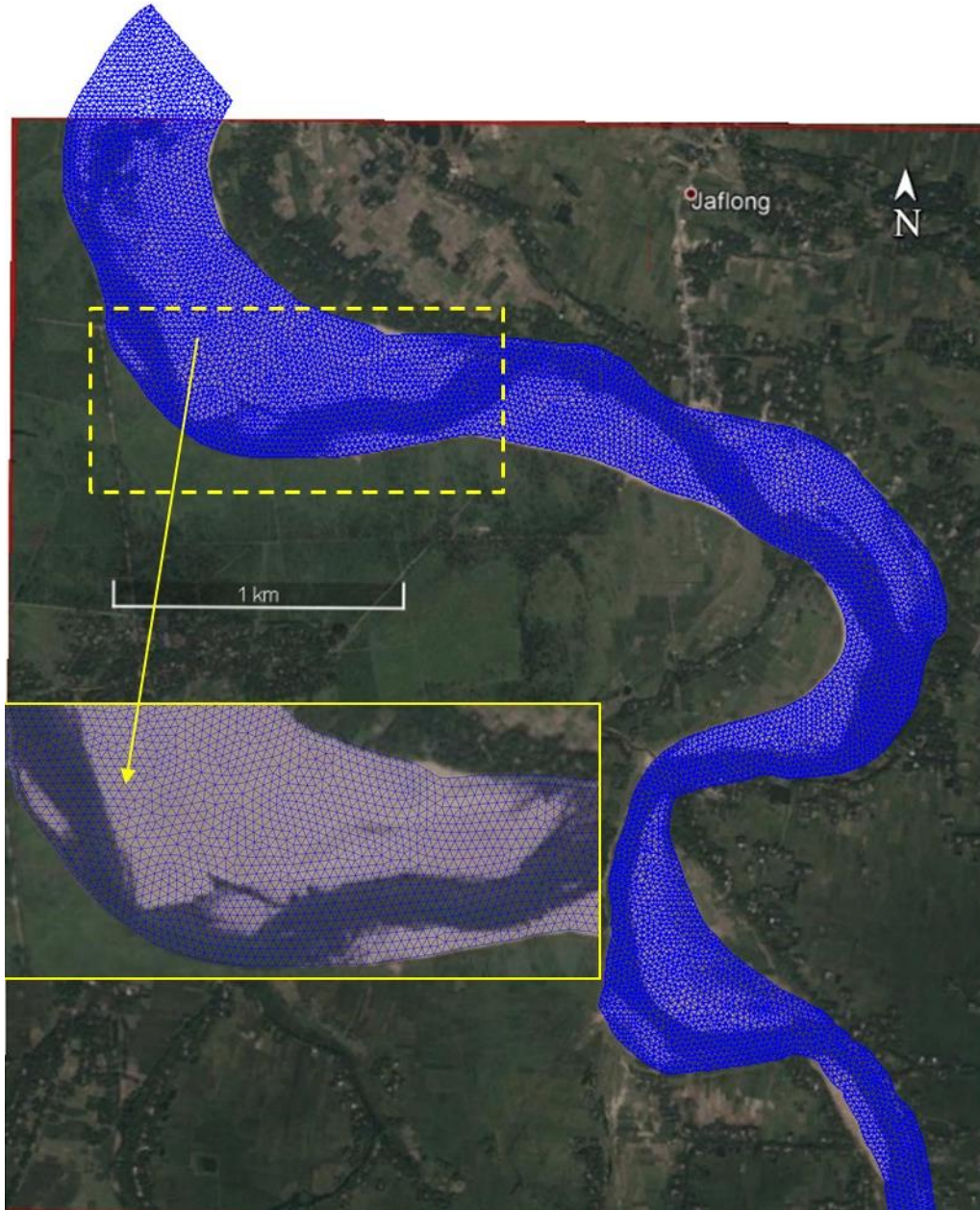
Figure 4.7 *G*eneration of unstructured mesh for the study domain

4.2.4 Results and discussions

In this section, results and discussions for each simulation are discussed separately and comparison is made at the end. The overall channel evolution at the end of the simulation, the spatial distribution of bed shear stress and velocity, channel cross-sectional change, etc. are analyzed and presented in this section.

1) Fixed bed case

The main purpose of simulating this case was to calibrate different model parameters and also check the overall hydrodynamic characteristics of the channel. The Manning's coefficient of 0.025 was adopted for the river bed and 0.02 for the banks. The model reproduced the observed discharge and water-level with reasonable accuracy. **Figure 4.8** represents the comparison of observed versus simulated discharge and the water-level. **Figure 4.9** depicts the water surface profile along the channel thalweg for t=55 days of simulation.
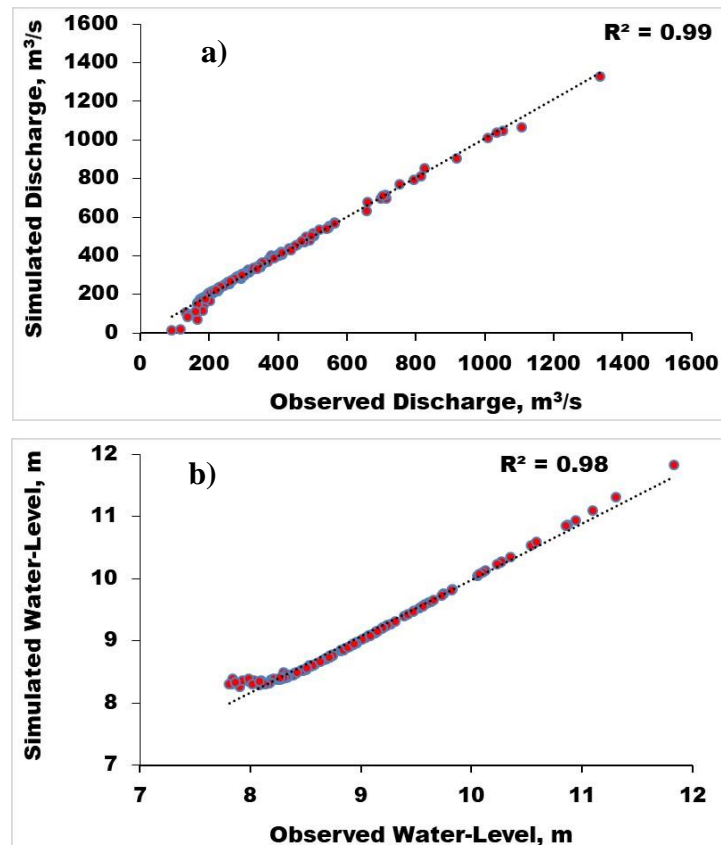
Figure 4.8 Scatterplot of observed v/s measured: a) discharge b) water-level
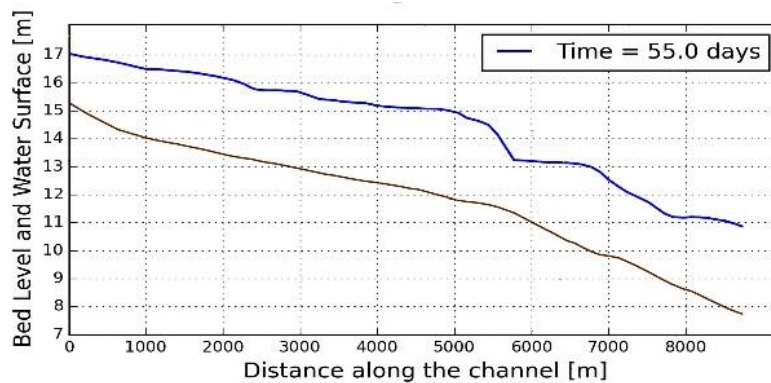
Figure 4.9 Water profile along the thalweg at t=55 days of simulation

80

1) Bed evolution without groynes

After calibrating the model parameters, coupled simulation of flow and sediment transport was carried out next, to understand the overall channel morphological characteristics as well as near bank phenomenon. The results from this simulation will be helpful in planning and designing the groynes. In this case, we first performed hydrodynamic simulation under the fixed bed for the inflow discharge of the first day of the input time series discharge until a steady state is reached. The results of this fixed bed simulation were used as an initial condition for the coupled simulation. The main purpose of doing this was to avoid any model instability or excessive scour due to the initial condition. The coupled simulation also reproduced the observed discharge and water-level with reasonable accuracy.

Figure 4.10 illustrates the channel evolution at the end of the simulation. The results of bed evolution showed higher erosion around the outer bank in general. Around the target bend where greater than 200m of bank erosion was observed through satellite images in **Figure 4.2,** erosion
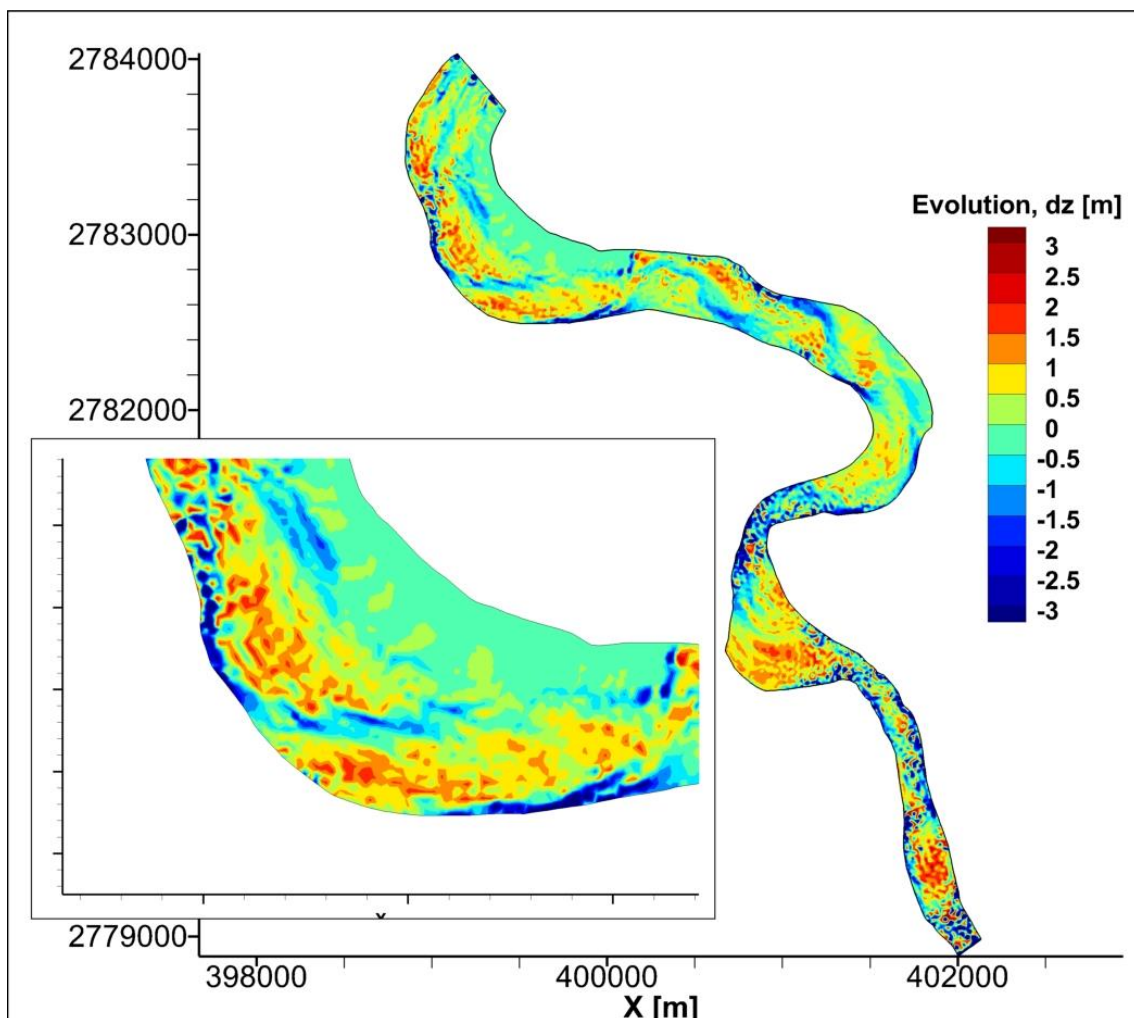
Figure 4.10 Bed evolution at the end (t=155 days) of simulation for the case without groynes

greater than 3m occurred in simulations. Erosion-deposition zones of the simulation are in close agreement with the observed trend in other locations too. This signifies the validity of the model to predict the real field scenarios.

The bed shear stress distribution as shown in **Figure 4.11** showed that during the peak flows, higher shear stress zone is located at the entrance and the exit of the bend. The higher shear stress is related to the higher velocity as **Figure 4.11** and **4.12** correspond to each other. The graph at the top right represents the time-series of the water level at the outlet and the line marks the water-level corresponding to the shear-stress distribution (bed evolution and velocity distribution too).

The spatial distribution of depth-averaged velocity is shown in **Figure 4.12.** It was found that during the low discharge, flow takes the path of the channel thalweg. Higher velocities occurred at the entrance and exit of the bend as shown in the zoomed figure of the target area in **Figure 4.12**. The zones of erosion and that of higher velocity correspond to each other signifying that these locations are prone to erosion.
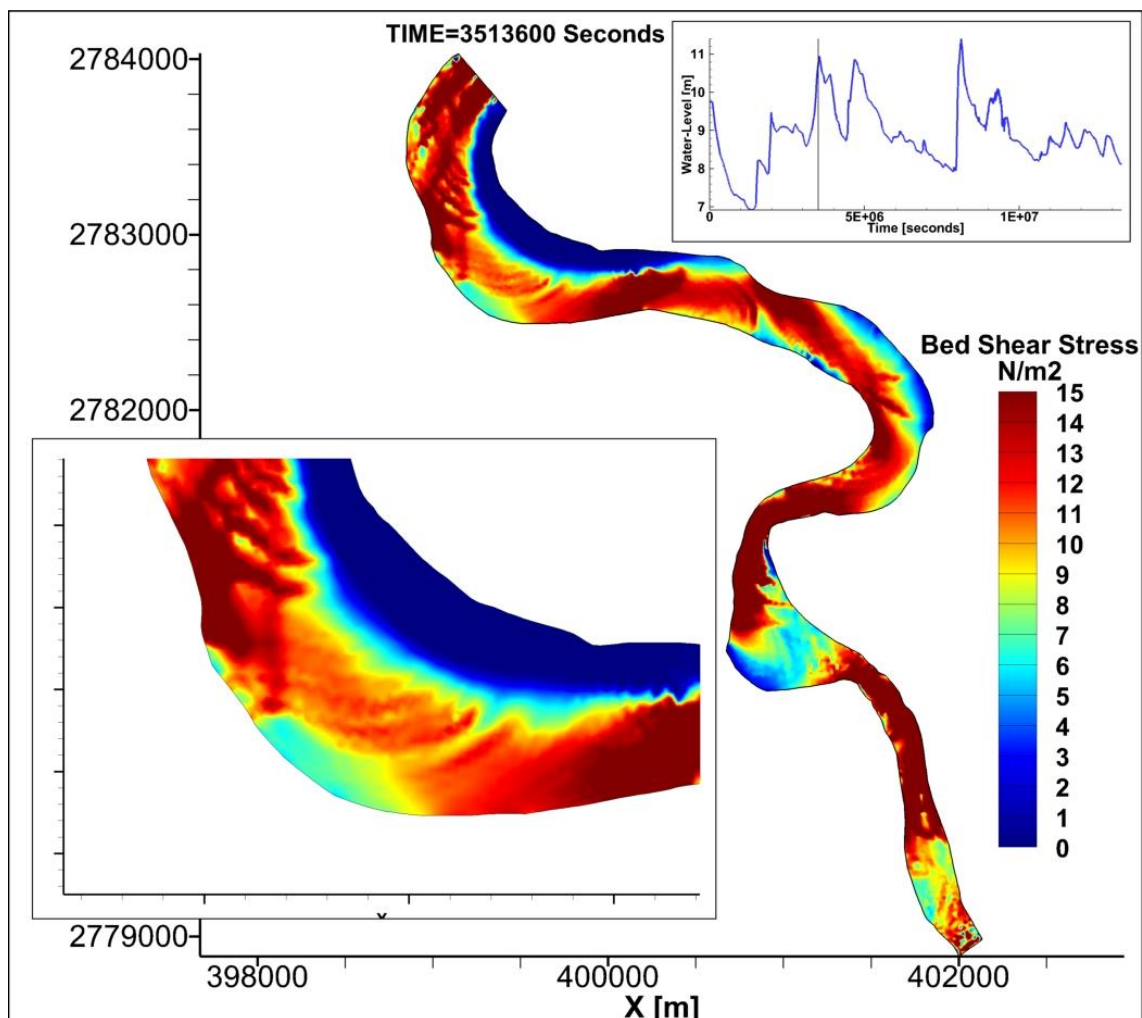
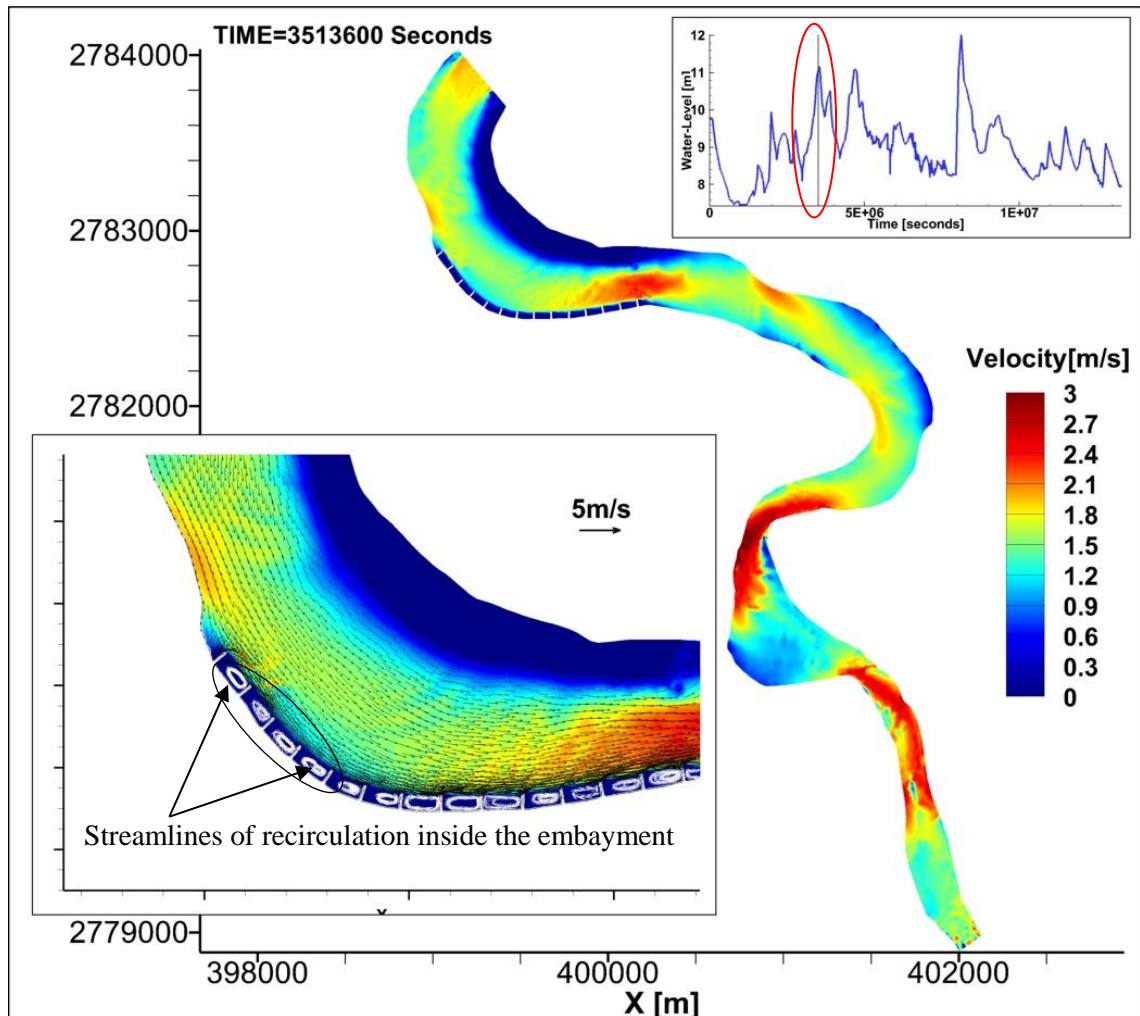**Figure 4.11** Bed shear stress distribution at the time (*t*=40 days) of simulation

82
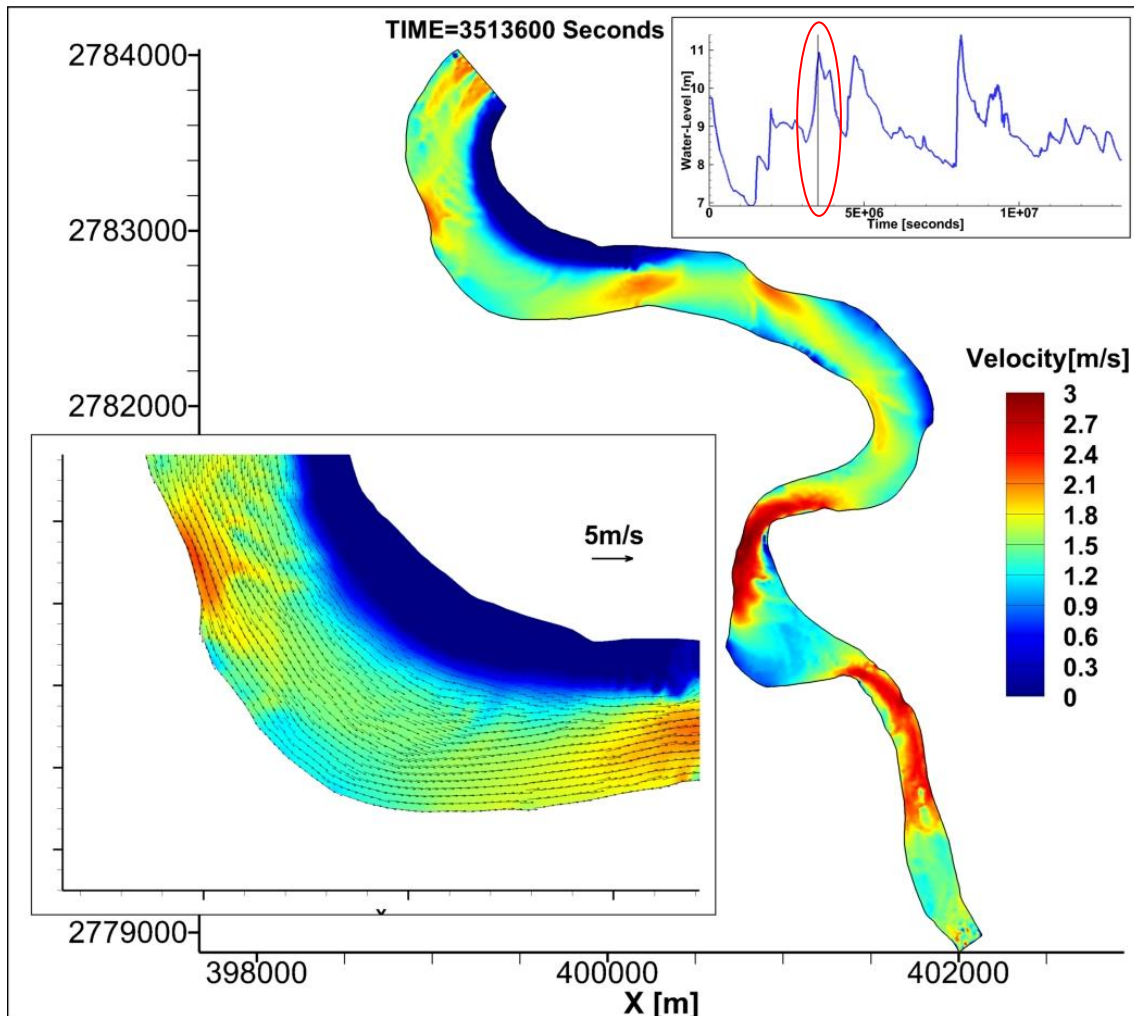
Figure 4.12 Depth-averaged velocity distribution at the time (t=40 days) of simulation

2) Bed evolution with 90^0 groynes

In the next simulation, we implemented the non-submerged impermeable rectangular groynes along the outer bank of the target area. The length of the groynes was set 40m while the width was 4.5m. The spacing between the groynes was fixed at 100m i.e. 2.5times the length of the groynes. The length of the groynes was decided based on the average channel width inside the target area. The average width of the channel was about 500m but the width occupied by the permanent type sand bars were excluded. The arrangement of the groynes and the generated mesh are illustrated in **Figure 4.13**. The aim of this simulation was to understand the effect of groynes in deflecting the high velocity and shear stress away from the outer banks.

After installing the groynes, the near bank erosion was greatly reduced and it was shifted towards the channel. However, groynes at the initial and those at the end suffered significant scour at their tip. This scour can be reduced by suitably modifying the groynes tip. The near bank region

just upstream of the first groynes still had higher erosion which suggests the need for additional protection of those areas by revetment or similar measures. If the erosion occurs in those areas, there are high chances that the flow might outflank the structures which will create an adverse effect. Groynes deflected the high-velocity zone towards the channel. Groynes at the beginning and the exit of the bend showed greater deflection tendency than those in between. Similarly, a considerable degree of recirculation flow was observed within the groynes.
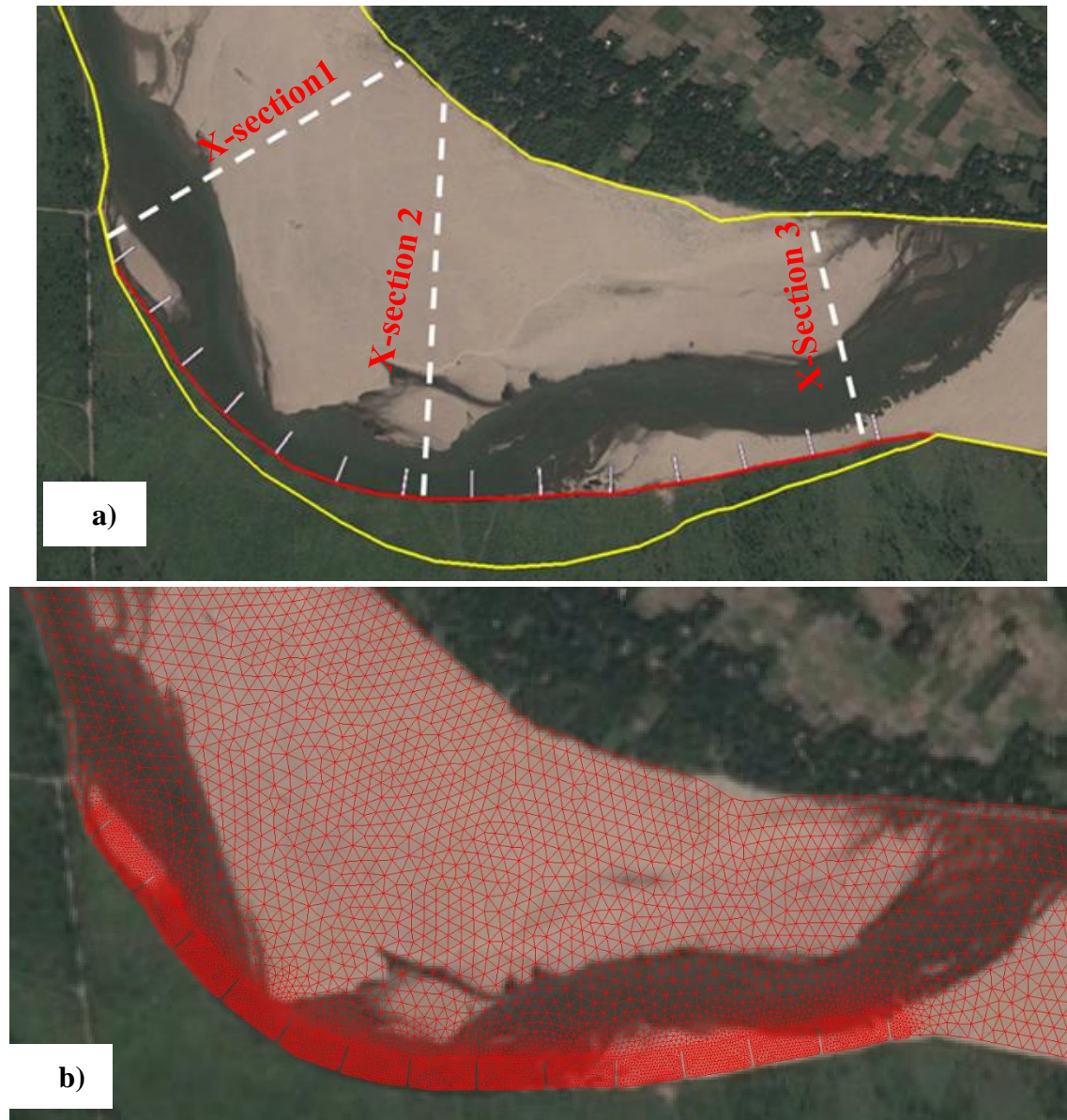
Figure 4.13 (a) Arrangement of groynes and (b) mesh generation for 90^0 groynes case

Figure 4.14 illustrates the channel evolution at the end of the simulation period of 155 days. The zoomed figure in the box shows the evolution around the groynes implemented area. It can
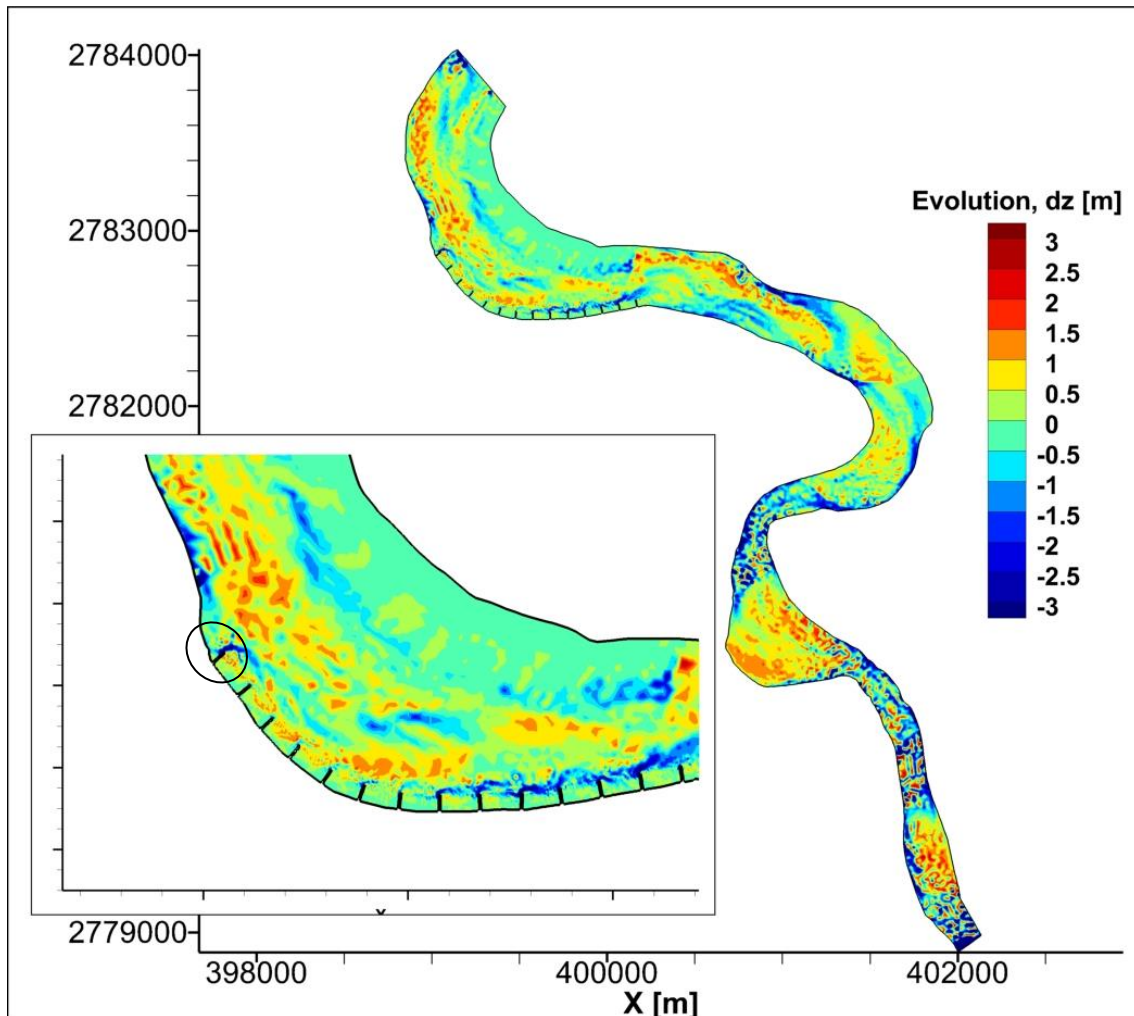
Figure 4.14 Bed evolution at the end (*t*=155 days) of simulation for the case without groynes

be seen that the scouring at the first groynes is higher. Similarly, slightly upstream of the first groynes erosion occurred near the outer bank. This phenomenon suggests that the first groynes as well as the area around it are vulnerable and requires additional protection. In the middle groynes, relatively scouring was lower and also the deposition in front of the groynes can be seen in this area. This is because the flow direction was away from the banks in this region. However, along the last seven groynes, the scouring at the tip was the highest. The flow was directed around these groynes due to the channel development process. This signifies that the groynes at the entry and the exit will have the major role in changing the channel flow behavior and morphology.

Figure 4.15 shows the bed shear stress distribution along the channel on the 40th day of simulation. It can be seen that the zone of higher bed shear stress is concentrated around the initial two groynes and the last seven groynes. This can be correlated with the distribution of depth-averaged velocity in **Figure 4.16** where the velocities were also higher around these areas.
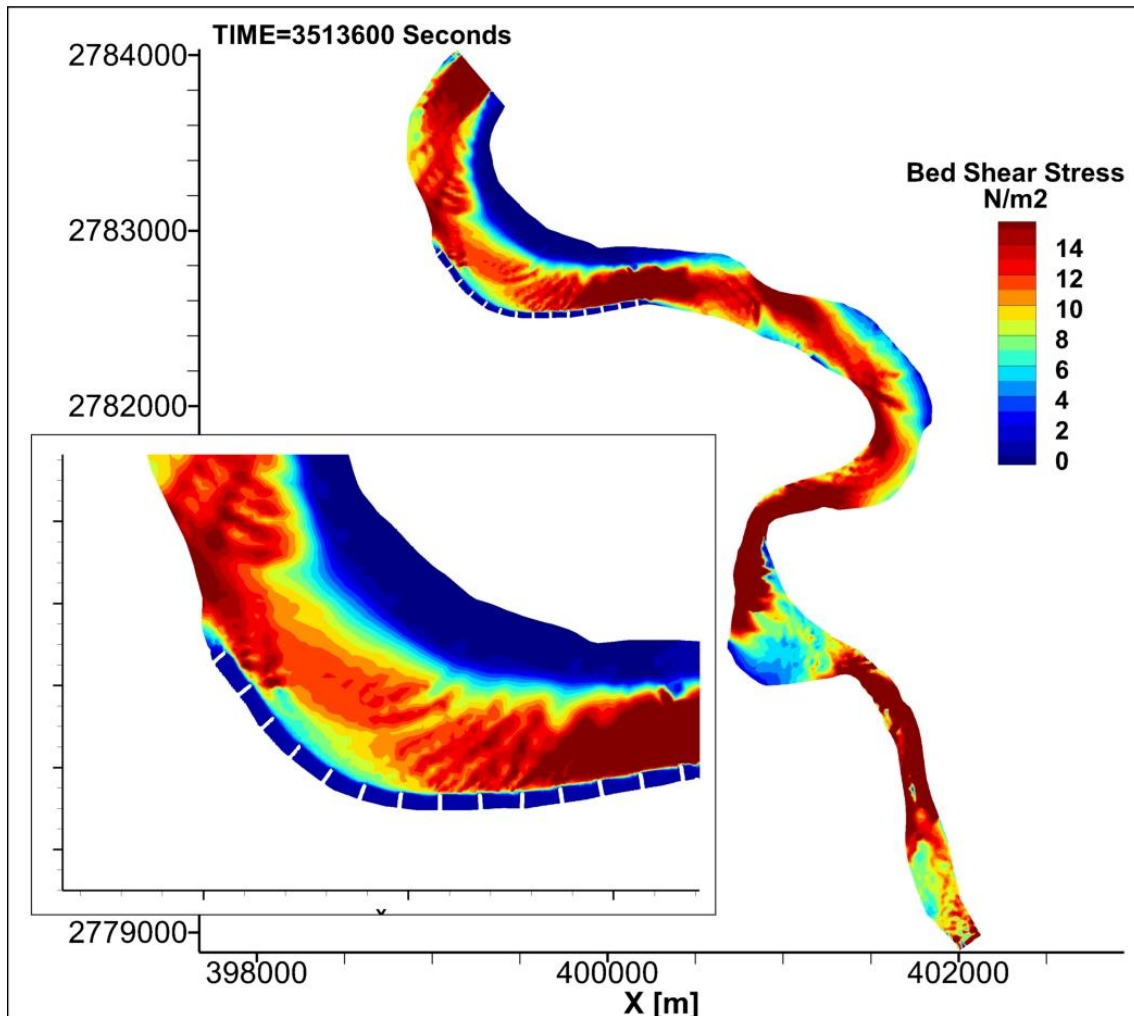
Figure 4.15 Bed shear stress distribution at the time (*t*=40 days) of simulation

As illustrated in **Figure 4.16**, throughout the channel higher velocities are in general, located around the bends. Velocities were even higher where the width along the channel was lower. The velocities in the embayment have reduced. However, recirculation was still higher in the embayment. The white circles inside the embayment area in **Figure 4.16** represent the streamlines of the recirculation flow. The recirculation flow was attached just upstream of each groyne whereas, at just downstream of the groynes, its strength was lower. The intensity of recirculation increased in the downstream direction. This phenomenon has a significant effect on the overall performance of the groynes in terms of reducing bank erosion by inducing the deposition. Notice the space between the groynes in **Figure 4.14** where the deposition is higher in the upstream groynes. The deposition is minimum in the last seven groynes. The degree of recirculation depends on the spacing of the groynes. At the apex of each bend, the velocity was usually higher than other locations of the bend.

86

Figure 4.16 Depth-averaged velocity distribution at the time (t=40 days) of simulation

3) Bed evolution with 120^0 groynes

In this case, the groynes were oriented at 120^0 to the bankline keeping other design parameters like the length, width and the spacing constant.

Figure 4.17 shows the bed evolution at the end of the simulation. Comparing with the case of 90^0 groynes, substantial deposition occurred just upstream of the groynes. The scour at the tip of the initial groynes was negligible compared to the previous case. Almost all of the first seven groynes didn't undergo any major scour and there was considerable deposition just upstream of all the initial seven groynes. This finding could be useful in the planning of river training works. The main phenomena that could have caused this effect are the smooth flow approach by attracting the flow towards the initial groynes. However, the erosion around the groynes was higher for the last six groynes compared to the 90^0 groynes. Also, the deposition in the embayment area was lower for these groynes.
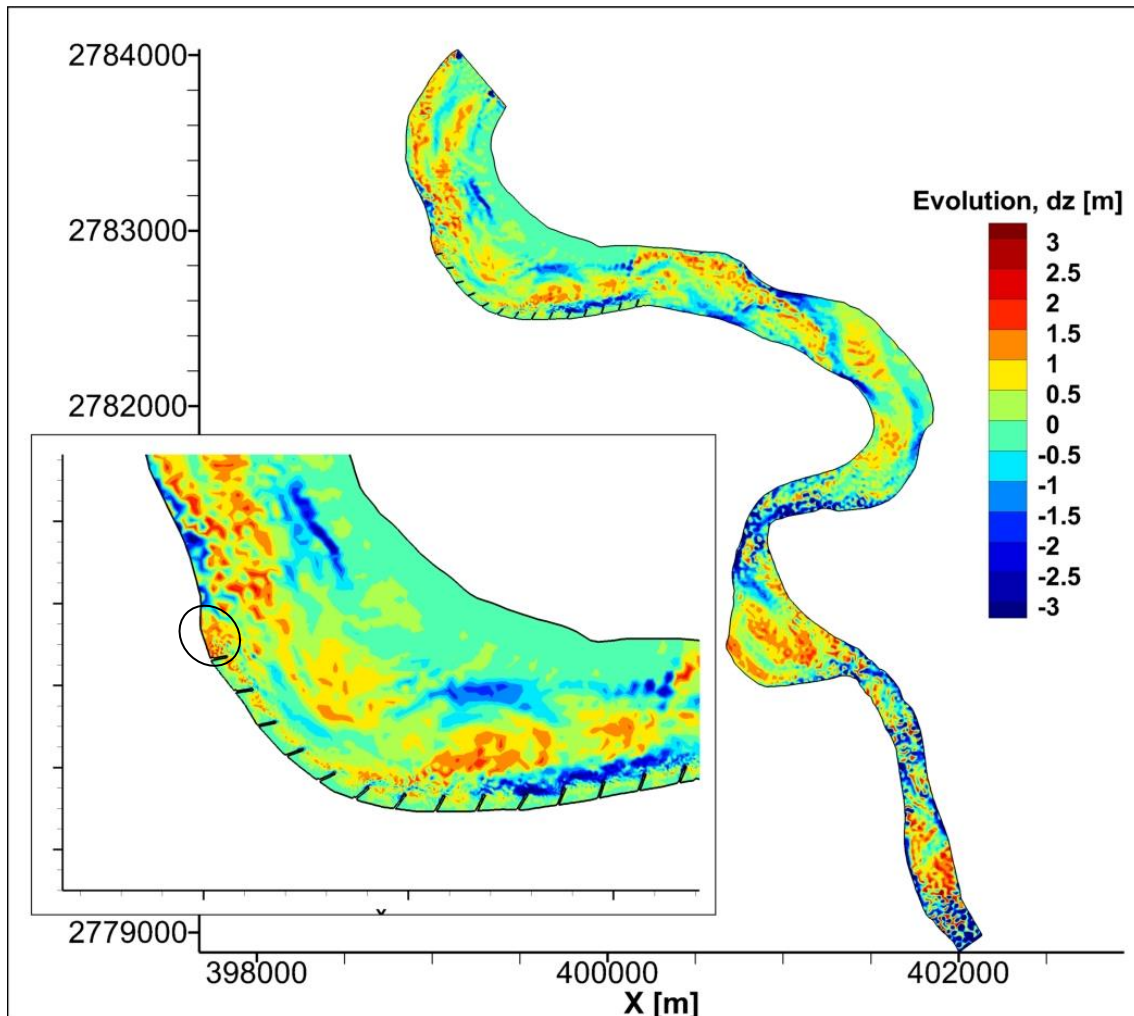
Figure 4.17 Bed evolution at the end (t=155 days) of simulation for the case without groynes

The distribution of bed shear stress which is illustrated in **Figure 4.18** shows little difference as compared to the previous case in **Figure 4.16**. However, compared to the 90^0 groynes, the zone of higher bed shear stress is slightly away from the groynes in this case. Consequently, the erosion around these areas was lower. However, the bed shear stress was higher than the previous case for groynes near the exit due to which greater scouring was observed around these locations. The erosion was higher in terms of both the depth and the total area. The overall extent of the higher bed shear stress zone was greater in 120^0 groynes case. At other locations along the channel, higher bed shear stress usually concentrated at the apex of the bend. If we notice the satellite images presented in **section 4.2.1**, the channel bed pattern in these locations clearly indicate that the low flow is concentrated exactly around these regions and consequently the erosion is also expected to be higher. So it suggests that the implementation of bank protection structures should consider such phenomena so that the structures are accurately positioned.

88
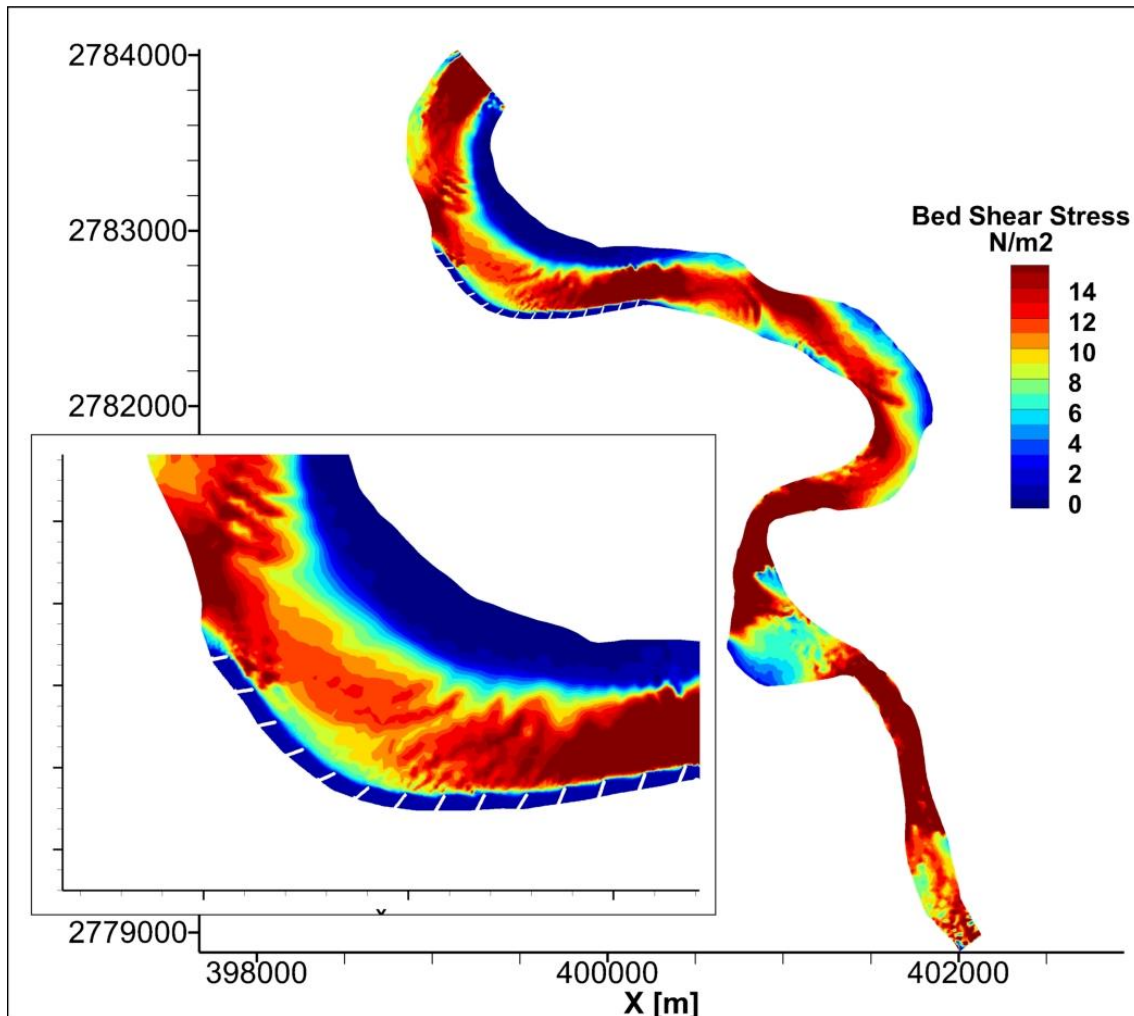
Figure 4.18 Bed shear stress distribution at the time (*t*=40 days) of simulation

In **Figure 4.19**, the distribution of the depth-averaged velocity including the streamline inside the embayment area is shown. The pattern of velocity and the bed shear stress distribution correspond to each other. The general velocity distribution pattern along the channel is similar to the previous case where the higher velocities concentrated around the initial two and the last seven groynes. However, the zone of higher velocity extended for greater length in this case. The other difference is the formation of the recirculation pattern whereas, in the 90^0 groynes case, the recirculation cell was attached just upstream of the groynes. In this case, the recirculation in most of the embayment covered all the area inside the embayment, not just the portion like the previous case. The strength of the recirculation was nearly the same in most of the groynes due to which the deposition in the embayment was quite similar. At other locations of the channel, velocity was higher where the channel width was narrower. Similarly, at the apex of every bend, channel velocity was higher.
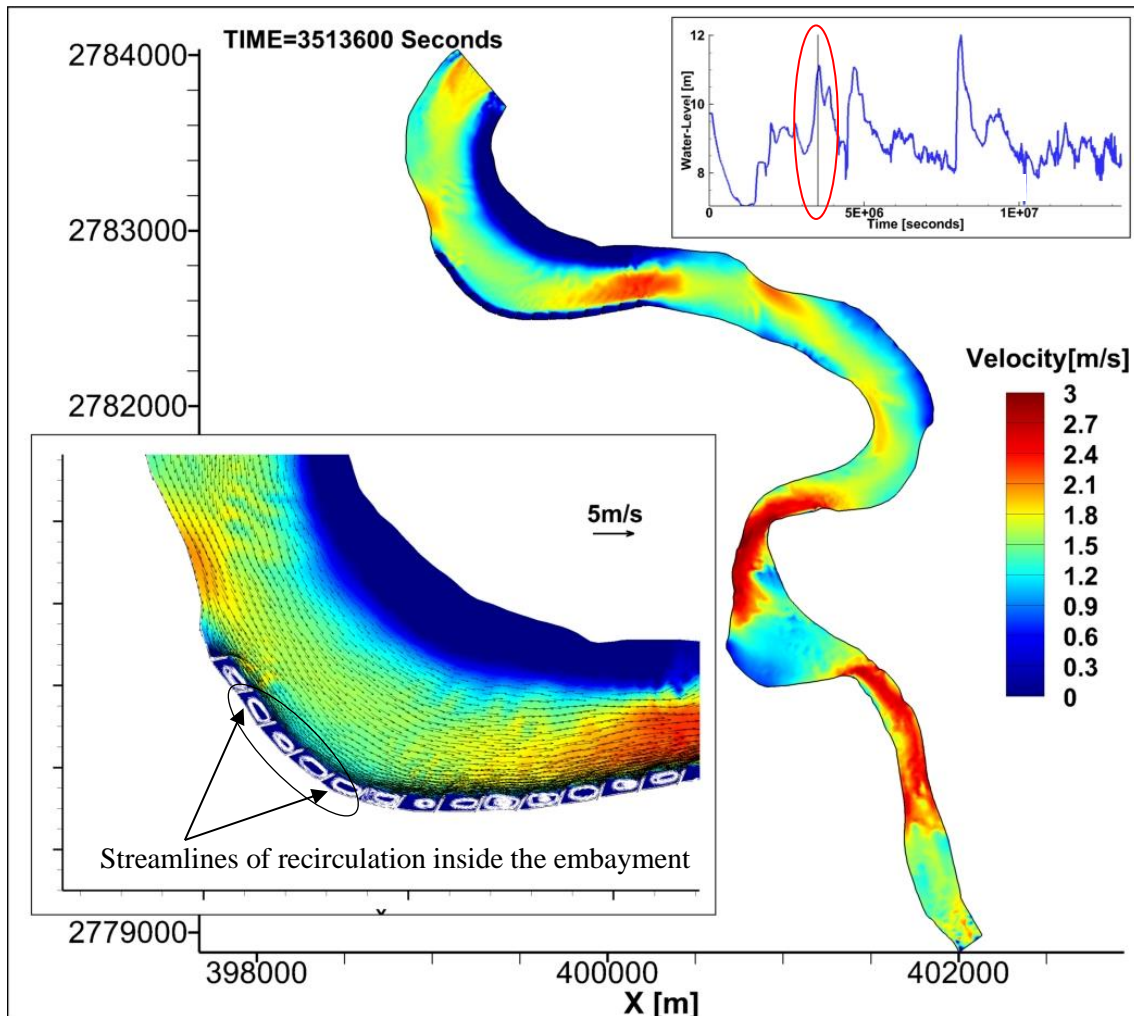
Figure 4.19 Depth-averaged velocity distribution at the time (t=40 days) of simulation

4) Overall Comparison

After analyzing the overall results in the previous sections, we tried to make a comparative analysis between three cases in terms of velocity deflection and the cross-sectional change.

Figure 4.20 (a-c) shows the cross-sectional velocity vectors respectively for the cases without groynes, with 90^0 and 120^0 groynes for the 26th day of simulation with the discharge of 656m^3/s. In the case without groynes in **Figure 4.20 (a)**, higher velocities are located in the near-bank region. These high near-bank velocities are responsible for the continuous erosion of banks as observed in the satellite images. To see the effect of groynes on mitigating the bank erosion by deflecting the high-velocity currents away from the banks, two different arrangement of groynes were examined. From the figure, it can be seen that the high-velocity zone has been deflected away from the banks in both cases of groynes. However, the recirculation flow developed in the embayment area.

90
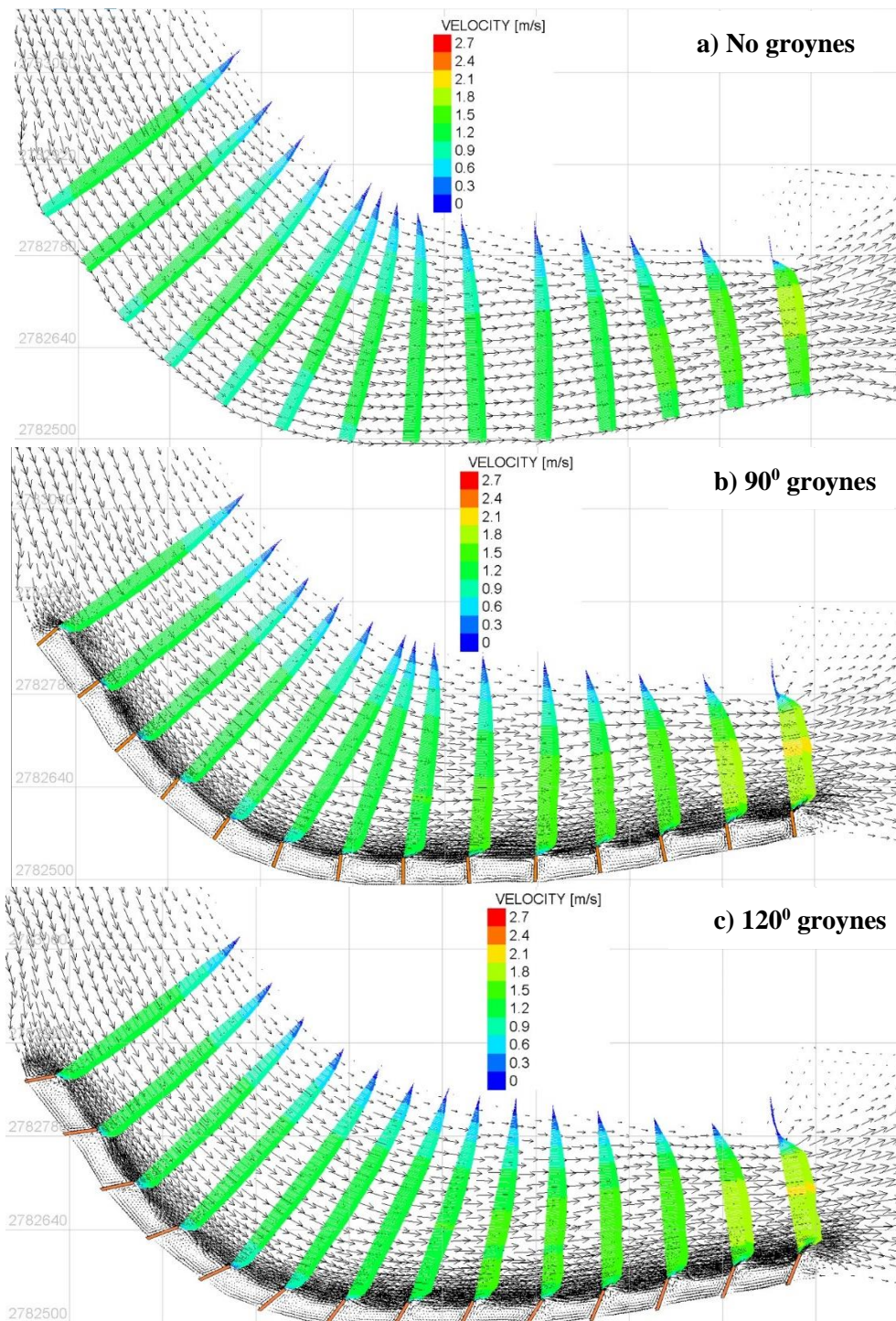
Figure 4.20 Velocity vectors at different x-sections along the groynes area

The comparison of the cross-sectional change along the three sections (see **Figure 13a** for the location of cross-sections) is presented in **Figure 4.21**. It can be seen that due to the erosion near the bank, deep scour are formed in the case without groynes. However, that was reduced in the case of groynes implementation.   Also, erosion has shifted away from the banks which are as
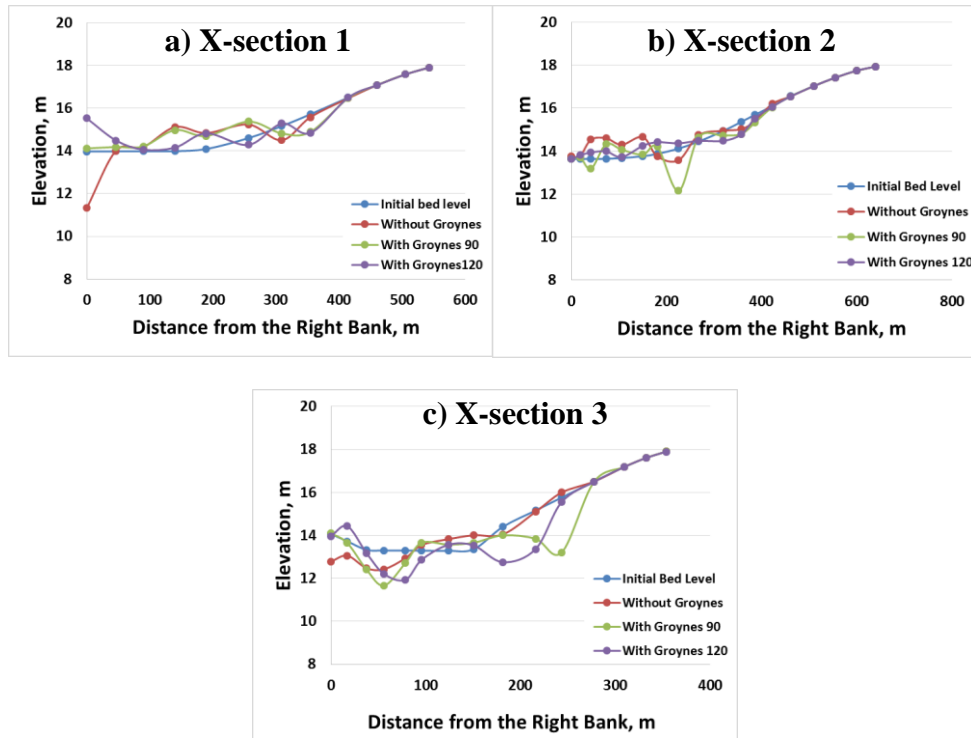
Figure 4.21 Cross-sectional evolution at the end of the simulation (see **Figure 4.13a**)
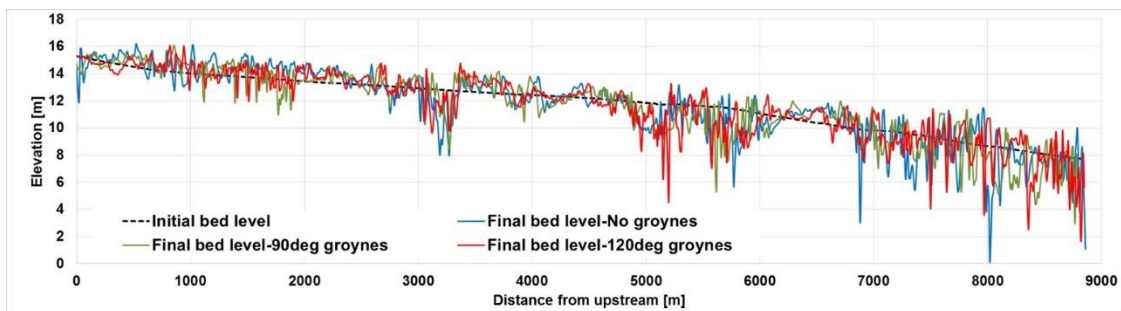
Figure 4.22 Elevation along channel thalweg at the end of simulations for all cases

desired for preventing the erosion of banks. Similarly, due to the overall effect of the series of groynes, the point bar located on the opposite bank has also been eroded especially at the most downstream x-section **Figure 4.21 (c).** Similarly, **Figure 4.22** represents the final elevation along the channel thalweg for all the cases.

Based on the results presented in this section, 2D simulations are computationally efficient in investigating different scenarios of groynes application. Applications of the 2D numerical models can reproduce the real field meandering channel morphological phenomena with reasonable accuracy. It can be said that the appropriate arrangement of groynes can provide a long-term solution to bank erosion problem in meandering rivers.

4.3 Uji River, Japan

The river reach of Uji selected for the current study is beginning from the confluence with Yamashina River near Mukaijima to about 4km downstream. Within this reach, the curved portion near the Ujigawa Open laboratory is analyzed in detail because of high bank erosion.
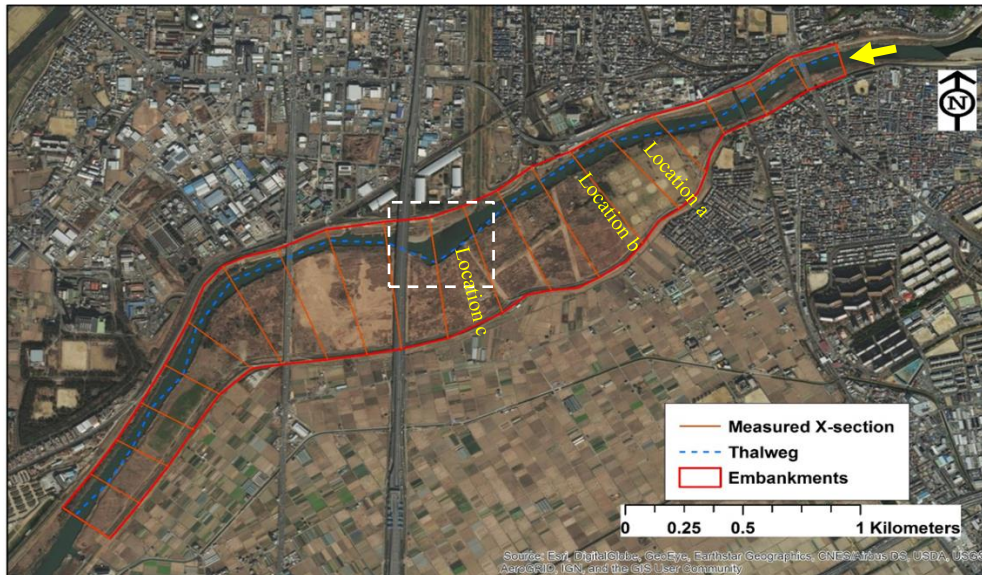
Figure 4.23 Study area of Uji River
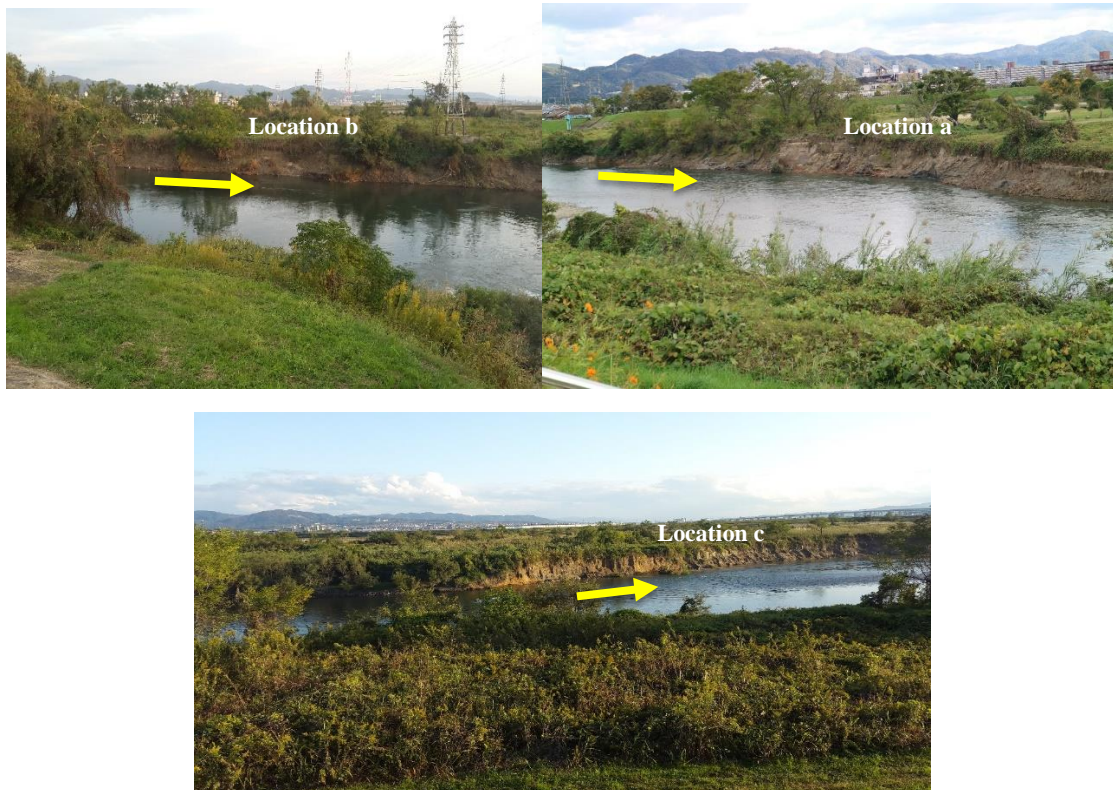
Photo 4.1 (a-c) Bank erosion in Uji River within the target area (Arrow indicate flow direction)

4.3.1 Satellite Imagery Analysis of Channel changes

Analysis of the river bankline changes and the corresponding areas eroded for this particular location are presented in **Photos 4.2** and **Figure 4.24**. It can be that continuous erosion has occurred along the outer bank while the point bar has formed along the inner bank.

Photos 4.2 (a-e) Bankline change due to the erosion of banks

94
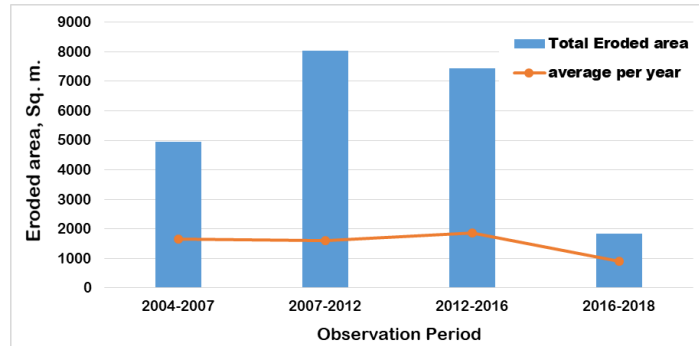
Figure 4.24 Rate of Bank erosion at the channel bend

4.3.2 Input data

In order to set-up the model for simulation, we needed to carefully prepare different types of input data. Different data used for the simulation are discussed in brief in the next sections.

1) River Bathymetry

River bathymetry was generated by the spatial interpolation of the cross-sections data obtained from the Ministry of Land Infrastructure and Transport, Japan. The cross-sections data were recorded at the end of the year 2015. **Figure 2.25** illustrates the interpolated River bathymetry. The typical cross-section across the river bend is shown inside the rectangle in the same figure. For the spatial interpolation, we used HEC-GeoRAS application in ArcGIS interface.
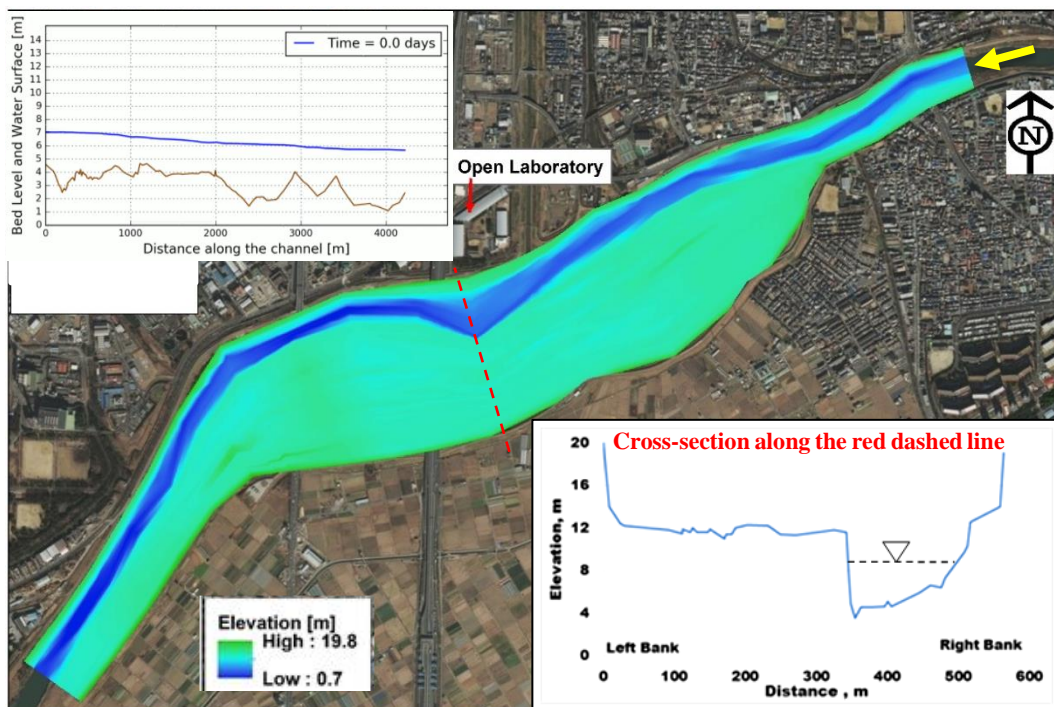
Figure 2.25 Bathymetry of the study reach of Uji River

2) Flow and Water Level

The inflow and outflow boundary for the model was given as the observed discharge and the observed water-level respectively. Since the river bathymetry was taken at the end of 2015, measured flow and water-level data of the year 2016 at Kumiyama-cho, Ohashiberi, Kyoto observing station were used for the simulation. The graph in **Figure 4.26** shows the observed discharge and water level for one year period of 2016. These data show highly regulated flows due to the operation of Amagashe dam in the upstream of Uji River.
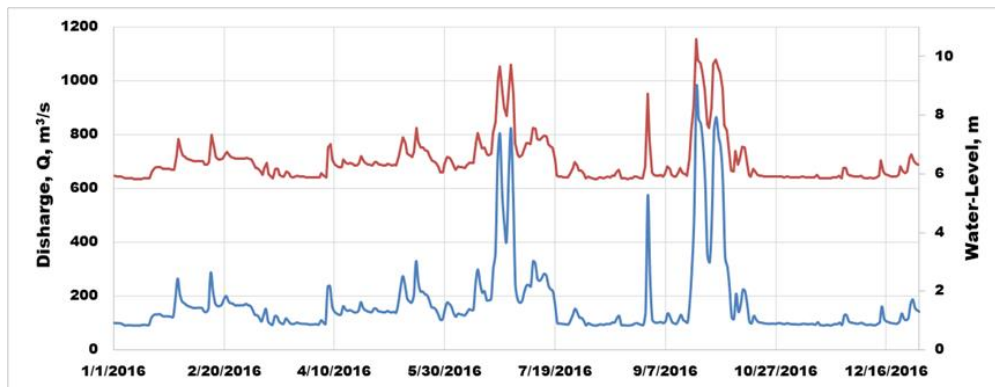
Figure 4.26 Observed water-level and the discharge data used for simulation

3) Sediment properties

Sediment samples of the river-bed were collected from the point bar at two different locations, one at the confluence of Yamashina River and the other in front of the Ujigawa open laboratory. Sieve analysis was performed on the collected sediment samples. **Figure 4.27 (a & b)** shows the particle size distribution curve of the two samples.
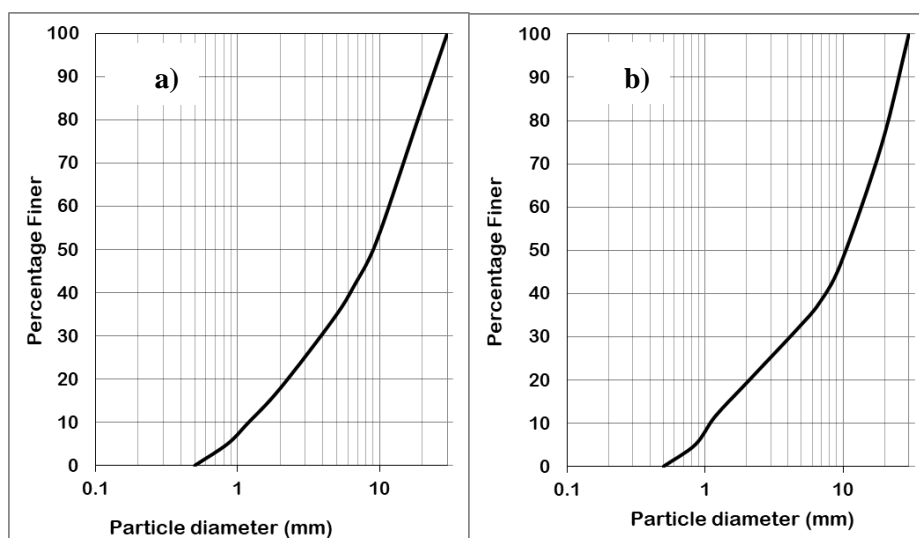
Figure 4.27 Sediment distribution curve near; a) Yamashina confluence b) Ujigawa open lab

96

4.3.3 Different Simulation Cases

After carefully preparing the required data, the model was set-up was done. **Figure 4.28** illustrates the mesh generated for the study reach. The simulation was first run under fixed-bed case for the calibration of the model. And in the next case, with a movable bed and finally the bank erosion case was performed.
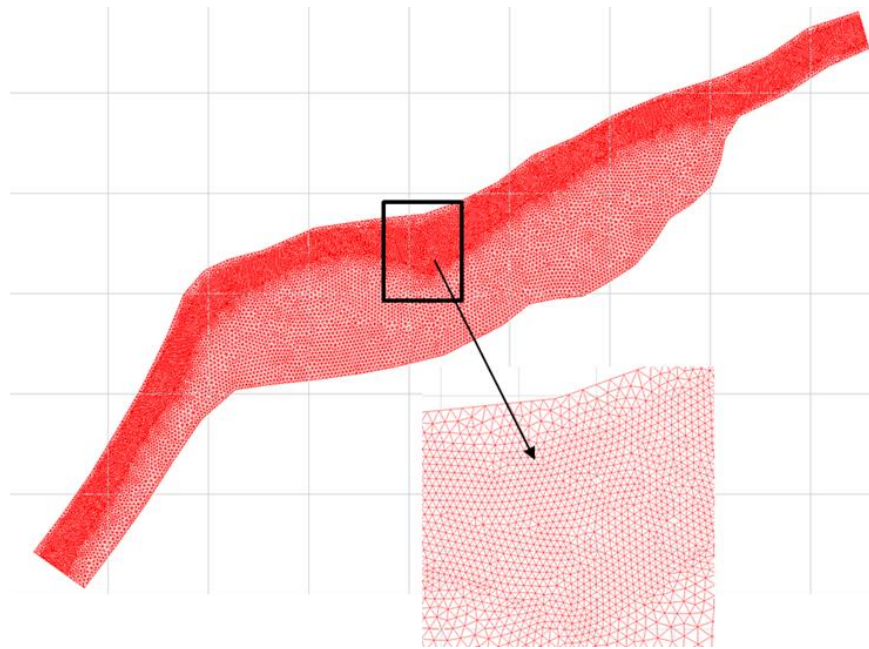
Figure 4.28 Unstructured mesh generated for the study domain

4.3.4 Results and discussions

1) Fixed bed case

The purpose of the fixed-bed simulation is to perform the model calibration. The results of the simulation showed good agreement with the observed data as shown in **Figure 4.29**. The R^2
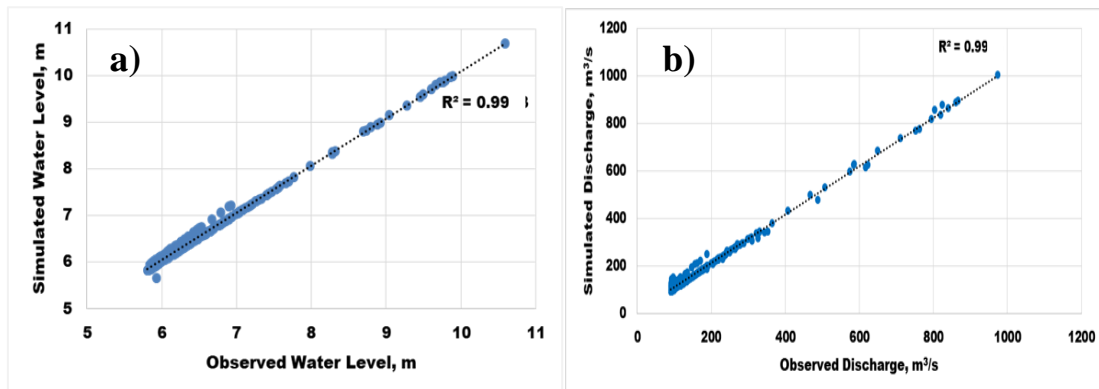
Figure 4.29 Scatter-plot of the observed vs measured a) water-level b) discharge
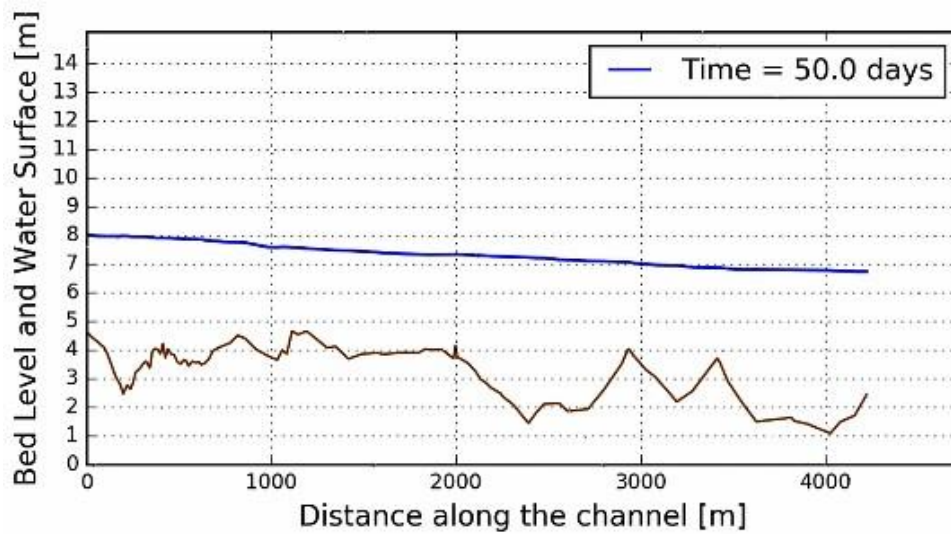
Figure 4.30 Water surface profile at 50th day of simulation [Q=200m^3/s]

values for both the discharge and the water level is greater than 0.99. This simulation of fixed bed case shows the model capability to compute the hydrodynamic variables under a range of inflow discharges. A typical water-surface profile is shown in **Figure 4.30** for the 50th day of simulation with an inflow discharge of about 200m^3/s. The difference in the water level between the upstream and the downstream boundary is about 1m.

2) Movable bed case

In the next step, we considered sediment transport with an objective to identify the channel morphological changes. However, the bed evolution was almost negligible. This might be due to the effect of coarser bed materials used in the simulation. Since the sediment sample was collected from the point bar instead of the actual river-bed. The main reason behind this could be the bed armoring due to the reduction in sediment supply by Amagashe dam.

Figure 4.31 illustrates the distribution of bed shear stress (represent velocity distribution and the bed shear stress (τ) for the low flow (Q=97m^3/s) and high-flow (Q=584m^3/s) condition. It can be observed during the low flow condition, higher bed shear stress zones are located closer to the banks. This is due to the fact that the flow alignment is close to the banks where the channel bed elevation is lower. On the other hand, during the high flow ,the higher bed shear stress zones are uniformly distributed across the channel or more along the channel center. The implication of this result is that the erosion of banks are most likely to be caused by the low flow condition rather than the high flow. Also during the receding period from high to low flow, there can be a sudden change in the bed shear stress which might result in the bank failure. Therefore while implementing the bank protection works, both high & low flow phenomena should be considered.
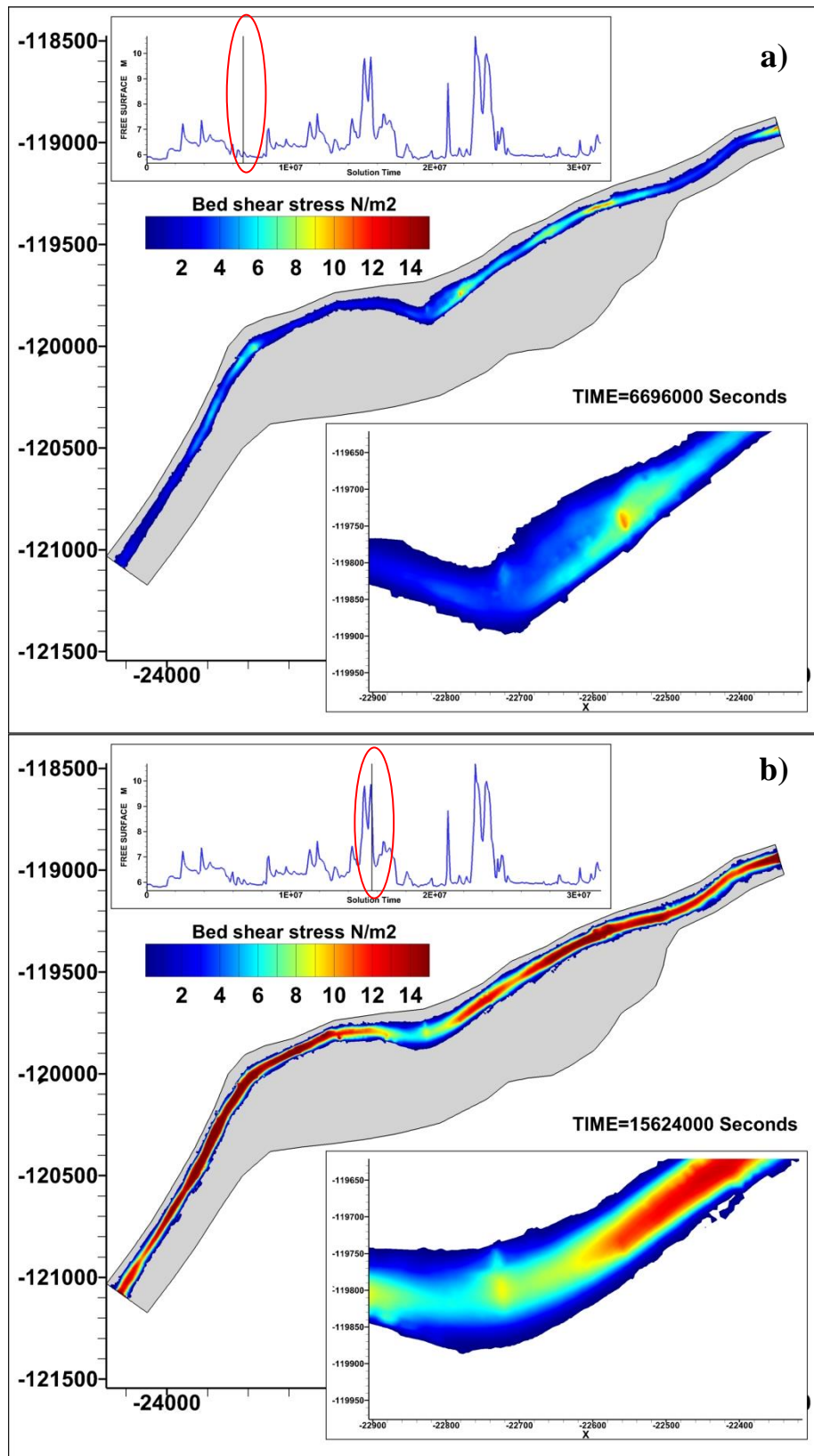
Figure 4.31 Bed shear stress (τ) distribution for a) low flow b) high-flow condition
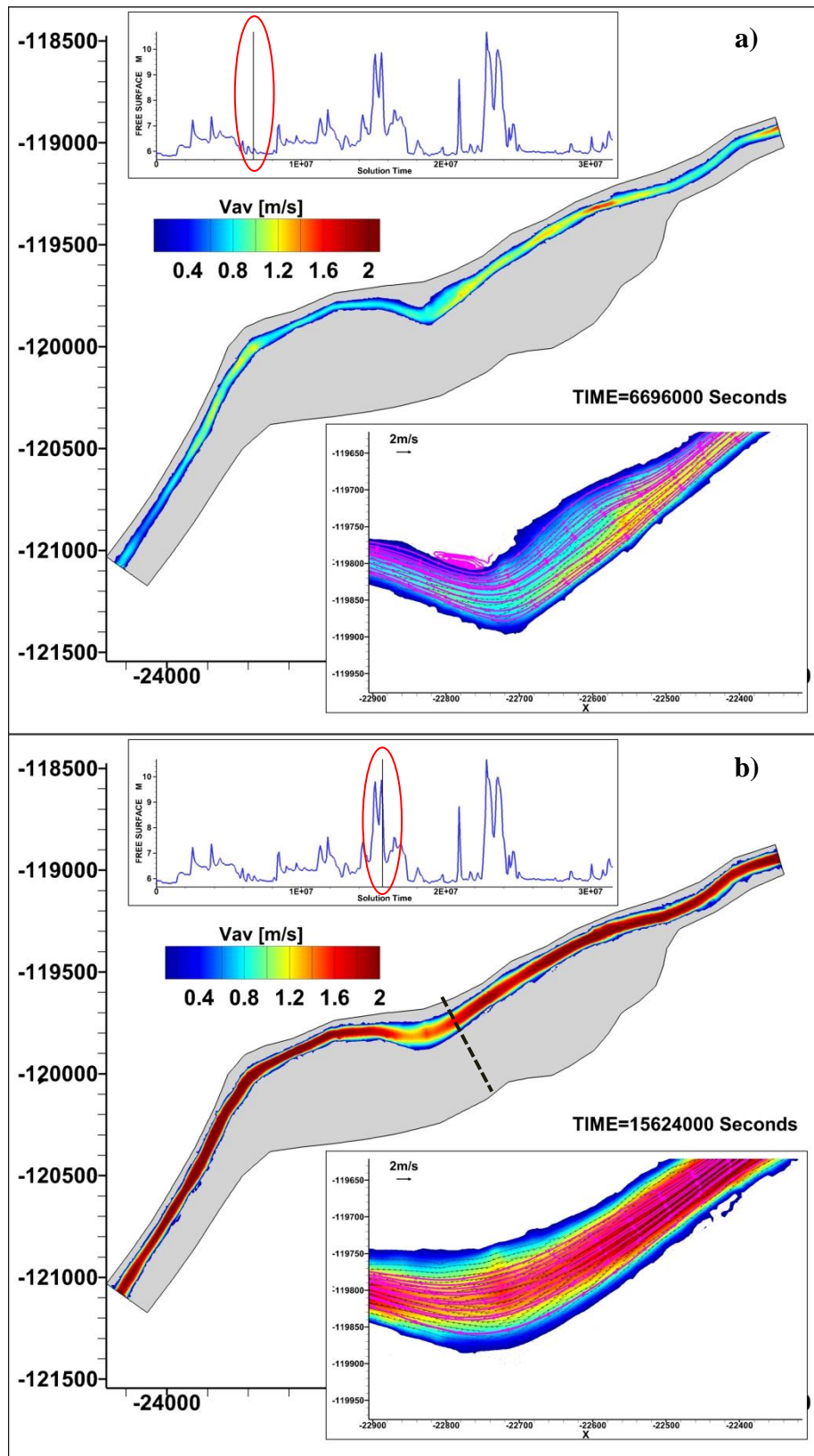
Figure 4.32 Depth-averaged velocity (m/s) distribution for a) low flow b) high-flow condition

(The pink lines in the figure indicate streamlines of depth-averaged velocity)
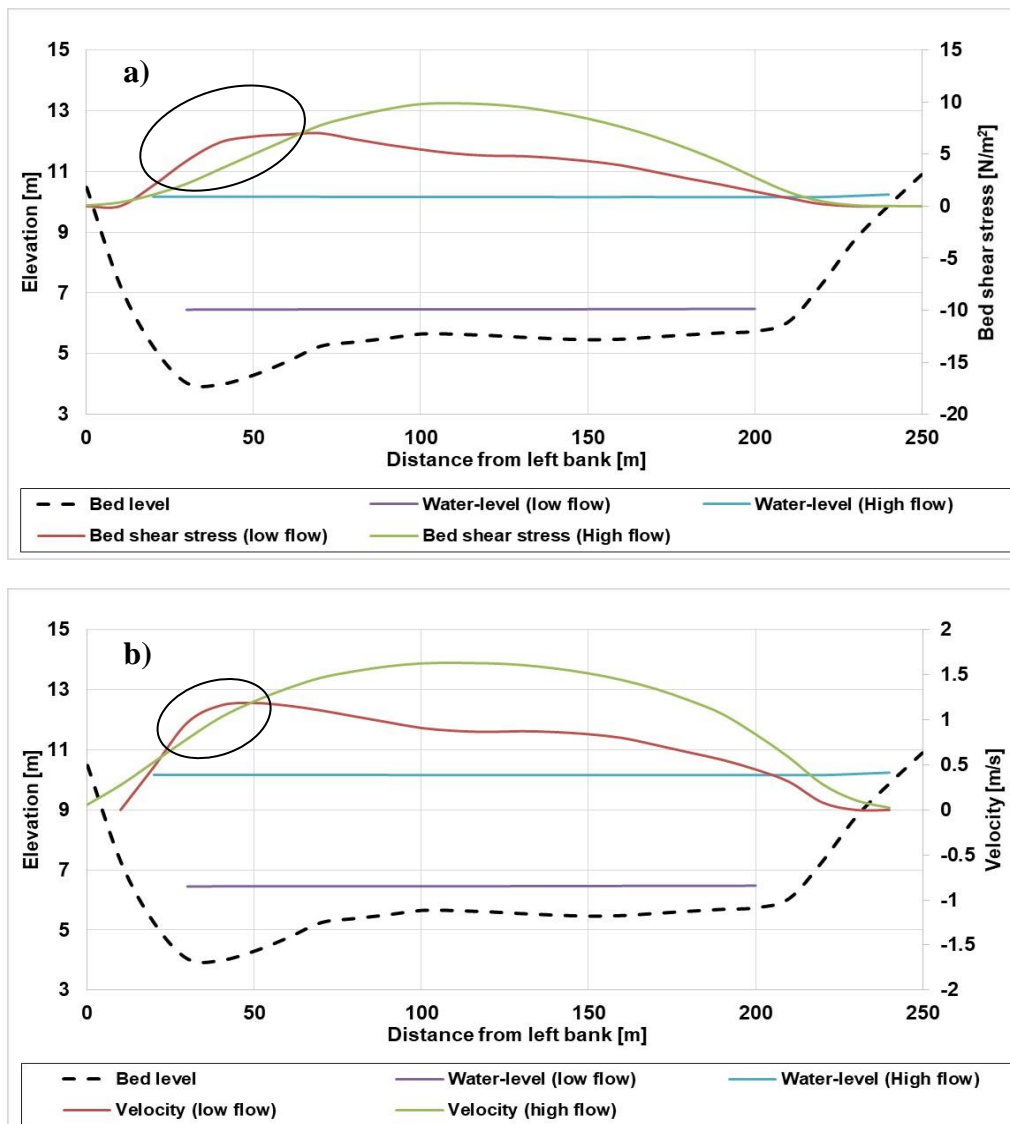
Figure 4.33 Cross-sectional variation of a)bed shear stress b)depth-averaged velocity
[See **Figure 4.32b** for the location of the x-section]

However, results showed that the overall channel evolution is insignificant in the Uji River. The reason behind this is the channel degradation that has been caused due to the construction of Amagashe dam in the upstream. The Amagashe dam cut the sediment supply to the river downstream. Consequently, the river degraded to such an extent that further river bed change became insignificant. This can be more clearly seen from the river profile data of the Uji River in **Figure 4.30**. The other reason might be the sediment size that we prescribed to the model which were relatively coarser. The shear stress necessary for the transport of such coarser materials could not be reached.

Similarly, in **Figure 4.32**, distribution of the depth-averaged velocity are plotted for the same flow conditions as above. It can be seen that the streamlines are more oriented towards the bank during the low flow while during the high flow, higher velocity flow is concentrated towards the channel center. For a more clear understanding, we plotted the cross-sectional variation of the bed shear stress and velocity in **Figure 4.33**. As mentioned above, it can be clearly seen that for the low flow condition, both near-bank bed shear stress and the velocity are greater than that for the high flow condition.

4.3.5 Bank erosion prediction in Uji River

In the 2D simulation of bed evolution, we identified that the overall channel evolution was insignificant along the study reach. However, it was observed from satellite imagery analysis that bank erosion at several locations is severe along the study reach. Therefore predicting the bank failure would be vital in the appropriate planning and implementation of bank erosion control measures. In this context, we made an effort to apply a bank erosion model to the study reach with an objective to check the dominant mode of bank erosion as well as evaluate model capability in predicting the bank erosion processes. In this regard, several bank failure algorithms have been formulated ranging from the simplified angle of repose approach to the more complex physically based models (El Kadi Abderrezzak et al., 2016;). Among various bank erosion models, Bank Stability and Toe Erosion Model (BSTEM) is a widely used model developed by the National Sedimentation Laboratory in Oxford, Mississippi, USA (Langendoen and Simon, 2008; Simon et al., 2010, 2000). A brief introduction on the science behind the BSTEM model and its application to the Uji River is presented in this section.

1) Model Description

BSTEM couples iterative planar bank failure analysis based on a fundamental force balance with a toe scour model that considers the interaction between the hydrodynamics and the toe scour/deposition. The two major modes of bank failure algorithms embedded into BSTEM are:

a) Bank Failure

Bank failure mode accounts for the geotechnical failure which computes a number of failure planes as required through the bank to determine if the gravitational forces exceed the resisting frictional forces. The bank stability model performs a series of iteration to select probable failure planes, calculate the factor of safety and converge on the most likely failure plane using the following steps (CEIWR-HEC, 2015):

i) Determine the factor of safety (FS) for nodes at several vertical points on the channel bank.

ii) Compute critical factor of safety, FS_{cr}) for each vertical location after selecting the bounding

failure planes (minimum and maximum angle)

iii) Select the most probable critical failure plane (FS_i~FS_{cr})

iv) Use the above information to update the critical failure plane ($FS_{i+1} \rightarrow FS_{cr}$)

v) Decide when the FS is close to FS_{cr} to stop

vi) If FS_{cr} is less than 1, fail the bank, update the cross-section, and supply the sediments to the channel for transport.
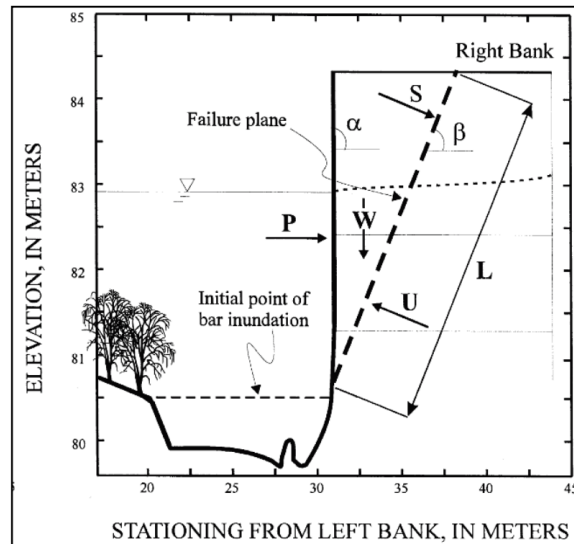
Figure 4.34 Force diagram for layer method [Adapted from (Simon, 2000)]

We used Layer method to compute the FS of a failure plane through the bank. In this method a non-iterative equation [**Eq. 4.1**] is solved to determine the FS which compares the disturbing or driving force to the balancing or resisting force. **Figure 4.34** illustrates the force diagram involved in this method.

[4.1]

$$FS = \frac{\sum_{i=1}^{I} c_i' L_i + S_i tan\emptyset_i^b + [W_i cos\beta - U_i + P_i cos(\alpha - \beta)]tan\emptyset_i'}{\sum_{i=1}^{I}(W_i\ sin\beta - P_i sin[\alpha - \beta])}$$

i=layer

L=length of failure plane

S=matrix suction force

U=hydrostatic lift

P=hydrostatic confining force of the water in the channel

$\emptyset'$= friction angle

$\emptyset^b$= relationship between matrix suction and apparent cohesion

c'= effective cohesion

β= angle of failure plane

$W_i sin\beta$= the component of soil weight down the failure plane, driving the soil downward

103

$W_i cos\beta tan\emptyset_i'$= frictional resisting of the soil along the failure plane.

$W_i cos\beta$=component of soil weight normal to failure plane

$\emptyset_i'$=friction angle of the soil

$c_i' L_i$=effective cohesion per unit length

$P_i cos(\alpha - \beta) tan\emptyset_i'$=the normal component of the hydrostatic confining forces the water in the channel

$-P_i sin[\alpha - \beta]$=the component of the hydrostatic confining forces acting along the failure plane

$U_i tan\emptyset_i'$=hydrostatic uplift force

$S_i tan\emptyset_i^b$=suction forces

b) Toe Erosion

The toe erosion module of BSTEM computes undermining of the bank toe as a result of fluvial erosion (Simon et al., 2000; Midgley et al., 2012). Excess shear stress formulation originally proposed by Partheniades (1965) is adopted to predict the erosion. Erosion rate, ε (m/s), is calculated as:

$$\varepsilon = k(\tau_0 - \tau_c)^a \qquad [4.2]$$

k is erodibility coefficient (m³N⁻¹S⁻¹), $\tau_0 = \gamma RS$ is average shear stress (Nm⁻²), τ_c is critical shear stress and a is exponent whose value is assumed as 1. The parameters k and τ_c depend on the properties of the soil. BSTEM divides the bank profiles into several nodes and for each of the nodes calculates τ_0 based on the flow segment affecting each node. Thus, a distribution of τ_0 is generated along the banks rather than just one average shear stress over the entire bank. To correct the boundary shear stress due to the effect of secondary flow in meandering channels, 'no-lag kinematic model' [**Eq. 4.3**] is used (Crosato, 2009).

$$\tau_0 = \frac{\gamma_w n^2 (u + U)^2}{R^{1/3}} \qquad [4.3]$$

where n is Manning's roughness coefficient, u is the channel-averaged flow velocity (m/s) and U is the increase in near-bank velocity due to superelevation (m/s).
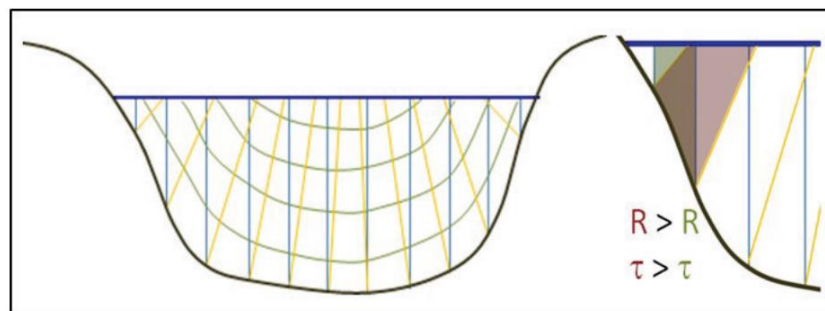
Figure 4.35 Division of cross-sections into vertical (blue) and radial prisms (yellow) perpendicular to isovels for determining near bank shear stress (CEIWR-HEC, 2015)
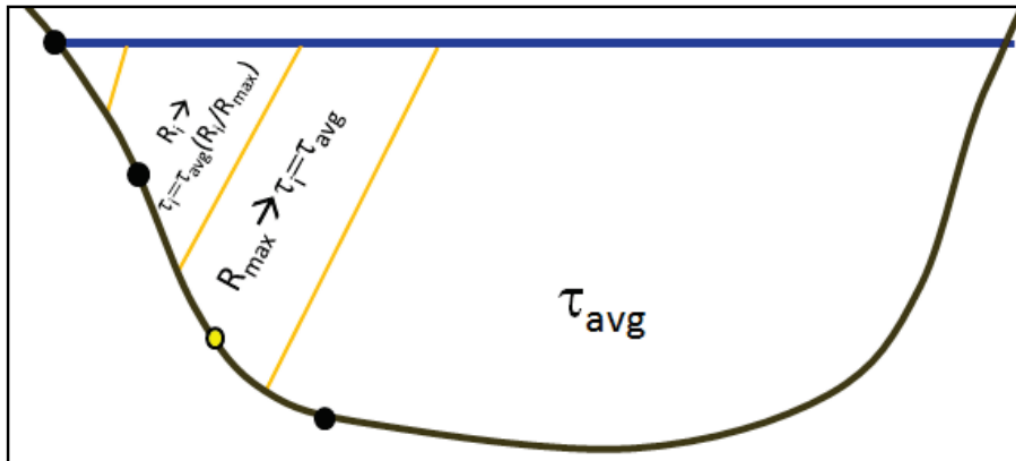
Figure 4.36 Partitioning the shear stress by the ratio of hydraulic radius of the radial prisms (CEIWR-HEC, 2015)

Figure 4.35 represents the division of the near bank area into number of radial prisms for calcualting the shear stress for each component. Similarly **Figure 4.36** represent the determination of the near bank shear stress for each radial prism according to the weightage of hydraulic radius of each radial prisms. The shear stress for any radial prism *i* is given by the following relation,

$$\tau_i = \tau_{avg}(\frac{R_i}{R_{max}}) \qquad [4.4]$$

R_{max} which is basically R_{toe} is the largest hydraulic radius among the radial prisms.

2) Model Input and set-up

BSTEM requires river bathymetry, flow hydrographs and the soil parameters data as an input to calculate bank erosion analysis. The flow and the river bathymetry data is the same as mentioned in **section 4.3.2**. However, the measured data on riverbank soil parameters were unavailable. Accordingly, we had to choose from the default data available in the model. The soil parameters for the selected material type is presented in **Table 4.1.** Similarly, the soil groundwater table data were also unavailable. Therefore we set the static groundwater level at 5m elevation.

Table 4.1 Soil parameters selected for the study reach [Adapted from (CEIWR-HEC, 2015)]

Default material type	Saturated Unit Weight (lb/ft³)	Friction angle ∅	Cohesion (lb/ft²)	∅ᵇ	Critical shear (lb/ft²)	Erodibility (ft³/lb-s)
Moderate soft clay	112.7	26.4	171.26	15	0.1044	2.86*10⁻⁴

Four cross-sections were selected where the rate of bank erosion was high depending on the satellite imagery as well as field observations. **Figure 4.37** illustrates the cross-sections chosen for the analysis of bank erosion.

3) Application in Uji River

Figure 4.38 shows the evolution of cross-sections due to the erosion of banks after one year of simulation. It can be seen that toe erosion is dominant in cross-sections 1-3 whereas bank failure mode is more prominent in cross-section 1. The rate of bank erosion was higher in cross-sections 2-4 which may be due to their location along the bend. The distribution of bed shear stress in **Figure 4.31** matches with the erosion locations. **Figure 4.39** compares the observed and the
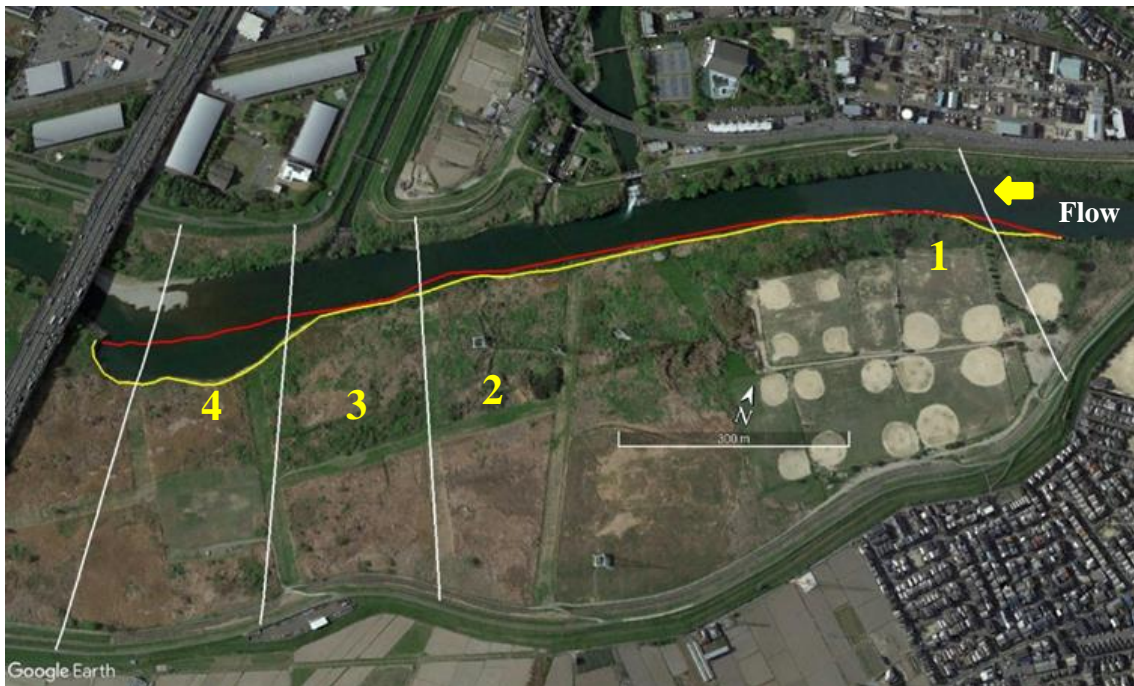
Figure 4.37 Cross-sections selected for bank erosion analysis

simulated bank erosion rate. The predicted bank erosion rate closely matches the observed value at cross-sections 1 and 4. However, at sections 2 and 3, the model over predicted the erosion rate. This might be due to several factors. First, the bank material properties are assumed based on the default model data which could lead to uncertainty in the prediction. Similarly, the erosion rate is calculated as an average of the last 14 years of data. If we consider only the recent year's data, the predicted value will lie closer to the observed.
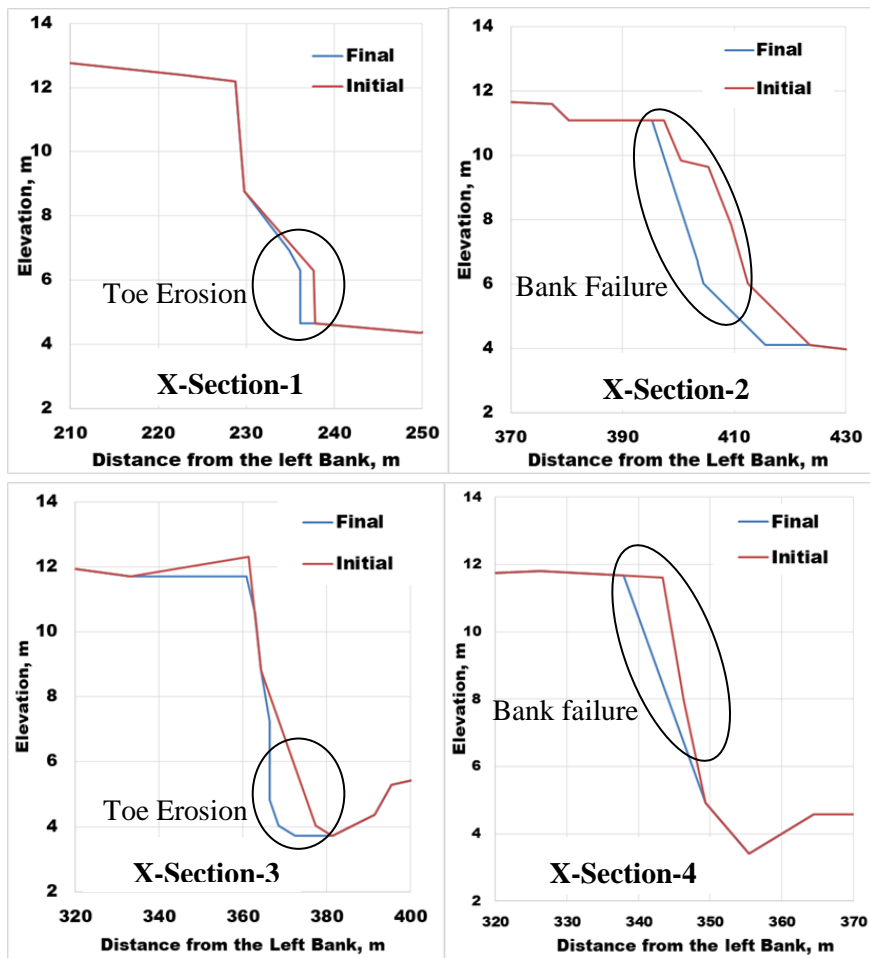
Figure 4.38 Comparison of bank evolution at selected cross-sections
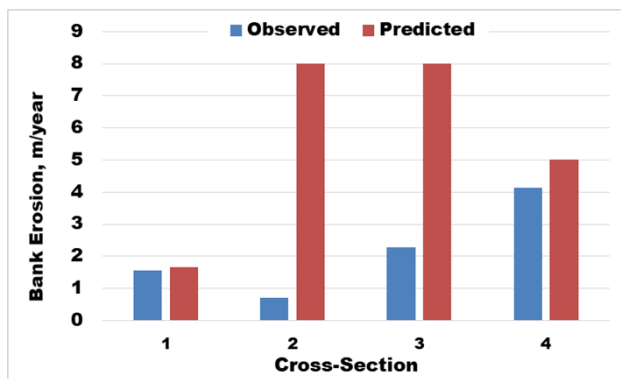
Figure 4.39 Comparison between the observed and the computed cross-sections

4.4 Summary

In this chapter, we discussed the two cases of field application of 2D numerical models. Application of numerical models to the real field cases is challenging due to the interaction of

various phenomena. Therefore, reproducing real field phenomena is a difficult task. Another hindrance is the availability of the measured data of river bathymetry, discharge, water-level, bed and bank materials, etc.

The application of 2D model showed it can reasonably reproduce the morphological phenomena of meandering rivers. In the case of Gowain River, Bangladesh initial bathymetry was largely assumed and obtained from the previous works. The channel evolution phenomena closely matched the observed trends. It was found that the channel erosion is mainly critical at the entry and the exit of a bend. The implementation of groynes suggested that it can have a significant effect on the overall channel bed evolution phenomena. The erosion near the banks was shifted away towards the channel. Two different orientation of groynes were examined. The results indicated that each of the orientation has its own pros and cons. Therefore, in order to achieve optimum functioning, the combination of both types of orientation is recommended.

Similarly, we performed another case of field application in Uji River, Japan. Due to the availability of the measured data, the initial bathymetry was more reliable in case of the Uji River. The results showed that the overall channel evolution phenomena are not so dominant. However, the analysis of satellite images revealed that bank erosion at different locations has become serious. The results also signified that the low flow condition is more responsible for the continuous erosion of banks because it was observed that the near bank bed shear stress and velocity were greater during the low flow. However, the sediment data from the actual river couldn't be obtained. By incorporating further reliable data, we can improve the results in the future and also examine varieties of scenarios of bed and bank evolution for supporting the river management practitioners and the planners. Results of the prediction of bank erosion indicated that fluvial erosion due to the scour near the bank toe is dominant at most of the locations in Uji River. Finally, it is suggested that in the case of implementation of river bank protection works, research and analysis through simulation might help to select the optimum methods.

Chapter 5

3-Dimensional numerical modeling of flow and morphology

5.1 Introduction

The meandering of natural rivers generates a complicated flow structure which is characterized by high turbulence and three-dimensional features. The flow field is further made complex due to the implementation of different structures in the river channels for bank protection. Understanding of the flow structures and channel evolution due to different bank protection structures are essential for the appropriate planning and implementation of such structures. Although 2D models can satisfactorily reproduce the bed morphological phenomena, they cannot fully capture the complicated flow processes generated by the interaction of channel curvature, bed evolution and the bank protection structures (Zeng et al., 2008). Therefore, three-dimensional models are useful in understanding the in-depth mechanism of the flow field evolution. Studies have shown that bank protection structures like groynes tend to disrupt the secondary flow and redistribute the vertical flow structures (Matsuura and Townsend, 2004). Even though several previous studies have tried to investigate the three-dimensional flow features in meandering channel or channel bends (Kashyap, 2012; Zeng et al., 2008), none of those has emphasized the role of channel sinuosity or curvature on the evolution of flow field. Previous studies considering the role of channel sinuosity and curvature have focused only on the channel evolution and depth-averaged velocity patterns (da Silva et al, 2006).

In this chapter, we applied a three-dimensional model to study channels with objectives to investigate the flow phenomena affecting channel bank erosion process and the effectiveness of groynes in minimizing the erosion by redistributing the velocity.

5.2 Model description

We used an open source library of Telemac-3D to formulate the 3D model that fits our case studies. Telemac-3D is developed by the LNHE (Laboratoire National d'Hydraulique et Environnement) of the Research and Development Division of EDF (EDF-R&D), France. Telemac-3D is a three-dimensional computational code which computes the 3D velocity field (U, V, W) and the water depth h (and, from the bottom depth, the free surface S) at each time step (Mattic, 2018). Although the non-hydrostatic assumption is also available, in this study, we used the hydrostatic pressure hypothesis.

Following assumptions are made under the hydrostatic hypothesis;

  i) Three-dimensional Navier-Stokes equations with a free surface changing in time,

  ii) Incompressible fluid i.e. the variation of density in mass conservation is negligible

  iii) Hydrostatic pressure hypothesis i.e. the total pressure at any given depth is the summation of the air pressure at the free surface plus the weight of the overlying water body,

  iv) Boussinesq approximation for the momentum (the density variations are only taken into account as buoyant forces)

5.2.1 Governing equations

The governing equations of the 3D model based on the above assumptions are;

$$\frac{\partial U}{\partial x} + \frac{\partial V}{\partial y} + \frac{\partial W}{\partial z} = 0 \qquad [5.1]$$

$$\frac{\partial U}{\partial t} + U\frac{\partial U}{\partial x} + V\frac{\partial U}{\partial y} + W\frac{\partial U}{\partial z} = -g\frac{\partial Z_s}{\partial x} + \vartheta\Delta(U) + F_x \qquad [5.2]$$

$$\frac{\partial V}{\partial t} + U\frac{\partial V}{\partial x} + V\frac{\partial V}{\partial x} + W\frac{\partial V}{\partial z} = -g\frac{\partial Z_s}{\partial y} + \vartheta\Delta(V) + F_y \qquad [5.3]$$

$$p = p_{atm} + \rho_0 g(Z_s - z) + \rho_0 g \int_Z^{Z_s} \frac{\Delta\rho}{\rho_0} dz' \qquad [5.4]$$

Z_s=free surface elevation

U, V, W=3-D components of velocity

p=pressure

p_{atm}=atmospheric pressure

g=acceleration due to gravity

ϑ=kinematic viscosity

z=vertical space components

t=time

x, y=horizontal space coordinates

F_x, F_y=source terms denoting bottom friction forces

h, U, V, W=unknown variables called 'computational variables'

5.2.2 Solution steps

As described in the user guide and the theoretical description of Telemac3D, the basic algorithm of solution for the equations can be divided into three computational steps (three fractional steps) which are;

i) In the first step, the advected velocity components are determined by only solving the advection terms.

ii) In the next step, the new velocity components are computed from the initially calculated advected velocities but taking into account the diffusion terms and the source terms in the momentum equations. These two solutions enable to obtain an intermediate velocity field.

iii) The third and the final step consists of computing the water depth from the depth integration of the continuity and the momentum equations but only including the pressure-continuity terms (where all the other terms have already been taken into account in the earlier two steps). The resulting two-dimensional equations (analogous to the Saint-Venant equations without diffusion, advection and source terms) can be represented as:

$$\frac{\partial h}{\partial t} + \frac{\partial (Uh)}{\partial x} + \frac{\partial (Vh)}{\partial y} = 0 \qquad [5.5]$$

$$\frac{\partial U}{\partial t} = -g\frac{\partial Z_s}{\partial x} \qquad [5.6]$$

$$\frac{\partial V}{\partial t} = -g\frac{\partial Z_s}{\partial y} \qquad [5.7]$$

The 2-D velocity components U and V are solved by the libraries in the Telemac2D code which allows to obtain the depth-averaged velocity and the water depth. This water depth makes it possible to re-compute the elevations of the various mesh points and then those of the free surface. The computation of the U and V velocities is achieved through a combination of the equations linking the velocities. Finally, from the continuity equation, the vertical velocity W is determined.

5.2.3 Bed Evolution Model

The mechanism involved for the coupling of hydrodynamic module of Telemac3D and the sediment transport module SISYPHE is basically the same as described in **section 3.3.2** of **chapter 3** of this thesis. The bed load transport method and the governing equations for the bed evolution model are the same as given in **equations [3.4-3.10].** A brief steps of the solution method for bed evolution is given below:

1. The hydrodynamic module Telamac3D runs for a time step and calculates the water depth and velocity components. This information is passed over to the sediment transport module.
2. With this information of velocity and water depth from Telemac3D module, sediment transport module solves the transport equation for a time step, thus calculating bottom elevation changes.
3. The new bed topography value is then used by the hydrodynamic module at the next time step, and so on.

5.2.4 Turbulence model

In this study, we applied a $k - \varepsilon$ turbulence model whose equations of which are:

$$\frac{\partial k}{\partial t} + U\frac{\partial k}{\partial x} + V\frac{\partial k}{\partial y} + W\frac{\partial k}{\partial z} = \frac{\partial}{\partial x}\left(\frac{v_t}{\sigma_k}\frac{\partial k}{\partial x}\right) + \frac{\partial}{\partial y}\left(\frac{v_t}{\sigma_k}\frac{\partial k}{\partial y}\right) + \frac{\partial}{\partial z}\left(\frac{v_t}{\sigma_k}\frac{\partial k}{\partial z}\right) + P - G - \varepsilon \quad [5.8]$$

$$\frac{\partial \varepsilon}{\partial t} + U\frac{\partial \varepsilon}{\partial x} + V\frac{\partial \varepsilon}{\partial y} + W\frac{\partial \varepsilon}{\partial z} = \frac{\partial}{\partial x}\left(\frac{v_t}{\sigma_\varepsilon}\frac{\partial \varepsilon}{\partial x}\right) + \frac{\partial}{\partial y}\left(\frac{v_t}{\sigma_\varepsilon}\frac{\partial \varepsilon}{\partial y}\right) + \frac{\partial}{\partial z}\left(\frac{v_t}{\sigma_\varepsilon}\frac{\partial \varepsilon}{\partial z}\right) + C_{1\varepsilon}\frac{\varepsilon}{k}[P + (1 - C_{3\varepsilon})G] - C_{2\varepsilon}\frac{\varepsilon^2}{k}$$

$$[5.9]$$

Wherein:

$k = \frac{1}{2}\overline{u_\iota' u_\iota'}$=turbulent kinetic energy

$u_i' = U_i - \overline{u_\iota}$=$i^{\text{th}}$ component of the fluctuation of **U**(U, V, W)

$\varepsilon = v\overline{\frac{\partial u_i'}{\partial x_J}\frac{\partial u_i'}{\partial x_J}}$=dissipation of turbulent kinetic energy

P=turbulent energy production term

G=source term due to the gravitational forces

$$P = v_t(\overline{\frac{\partial U_\iota}{\partial x_J}} + \overline{\frac{\partial U_\iota}{\partial x_\iota}})\overline{\frac{\partial U_\iota}{\partial x_J}}; \quad G = -\frac{v_t}{Pr_t}\frac{g}{\rho}\frac{\partial \rho}{\partial z}$$

$$v_t = C_\mu\frac{k^2}{\varepsilon}$$

$C_\mu, Pr_t, C_{1\varepsilon}, C_{2\varepsilon}, C_{3\varepsilon}, \sigma_k, \sigma_\varepsilon$ are constants in $k - \varepsilon$ model.

5.2.5 Mesh Discretization

Mesh generation and its discretization is an important aspect of any modeling studies. Furthermore, in 3D simulation, proper care needs to be given for the appropriate methods of mesh discretization because the model results and reliability can be affected by the mesh. Mesh in Telemac3D could be transformed from the 2D mesh generated for Telemac2d. The mesh discretization

i) The Telemac3D mesh structure is made of prisms (possibly split in tetrahedrons) a two-dimensional mesh comprising triangles which cover the computational domain (the bottom) in a plane is first constructed.

ii) The second step consists in duplicating that mesh along the vertical direction in a number of curved surfaces known as "planes".

iii) Between two such planes, the links between the meshed triangles make up prisms.

iv) The computational variables are defined at each point of the three-dimensional mesh, inclusive of bottom and surface.

U, V, W are "three-dimensional variables" and the water depth and the bottom depth which are defined only once along a vertical. Thus, they are "two-dimensional variables". Some Telemac3D actions are then shared with Telemac2D and use the same libraries, such as the water depth computation library. Therefore, it is well understood that Telemac3D should manage a couple of mesh structures: the first one is two-dimensional and is the same as that used by Telemac2D, and the second one is three-dimensional. **Figure 5.1** illustrates the mesh structure adopted in Telemac3D.
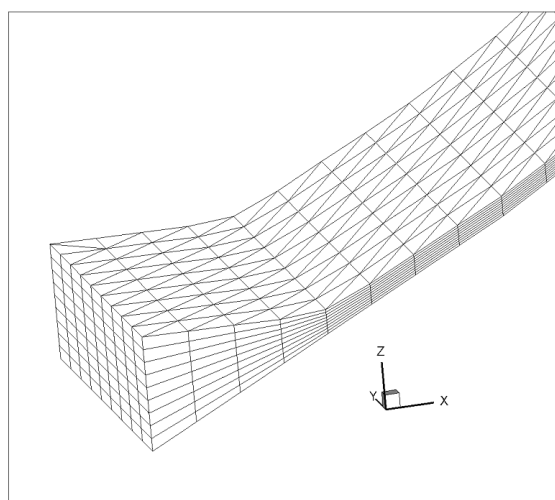
Figure 5.1 A three-dimensional mesh [adapted from the user manual of Telemac3d]

5.3 Model Set-up and Simulation cases

After preparing the mesh, the next step includes the setting up the model. Model set-up involves selecting the appropriate parameters for the simulation. The selection of different schemes for the solution of the underlying governing equations is a choice between the required accuracy and the computational time. Combination of different schemes was tested to select the optimum one. **Table 5.1** shows the model parameters selected for the simulation.

Table 5.1 Model parameters used for the simulation

Model parameters	Telemac-3D code	Scheme used
Mesh transformation	1	Sigma transformation
Number of horizontal levels	10	
Scheme for advection of velocities	1	Method of characteristics
Scheme for advection of depth	5	Explicit + Multidimensional Upwind Residual Distribution (MURD) Positive Streamwise Invariant (PSI) Scheme
Horizontal turbulence model	3	$k - \varepsilon$
Vertical turbulence model	2	Mixing length
mixing length model	3	Nezu and Nakagawa
Coefficient for diffusion of velocity	1.00E-06	
Solver for propagation	1	Conjugate gradient
Solver for vertical velocity	7	Generalized Minimal Residual (GMRES) method
Solver for diffusion of velocity	1	Conjugate gradient

Table 5.2 3D simulation cases in this study

Cases	Symbol		Duration
	Ch-45	Ch-60	
No groynes	Ch45NG	Ch60NG	60 minutes
Rectangular Groynes	Ch45G	Ch60G	60 minutes

For 3D simulation, we considered a total of four cases, two in each of the channels. In each channel, one case without any structure and the other with the structure were performed. **Table 5.2** represents the 3D simulation cases performed. Mesh resolution for different cases are presented in **Table 5.3.**

Table 5.3 Mesh resolution used for different cases of simulation.

Cases	Edge length (m)	No. of elements	No. of nodes
Ch45NG	0.02	5456	3078
Ch45G	0.02	7816	4321
Ch60NG	0.02	5936	3348
Ch60G	0.02	9492	5256

5.4 Model Validation

Before applying the model for the cases of this study, we validated it with the published experimental data. We considered two different cases; one for flow field under fixed bed experiments and the other for bed evolution considering the movable bed. The two validation cases are separately discussed in the next sections.

5.4.1 Validation case for flow field

We used the experimental data of (de Vriend, 1979) to validate the model. The experimental channel is shown in **Figure 5.2** which consists of a U-shaped channel bend. The hydraulic condition of the experiments is presented in **Table 5.4.** This experimental case was chosen mainly because of the availability of the measured data.

Table 5.4 Hydraulic condition in the experiments of de Vriend (1979)

Bed slope, S_o	Discharge, Q (m^3/s)	Mean flow depth, h_{av} (m)	Channel width, B (m)	Length (m)	Inner radius (m)	Outer radius (m)
0.00	0.189	0.18	1.7	25.35	3.4	5.1
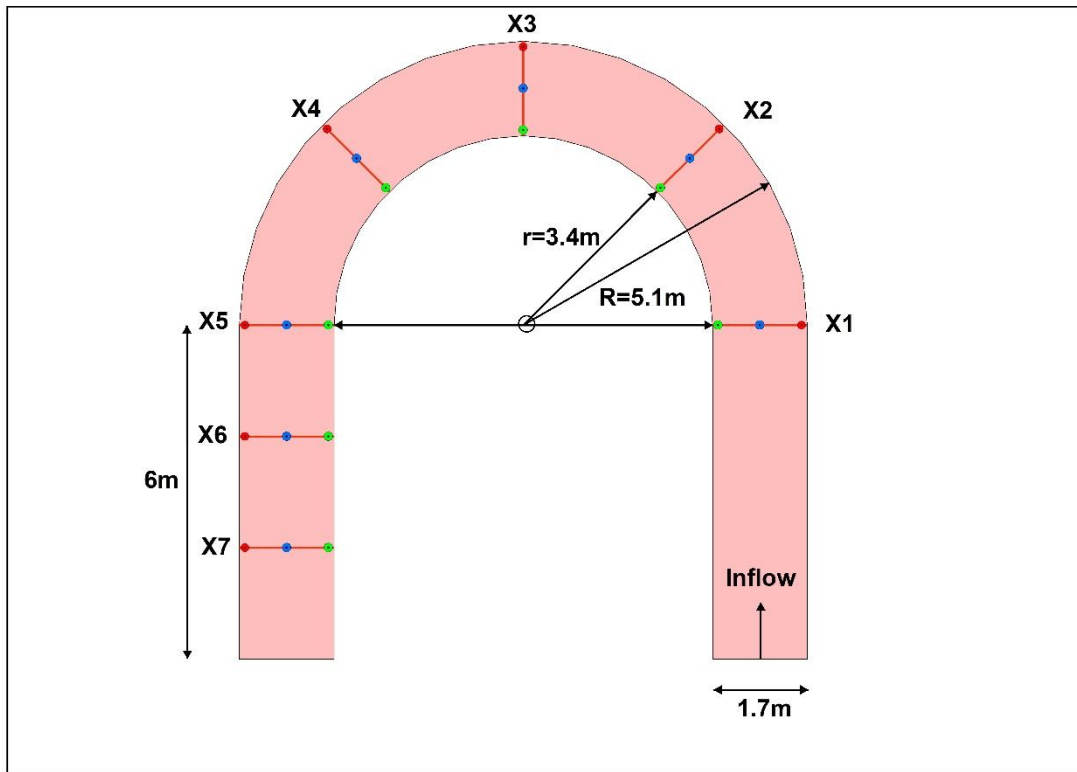
Figure 5.2 De Vriend experimental channel and the x-section locations for model validation.
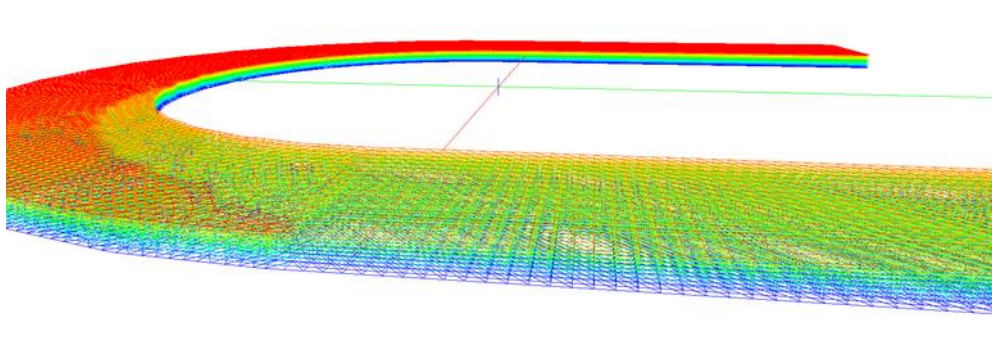
Figure 5.3 3-D mesh of the experimental domain used for the simulation.

The U-shaped bend is connected with straight rectangular channel of length 6m at the inlet and the outlet as shown in **Figure 5.2.** The channel bed is rigid and horizontal and the banks are fixed**.** For comparing the observed and the simulated data, we considered seven cross-sections (*X1-X7*) as indicated in the above **Figure 5.2**. The vertical velocity distribution is compared at X-section *X3* located across the apex of the bend and *X4* along the inner bank, center and the outer-bank as marked by the green, blue and the red dots respectively at each cross-section. Similarly, the water level is also compared along the inner, center and the outer bank separately. The inner and the outer bank points are located 10cm from the walls of the channels.

116
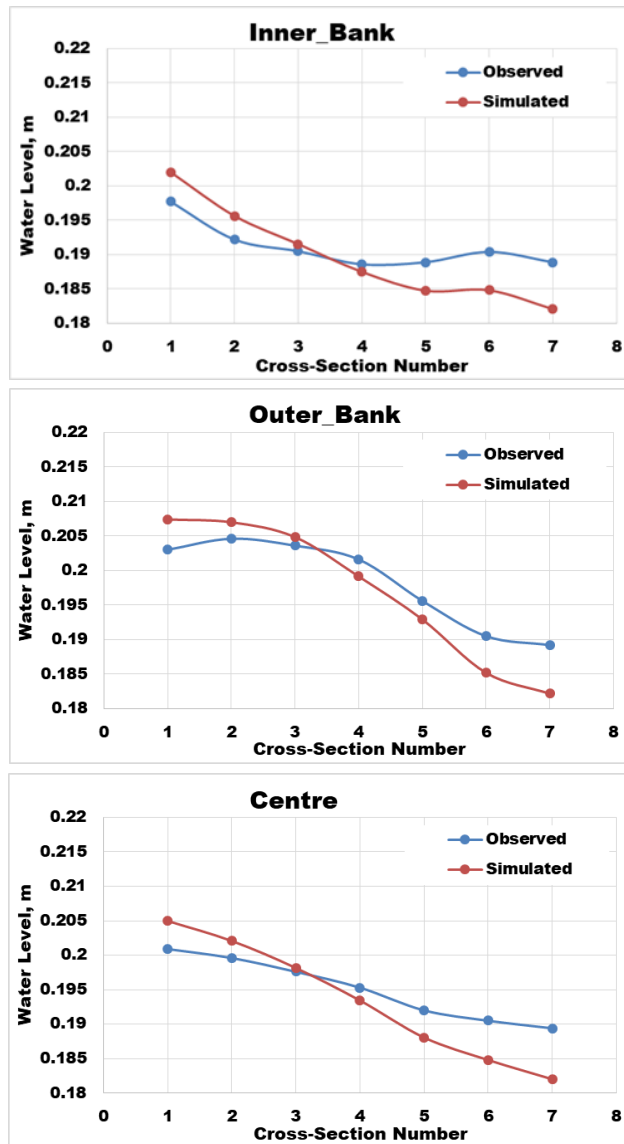
Figure 5.4 Comparison of the experimental and simulated water-levels.

Figure 5.4 illustrates the comparison between the experimental and simulated water-level along the inner, center and the outer bank of the cross-sections indicated as indicated in **Figure 5.2**. It can be seen that the simulation has satisfactorily matched the water-level pattern of the experiments. However, there is a slight overestimation near the inlet while a slight underestimation at the outlet. While at the middle sections *X2-X5,* the simulated result is more close to the observed ones. This slight deviation might be due to the bed and banks friction coefficients which couldn't be exactly determined for the simulation.

Similarly, **Figure 5.5** shows the comparison between the observed and the simulated velocity magnitude along with the depth at sections *X3* and *X4.* It can be seen that the vertical velocity distribution at the center of the channel is nearly the same in both cases. Similarly the distribution

117
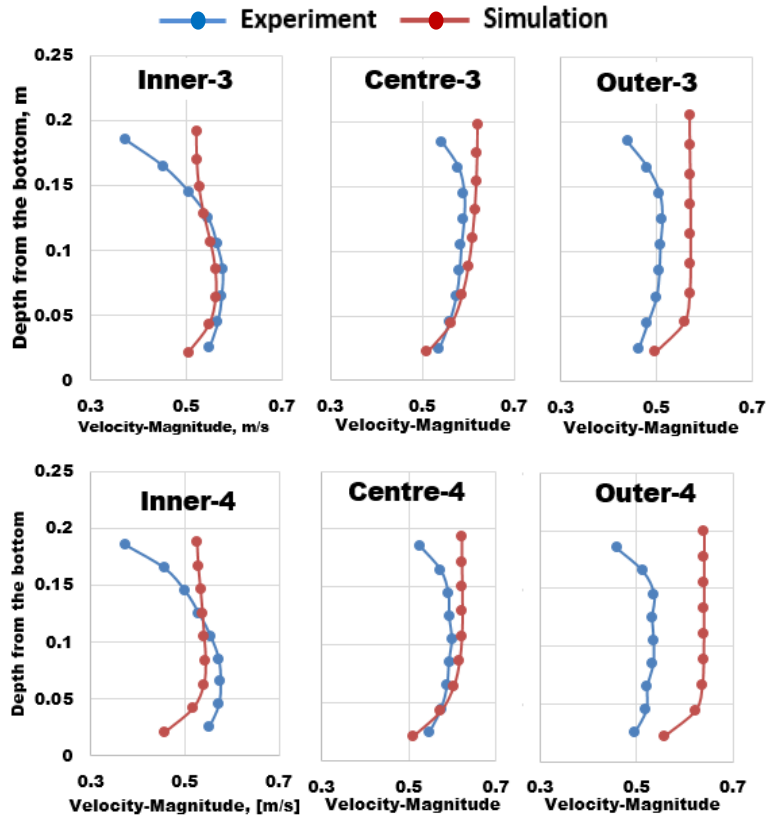
Figure 5.5 Comparison of vertical velocity at *X3* and *X4*.

is satisfactory at the inner bank too. However, at the outer bank, the simulation has slightly overestimated the observed results. Also in all the cases, the velocity at the surface is slightly higher than the observed. In overall, the simulated and observed results are in a close agreement. Therefore, this model could be applied to further cases. These variations at the different locations might be due to the effect of channel boundary roughness.

5.4.2 Validation case for bed evolution

After validating the model for fixed bed case, we performed another case of validation for the bed evolution incorporating the sediment transport. The experimental data for this case is the same as mentioned in the validation case of the 2D model in **section 3.3** of this thesis. The model was set-up in the same procedure as mentioned in **section 5.3** of this chapter.

With an average edge length of 4cm, a total of 9717 nodes and 18524 elements made up the computational mesh. The bottom 2D mesh was transformed vertically into 10 horizontal planes from the bottom to the top similar to Figure of the previous case. The simulation begins with a uniform depth i.e. 5cm of water throughout the channel. Since the computational time for 3D simulation is usually significantly greater than 2D, we used parallel computing with 4 cores. This enabled to reduce the computational time.

118
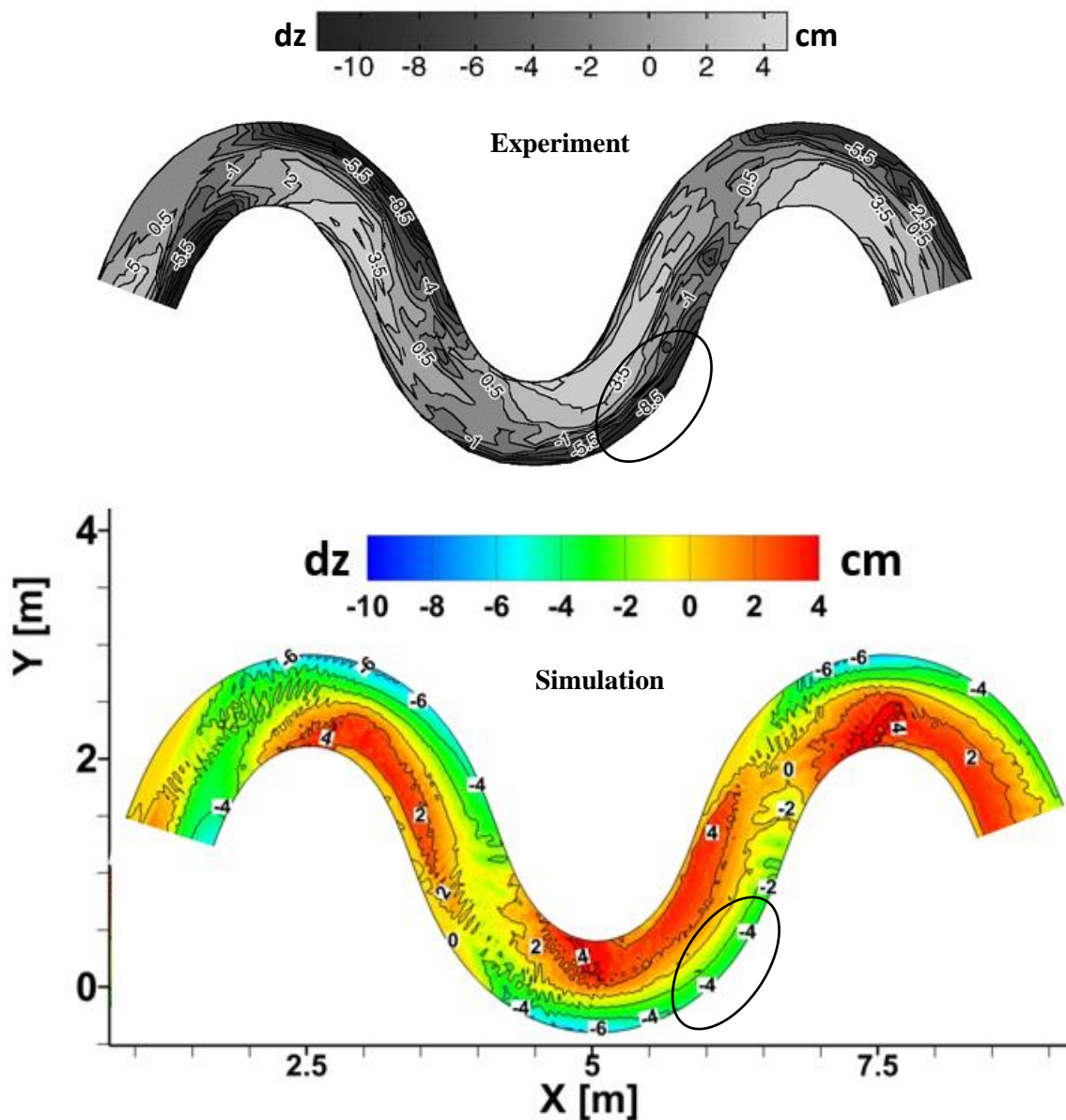
Figure 5.6 Comparison of bed evolution in experiment (top) and the 3D simulation (bottom).

Figure 5.6 depicts the final bed evolution at the end of the experiment and the simulation. It can be seen that the erosion-deposition pattern is nearly the same in both cases. The bed morphological features like the formation of the point bar and the deep pools are similar. The size and the location of these point bars and the erosion zones also match closely. However, at some locations, the erosion depth is underestimated in the simulation. This underestimation might be due to the channel bed and the wall friction coefficients whose value couldn't be sure about. The mesh size might also affect the result. Also, the complete sediment distribution data used in the experiments couldn't be obtained. With additional data, the results could be further improved. Nonetheless, the overall channel erosion-deposition pattern has been reasonably reproduced.

5.5 Application to the cases of this study

After performing the validation case for flow field and the bed evolution, we applied the model to four different cases of this study as already mentioned in **Table 5.3.** Here we present the results and discussions of the 3D simulation cases. For the analysis of the 3D flow field, we selected some representative cross-sections as shown in **Figure 5.7.** In each of the channels, for both cases of no groynes and with groynes, we selected one cross-section at the entry of the bend, at the apex, at the d/s of apex, the crossover and the final apex on the third bend. Across each cross-sections, velocity data were extracted at 11 points. From each banks, the first two points are 1cm apart and rest of the points are 2cm apart from each other. These cross-sections were chosen mainly due to their locations where the change in flow direction occurs. Analysis of the vertical velocity distribution, bed evolution, etc. are presented.
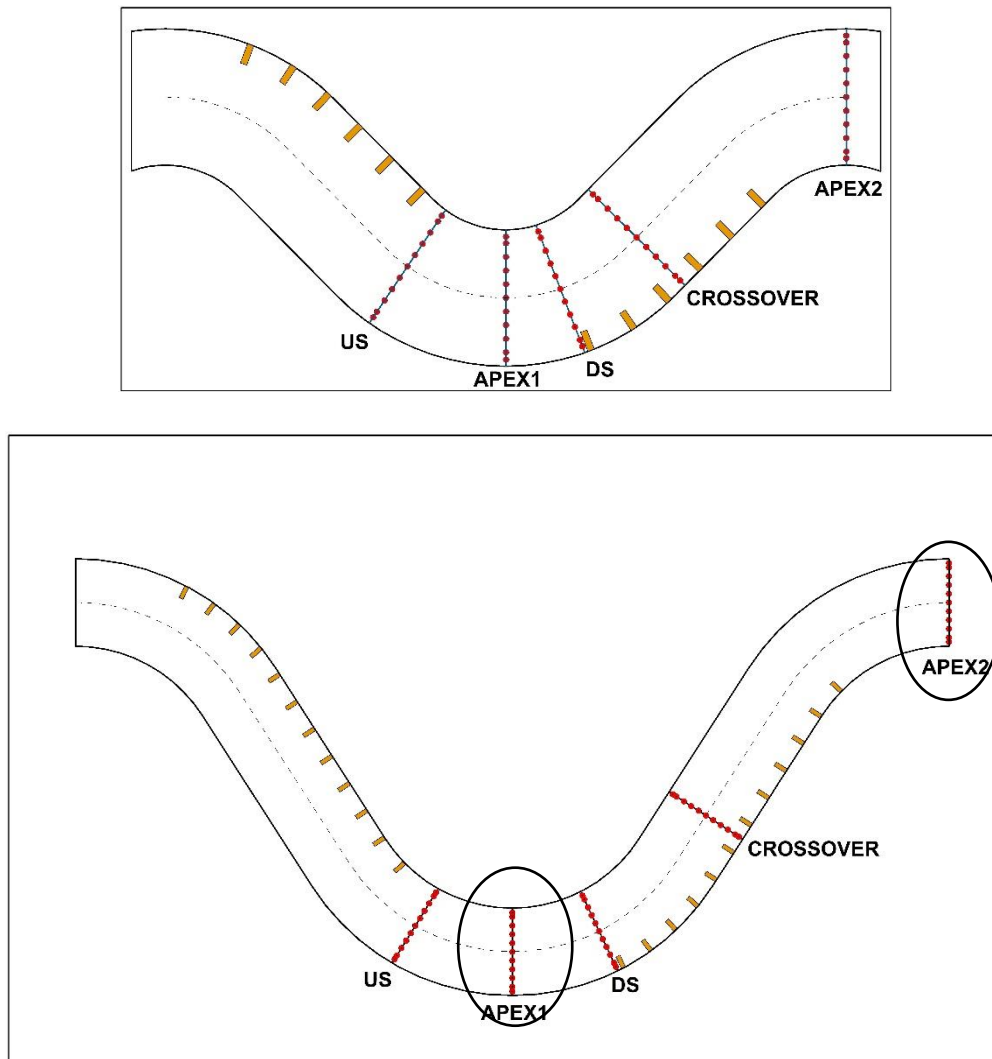
Figure 5.7 Locations of the x-sections for the analysis of 3D flow field

5.5.1 Results and Discussions

1) Channel Evolution

Bed evolution at the end of the simulation (t=60min) is presented in **Figure 5.8** for all cases of Ch-45 and Ch-60. Negative and positive values indicate erosion and deposition respectively. As expected in case *Ch45NG*, the zone of erosion is located downstream of the apex around the crossover region (**Figure 5.8 (a)**). This indicates a phase lag in the maximum erosion zone with the channel curvature   The point bar are formed downstream from the inner bend apex and extend nearly half of the bank length. After the groynes were implemented in case *Ch45G*, the erosion of the outer banks shifted towards the channel. In the first series of groynes, the scour near the tip was minimum. However, in the second series, scouring was greater in the initial groynes and decreased towards the downstream groynes. The shift of the flow towards the channel suppressed the growth of the point bar as it can be seen in **Figure 5.8 (b)** that its size and the extent has been considerably reduced. Just downstream of the last groynes in each series, greater deposition occurred due to the reduced velocity near the bank.
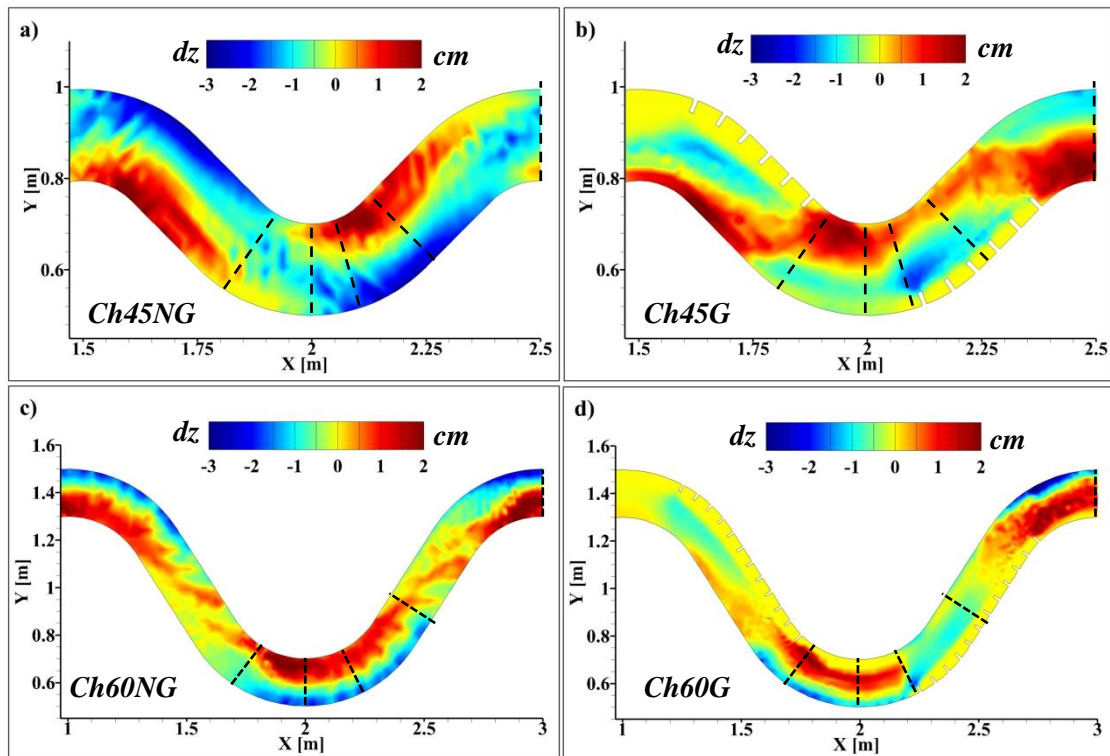
Figure 5.8 Bed evolution at the end of the simulation (a, b) Ch-45 (c, d) Ch-60

In Ch-60, it can be seen that in the absence of the groynes, erosion started slight upstream of the outer bank apex and extended near to the crossover region which indicates the erosion zones are in phase with the channel curvature. Accordingly, the location and the length of the point bar extended near to the same location on the opposite bank. It indicates that with an increase

in deflection angle, the location of maximum erosion shifts upstream towards the outer bank apex. With groynes, the erosion in the first bend was shifted towards the channel in front of the groynes. The point bar on the opposite bank downstream of the apex nearly disappeared in both bends. As in the case of *Ch45NG*, the deposition occurred downstream of the last groynes. The distribution of the depth-averaged longitudinal velocity in **Figure 5.11** (purple lines in the figure indicate streamlines of *UV* velocity) can be correlated with the locations of the maximum erosion-deposition zones for a clear understanding.

2) Flow Field
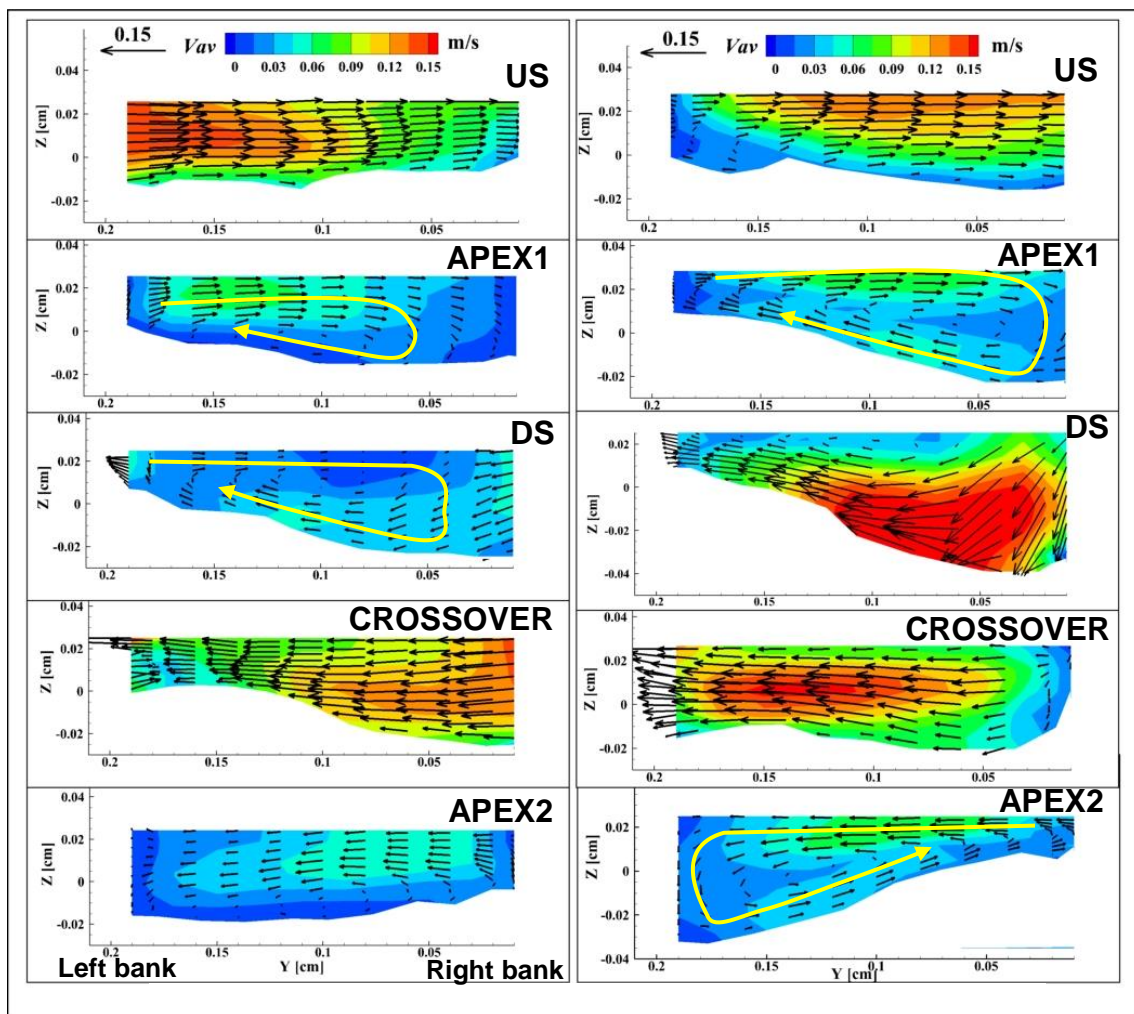
Column 1) Case *Ch45NG*, Without Groynes   Column 2) Case *Ch45G*, With Groynes

Figure 5.9 Cross-sectional distribution of *VW* velocity at different x-sections of Ch-45

To characterize the three-dimensional flow field, variation of velocity across different cross-sections were plotted as depicted in **Figure 5.9 (Column 1 and 2)**. The vectors indicate resultant of *VW*; the velocity component in *Y* and *Z* direction while the contour map indicates $\sqrt{V^2 + W^2}$.

There is a clear redistribution of velocity due to the effect of groynes. At section *US* without groynes, higher velocity is concentrated at the left bank but the flow is directed towards the opposite banks. But at the same section in case *Ch45G*, the higher velocity is shifted towards the channel with increased velocity on the opposite bank (Column 2, *US*). The tendency is similar for section *CROSSOVER* with higher velocities shifting to channel center with the reduction in bed elevation due to the erosion of point bar on the opposite bank. For section *APEX1*, since the approach flow in case *Ch45NG* is more directed towards downstream of the apex (**Figure 5.11a**), the velocity is still higher near the inner bank compared to the outer bank with minimum secondary circulation. But when the groynes were implemented in case *Ch45G*, the velocity variation increased with strong secondary circulation due to the presence of groynes in the downstream. This strong secondary current enhanced the transport of sediment towards the apex of the opposite bank as indicated by the deposition just downstream of the last groynes in **Figure 5.8(b)**. A similar pattern could be observed in section *APEX2*.

Column 1) Case *Ch60NG*, Without Groynes   Column 2) Case *Ch60G*, With Groynes
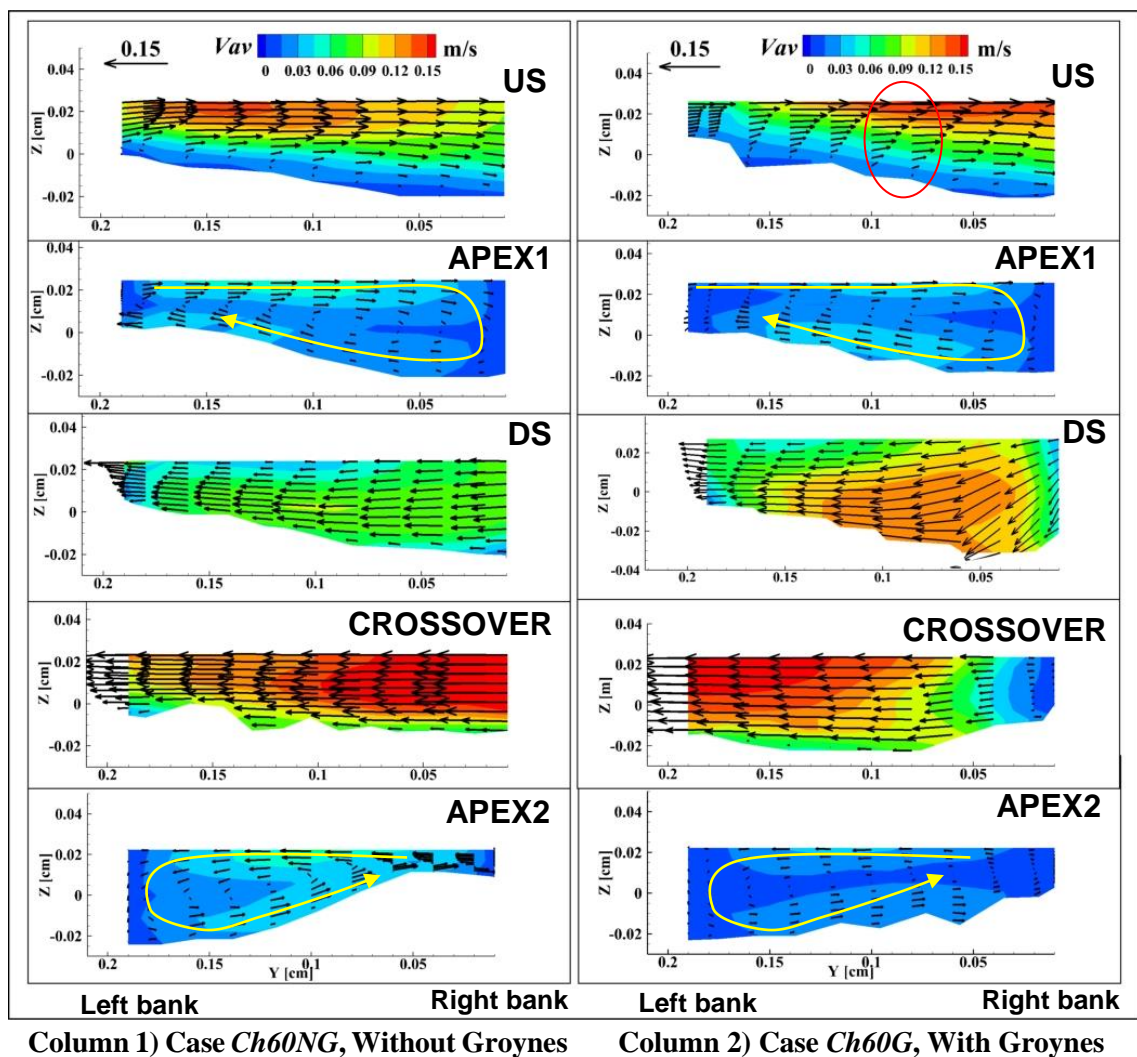
Figure 5.10 Cross-sectional distribution of *VW* velocity at different x-sections of Ch-60

The cross-stream velocity variation for the two cases of Ch-60 are plotted in **Figure 5.10** (Column 1 and 2). At section *US* (Column 1), the divergence of flow already begins slightly upstream (**Figure 5.11c**) due to which the high-velocity core doesn't exactly coincide with the left bank unlike in the previous case of *Ch45NG*. With groynes (Column 2, *US*), vertical velocity gradient increased with smaller velocity near the bed and greater velocity near the surface. At the same time, the higher velocity is shifted towards the right bank. At section *APEX1*, the secondary currents have reduced due to groynes which had increased in case *Ch45G*. Since this section is located between the two groynes on either bank, the accelerated flow from one groyne is damped by the next groynes. Also, the direction of the approach flow might be changed due to groynes and redistributed the secondary currents. Similarly, at section *DS* which is located just upstream of the first groynes, flow is nearly uniform but more directed in the transverse direction in the case without groynes. However, after the groynes were placed the near bank velocity was reduced and at the same time higher velocity zone developed towards the channel center with the strong downward flow around the groynes tip. This might be attributed to the vortex phenomena developed around the groynes. But in section *CROSSOVER* which is located exactly between the two groynes on the same bank, no such downward velocity vectors formed instead velocity reduced near the bank region as indicated in **Figure 5.10** (Column, 2, *CROSSOVER*). This velocity was higher near the right bank in case without groynes. Finally, at section *APEX2* located at the third apex, before the groynes placement, there was a significant secondary recirculation.
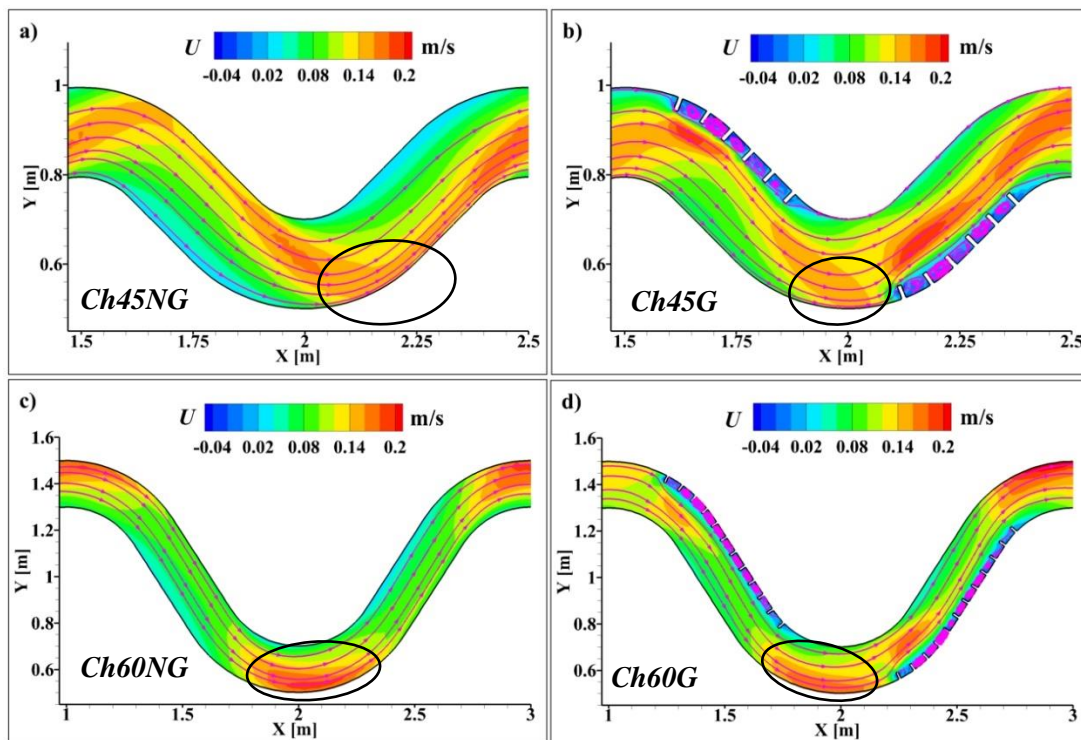
Figure 5.11 Distribution in plan the depth-averaged longitudinal component of velocity, *U*

However, in the case with groynes, the strength of the recirculation was reduced. This is due to the fact that the groynes on the opposite bank tend to converge the flow more upstream of the apex and thus the longitudinal component of velocity becomes more dominant than the cross-stream velocity which can be clearly observed from **Figure 5.11(d)**.

5.6 Summary

In order to overcome the limitations of 2D model, 3D simulations were carried out with an objective to investigate the three-dimensional flow field. The effect of the channel curvature on the depth-wise velocity distribution is analyzed. At the same time, the effect of groynes in reshaping the cross-sectional velocity distribution was studied.

We presented the analysis on the results of three-dimensional simulation of flow and morphology in meandering channels with and without groynes under different sinuosity and deflection angle. Results indicated a considerable difference in the flow and morphological characteristics with changing channel parameters. The flow pattern and locations of the maximum erosion-deposition zones indicated that the lower sinuosity channel is likely to translate or migrate downstream whereas higher sinuosity channels tend to expand laterally increasing the amplitude. Analysis on the cross-stream flow field indicated that the cross-sectional velocity variability is greater in high curvature bend i.e. 45^0 channel (R_c/B=1.25) showed greater variability than 60^0 channel (R_c/B =2.25). The cross-sectional variation in the velocity field is dominant at the entry and the exit of the bend whereas the secondary flow is mostly stronger at the apex sections in both channels. Groynes minimized the near bank velocity in both cases. However, the redistribution of secondary recirculation at the bend apex was different for both channels which could be due to the position of the groynes.

Chapter 6

Conclusions and recommendations

6.1 Conclusions

The conclusions based on the findings from this study are enlisted below:

Experimental observations

- The initial bed development process is more rapid in low sinuous channels. Accordingly, the rate of bank erosion was higher for such channels.
- The formation of common characteristics of meandering channels like point bar and deep pools are distinct in low sinuous channels. With increasing sinuosity, bed morphology tends to be more irregular and complicated.
- Another important observation was the location of the maximum bank erosion which was different for each channel. In low sinuosity (and low deflection angle) channel, maximum bank erosion zone begins downstream of outer bank apex and extends to further downstream near inner (convex) bend apex while that location shifts further upstream with increasing deflection angle. As it was observed that maximum bank erosion located upstream of apex to near the crossover region in higher sinuosity channel. This phenomenon is basically governed by the direction of the approach flow which varied with channel deflection angle.
- The flow pattern and locations of the maximum erosion-deposition zones indicated that the lower sinuosity channel is likely to translate or migrate downstream whereas higher sinuosity channels tend to expand laterally increasing the amplitude.

127

- Results showed that the erosion of the outer banks can be significantly reduced by implementing groynes. The high-velocity zone was shifted away from the banks around the groynes field which suppressed the growth and expansion of the point bar on the opposite inner bank. However, the strong recirculation in the embayment can cause erosion to continue in that area.

- At the first groynes where the impact of approach flow is greater, higher scour occurs near the tip increasing the risk of failure of the groynes. Although groynes reduced the bank erosion, they also tend to transfer the erosion from one point to another. Experiments revealed higher erosion in the near-bank area upstream of the first groynes in higher sinuosity channels suggesting increased protection of the area. This tendency was relatively lower in a low sinuous channel which is due to the convergence of approach flow downstream of the apex with less attack on the first groynes.

2D numerical simulation

- Validation results revealed that the 2D models can reasonably predict the bed morphological evolutions in meandering channels.

- The application of 2D models to this study showed that in low sinuosity channel, the groynes positioned downstream of the apex are more effective in reducing the scour depth at the groynes tip, shifting high-velocity core and high near-bank shear stress towards the channel. However, with increasing sinuosity, the position of groynes needs to be shifted upstream around the apex for improving the performance. As it was recognized in case of high sinuosity channel that the groynes positioned exactly at the apex have a slightly better effect of shifting the high-velocity core and high bed shear stress away from the banks.

- The comparison of results between the change in groynes orientation (angle) and location signified that the meandering channel morphology and flow features are more sensitive to the change in location of the groynes than the orientation.

Real field application of 2D model

- The application of the 2D model to the real field cases reasonably reproduced the observed trend. In the case of Gowain River, it was observed that the groynes oriented at 90^0 are more effective in shifting the high velocity from the banks but could promote erosion behind the initial groynes. On the other hand, groynes placed at 120^0 induce greater deposition in the initial groynes. Therefore it was concluded that rather than adopting a single orientation, a combination of two or more arrangements would enhance the effectiveness of the groynes depending upon the field condition.

- Simulation in the Uji River suggested that the overall channel evolution is insignificant but the bank erosion is dominant at several locations. It was also concluded that the bank erosion is mainly caused by the undercutting of the bank toe due to the low flow condition which induces high near bank bed shear stress and a high near bank velocity. With higher flow discharge, the zone of maximum velocity tends to shift more towards the channel center.

<u>3D simulation</u>

- Results indicated that the cross-sectional flow variability is higher in high curvature bend i.e. 45^0 channel (R_c/B=1.25) showed greater variability than 60^0 channel (R_c/B =2.25).
- The cross-sectional variation in the velocity field is dominant at the entry and the exit of the bend whereas the secondary flow is mostly stronger at the apex sections in both channels.
- Groynes minimized the near bank velocity in both cases. However, the redistribution of secondary recirculation at the bend apex was different for both channels which could be due to the position of the groynes.

6.2 Recommendations for future studies

With regard to the scope of the works undertaken, the current study had various limitations. Nevertheless, there is room for expanding the current methodology and analysis. In this regard, some of the possible issues that could be considered in the future works could be listed as;

- Only two meandering channels (deflection angle 45^0 and 60^0) were considered in the current study. The analysis could have been made broader and generalized if two additional channels: one having a deflection angle below 45^0 and the other above 60^0 were incorporated.
- Due to the rapid erosion of channel banks leading to loss of meandering planform, duration of experiments were limited to the quasi-equilibrium state. Strengthening the banks will favor the longer experimental time which would allow the analysis of the equilibrium stage.
- Owing to the size of the experimental domain along with the continuous change of channel planform, the three-dimensional flow field couldn't be measured during the experiments. Thus, it is recommended to consider a smaller domain and carry the experiments sequentially first under the fixed-bed and fixed banks, then the erodible bed and fixed bank and finally considering both the bed and banks erodible. This would

allow the measurement of flow variables with less difficulty and also enable more detailed analysis.

- Groynes in natural channels are subject to unsteady flow situations which lead to alternate submergence and emergence of groynes. To represent a more realistic scenario, experiments with variable flow discharge and submerged condition could be incorporated.

- Alternative countermeasures like bandal-like structures could also be tested for their applicability in meandering channels.

- The results of real field simulations could be further improved if the accurate measurement of river channel bathymetry and other field variables could be done.

References

Abad, J.D., Buscaglia, G.C., Garcia, M.H., 2008. 2D stream hydrodynamic, sediment transport and bed morphology model for engineering applications. Hydrol. Process. 22, 1443–1459. https://doi.org/10.1002/hyp.6697

Ashida, K., Michiue, M., 1973. Studies on bed load transport rate in alluvial streams. Trans. JSCE 4.

Barkdoll, B., Ettema, R., Melville, B.W., 2007. Countermeasures to protect bridge abutments from scour. Washington, DC.

Bhuiyan, F., Hey, R.D., Wormleaton, P.R., 2010. Bank-Attached Vanes for Bank Erosion Control and Restoration of River Meanders. J. Hydraul. Eng. 136, 583–596. https://doi.org/10.1061/(ASCE)HY.1943-7900.0000217

Blanckaert, K., 2015. Flow separation at convex banks in open channels. J. Fluid Mech. 779, 432–467.

Blanckaert, K., 2011. Hydrodynamic processes in sharp meander bends and their morphological implications. J. Geophys. Res. Earth Surf. 116, 1–22. https://doi.org/10.1029/2010JF001806

Braudrick, C.A., Dietrich, W.E., Leverich, G.T., Sklar, L.S., 2009. Experimental evidence for the conditions necessary to sustain meandering in coarse-bedded rivers. Proc. Natl. Acad. Sci. U. S. A. 106, 16936–16941. https://doi.org/10.1073/pnas.0909417106

Cao, Z., Day, R., Egashira, S., 2002. Coupled and decoupled numerical modelling of flow and morphological evolution in alluvial rivers. ,. J. Hydraul. Eng. 128.

CEIWR-HEC, 2015. HEC-RAS: USDA-ARS Bank Stability & Toe Erosion Model (BSTEM) Technical Reference & User's Manual 34. https://doi.org/CPD-68B

Chang, H.H., 2008. River morphology and river channel changes. Trans. Tianjin Univ. 14, 254–262. https://doi.org/10.1007/s12209-008-0045-3

Church, M., 2006. Bed Material Transport and the Morphology of Alluvial River Channels. Annu. Rev. Earth Planet. Sci. 34, 325–354.

Crosato, A., 2009. Physical explanations of variations in river meander migration rates from model comparison. Earth Surf. Process. Landforms 34, 2078–2086. https://doi.org/10.1002/esp

da Silva, A.M.F., El-Tahawy, T., 2008. On the location in flow plan of erosion–deposition zones in sine–generated meandering streams. J. Hydraul. Res. 46, 49–60. https://doi.org/10.1080/00221686.2008.9521939

da Silva, A.M.F., El-Tahawy, T., Tape, W.D., 2006. Variation of Flow Pattern with

Sinuosity in Sine-Generated Meandering Streams. J. Hydraul. Eng. 132, 1003–1014. https://doi.org/10.1061/(ASCE)0733-9429(2006)132:10(1003)

de Vriend H.J., 1987. 2DH mathematical modelling of morphological evolutions in shallow water. Coast. Eng. 11, 1–27.

de Vriend, H.J., 1979. Flow measurements in a curved rectangular channel. Internal report no. 9-79, Laboratory of Fluid mechanics, Department of Civil Engineering Delft University of Technology.

de Vriend, H.J., 1977. A mathematical model of steady flow in curved shallow channels. J. Hydraul. Res. 15, 37–54.

Dehghani, A.A., Azamathulla, H.M., Hashemi Najafi, S.S., Ayyoubzaeh, S.A., 2013. Local scouring around L-head groynes. J. Hydrol. 504, 125–131.

Dulal, K.P., Shimizu, Y., 2010. Experimental simulation of meandering in clay mixed sediments. J. Hydro-Environment Res. 4, 329–343.

Ebrahimi, M., 2015. Flow patterns, bank erosion and planimetric changes in meandering streams: an experimental study. PhD Thesis Queen's University.

El Kadi Abderrezzak, K., Die Moran, A., Tassi, P., Ata, R., Hervouet, J.M., 2016. Modelling river bank erosion using a 2D depth-averaged numerical model of flow and non-cohesive, non-uniform sediment transport. Adv. Water Resour. 93, 75–88. https://doi.org/10.1016/j.advwatres.2015.11.004

Elhakeem, M.P., N.Thanos, A., Wilson, C.G., 2017. Implementing streambank erosion control measures in meandering streams: design procedure enhanced with numerical modelling. Int. J. River Basin Manag. 15, 317–327. https://doi.org/10.1080/15715124.2017.1315816

Engelund, F., 1974. Flow and bed topography in channel bends. J. Hydraul. Div. 1631–1648.

Fujita, I., Muste, M., Kruger, A., 1998. Large-scale particle image velocimetry for flow analysis in hydraulic engineering applications. J. Hydraul. Res. 36, 397–414. https://doi.org/10.1080/00221689809498626

Giri, S., Shimizu, Y., 2004. Observation on bed variation in a meandering like flume with river training structures. Annu. J. Hydraul. Eng. JSCE 48, 1069–1074.

Giri, S., Shimizu, Y., Fujita, M., 2003. Flow characteristics in a mildly meandering channel with & without river training structures. Annu. J. Hydraul. Eng. JSCE 47, 835–840.

Guan, M., Wright, N., Sleigh, P., 2015. Multimode morphodynamic model for sediment-laden flows and geomorphic impacts. J. Hydraul. Eng. 141.

Guan, M., Wright, N.G., Sleigh, P.A., Ahilan, S., Lamb, R., 2016. Physical complexity to model morphological changes at a natural channel bend. Water Resour. Res. 52, 6348–

6364. https://doi.org/10.1002/2015WR017917

Güneralp, I., Abad, J.D., Zolezzi, G., Hooke, J., 2012. Advances and challenges in meandering channels research. Geomorphology 163–164, 1–9. https://doi.org/10.1016/j.geomorph.2012.04.011

Hashimoto, M., Kawaike, K., Hasegawa, Y., Deguchi, T., Paul, A., Salehin, M., Nakagawa, H., 2017. Flash flood inundation analysis considering the aggradation of riverbed in gowain river , bangladesh, in: Proceedings of the 37th IAHR World Congress. Kuala Lumpur, pp. 1840–1847.

Hervouet, J.-M., 2007. Hydrodynamics of Free Surface Flows, Hydrodynamics of Free Surface Flows. https://doi.org/10.1002/9780470319628

Hervouet, J.M., Bates, P., 2000. The telemac modelling system special issue. Hydrological Processes. Hydrol. Process. 2207–2208.

Hickin, E.J., Nanson, G.C., 1984. Lateral Migration Rates of River Bends. J. Hydraul. Eng. 110, 1557–1567. https://doi.org/10.1061/(ASCE)0733-9429(1984)110:11(1557)

Hickin, E.J., Nanson, G.C., 1977. Lateral migration rates of river bends. J. Hydraul. Eng. 110, 1557–1567.

Hirano, M., 1971. On river bed variation with armoring, in: Proceedings of the JSCE. pp. 55–65.

Hooke, J., 2003. River meander behaviour and instability : 238–253.

Hooke, J.M., 2013. River Meandering, Treatise on Geomorphology. Elsevier Ltd. https://doi.org/10.1016/B978-0-12-374739-6.00241-4

Iwagaki, Y., 1956. Hydrodynamical study on critical tractive force. Trans. JSCE 41, 1–21. https://doi.org/10.2208/jscej1949.1956.41_1

Jamieson, E.C., Rennie, C.D., Townsend, R.D., 2013. 3D Flow and Sediment Dynamics in a Laboratory Channel Bend with and without Stream Barbs. J. Hydraul. Eng. 139, 154–166. https://doi.org/10.1061/(ASCE)HY.1943-7900.0000655.

Jia, Y., Scott, S., Xu, Y., Wang, S.S.Y., 2009. Numerical study of flow affected by bendway weirs in Victoria Bendway, the Mississippi River. J. Hydraul. Eng. 135, 902–916.

Johannesson, H., Parker, G., 1989. Velocity redistribution in meandering rivers. J. Hydraul. Eng. 115, 1019–1039.

Karki, S., Nakagwa, H., Kawaike, K., 2018. Evolution of Alluvial Meandering Channels : Comparison between Laboratory Experiments and Natural Channels. DPRI Annu. 655–667.

Kashyap, S., 2012. A 3-D Numerical Study of Flow, Coherent Structures, and Mechanisms Leading to Scour in a High Curvature 135° Channel Bend With and Without Submerged Groynes. PhD Thesis Univ. Ottawa 294.

Knighton, D., 1988. Fluvial forms and processes, a new perspective, Arnold. London.

Koch, F., Flokstra, C., 1980. Bed level computations for curved alluvial channels. , New Delhi., in: Proceedings of the XIXth Congress of the Int. Ass. for Hydr. Res. New Delhi.

Kurdistani, S.M., Pagliara, S., 2017. Experimental study on cross-vane scour morphology in curved horizontal channels. J. Irrig. Drain. Eng. 143, 1–9. https://doi.org/10.1061/(ASCE)IR.1943-4774.0001183

Lagasse, P.F., Clopper, P.E., Pagan-Ortiz, J.E., Zevenbergen, L.W., Arneson, L.A., Schall, J.D., Girard, L.G., 2009. Bridge Scour and Stream Instability Countermeasures: Experience, Selection, and Design Guidance-Third Edition Volume 2. Publication No. FHWA-NHI-09-112. Hydraul. Eng. Circ. 2, 376.

Lagasse, P.F., Spitz, W.J., Zevenbergen, L.W., 2004. Handbook for predicting stream meander migration. Washington D.C.

Langendoen, E.J., 2000. CONCEPTS-CONservation Channel Evolution and Pollutant Transport System, Stream Corridor Version 1.0 180.

Langendoen, E.J., Mendoza, A., Abad, J.D., Tassi, P., Wang, D., Ata, R., El kadi Abderrezzak, K., Hervouet, J.M., 2016. Improved numerical modeling of morphodynamics of rivers with steep banks. Adv. Water Resour. 93, 4–14. https://doi.org/10.1016/j.advwatres.2015.04.002

Langendoen, E.J., Simon, A., 2008. Modeling the Evolution of Incised Streams. II: Streambank Erosion. J. Hydraul. Eng. 134, 905–915. https://doi.org/10.1061/(asce)0733-9429(2008)134:7(905)

Leopold, L.B., Langbein, W.B., 1966. River meanders. Sci. Am. 6, 60-.

Leopold, L.B., Langbein, W.B., 1960. River Meanders. Geol. Soc. Am. Bull. 71, 1–7. https://doi.org/10.1130/0016-7606(1960)71[769:RM]2.0.CO;2

Leopold, L.B., Wolman, M.G., 1957. River Channel Patterns: Braided, Meandering and Straight. Cross Sect. 282.

Leopold, L.B., Wolman, M.G., Miller, J.P., 1964. Fluvial Processes in Geomorphology. Freeman Press, San Francisco.

Lyn, D.A., Cunningham, R., 2016. A Laboratory Study of Bendway Weirs as a Bank Erosion Countermeasure. J. Hydraul. Eng. 142, 1–21. https://doi.org/10.5703/1288284314249

Matsuura, T., Townsend, R., 2004. Stream-barb installations for narrow channel bends – a laboratory study. Can. J. Civ. Eng. 31, 478–486.

Mattic, O., 2018. Telemac3d User Manual. v7p3, 92p.

Mendoza, A., Abad, J.D., Langendoen, E.J., Wang, D., Tassi, P., Abderrezzak, K. El, 2016. Effect of sediment transport boundary conditions on the numerical modeling of bed morphodynamics. J. Hydraul. Eng.

Meyer-Peter, E., Müller, R., 1948. Formulas for Bed-Load Transport. Proc. 2nd Meet. Int. Assoc. Hydraul. Res. 39–64. https://doi.org/1948-06-07

Midgley, T.L., Fox, G.A., Heeren, D.M., 2012. Evaluation of the bank stability and toe erosion model (BSTEM) for predicting lateral retreat on composite streambanks. Geomorphology 145–146, 107–114. https://doi.org/10.1016/j.geomorph.2011.12.044

Mosselman, E., Shishikura, T., Klassen, G.J., 2000. Effect of bank stabilization on bend scour in anabranches of braided river. Phys. Chem. Earth 25, 699–704.

Motta, D., Abad, J.D., Langendoen, E.J., Garcia, M.H., 2012. A simplified 2D model for meander migration with physically-based bank evolution. Geomorphology 163–164, 10–25. https://doi.org/10.1016/j.geomorph.2011.06.036

Nagata, N., Hosoda, T., Muramoto, Y., 2000. Numerical analysis of river channel process with bank erosion. J. Hydraul. Eng. 243–252.

Nakagawa, H., Zhang, H., Baba, Y., Kawaike, K., Teraguchi, H., 2013. Hydraulic characteristics of typical bank-protection works along the Brahmaputra/Jamuna River, Bangladesh. J. Flood Risk Manag. 6, 345–359. https://doi.org/10.1111/jfr3.12021

Partheniades, E., 1965. Erosion and deposition of cohesive soils. J. Hydraul. Div. 91, 105–139.

Przedwojski, B., 1995. Bed topography and local scour in rivers with banks protected by groynes. J. Hydraul. Res. 33, 257–273. https://doi.org/10.1080/00221689509498674

Rhoads, B.L., Welford, M.R., 1991. Initiation of river meandering. Prog. Phys. Geogr. 15, 127–156.

Schumm, S.A., 1963. Sinuosity of alluvial rivers on the Great Plains. Geol. Soc. Am. Bull. 74, 1089–1100.

Schumm, S.A., 1960. The Shape of Alluvial Channels in Relation To Sediment Type. USGS Numbered Ser. 24. https://doi.org/10.3133/pp352B

Seminara, G., 2006. Meanders. J. Fluid Mech. 554, 271. https://doi.org/10.1017/S0022112006008925

Sharma, K., Mohapatra, P.K., 2012. Separation Zone in Flow past a Spur Dyke on Rigid Bed Meandering Channel. J. Hydraul. Eng. 138, 897–901. https://doi.org/10.1061/(ASCE)HY.1943-7900.0000586

Simon, A., Bankhead, N., Thomas, R.E., 2010. Iterative bankstability and toe-erosion modeling for predicting streambank loading rates and potential load reductions, in: Paper Presented at Joint Federal Interagency Conference, Subcomm. on Hydrol. and Sediment., Advis. Comm. on Water Info. Las Vegas, Nevada.

Simon, A., Curini, A., Darby, S.E., Langendoen, E.J., 2000. Bank and near-bank processes in an incised channel. Geomorphology 35, 183–217.

Song, C.G., Seo, I.W., Kim, Y.D., 2012. Analysis of secondary current effect in the modeling of shallow flow in open channels. Adv. Water Resour. 41, 29–48.

Song, X., Xu, G., Bai, Y., Xu, D., 2016. Experiments on the short-term development of sine-generated meandering rivers. J. Hydro-Environment Res. 11, 42–58. https://doi.org/10.1016/j.jher.2016.01.004

Struiksma, N., Olesen, K.W., Flokstra, C., De Vriend, H.J., 1985. Bed deformation in curved alluvial channels. J. Hydraul. Res. 23, 57–79. https://doi.org/10.1080/00221688509499377

Tal, M., Narteau, C., Jerolmack, D., 2010. Single-thread channels as the result of localized erosion and deposition driven by vegetation, in: RCEM. pp. 587–593.

Tape, W.D., 2001. Experimental investigation of flow patterns in meandering channels of moderate sinuosity. Univ. Wind.

Tassi, P., 2018. Sisyphe User Manual. V7p3, 70.

Teraguchi, H., 2011. Study on hydraulic and morphological characteristics of river channel with groynes structures. Kyoto University.

Teraguchi, H., Nakagawa, H., Kawaike, K., Baba, Y., Zhang, H., 2011. Effects of hydraulic structures on river morphological processes. Int. J. Sediment Res. 26, 283–203.

Thielicke, W., Stamhuis, E.J., 2014. PIVlab − Towards User-friendly, Affordable and Accurate Digital Particle Image Velocimetry in MATLAB. J. open Softw. Res. 2, 30.

Uijttewaal, W.S., 2005. Effects of Groyne Layout on the Flow in Groyne Fields: Laboratory Experiments. J. Hydraul. Eng. 131, 782–791. https://doi.org/10.1061/(ASCE)0733-9429(2005)131:9(782)

Villaret, C., Hervouet, J.M., Kopmann, R., Merkel, U., Davies, A.G., 2013. Morphodynamic modeling using the Telemac finite-element system. Comput. Geosci. 53, 105–113. https://doi.org/10.1016/j.cageo.2011.10.004

Whiting, P., Dietrich, W., 1993. Experimental Studies of Bed Topography and Flow Patterns in Large Amplitude Meanders. 1. Observations. Water Resour. Res. 3605–3614.

Wu, W., 2004. Channels, Depth-averaged two-dimensional numerical modeling of unsteady flow and nonuniform sediment transport in open. J. Hydraul. Eng. 130.

Xiao, Y., Zhou, G., Yang, F.S., 2016. 2D numerical modelling of meandering channel formation. J. Earth Syst. Sci. 125, 251–267. https://doi.org/10.1007/s12040-016-0662-5

Xu, D., Bai, Y., 2013. Experimental study on the bed topography evolution in alluvial meandering rivers with various sinuousnesses. J. Hydro-Environment Res. 7, 92–102. https://doi.org/10.1016/j.jher.2012.06.003

Yossef, M.F.M., 2002. The effect of groynes on rivers: Literature review. Delft Clust. Publ. 03.03. 04.

Yossef, M.F.M., Vriend, H.J. de, 2010. Sediment Exchange between a River and Its Groyne Fields: Mobile-Bed Experiment. J. Hydraul. Eng. 136, 610–625. https://doi.org/10.1061/(ASCE)HY.1943-7900.0000226

Zeng, J., Constantinescu, G., Blanckaert, K., Weber, L., 2008. Flow and bathymetry in sharp open-channel bends: Experiments and predictions. Water Resour. Res. 44. https://doi.org/10.1029/2007WR006303

Zhang, H., Nakagawa, H., 2009. Characteristics of local flow and bed deformation at impermeable and permeable spur dykes. Annu. J. Hydraul. Eng. JSCE 53, 145–150.

List of Figures

142

List of Photos

List of Tables

Curriculum Vitae

Name   KARKI Saroj

Citizenship   Republic of Nepal

Date of Birth   23 September, 1985

Key Qualification

Ph.D. Student (2016 ~ 2019)

Department of Civil and Earth Resources Engineering,

Kyoto University, Kyoto, Japan

M. Sc. (2010 ~ 2012)

Department of Water Resources Engineering

Institute of Engineering (IOE), Pulchowk Campus, Tribhuvan University (TU), Nepal

B.E. (2005 ~ 2010)

Department of Civil Engineering

Institute of Engineering (IOE), Pulchowk Campus, Tribhuvan University (TU), Nepal

Key Employment Record

From July 2012 to Present (On a study leave during Ph.D.)

Employer: Ministry of Water-Resources and Irrigation, Government of Nepal

Position Held: Irrigation Engineer

From July 2010 to Jan 2011

Employer: Hydro-Solutions Pvt. Ltd.

Position Held: Design Engineer (Hydropower)

Paper based on the Thesis

Karki S., Nakagawa H., Kawaike K. and Hashimoto M.: Experimental Study on the Performance of Slope-crested Groynes in Erodible Meandering Channels of Different Sinuosity, *Journal of Japan Society for Natural Disaster Science*, Vol. 37, 93-105, 2018.

Karki S., Nakagawa H., Kawaike K., Hashimoto M. and Hasegawa Y.: Morphological Variations with Sinuosity in Sine-Generated Meandering Channels with and Without Groynes, *Journal of Japan Society of Civil Engineers*, Ser. B1 (Hydraulic Engineering) Vol. 74, No. 5, I_967-I_972, 2018.

Karki S., Hasegawa Y., Hashimoto M., Nakagawa H. and Kawaike K.: Short-Term Evolution of Flow and Morphology in an erodible Meandering Channel with and without groynes, *Journal of Japan Society of Civil Engineers*, Ser. B1 (Hydraulic Engineering) Vol. 74, No. 4, I_1147-I_1152, 2018.

Karki S, Hashimoto M, Nakagawa H, Kawaike K and Hasegawa Y.: A 2D Numerical Analysis of the Hydro-Morphodynamic Behaviour of Meandering Channel with Groynes: A Case of Piyan River in Bangladesh, Book of extended Abstract, *7th International Conference on Water and Flood Management-ICWFM 2019*, Dhaka, Bangladesh, 85-86, 2019.

Karki S, Nakagawa H and Kawaike K.: Evolution of Alluvial Meandering Channels: Comparison between Laboratory Experiments and Natural Channels, *Annuals of the Disaster Prevention Research Institute*, Kyoto University, Vol. 61B, 655-667, 2018.

Karki S., Nakagawa H., Kawaike K., Hashimoto M., Hasegawa Y., Langendoen E. J., Ata R., Tassi P. and Abderrezzak K E K.: Experimental and 2D Numerical Modelling of Morphology and Bank Erosion in Meandering Channels of Different Sinuosity, *38th IAHR World Congress*, Panama City, Panama, September 1-6, 2019 (**Accepted**)

Karki S., Nakagawa H., and Kawaike K.: Meandering Channels Response to a Series of Permeable and Impermeable Structures under Different Sinuosity, *Journal of Japan Society of Civil Engineers*, Ser. B1 (Hydraulic Engineering), 2019 (**Accepted**)

Karki S, Nakagawa H and Kawaike K.: 3-Dimensional modeling of flow and morphology in meandering channels of different sinuosity with bank protection structures, 14th *International Symposium on River Sedimentation*, Chengdu, China, September 16-19, 2019 (**Accepted**).

Karki S, Nakagawa H, Kawaike K. and Hashimoto, M.: Numerical Study on the Hydro-Morphological and Bank Erosion Characteristics of Uji River, Japan, *Annuals of the Disaster Prevention Research Institute*, Kyoto University, 2019 (**In print**).